

THE TEMPORAL SPOTLIGHT OF ATTENTION:  
COMPUTATIONAL AND ELECTROPHYSIOLOGICAL EXPLORATIONS

A THESIS SUBMITTED TO  
THE UNIVERSITY OF KENT AT CANTERBURY  
IN THE SUBJECT OF COMPUTER SCIENCE  
FOR THE DEGREE  
OF DOCTOR OF PHILOSOPHY

By  
Srivas Chennu  
December 2009

# Contents

<b>List of Tables</b>	<b>ix</b>
<b>List of Figures</b>	<b>x</b>
<b>Abstract</b>	<b>xiii</b>
<b>Acknowledgements</b>	<b>xiv</b>
<b>I Background</b>	<b>1</b>
<b>1 Introduction</b>	<b>2</b>
1.1 Overview . . . . .	2
1.1.1 Temporal Attention . . . . .	2
1.1.2 Human Electrophysiology . . . . .	5
1.1.3 Cognitive Modelling . . . . .	6
1.2 Central Hypotheses . . . . .	7
1.3 Organisation . . . . .	9
1.4 Collaborations and Publications . . . . .	12
<b>2 Prior Research</b>	<b>13</b>
2.1 Temporal Attention and TAE . . . . .	13
2.2 Rapid Serial Visual Presentation . . . . .	15
2.3 The Attentional Blink . . . . .	16
2.3.1 The Task . . . . .	16
2.3.2 AB Phenomena . . . . .	16

2.4	The Electrophysiology of Attention and Consciousness . . . . .	19
2.4.1	Electroencephalography . . . . .	19
2.4.2	Event-related Potentials . . . . .	20
2.4.3	ERP Components . . . . .	20
2.4.4	ERPimages . . . . .	24
2.5	Feature Binding in Vision . . . . .	25
2.5.1	Feature Binding in the Temporal Dimension . . . . .	28
2.5.2	Modelling Temporal Feature Binding . . . . .	33
2.6	Conclusions . . . . .	40
<b>3</b>	<b>Models of the Temporal Spotlight</b>	<b>41</b>
3.1	The ST <sup>2</sup> Model . . . . .	41
3.1.1	Types and Tokens . . . . .	42
3.1.2	Stage 1 of Neural-ST <sup>2</sup> . . . . .	43
3.1.3	Stage 2 of Neural-ST <sup>2</sup> . . . . .	44
3.1.4	Transient Attentional Enhancement: the Blaster . . . . .	44
3.1.5	How the Model Blinks - Suppression of TAE . . . . .	45
3.2	The LC-NE Model . . . . .	46
3.2.1	Behavioural Network . . . . .	46
3.2.2	The Locus Coeruleus . . . . .	47
3.2.3	How the Model Blinks - The LC Refractory Period . . . . .	48
3.3	Related Work . . . . .	48
3.3.1	The Global Workspace Model . . . . .	48
3.3.2	The CODAM Model . . . . .	49
3.3.3	The eSTST Model . . . . .	49
3.3.4	The Boost and Bounce Model . . . . .	50
3.4	Conclusions . . . . .	50
<b>4</b>	<b>Connecting Modelling and Electrophysiology</b>	<b>51</b>
4.1	Introducing Virtual ERPs . . . . .	51
4.2	Generating Virtual ERPs . . . . .	53
4.2.1	Grand Average Virtual ERPs . . . . .	56

4.2.2	Virtual ERPimages . . . . .	56
4.3	Virtual ERP Components . . . . .	57
4.3.1	Early Visual Processing - The Virtual ssVEP . . . . .	57
4.3.2	Transient Attentional Enhancement - The Virtual N2pc . . . . .	58
4.3.3	Working Memory Encoding - The Virtual P3 . . . . .	59
4.4	Conclusions . . . . .	59
 <b>II Explorations of the Temporal Spotlight</b>		<b>60</b>
 <b>5 Comparing the ST<sup>2</sup> and the LC-NE models</b>		<b>61</b>
5.1	Introduction . . . . .	61
5.2	TAE in the ST <sup>2</sup> Model: The Blaster . . . . .	63
5.2.1	Internal Structure . . . . .	64
5.3	TAE in the LC-NE Model: The Locus Coeruleus . . . . .	65
5.3.1	The Locus Coeruleus & Norepinephrine . . . . .	66
5.4	Assessment of Models . . . . .	68
5.4.1	The ST <sup>2</sup> Model . . . . .	69
5.4.2	The LC-NE Model . . . . .	73
5.4.3	Discussion . . . . .	77
5.5	Extension of the LC-NE Model . . . . .	80
5.5.1	Performance of the Extended LC-NE Model . . . . .	81
5.6	Final Discussion . . . . .	82
5.6.1	The Blaster and the LC . . . . .	83
5.6.2	Correlates of the P3 . . . . .	84
5.7	Conclusions . . . . .	85
 <b>6 Target Discriminability and Temporal Perception</b>		<b>86</b>
6.1	Introduction . . . . .	86
6.1.1	Motivation and Overview . . . . .	89
6.2	The Single Target Experiment . . . . .	89
6.3	Target Processing in Onset Presentation . . . . .	90

6.3.1	Behaviour . . . . .	90
6.3.2	Early Components . . . . .	90
6.3.3	The P3 . . . . .	91
6.4	Modelling Onset Presentation with the ST <sup>2</sup> Model . . . . .	92
6.4.1	Step 1: Simulating Early Components . . . . .	92
6.4.2	Step 2: Simulating the P3 . . . . .	94
6.4.3	Step 3: Simulating Behavioural Accuracy . . . . .	97
6.5	Discussion . . . . .	99
6.5.1	Early Components vs. the ssVEP . . . . .	99
6.5.2	Lag 1 Sparing and Onset Presentation . . . . .	100
6.5.3	Is Onset Presentation an Equal Substitute for RSVP? . . . . .	101
6.6	Conclusions . . . . .	102
<b>7</b>	<b>The Temporal Precision of Attention</b>	<b>103</b>
7.1	Introduction . . . . .	103
7.1.1	Attentional Precision and the ST <sup>2</sup> Model . . . . .	104
7.2	The Two Target Experiment . . . . .	105
7.3	Behavioural Analysis . . . . .	105
7.4	ERP Analysis . . . . .	106
7.5	Single-Trial Analysis . . . . .	110
7.5.1	Analysis of ITC and ERSP . . . . .	110
7.5.2	Analysis of ERPimages . . . . .	116
7.5.3	Analysis of Phases . . . . .	119
7.6	Explaining Temporal Precision using the ST <sup>2</sup> Model . . . . .	125
7.6.1	Simulated Behavioural Accuracy . . . . .	125
7.7	Virtual ERPs . . . . .	125
7.7.1	Virtual ERPimages . . . . .	128
7.8	Discussion . . . . .	134
7.9	Related Work . . . . .	136
7.9.1	Chun (1997), Popple and Levi (2007) . . . . .	136
7.9.2	Vul, Nieuwenstein and Kanwisher (2008) . . . . .	137

7.9.3	Sergent, Baillet and Dehaene (2005)	139
7.10	Conclusions	139
<b>8</b>	<b>Attention and Temporal Feature Binding</b>	<b>141</b>
8.1	Introduction	141
8.2	The Two-Feature Extension to ST <sup>2</sup> : The 2f-ST <sup>2</sup> Model	142
8.2.1	Rationale	142
8.2.2	Architecture	144
8.2.3	Dynamics	150
8.2.4	Configuration	152
8.3	Behavioural Predictions of the 2f-ST <sup>2</sup> Model	154
8.3.1	Manipulation of the Key Feature Pathway	155
8.3.2	Manipulation of the Response Feature Pathway	159
8.3.3	Summary	162
8.4	Reaction Times for Response Positions	162
8.5	The Temporal Binding Experiment	167
8.6	Conclusions	170
<b>9</b>	<b>Neural Dynamics of Temporal Feature Binding</b>	<b>172</b>
9.1	Virtual ERPs from 2f-ST <sup>2</sup>	172
9.2	Determinants of the P3	174
9.3	ERP Predictions of the 2f-ST <sup>2</sup> Model	177
9.3.1	Combined Key-locked and Response-locked Averages	177
9.3.2	Correct Reports, Pre-target Errors and Post-target Errors	180
9.3.3	Manipulation of the Key Feature Pathway	183
9.3.4	Manipulation of the Response Feature Pathway	186
9.4	The Temporal Binding Experiment	191
9.4.1	Combined Key-locked and Response-locked Averages	191
9.4.2	Correct Reports, Pre-target Errors and Post-target Errors	193
9.4.3	Manipulation of the Key Feature Pathway	198
9.4.4	Manipulation of the Response Feature Pathway	202
9.4.5	Summary	203

9.5	Conclusions . . . . .	204
<b>III</b>	<b>Discussion</b>	<b>206</b>
<b>10</b>	<b>Conclusions, Contributions and Outlook</b>	<b>207</b>
10.1	Conclusions . . . . .	207
10.2	Contributions . . . . .	211
10.3	Future Outlook . . . . .	213
10.3.1	Experimental Directions . . . . .	213
10.3.2	Theoretical Directions . . . . .	216
<b>IV</b>	<b>Appendix</b>	<b>220</b>
<b>A</b>	<b>Computational Methods</b>	<b>221</b>
A.1	The ST <sup>2</sup> Model . . . . .	221
A.1.1	On-Off Circuits . . . . .	221
A.1.2	Gate-Trace Pair . . . . .	222
A.1.3	Weights and Connectivity . . . . .	224
A.1.4	Model Configuration . . . . .	224
A.2	The Re-implemented LC-NE Model . . . . .	225
A.2.1	Simulating Blanks in the LC-NE Model . . . . .	225
A.3	The Extended LC-NE Model . . . . .	225
A.3.1	Extension Parameters . . . . .	226
A.4	The 2f-ST <sup>2</sup> Model . . . . .	227
A.4.1	Architecture . . . . .	227
A.4.2	Dynamics . . . . .	230
A.4.3	General Configuration . . . . .	230
A.4.4	Configuration for Behavioural Simulations in Section 8.3 . . . . .	231
<b>B</b>	<b>Experimental Methods</b>	<b>233</b>
B.1	Experiment 1 . . . . .	233
B.1.1	Participants . . . . .	233

B.1.2	Stimuli and Apparatus . . . . .	233
B.1.3	Procedure . . . . .	233
B.1.4	EEG Recording and Analysis . . . . .	235
B.1.5	Computational Modelling . . . . .	237
B.2	Experiment 2 . . . . .	237
B.2.1	Participants . . . . .	237
B.2.2	Stimuli and Apparatus . . . . .	238
B.2.3	Procedure . . . . .	238
B.2.4	EEG Recording and Analysis . . . . .	239
B.2.5	Computational Modelling . . . . .	242
B.3	Experiment 3 . . . . .	243
B.3.1	Participants . . . . .	243
B.3.2	Stimuli and Apparatus . . . . .	243
B.3.3	Procedure . . . . .	244
B.3.4	EEG Recording and Analysis . . . . .	246
B.3.5	Computational Modelling . . . . .	247
	<b>Bibliography</b>	<b>249</b>

# List of Tables

1	Connection weights in the ST <sup>2</sup> model that were modified in this thesis . . . .	224
2	Leak current values in Stage 1 of the response pathway of the 2f-ST <sup>2</sup> model	228
3	Connection weights in Stage 1 of the response pathway of the 2f-ST <sup>2</sup> model .	229
4	Connection weights in Stage 2 of the 2f-ST <sup>2</sup> model . . . . .	229
5	Conditions of interest analysed in Experiment 2 . . . . .	240
6	Conditions of interest analysed in Experiment 3 . . . . .	247

# List of Figures

1	RSVP stream similar to that used by Lawrence (1971) . . . . .	15
2	Human performance in the AB task, reported by Chun and Potter (1995) (Bowman & Wyble, 2007) . . . . .	17
3	Generating ERPs from EEG . . . . .	21
4	Examples of ERP components (Woodman & Luck, 2003) . . . . .	22
5	ERPs vs. ERPimages. . . . .	24
6	Visual information processing in the brain . . . . .	26
7	The binding problem (Wolfe & Bennett, 1997) . . . . .	27
8	Sample response distributions from temporal binding experiments reported in Botella, Garcia, and Barriopedro (1992) . . . . .	30
9	Influence of the AB on temporal feature binding (Chun, 1997a; Vul, Nieuwenstein, & Kanwisher, 2008) . . . . .	32
10	The Botella, Barriopedro, and Suero (2001) model . . . . .	35
11	The Neural-ST <sup>2</sup> model (Craston, Wyble, Chennu, & Bowman, 2009) . . . . .	42
12	The LC-NE model (Nieuwenhuis, Gilzenrat, Holmes, & Cohen, 2005) . . . . .	47
13	The role of virtual ERPs in cognitive science research . . . . .	53
14	Node-level activation dynamics in Neural-ST <sup>2</sup> . . . . .	54
15	Virtual ERPs from the ST <sup>2</sup> model . . . . .	57
16	The dynamics and circuitry of the blaster in Neural-ST <sup>2</sup> (Bowman & Wyble, 2007) . . . . .	64
17	Dynamic behaviour of the LC-NE system . . . . .	66
18	ST <sup>2</sup> model performance in the AB task (Bowman & Wyble, 2007) . . . . .	69

19	T2 consolidation delay by lag for the ST <sup>2</sup> model (Bowman, Wyble, Chennu, & Craston, 2008) . . . . .	72
20	Standard blink conditions generated from the re-implemented LC-NE model (Bowman et al., 2008) . . . . .	74
21	T2 consolidation delay by lag for the LC-NE model (Bowman et al., 2008) . . . . .	76
22	The extended LC-NE model (Bowman et al., 2008) . . . . .	79
23	Standard blink conditions generated from the extended LC-NE model (Bowman et al., 2008) . . . . .	81
24	Behavioural accuracy scores from AB studies using Onset presentation (Ward, Duncan, & Shapiro, 1997; McLaughlin, Shore, & Klein, 2001; Visser, Bischof, & Di Lollo, 2004; Rolke, Bausenhardt, & Ulrich, 2007) . . . . .	88
25	Fast fourier transforms (FFT) of the ERPs for the RSVP (left) and Onset (right) conditions (Chennu, Craston, Wyble, & Bowman, 2009b) . . . . .	90
26	Human P3 for targets in RSVP and Onset presentation (Chennu et al., 2009b)	91
27	Step 1 of simulating Onset presentation . . . . .	92
28	Virtual ssVEP wave for the RSVP and early components for the Onset conditions (Chennu et al., 2009b) . . . . .	93
29	Step 2 of simulating Onset presentation (Chennu et al., 2009b) . . . . .	95
30	After Step 2: Virtual P3 for the RSVP and Onset conditions (Chennu et al., 2009b) . . . . .	96
31	Step 3 of simulating Onset presentation . . . . .	97
32	After Step 3: Virtual P3 for the RSVP and Onset conditions . . . . .	98
33	Human ERPs for targets presented outside and inside the AB . . . . .	107
34	Human ERPs for targets seen outside and inside the AB . . . . .	109
35	ITC evoked by targets inside and outside the AB . . . . .	112
36	ERSP evoked by targets inside and outside the AB . . . . .	115
37	Human N2pc ERPimages for targets seen outside and inside the AB . . . . .	117
38	Human P3 ERPimages for targets seen outside and inside the AB . . . . .	118
39	Human P3 ERPimages for the T2 Lag 8 and T1 Lag 3 conditions . . . . .	123
40	Virtual ERPs for targets seen outside and inside the AB . . . . .	126

41	50% area latency-sorted virtual N2pc ERP images for targets seen outside and inside the AB . . . . .	129
42	50% area latency-sorted virtual P3 ERP images for targets outside and targets inside the AB . . . . .	130
43	The 2f-ST <sup>2</sup> model . . . . .	145
44	Temporal feature binding in the 2f-ST <sup>2</sup> model . . . . .	150
45	Key feature manipulation in Botella et al. (2001) simulated by 2f-ST <sup>2</sup> . . . . .	157
46	Response feature manipulation in Botella et al. (2001) simulated by 2f-ST <sup>2</sup> . . . . .	160
47	Reaction time data from Botella (1992) explained by the 2f-ST <sup>2</sup> model . . . . .	163
48	Simulation of behavioural data from Experiment 3 by the 2f-ST <sup>2</sup> model . . . . .	168
49	Virtual ERPs from the 2f-ST <sup>2</sup> model . . . . .	174
50	Virtual ERPs from the 2f-ST <sup>2</sup> model combining across all response positions, time-locked to the key feature and response feature in each trial . . . . .	178
51	Key-locked and response-locked virtual ERPs from the 2f-ST <sup>2</sup> model for correct reports, pre-target and post-target errors . . . . .	181
52	Early and late key feature conditions from the 2f-ST <sup>2</sup> model . . . . .	184
53	Early and late response feature conditions from the 2f-ST <sup>2</sup> model . . . . .	187
54	Behaviour and ERPs from Experiment 3 . . . . .	192
55	ERPs evoked by correct reports, pre-target errors and post-target errors . . . . .	194
56	Behaviour and ERPs for the letter and symbol conditions . . . . .	199
57	An on-off circuit . . . . .	222
58	A gate-trace pair . . . . .	223
59	Weight types and connectivity patterns in the ST <sup>2</sup> model . . . . .	223
60	The RSVP and Onset presentation paradigms . . . . .	234
61	The two-target bilateral RSVP paradigm used in Experiment 2 (Craston et al., 2009) . . . . .	238
62	The single-target coloured bilateral RSVP paradigm used in Experiment 3 . . . . .	244

# Abstract

The study of attention aims to understand how the visual system focuses its resources on salient targets presented amongst competing distractors. In a continuously changing environment, temporal attention must pick out targets presented in between spatially coincident distractors that are offset in time. Cognitive theories have proposed that this task is mediated by a temporal ‘spotlight’ of attention. This thesis combines evidence from behaviour and electrophysiology (EEG) with theoretical insights from neural network modelling to investigate the interplay between this spotlight and conscious perception.

The experiments described in this thesis investigate the electrophysiology of temporal visual perception using the Rapid Serial Visual Presentation (RSVP) paradigm. Building upon behavioural research, we use EEG to investigate the influence of target discriminability, the Attentional Blink (AB) and feature integration on the temporal dynamics of visual perception. These findings characterise the influence of pre-attentional processes on attentional deployment, and the subsequent influence of this deployment on perception and behaviour. In addition, they provide the basis for a complementary computational elucidation.

The theoretical component of this thesis is based on the  $ST^2$  neural network model. The notion of Transient Attentional Enhancement (TAE) embodied therein is the computational equivalent of the temporal spotlight. Its function is evaluated within the  $ST^2$  model and in relation to other modelling approaches. In addition, human ERP (Event-Related Potential) data from the experiments are compared with the model’s equivalent activation traces, termed *Virtual ERPs*. This combination of theory and experiment broadens our understanding of temporal visual perception, and in conjunction, highlights the role of neural modelling in informing EEG research.

# Acknowledgements

My first foray into the topic of human cognition, consciousness, and ‘all that’ began with a reading of *Phantoms in the Brain* by Vilayanur S. Ramachandran. For handing me a well-worn copy of that book, I have only my mother Devaki and brother Arjun to thank.

However, my nascent interest in the topic would not have gotten very far if not for the enthusiasm displayed by Howard Bowman in taking me on as a student. He has been a most supportive and meticulous adviser all through my PhD, guiding my research with characteristically gentle persuasion. In same breath, I thank Brad Wyble for his convoluted code and straight answers. Owing to Brad and the continuing comradeship of Patrick Craston, I got my research off to a running start for which I will always be grateful. In addition, I was lucky to receive advice and support from Dinkar Sharma, Rosie Cowell, Dominique Chu and Alex Freitas at the University of Kent. Thanks are also due to Dinkar and John Duncan from the MRC Cognition and Brain Sciences Unit at Cambridge for agreeing to examine this thesis.

More heartfelt thanks go to Damian Dimmich, Poul Henriksen, Katherine Johnson, Sabrina Panëels, Tara Puri, Edward Suvanaphen and Bryony Worthington, for being great company during the highs and lows of my charmed life as a PhD student.

Lastly, I should be remiss not to thank the School of Computing at the University of Kent for their support, in the form of a research scholarship and the concomitant peace of mind with which to pursue my research to fruition.

# Part I

# Background

# Chapter 1

## Introduction

We introduce this thesis with an overview of the three overarching themes which form the basis of the research described here, namely temporal attention, human electrophysiology and cognitive modelling. Following that, we outline the general organisation of its contents into parts and chapters. In the last section of this chapter, we highlight the strongly collaborative aspect of this thesis and list the publications that have resulted from the research leading up to it.

### 1.1 Overview

#### 1.1.1 Temporal Attention

Within the science of cognitive psychology, the study of *attention* is targeted at understanding how the mind focuses its processing resources on information that is contextually salient in its environment, while suppressing irrelevant distracting information (Driver, 2001). In the context of the visual system, this filtering mechanism is essential to its information processing hierarchy (Hochstein & Ahissar, 2002). It enables the system to select a comparatively small amount of task-relevant information from a large quantity of sensory data. The nature of attention, especially within the research into visual awareness, is one of the most studied and debated aspects of human cognition, both as a conduit to the conscious mind (James, 1890; Broadbent, 1958; Kahneman, 1973; Pashler, 1996) and as a metaphor

for the underlying neural dynamics (Wurtz, Goldberg, & Robinson, 1980; Posner & Peterson, 1990; Luck, 1998).

Visual attention has been extensively investigated in the spatial domain, i.e., in which stimuli are presented simultaneously but are spatially offset in the visual field. This is a situation quite common in everyday circumstances. Consequently, the role of *spatial attention* in selectively enhancing task-relevant stimuli in the visual field, especially in visual search paradigms, has been explored in much breadth and depth (Broadbent, 1958; Deutsch & Deutsch, 1963; Duncan, 1980, 1981; Treisman & Gelade, 1980; Desimone & Duncan, 1995; Luck, Chelazzi, Hillyard, & Desimone, 1997; Treisman, 1998). In this context, attention has been popularly thought of as a ‘spotlight’ that highlights a specific location of the visual field for further processing, while suppressing irrelevant surrounding information (Sperling, 1960; Averbach & Coriell, 1961; Posner, Snyder, & Davidson, 1980; Winer & Cottrell, 1996). Studies that have characterised this *spatial spotlight* have found that it can ‘illuminate’ regions of varying size (C. W. Eriksen & St James, 1986), has limits to the spatial resolution within its central focus (Bouma, 1970; B. A. Eriksen & Eriksen, 1974; J. Miller, 1991; He, Cavanagh, & Intriligator, 1996), and degrades in efficiency with increasing distance from this centre (C. W. Eriksen & Yeh, 1985; Downing & Pinker, 1985).

Based on a large body of evidence, researchers have debated the extent to which the spotlight metaphor is applicable for spatial attention (see Cave & Bichot, 1999). This is because experiments have found that humans can divide their attention between multiple tasks (Corbetta, Miezin, Dobmeyer, Shulman, & Petersen, 1991; Bichot & Schall, 1999; though see Castiello & Umiltà, 1992; McCormick, Klein, & Johnston, 1998), and track the movement of multiple objects in their visual field (Pylyshyn & Storm, 1988; Pylyshyn, 1989; though see Yantis, 1992). In addition, it has been proposed that attention can operate at the level of objects rather than location (Duncan, 1984; Kanwisher & Driver, 1992). Such object-based selective attention is influenced by perceptual grouping of visual features (Driver & Baylis, 1989; Behrmann, Zemel, & Mozer, 1998; Cave & Bichot, 1999), and is thought to be achieved using internal mental representations referred to as ‘object files’ (Kahneman & Treisman, 1984; Kahneman, Treisman, & Gibbs, 1992; Chun, 1997b; Kanwisher & Driver, 1992).

On the other hand, *temporal attention*, relating to how salient stimuli are selected in

time, when presented with competing stimuli occupying the same spatial location but offset in time, is relatively less well understood. For the most part, this is because humans have been found to be extremely good at quickly extracting meaning from rapidly changing visual information (Sperling, Budiansky, Spivak, & Johnson, 1971; Lawrence, 1971; Potter, 1975; Reeves & Sperling, 1986; Weichselgartner & Sperling, 1987). As a result, the limits of temporal attention do not become evident in most everyday circumstances. However, with the progressively ubiquitous use of technology in our daily environment, the pace of human life is continually increasing. We are being exposed to real-life situations in which the temporal limits of our perceptual abilities are often reached. Common examples are scenarios involving automobile drivers and pilots, who have to selectively respond and act according to fleeting stimuli from numerous sources of information if they are to avoid potentially disastrous consequences. As a result, now more than ever, it has become important to understand and characterise the temporal capacity limits of human attention and vision. Therefore, fundamental research in this direction would be very beneficial, and could have significant implications for the design of the next generation of human-computer interface technologies (Su, Bowman, Barnard, & Wyble, 2008; Bowman, Su, Wyble, & Barnard, 2009; Makeig, 2009).

This thesis works towards addressing this gap in knowledge, and focuses on the empirical and theoretical study of temporal attention and perception. In this context, the *temporal spotlight of attention*, or more accurately, *Transient Attentional Enhancement* (TAE), describes the cognitive mechanism that provides a short-lived burst of enhancement to fleeting visual targets. Thus, the temporal spotlight highlights a brief window of time at a particular spatial location. In this sense, it is effectively spatially *and* temporally specific<sup>1</sup>. The temporal spotlight plays a crucial role in ensuring that briefly presented stimuli generate enough neural activation to reach the level of conscious awareness. In this thesis, *temporal perception* refers to the temporal dynamics of visual perception that result from the action of this spotlight. In the following sections, we highlight the two main techniques that we will use to investigate the mechanisms of temporal attention and perception: electrophysiology (EEG) and cognitive modelling.

---

<sup>1</sup>In comparison, the spatial spotlight discussed previously highlights regions of space (or objects within them) for sustained periods of time.

### 1.1.2 Human Electrophysiology

Experimental psychology since the ‘cognitive revolution’ (Broadbent, 1958; Neisser, 1967) has relied on behavioural metrics to characterise the unseen but indirectly observable processes underlying human cognition. Though behavioural psychology has been very successful in adding to our understanding of the mind, it is limited in its ability to directly study cognitive processes. In many situations, like in the case of attention, the processes being studied come into play at a very early stage after the visual onset of information, and are far removed from the eventual behavioural outcome. More recently, the field of cognitive neuroscience has attempted to bring the power of neuroimaging technologies to bear upon this problem (Gazzaniga, Ivry, & Mangun, 2002). Techniques like fMRI (functional Magnetic Resonance Imaging), EEG (Electroencephalography), MEG (Magnetoencephalography) and PET (Positron Emission Tomography) are attempting to directly capture the brain in action as it is processing information and executing behaviour. Using these tools, cognitive neuroscientists aim to discover the neural substrates and mechanisms in the brain that support the complex machinery of the mind.

For the purposes of studying temporal perception in humans, non-invasive, scalp-recorded electrical activity (EEG) (and increasingly, MEG) is a particularly useful tool. This is mainly because it is a moment-by-moment electrical signature of neural dynamics, which provides researchers with markers of short-lived brain events occurring very soon after the visual onset of stimuli. In particular, within a controlled laboratory setting, changes in ongoing EEG activity have been shown to be reproducibly time-locked to the occurrence of task-relevant stimuli. Such *event-related* EEG dynamics are thought to reliably reflect temporal characteristics of the pre-conscious neural processing of such stimuli (Hillyard & Picton, 1987; Luck & Hillyard, 1990; Hillyard & Anllo-Vento, 1998; Luck, 1998). Hence, in conjunction with behavioural techniques, event-related EEG has become a part of a methodology that provides the fine-grained resolution essential for empirical study of temporal attention (Luck, 2005; Makeig, Debener, Onton, & Delorme, 2004; Makeig & Onton, 2009). In this thesis, we will employ a combination of behavioural and EEG data to investigate temporal attention and perception. The findings therefrom will be an important source of empirical information to constrain and inform our theoretical explorations of the temporal spotlight of attention.

### 1.1.3 Cognitive Modelling

Theoretical descriptions have a long-standing tradition in cognitive psychology, and aim to consolidate and explain the variety of observable human behaviour within broad-based explanations focused on fundamental principles. Cognitive models can be thought of as computationally explicit manifestations of theoretical hypotheses, and encapsulate our knowledge of some aspect of behaviour. In addition to explaining known patterns of behaviour, a cognitive model allows researchers to generate new predictions about as yet unknown behaviour, and thus generate unambiguous and therefore falsifiable tests of the theory underlying the model. The empirical verification of these predictions serves to validate some theories and refute competing ones, thereby advancing our understanding and completing the cycle of theory and experiment.

Cognitive models can be broadly classed into *symbolic* and *sub-symbolic*, based on the level of explanation they adhere to. Symbolic, or computationalist models view the mind as a information processing system in which mental states are symbolic representations that are operated upon by mental processes (Turing, 1937; Newell & Simon, 1976; Fodor, 1975; Pylyshyn, 1984). In this view, the functioning of cognition can be thought of as ‘symbol manipulation’, beginning with input symbols that are successively processed and transformed into output symbols. Consequently, symbolic models focus on explanations of human cognition at this level, describing it in terms of symbolic information processing. Sub-symbolic models, on the other hand, view cognition as being embodied in multi-layered, flexible neural networks in the brain (Turing, 1948; Hebb, 1949; Rosenblatt, 1958). In recent times, concomitant with the development of cognitive neuroscience, *connectionist* approaches to sub-symbolic modelling have gained popularity as a means of bridging the ‘brain-mind barrier’. They attempt to explain how symbolic mental concepts are implemented by the interactions within and between brain networks (Marr, 1982). Connectionism aims to explain the complexities of cognition and behaviour as emerging out of the parallel, distributed interactions of a large number of relatively simple and uniform units of computation (Rumelhart, McClelland, & the PDP Research Group, 1986; Chalmers, 1990; Elman, 1991). Connectionist models are typically implemented as neural networks consisting of interconnected artificial neurons, wired up in architectures inspired by our understanding of brain anatomy

and function. Effectively, by remaining faithful to the forms of computation known to be possible in the brain, such cognitive neural networks attempt to understand how mental processes are embodied in their neural substrate.

As part of the theoretical component of this thesis, we will focus on cognitive modelling that draws upon these different approaches, to embody high-level cognitive constructs in functional neural network descriptions. In doing so, we show that such modelling approaches can provide an important complement to empirical research in cognitive neuroscience. Specifically, modern neuroimaging techniques are capable of generating large quantities of data about brain dynamics, which can be difficult to interpret without a priori hypotheses. Connectionist models of cognition can fill this need, as they generate hypotheses at multiple levels of explanation. This is because, in addition to making testable predictions about behaviour, sub-symbolic descriptions also make predictions about the underlying neural dynamics that produce it. Hence, behavioural and neuroimaging research can be combined with such models to explain patterns of effect in data from these disparate sources within a common explanatory framework. In this thesis, we will mostly employ and extend the Simultaneous Type, Serial Token (ST<sup>2</sup>) model (Bowman & Wyble, 2007), a neural network model of temporal attention and working memory. We will apply a novel methodology for generating virtual activation traces from the model that are comparable to human EEG. In conjunction with generating hypotheses about behaviour, this will enable us to make predictions about the electrophysiology of temporal attention and perception.

## 1.2 Central Hypotheses

The research presented in this thesis investigates a set of inter-related hypotheses about the nature of transient attentional enhancement and its role in human visual cognition. These are described below in turn.

### **The Existence of TAE**

We propose that there exists in the human cognitive architecture a mechanism that provides a transient attentional enhancement to visual stimuli. It generates a short-lived burst of excitation, intended to benefit the representations of task-relevant stimuli and aid their

consolidation into working memory. In this sense, TAE functions like an attentional gate, which briefly opens to allow important information to be made available for conscious access. It performs this function by highlighting a short window of time and a region of space around the presentation of a task-relevant stimulus. The ST<sup>2</sup> neural network model implements the mechanism of TAE as conceptualised here. It forms the basis of the theoretical explorations of TAE described in this thesis. Chapter 5 evaluates the implementation of TAE in ST<sup>2</sup>, highlighting how its characteristics explain human behaviour in the context of temporal visual perception.

### **The Task Relevance of Stimuli and TAE**

Transient attentional enhancement is triggered by the presentation of task-relevant stimuli to the visual system. Specifically, we suggest that it is selectively activated by the detection of task relevance. This detection can happen earlier or later in the sequence of visual information processing, effectively altering the time at which TAE is triggered. In chapter 6, we will investigate the influence of target discriminability on the latency of conscious perception as measured by EEG. We then interpret our findings as an outcome of variation in the triggering latency of TAE in the ST<sup>2</sup> model.

Once activated, TAE provides a burst of excitation that is temporally and spatially specific, but is *not* feature specific. To elaborate, though TAE is triggered by the detection of task-relevant stimulus features, its benefit is not restricted to the stimulus that triggered it. Rather, it enhances the mental representations of all stimuli that happen to be active.

### **Suppression of TAE by Working Memory Encoding**

Once TAE initiates the process of consolidating a stimulus into working memory, it is actively suppressed by this very process. Hence, it is prevented from being triggered again for subsequent stimuli, until the consolidation of the first stimulus has been completed. The duration of this suppression depends on the time taken for consolidation. In turn, this time is influenced by the strengths of the mental representations generated by the stimulus. In chapter 5, we describe how the ST<sup>2</sup> model characterises this temporal relationship. Further, we comparatively evaluate it against other modelling approaches to TAE.

## **The Influence of TAE on the Temporal Precision of Perception**

We hypothesise that TAE provides visual perception with temporal precision. The unimpaired availability of TAE ensures that the amount of time taken to consolidate a stimulus into working memory is relatively stable, depending only on its strength. When TAE is impaired, the temporal acuity of perception is adversely affected. In particular, this results in increased variability and reduced accuracy in the temporal dynamics of visual perception. This role of TAE is the topic of chapter 7. Therein, we mine EEG data to uncover differences in temporal precision produced by the impairment of TAE. Further, we inform these findings in light of predictions drawing upon its dynamics in  $ST^2$ .

## **The Role of TAE in Temporal Feature Binding**

We consider transient attentional enhancement to play a pivotal role in the efficient combination of stimulus features in time. This function becomes important in scenarios where the visual system is presented with stimuli comprising multiple task-relevant features. Such features of briefly presented stimuli are likely to generate concurrently active, temporally overlapping mental representations. In this context, we suggest that TAE mediates the *binding* of the target's features into working memory. It determines the temporal dynamics of this process, in which task-relevant features benefit from its enhancement and get bound together into conscious perception. Chapters 8 and 9 describe an extension to  $ST^2$ , termed the 2f- $ST^2$  model, which simulates the temporal binding of pairs of stimulus features, and the role of TAE therein. In these chapters, we will also present results from behavioural and EEG data that test and verify the functional role of TAE in temporal feature binding.

## **1.3 Organisation**

The contents of this thesis are organised into three parts. Part I provides the required background, beginning with this introductory chapter. Chapter 2 follows on and serves as a review of the previous research relevant to the topic of temporal attention. It discusses commonly used experimental techniques employed to study the Attentional Blink (AB) phenomenon. It also describes previous research in the area of temporal feature binding, and introduces the terminology that will be referred to in later chapters.

Chapter 3 continues the literature review, and focuses on two computationally explicit models that have described the role of the temporal spotlight of attention in visual information processing: the  $ST^2$  and the LC-NE models. The  $ST^2$  model in particular, forms the basis of the theoretical component of this thesis. Also, this description is revisited in Chapter 5, which conducts a comparative assessment of these models and the mechanism of Transient Attentional Enhancement (TAE) embodied in them.

Chapter 4 concludes Part I with an introduction to virtual ERPs (Event-Related Potentials) from the  $ST^2$  model. There, we provide a rationale for the use of virtual ERPs in extending the flow of ideas between empirical and theoretical research with the aid of EEG data. In addition, we describe the methodology for generating specific virtual ERPs from the  $ST^2$  model, which are qualitatively comparable to human ERPs, both at the level of grand averages and single trial dynamics.

Part II forms the main body of this thesis, and describes a collection of explorations of the temporal spotlight of attention. It begins with a comparative evaluation of the  $ST^2$  and LC-NE models in chapter 5. Starting with a description of TAE as embodied in these two models, we conduct a detailed assessment of how both models fare in terms of explaining the main phenomena that characterise the AB. We also introduce a potential extension to the LC-NE model, borrowing concepts from  $ST^2$  to bridge the levels of explanation encompassed by the two models.

In chapter 6, we explore the question of how the discriminability of targets from distractors affects the temporal dynamics of visual perception. This issue is explored using evidence from EEG data, and complemented by neural network modelling using the  $ST^2$  model. In particular, we compare two contrasting conditions, one in which targets are discernible by their visual onset, and another in which a categorical discrimination must be made to distinguish targets. We then examine the effect of this difference on EEG activity, and investigate the observed pattern of changes using simulations from the  $ST^2$  model. In doing so, we perform a sequence of justifiable alterations to the model, which affect the way in which TAE is triggered by the occurrence of targets. By generating virtual ERPs that have differences similar to their human counterparts, we propose an explanation for how target discriminability influences the deployment of the temporal spotlight of attention.

Chapter 7 continues our exploration of the temporal spotlight, and investigates its role

in providing perception with temporal precision. Using the Attentional Blink (AB) as a modulatory mechanism and EEG as an index of neural dynamics, we show how impairing the temporal spotlight adversely affects conscious perception. We go beyond traditional ERPs to investigate single-trial dynamics using time-frequency analysis of data from an EEG experiment, and compare the temporal precision of perception outside and inside the AB window. We then interpret our findings using virtual ERPs from the  $ST^2$  model, to propose a theoretical explanation of the influence of the AB on the precision of temporal attention and perception.

Chapter 8 extends beyond the visual processing of targets with single features, and investigates the role of the temporal spotlight in feature binding. We introduce the *2f-ST<sup>2</sup>* model, an extension to  $ST^2$  that enables it to simulate the binding of features of items presented in rapid succession. Starting with a rationale for the development of the *2f-ST<sup>2</sup>* model, we describe its neural network architecture, and how it provides a sub-symbolic description of the binding of visual features in time. We then generate behavioural predictions from the model about the effect of systematic experimental manipulations, and validate them using existing and new data.

In chapter 9, the last one in Part II, we take the *2f-ST<sup>2</sup>* model further, and employ it to make a range of testable predictions about EEG responses evoked during temporal feature binding. We also present new EEG data describing the neural dynamics of temporal binding. We use this data to verify some of the main ERP predictions from the *2f-ST<sup>2</sup>* model and comparatively evaluate it against previous modelling approaches.

Part III concludes this thesis, combining its main conclusions, contributions and future directions in chapter 10. Therein, we return to the central hypotheses outlined in section 1.2 and highlight how the research described in Part II has addressed each one of them. We then discuss the main contributions of this thesis to current research. Finally, we look forward to suggest potential experimental and theoretical directions in which the research themes explored in this thesis could be advanced.

## 1.4 Collaborations and Publications

The research described in the main body of this thesis has benefited significantly from intensive collaboration with Patrick Craston (PC), Brad Wyble (BW) and Howard Bowman (HB). In addition, most of this research has been published in peer-reviewed journals and conferences.

The ST<sup>2</sup> model, which forms the basis of most of the theoretical explorations herein, was previously developed by HB and BW (Bowman & Wyble, 2007). As a part of his thesis, PC developed a general methodology for the generation of virtual ERPs from the model (Craston, 2009). For the research leading up to this thesis, I applied the virtual ERP methodology to generate virtual N2pc traces.

For the research described in chapter 5, I re-implemented the LC-NE model published by Nieuwenhuis, Gilzenrat, et al. (2005). With this re-implementation, I performed a comparative assessment of the ST<sup>2</sup> and LC-NE models, and then developed an extension to the LC-NE model. This work was conducted in collaboration with HB, with input from BW and PC. It has been published in the journal *Brain Research* (Bowman et al., 2008).

Experiment 1, the data from which is used to study the influence of target discriminability on temporal perception in chapter 6, was originally designed by PC and BW, with input from HB. It was conducted by PC and me. Consequently, PC and I performed the data analysis and computational modelling presented in chapter 6. This work has been published in the *Proceedings of the 31st Annual Conference of the Cognitive Science Society* (Chennu et al., 2009b).

Experiment 2 was designed by PC and BW with input from HB, and conducted by PC and me. I performed the data analysis and computational modelling presented in chapter 7 in collaboration with PC, with input from BW and HB. This work has been published in the journal *PLoS Computational Biology* (Chennu, Craston, Wyble, & Bowman, 2009a).

For the research described in chapters 8 and 9, I developed the 2f-ST<sup>2</sup> model and performed the computational modelling described therein. In particular, I extended the virtual ERP methodology to generate virtual N2pc and P3 traces from 2f-ST<sup>2</sup>. In addition, I designed, conducted and analysed data from Experiment 3. This work benefited from discussions with HB, BW and PC.

## Chapter 2

# Prior Research

This chapter provides an overview of the previous research relevant to the topic of temporal attention. We begin by discussing the experimental techniques conventionally employed in this regard, focusing in particular on the Attentional Blink (AB) phenomenon. We then move on to a brief introduction to human electrophysiology (EEG) and the principles involved in EEG data analysis. In the final section, we review experimental research in the area of temporal feature binding, and introduce the related terms, concepts and modelling work that we will revisit later in this thesis.

### 2.1 Temporal Attention and TAE

The study of temporal attention for the purposes of this thesis refers to the exploration of how salient visual information is selected for further processing when presented with competing information occupying the same spatial location but offset in time. In this context, a *temporal spotlight of attention* is hypothesised to selectively highlight and enhance processing of salient information, thereby increasing the chances that this information gets successfully encoded into working memory (WM).

In the real world, most visual stimuli are available long enough to generate sufficient sensory activation to ensure their successful encoding. The Rapid Serial Visual Presentation (RSVP) paradigm, on the other hand, is designed to test the limits of temporal perception by presenting the visual system with a stream of fleeting stimuli at high rates such that they generate very little sensory activation, and hence are unlikely to reach conscious perception.

The Attentional Blink (AB) is a phenomenon commonly observed in RSVP (Chun & Potter, 1995; Raymond, Shapiro, & Arnell, 1992) tasks in which two targets are embedded in the sequence of stimuli constituting an RSVP stream. It has been found that if the first target (T1) is correctly reported, performance on the second target (T2) is impaired when it appears within 200 to 500ms of the onset of the first target. In such circumstances, the key role of this temporal spotlight of attention in visual perception can be studied in detail. A transient attentional enhancement (TAE) is hypothesised to provide additional activation to a salient stimulus in an RSVP stream, significantly increasing its chances of being consciously perceived.

This notion of the temporal spotlight is supported by experimental findings, in particular by one of the trademarks of the Attentional Blink, lag 1 sparing (Potter, Chun, Banks, & Muckenhoupt, 1998). The fact that a T2 occurring immediately after T1 is reported at baseline levels suggests that it gets the benefit of the attentional enhancement triggered by T1. The role of TAE is also supported by previous research. Drawing upon their experimental data, Weichselgartner and Sperling (1987) referred to a first attentional ‘glimpse’ triggered by cued targets. Later, Nakayama and Mackeben (1989) described two forms of covert visuospatial attention: one sustained component that was slow to deploy, and the other a transient component with behavioural effects that began 50ms after a task relevant cue, but then fading within 150ms. In addition, Müller and Rabbitt (1989) reported improved performance when cues preceded a fleeting target by 100 or 175ms. They found the same pattern as Nakayama and Mackeben (1989); that is, peripheral cues first evoked a transient pattern of improved accuracy, which then fell to a baseline defined by the sustained component of attention. Recent work exploring transient attention has identified similar effects (Kristjansson, Mackeben, & Nakayama, 2001; Kristjansson & Nakayama, 2003). In general, the transient component appears to be triggered exogenously, by the occurrence of a salient stimulus (Posner et al., 1980). However, it is regulated by endogenously configured task goals (Yantis, 1998). This notion of transient attentional enhancement has been previously studied in different paradigms, and has informed the explorations reported in this thesis. The following sections describe the relevant paradigms and phenomena in greater detail, before providing an overview of the current research and methodologies in this field.

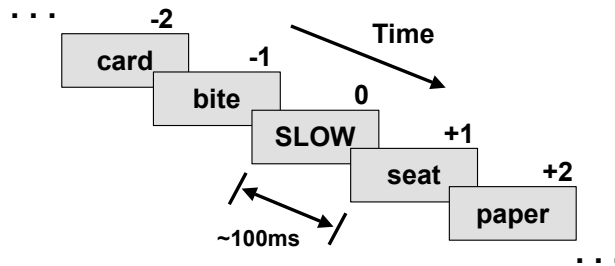


Figure 1 **RSVP stream similar to that used by Lawrence (1971)**. Participants were required to identify the only word in uppercase, embedded in a stream of lowercase distractor words.

## 2.2 Rapid Serial Visual Presentation

In the study of temporal attention and conscious perception, the Rapid Serial Visual Presentation (RSVP) paradigm has a long history (Broadbent & Broadbent, 1987; Lawrence, 1971) as a means to enforce tight temporal constraints on visual information processing. In a typical RSVP experiment, visual stimuli are presented in rapid succession at the same spatial location on a screen, with each stimulus staying on for a very short period of time, approximately 100ms. This rate of presentation is called the *Stimulus Onset Asynchrony* (SOA). Embedded in such a stream of task-irrelevant stimuli, called distractors, are task-relevant targets that have been deemed to be salient, depending on the experimental instructions. As an early example, figure 1 shows a sample sequence of stimuli similar to those used by Lawrence (1971).

At the speeds of presentation common in RSVP, the early visual system is able to form only fleeting mental representations of items before they are overwritten by following items. Further, in the early stages of the visual processing pathway, the traces of successive items overlap in time. RSVP hence makes the task of temporal selection and perception harder than in everyday circumstances, bringing down performance from ceiling levels and inducing participants to make errors in perception. Thus, RSVP allows experimenters to study the dynamics of selective attention in time, in addition to the influence of distractor processing and the nature of visual masking.

## 2.3 The Attentional Blink

### 2.3.1 The Task

As introduced previously, the Attentional Blink (AB), often referred to as ‘the blink’ in this thesis, is a phenomenon commonly observed in RSVP (Chun & Potter, 1995; Raymond et al., 1992) tasks in which two targets are embedded in the sequence of stimuli constituting an RSVP stream. It has been found that if the first target (T1) is correctly reported, performance on the second target (T2) is impaired when it appears within 200 to 500ms of the onset of the first target. This behavioural impairment is termed the Attentional Blink, and has been shown to occur with a variety of visual stimuli, including alphanumeric stimuli (Craston et al., 2009; Chun & Potter, 1995), words (Luck, Vogel, & Shapiro, 1996), faces (Fox, Russo, & Georgiou, 2005) and pictures (Trippe, Hewig, Heydel, Hecht, & Miltner, 2007). In this thesis, most of the focus will be on the ‘letters-in-digits’ task (with letter targets and digit distractors) used by Chun and Potter (1995). This variant of the AB task can be considered to be a *pure* test involving categorical discrimination between targets and distractors. Furthermore, it avoids introducing a task switch between T1 and T2, which has been argued to introduce a potential confound (Chun & Potter, 2000).

### 2.3.2 AB Phenomena

A large amount of research literature has identified a variety of phenomena that characterise the AB, discussed below in turn. Though the occurrences of these phenomena vary depending on the actual RSVP task and the stimuli therein, they serve to inform theoretical understanding of the AB effect, and constrain computational accounts of it.

#### The Basic Blink

A typical AB serial-position curve, arising from the letters-in-digits task (Chun & Potter, 1995), describes the Basic Blink condition in figure 2. As is evident, the AB is a 200-500ms (approx) interval post-T1 onset in which performance on T2, conditional on correct report of T1, (i.e.  $T2|T1$ ) is significantly reduced. Also, generally the blink has a sharper onset than offset. Finally, if T2 immediately follows T1 it is reported at baseline levels, which is described as lag 1 sparing.

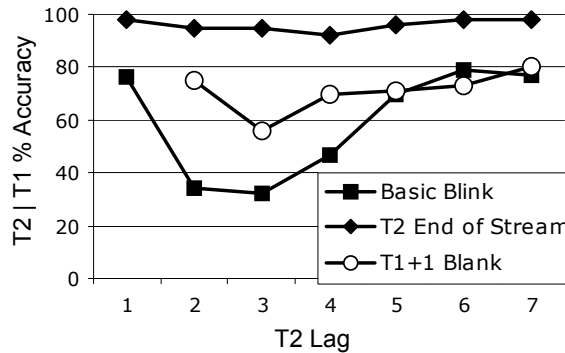


*Figure 2* **Human performance in the AB task, reported by Chun and Potter (1995).** X-axis denotes lag position of T2, while Y-axis denotes percentage accuracy of T2 report, conditional on the correct report of T1. Note that in the T1+1 Blank condition, there is no lag 1, as that slot is blank. Reproduced from Bowman and Wyble (2007).

### Increased Processing of T1+1 Slot

There is a good deal of evidence that the item (whether it be a distractor or a target) immediately after the first target in a dual target RSVP stream is particularly deeply processed. For example, in a letter detection AB paradigm (Chua, Goh, & Hon, 2001) found that a distractor immediately following a T1 primes a later T2 more than it would at other positions relative to T1. This finding suggests that the T1 opens up a short window of transient attentional enhancement, which includes the following distractor. Furthermore, lag 1 sparing suggests increased processing when the T1+1 item is a target. Indeed, T2 at lag 1 can even have better accuracy than the T1 preceding it (Craston et al., 2009). Thus, it seems clear that the occurrence of the T1 initiates a brief window of generalised enhancement. Furthermore, there is evidence that this window has a fixed minimal extent; that is, it lasts at least 120ms (Potter, Staub, & O'Connor, 2002; Wyble, Bowman, & Nieuwenstein, 2009; Bowman & Wyble, 2007; Nieuwenhuis, Gilzenrat, et al., 2005). The emphasis here is on ‘minimal extent’, as there is evidence that the window can be extended when a sequence of target items is presented, as described in section 2.3.2.

### Spatial Specificity of Lag 1 Enhancement

As previously discussed, the lag 1 attentional enhancement is generalised, in the sense that an enhancement is observed whatever the lag 1 item. However, there is evidence that the enhancement is not spatially generalised. In particular, Visser, Bischof, and Di Lollo (1999)

have shown that there is no sparing if a lag 1 T2 appears in a different spatial location to T1, suggesting that the enhancement is restricted to the location of the initiating stimulus. This finding has been generalised to a spatial cueing setting (Wyble, Bowman, & Potter, 2009).

### **T1-T2 Costs at Lag 1**

Lag 1 sparing does not come free of cost. Initial evidence for this perspective is that T1 performance is reduced at lag 1, suggesting competition between T1 and T2 at this lag (Potter et al., 2002; Craston et al., 2009). Further evidence of lag 1 costs arises from data on temporal order confusion; that is, situations in which T1 and T2 are both identified, but are ‘perceived’ in the wrong order. Data from Chun and Potter (1995) suggests that participants are only about 70% accurate at reporting the temporal order of targets. This deficit in order report disappears rapidly as the two targets are moved apart, reaching 95% by lag 3.

### **Blink Attenuation with T1+1 Blank**

The blink is attenuated if a blank is placed in the T1+1 position, but not if the blank is placed at T1+2, as can be inferred from figure 2. This suggests that when T1 is easier to perceive, T2 is also more easily perceived <sup>1</sup>.

### **Blink Attenuation with T2+1 Blank**

In the same spirit, the strength of the T2 trace also affects blink depth. Although empirical studies have not directly assessed this fact, it has been shown that the blink is absent if T2 is the last item in the stream (Giesbrecht & Di Lollo, 1998), where it is effectively unmasked, see figure 2. This finding has been confirmed by Vogel and Luck (2002). Thus, on the whole, ease of target processing modulates blink depth. However, it is possible that this apparent blink attenuation is partly also due to the ceiling effect in T2’s performance, caused by its unmasking.

---

<sup>1</sup>However, findings by Chua (2005) suggest a more complicated relationship between T1 luminance and T2 performance.

## Delayed T2 Consolidation

In typical AB studies, the blink is not total; that is, T2 performance is never zero at any lag. This raises the question of the fate of T2s seen during the blink. There are two extreme positions; that seen T2s ‘break-through’ or ‘outlive’ the blink. Here, the break-through scenario describes a T2 that is seen during the blink because it manages to override the impairment of attention. In contrast, the outliving scenario suggests that the T2 waits and hence survives the impairment of attention until T1 processing is completed. T2 manipulations that attenuate the blink (e.g. increasing the personal or emotional salience of the T2 (Anderson, 2005) are sometimes described as T2 break-through effects. On the other hand, ERP studies also suggest that T2 consolidation is delayed during the blink (Martens, Munneke, Smid, & Johnson, 2006; Vogel & Luck, 2002), arguing in favour of T2 outliving the AB. Indeed, it might be that some mixture of these two scenarios is occurring from one trial to the next in an AB experiment.

## Spreading the Sparing

There is recent evidence that the blink is not absolute, in the sense that the sparing window can be extended beyond lag 1 if a continuous stream of targets is presented (Di Lollo, Ghorashi, & Enns, 2005; Olivers, Stigchel, & Hulleman, 2005). Spreading the sparing is in fact suggested by the finding of spared performance at lag 2 in the T1+1 blank condition in figure 2.

## 2.4 The Electrophysiology of Attention and Consciousness

This section shifts focus to introduce the key ideas in human electroencephalography (EEG) relevant to this thesis. Beginning with a general description of research methods and analysis techniques, it reviews the literature on the EEG components focused on in later chapters.

### 2.4.1 Electroencephalography

The neurophysiological measurement of electrical brain activity on the scalp is known as *electroencephalography*. Richard Caton, an English physician in the late 19th century discovered that electrical currents were generated inside the brain (Swartz, 1988) in correlation

with neural activity. This finding laid the groundwork for later work by the German neurologist Hans Berger, who in 1924, found that electrical currents could also be recorded non-invasively using sensitive electrodes placed on the scalp (Berger, 1929). Since then, EEG research has made significant progress in the collection and analysis of the raw EEG time series data recorded off the scalp. In particular, researchers have discovered many EEG “correlates” of different aspects of cognitive processing. The following sections introduce the correlates that are relevant to this thesis, and the methodologies used to extract and analyse them.

### **2.4.2 Event-related Potentials**

In modern EEG experiments, participants perform cognitive tasks while their EEG is recorded continuously from multiple electrodes near their scalp. The large amount of raw EEG data thus generated is reduced in its dimensionality to extract *Event-related Potentials* (ERP) (also called Evoked Potentials), which represent the average response of the brain to a cognitive event of interest in the context of the experiment. The steps in this process are illustrated in figure 3. Raw EEG recorded at an electrode is represented as time series data, and segmented into chunks time-locked to the occurrence of externally generated cognitive events. These chunks are then averaged together to generate the ERP. The averaging process increases the signal-to-noise ratio by attenuating EEG activity that is not time-locked to the cognitive event. The resulting ERP waveform contains a number of positive and negative deflections evoked by the event, which are referred to as ERP components. A number of these ERP components have been associated with key cognitive processes occurring in the brain. Researchers correlate ERP evidence across multiple experiments to infer the nature and dynamics of neural processing occurring in response to stimuli, and they predict the consequences of experimental manipulations on this processing, as reflected by EEG data.

### **2.4.3 ERP Components**

We now focus on ERP components that are relevant to this thesis. These components will be generated and analysed using data from the experiments discussed later, and used to inform theoretical hypotheses about attention and conscious perception.

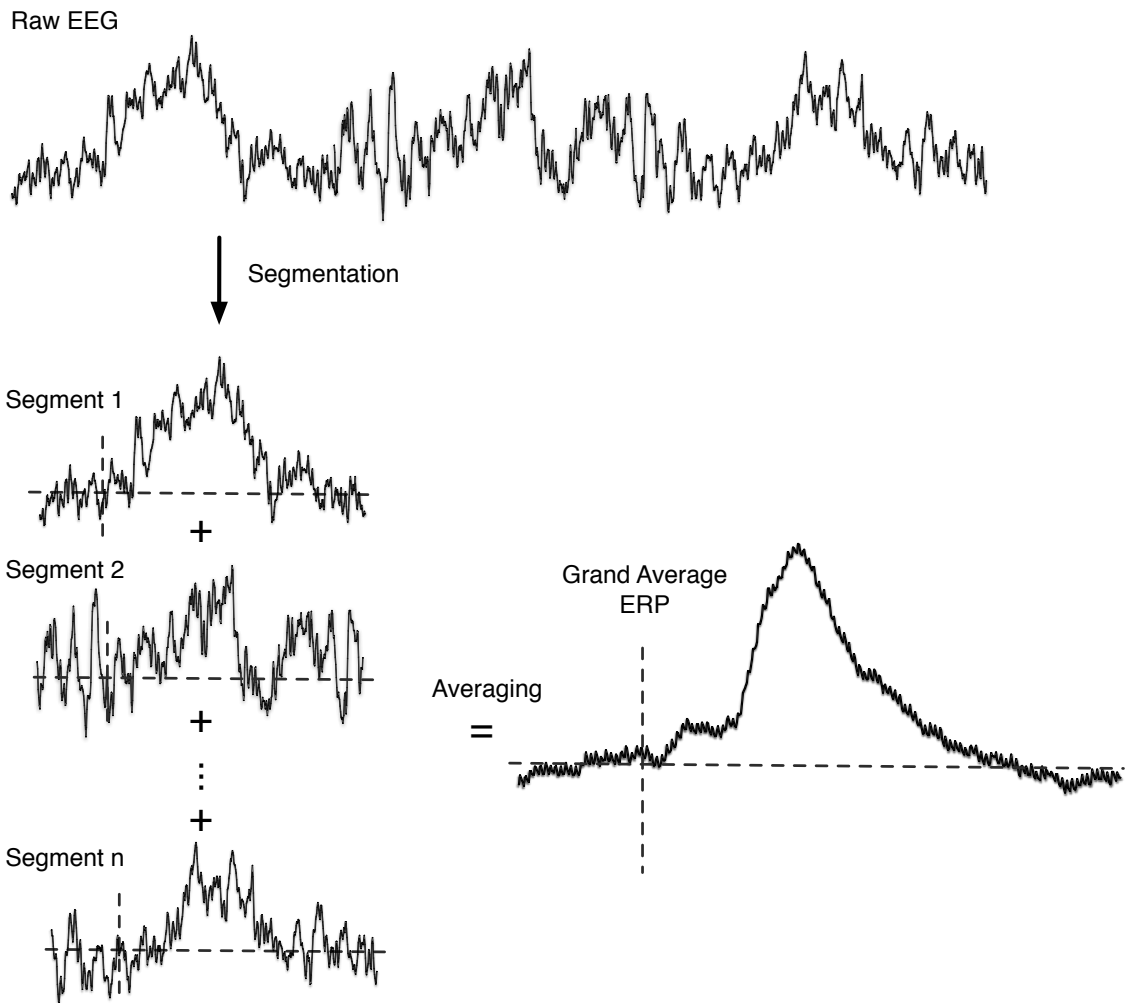


*Figure 3* **Generating ERPs from EEG.** The process of averaging segments of raw EEG to extract event-related potentials. Positive is plotted upwards.

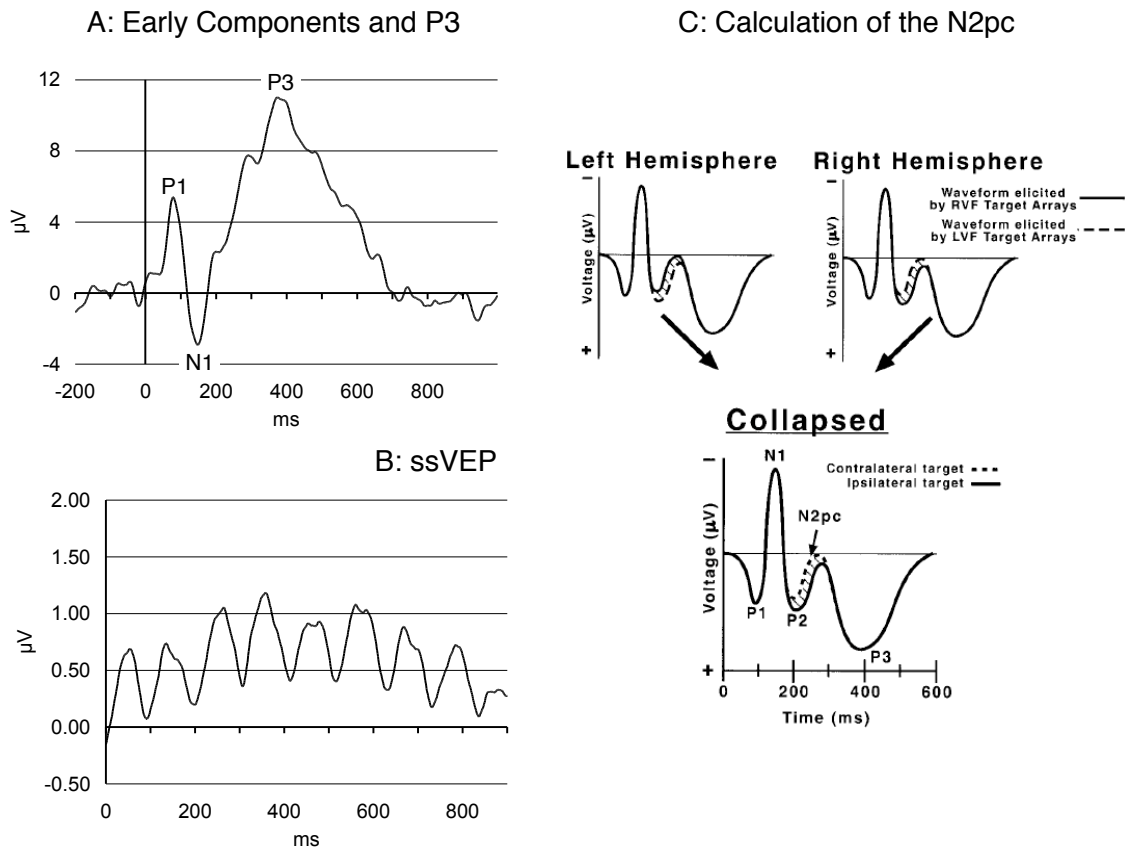


*Figure 4* **Examples of ERP components.** Panel A: A sample ERP showing the P1, N1 and P3 ERP components. Positive is plotted upwards. Panel B: A sample ssVEP wave oscillating at 10Hz. Positive is plotted upwards. Panel C: An illustration of how to extract a lateralised ERP component, such as the N2pc. Negative is plotted upwards. Reproduced from Woodman and Luck (2003).

**Early sensory processing** When individual stimuli are presented to the visual system, initial positive and negative deflections in the ERP, called the P1 and N1 (Figure 4A), are elicited. They typically occur around 100-200ms after stimulus presentation, and are commonly associated with early sensory processing (Hillyard & Anllo-Vento, 1998) in the occipital visual cortex, where these components are strongest.

On the other hand, when a sequence of items are presented in rapid sequence, like in RSVP, the steady-state Visually Evoked Potential (ssVEP) is elicited (Figure 4B). This is a wave, also strongly centred around the occipital electrodes, oscillating at the same frequency as the presentation rate of the items (Mueller & Hubner, 2002; Mueller et al., 1998; Di Russo, Teder-Sälejärvi, & Hillyard, 2003).

**Attentional selection** The N2pc ERP component has been described as a correlate of attentional selection when subjects are required to detect task-relevant targets among irrelevant distractor items (Luck & Hillyard, 1994; Eimer, 1996; Hopf et al., 2000). Importantly, previous research has shown that the N2pc reflects an endogenous attentional response selective to the presentation of task-relevant information (Kiss, Jolicoeur, Dell'Acqua, & Eimer, 2008). In contrast to early visual components, task relevance rather than psychophysical characteristics of stimuli are known to modulate it. The N2pc occurs around 150-300ms post-stimulus presentation and is a lateralised negative deflection of the ERP. In order to elicit an N2pc, participants are instructed to selectively attend to stimuli presented laterally relative to a central fixation point. This results in the attended stimulus being more extensively processed in the contralateral hemisphere of the brain. Consequently, as illustrated in figure 4C, the N2pc is usually observed at parietal and occipital electrodes, in the difference waveform calculated by subtracting the ipsilateral waveform from the contralateral waveform.

**Working memory consolidation** The distinctive P3 (or P300) is the third positive peak of the ERP, usually centred at parietal electrodes and occurring between 300 and 600ms post-stimulus presentation (Figure 4A). The P3 is one of the most widely studied ERP components elicited in a variety of experimental settings. The exact cognitive processes underlying the P3 have been subject to much debate (see Donchin & Coles, 1988 and Verleger, 1988 for details). However, for the purposes of this thesis, the P3 component is considered to be a correlate of the consolidation of targets into working memory (Donchin, 1981; Vogel, Luck, & Shapiro, 1998). This assumption is supported by a considerable body

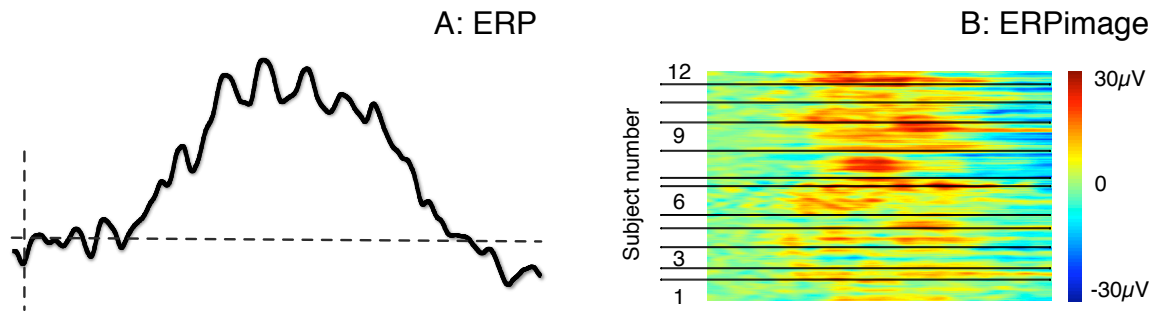


*Figure 5* **ERPs vs. ERPimages.** Panel A: ERP with time plotted on the x-axis and average amplitude variation on the y-axis. Positive is plotted upwards. Panel B: ERPimage corresponding to the ERP in Panel A. Time is plotted on the x-axis, and individual EEG trials are plotted in a stacked fashion along the y-axis. Amplitude variation is displayed using a colour scale, visual smoothing is applied across trials to reduce noise and aid interpretation.

of prior research, which has found that the occurrence of a P3 is strongly correlated with correctly reported targets. Conversely, targets that are missed do not elicit a P3 (Kranzloch, Debener, & Engel, 2003; Vogel et al., 1998).

#### 2.4.4 ERPimages

ERP analysis is a powerful tool for experimental research in cognitive psychology. However, when generating an ERP average (Figure 5A), multi-dimensional raw EEG data is reduced to a one-dimensional dataset displaying a sequence of voltage fluctuations over time. The averaging process extracts EEG activity that is consistently time-locked to the stimulus, whereas the rest of the signal is treated as irrelevant background noise. The problem with this approach (which is common to the averaging process in general) is that although it extracts the overall trends present in the data, information that is specific to individual observations - but not present in a temporally consistent fashion throughout the data - is lost. Average ERPs capture general trends in the data, but do not provide any measure of the variance of the underlying distribution of trials, a potentially important source of information about neural processing. ERPimages (Makeig, Debener, et al., 2004; Delorme & Makeig, 2004) provide one way to address this issue, by allowing researchers to visualise patterns in single-trial EEG data, make observations, and draw conclusions from patterns of inter-trial variation.

As an example, figure 5B depicts the ERPimage corresponding to the grand average ERP

in Figure 5A. It displays the raw EEG trials stacked on top of each other. Voltage values per timepoint are expressed by means of a colour scale in which blue indicates negative and red indicates positive values. The individual trials comprising the grand average are stacked vertically along the y-axis. The trials making up the ERPimage can be sorted by a number of criteria, including subject number (as in Figure 5B), amplitude, temporal latency of a cognitive event, oscillatory phase at a given frequency Makeig, Delorme, et al. (2004), etc. In order to reduce visual noise and aid interpretation, ERPimages are usually smoothed by averaging over small subsets of trials using a sliding smoothing window. ERPimages thus generated can be used to investigate inter-trial variability not visible in the grand average. Furthermore, as will be demonstrated in later chapters, they can be used to compare differences in the dynamics of neural processing across experimental conditions, at a level of detail that conventional ERP analyses cannot achieve.

## 2.5 Feature Binding in Vision

This section introduces another focus of this thesis: the role of temporal attention in visual feature binding. It introduces the key concepts and terminology that forms the basis of the research described in later chapters, and reviews previous literature in this context.

The ventral visual processing pathway in the human brain progressively integrates the large quantities of information received from the eyes. A conceptual view of this processing hierarchy is depicted in figure 6A, and figure 6B highlights the location of these constituent processing layers within the brain. The earliest layer, V1 represents basic constituent features of objects in the visual field, like orientation, colour, etc. in specialised neuronal maps. Successive layers progressively integrate information from previous ones, representing increasingly complex information about the visual input.

But in addition to this bottom-up processing hierarchy, top-down, goal-driven attention plays a key role in the process of feature binding in vision: the process by which featural information represented in the hierarchy is selectively enhanced and integrated, or ‘bound’ together to create coherent representations in working memory (Treisman & Gelade, 1980; Wolford, 1975; Prinzmetal, 1981). In this context, how the brain solves the *binding*

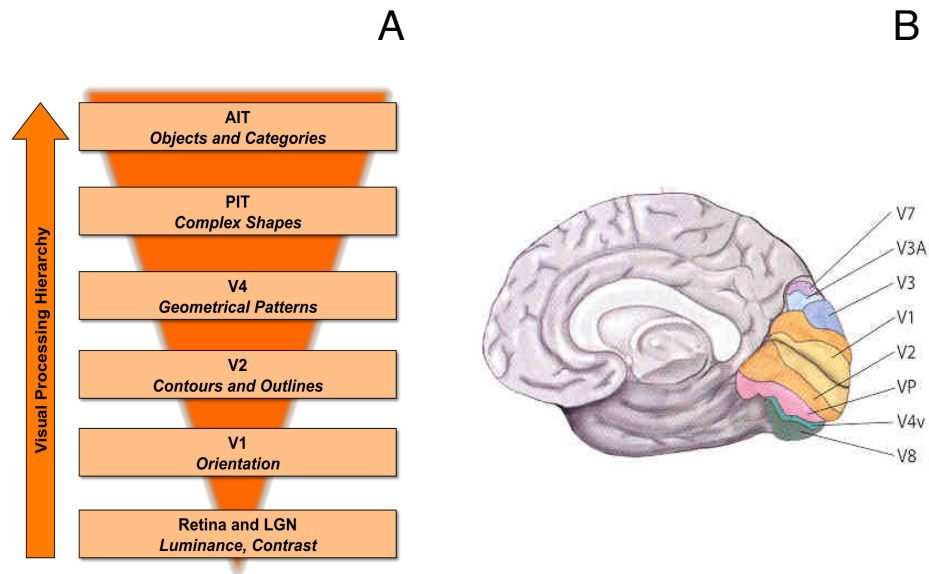


*Figure 6* **Visual information processing in the brain.** Panel A: The ventral visual processing hierarchy. Successive layers integrate progressively more complex information. Panel B: The early layers of the ventral visual processing hierarchy highlighted in a sagittal view of the brain.

*problem* refers to the cognitive and neural mechanisms by which feature binding is accomplished (Treisman, 1996; Wolfe & Cave, 1999). The essence of the hypothesised binding problem is depicted in figure 7A: when presented with a red square and a blue triangle, how does the visual system correctly associate “redness” with “squareness”, and “blueness” with “triangleness”, instead of the other way around? The assumption that feature binding is indeed a problem (which the brain normally solves quite efficiently) derives from multiple arguments (Wolfe & Cave, 1999). Firstly, referring back to figure 6, our knowledge of neuroanatomy suggests that basic features like colour and shape are represented in different regions of the primary visual cortex (V1), and must be combined at a later stage of processing. Secondly, visual search experiments have shown that searching for feature conjunctions is much harder than searching for single features. For example, in figure 7B, finding a oddly-oriented bar in the search display on the left is relatively easy and almost instantaneous, as the target item has a unique discriminating characteristic, namely orientation. In comparison, finding a red vertical bar in the display on the right is much more difficult and effortful, as the discriminating characteristic of the target item is a combination

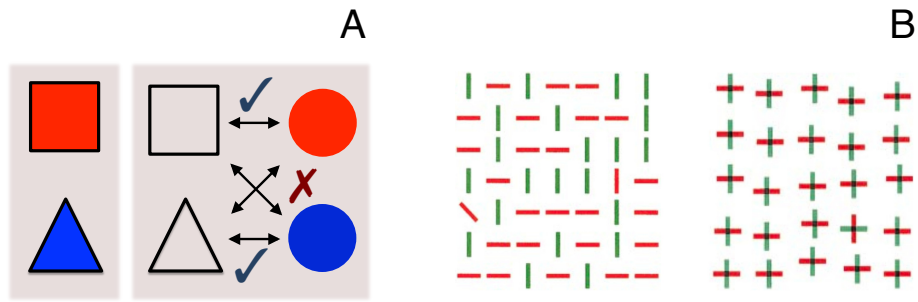


*Figure 7* **The binding problem.** Panel A: The essence of the binding problem. The brain must correctly combine “squareness” and “triangleness” with “redness” and “blueness”, respectively. Panel B: A demonstration of the fact that binding is indeed a problem. Finding a oddly-oriented bar in the display on the left is easy, because of the unique target-discriminating characteristic (orientation). Finding a red vertical bar in the display on the right is difficult, because the discriminating characteristic is a combination of two basic features (orientation and colour). Adapted from Wolfe and Bennett (1997).

of two basic features, namely orientation and colour. The factors that influence this apparent difference in the difficulty and efficiency of visual search have been extensively explored and debated (see Wolfe, 1998 for a review. Also see Duncan & Humphreys, 1989; Treisman, 1991; Duncan & Humphreys, 1992). In a similar vein, researchers have found that under experimental conditions that impede the focusing of attention on specific objects, participants can be induced to produce errors in binding, generally referred to as *conjunction errors*. Under such circumstances, they often consciously perceive *illusory conjunctions* of visual features, which are defined as ‘miscombination of features actually presented in a single display’ (Treisman & Gelade, 1980).

Since the pioneering work by Treisman and Wolford, the various aspects of feature binding in space have been extensively explored in numerous experiments over the past two decades (Ivry & Prinzmetal, 1991; Cohen & Ivry, 1989; Treisman & Schmidt, 1982) (see Prinzmetal (1995) for a review). On the empirical front, the nature and verity of illusory conjunctions in this context has been debated (Donk, 1999; Prinzmetal, Diedrichsen, & Ivry, 2001; Donk, 2001). On the theoretical front, various models have been proposed to explain the cognitive mechanisms that subservise spatial feature binding (Ashby, Prinzmetal, Ivry, & Maddox, 1996; Wolfe, 1994; Treisman & Gormican, 1988; Treisman & Gelade, 1980). But in comparison, much less research has been devoted to feature binding and the formation of illusory conjunctions *in time*. In an attempt to address this gap in knowledge, later chapters

of this thesis focus on the experimental and theoretical study of temporal feature binding. The following sections now lay the foundation for the research described in those chapters.

### 2.5.1 Feature Binding in the Temporal Dimension

Temporal feature binding refers to combination of features of objects presented one after the other, in the same spatial location. In this context, illusory conjunctions are made up of features that were not presented simultaneously, but in sequence. Experiments involving feature binding in time usually employ the RSVP paradigm, where a stream of stimuli is presented in rapid succession, whose features evoke short-lived activation in the early visual system. The earliest report of the occurrence of temporal illusory conjunctions came from experiments conducted by Lawrence (1971). Figure 1 depicts the kind of RSVP streams used therein. When asked to identify the only uppercase word in a rapidly presented stream of lowercase words, participants often made mistakes, and reported words occurring in temporal positions around the correct target position. Under such demanding experimental conditions, successive stimuli overwrite the activation generated by items presented before, leading to the possibility of the formation of illusory conjunctions. This highlights an important distinction between feature binding in space and time: features of items simultaneously presented in different spatial locations are thought to have some amount of location information associated with them (Wolfe & Cave, 1999). However, features of items presented in rapid succession at the same spatial location lack such distinction. Hence, in this context, the visual system has the task of solving the binding problem in time: it must pick out the features of targets in the RSVP stream, amongst multiple, temporally overlapping features of distractors.

Before going further, we now list some relevant terms and definitions, previously used by Botella et al. (2001). These are applicable across experiments involving temporal binding, and are useful in the theoretical elucidation of the data generated therefrom.

RSVP streams like that depicted in figure 1 contain sequences of items, consisting of targets embedded within distractors. Each such item is set up to have featural properties that vary along orthogonal and independent feature dimensions. In this context, it is important to note that the term *feature*, as used here and later in this thesis, is defined in a relatively general sense. In this context, it refers to any task-relevant categorical property

of a stimulus. Hence, psychophysical characteristics like colour, orientation, etc., as well as more high-level characteristics, like semantic identity, case and frequency of alphanumeric symbols and words are considered to be ‘features’. This definition subsumes and extends beyond the traditional definition of features as basic visual properties of stimuli that are processed in the primary visual cortex.

In a typical temporal feature binding experiment, each item in the RSVP stream has a constituent pair of features relevant to the task, which we refer to as the *key* and *response* feature of the item.

Amongst these, the features relevant in the context of temporal feature binding in RSVP are the following:

**Key feature** is the task-defining feature that is present *only* in a target item. Typically, this is the feature that participants are asked to look for.

**Response feature** is the feature of the target item that is asked to be identified and reported. Importantly, every item in the RSVP stream will have a reportable response feature.

Referring to the example of the Lawrence (1971) experiment, the key feature would be “uppercaseness”, and the response feature would be word identity. In this context, participants can produce one of three possible responses:

**Correct reports** are responses where the response feature reported matches that of the target item(s).

**Feature errors** occur when participants report a response feature that was not presented in temporal proximity to the target item, or one that was not presented at all.

**Conjunction errors** occur when participants report a response feature from an item presented in close temporal proximity to the target, either before or after it.

Conjunction errors as described above can be further classified into one of the following types.

**Pre-target Errors** also called a *pre-target intrusion*, occur when the response feature reported is from an item presented *before* the target in the RSVP stream.

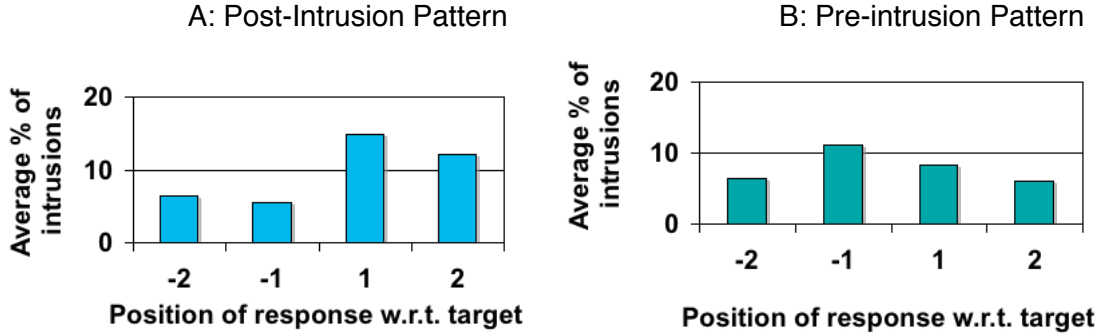


*Figure 8* **Sample response distributions from temporal binding experiments reported in Botella et al. (1992).** Panel A: A post-intrusion pattern with API 0.53. The key feature is “uppercaseness” and the response feature is word colour. Panel B: A pre-intrusion pattern with API -0.11. The key feature is “uppercaseness” and the response feature is word identity.

**Post-target Errors** also called a *post-target intrusion*, occur when the response feature reported is from an item presented *after* the target in the RSVP stream.

Over a large number of trials in a typical experiment, participants produce a distribution of responses, which can be plotted as a histogram of positional frequencies. These histograms, also called *intrusion patterns*, plot the frequency of responses from each position around and including the target item. Sample response distributions from results reported in Botella et al. (1992) are shown in figure 8. The x-axis in these histograms denotes the position of the intrusion relative to the target’s position, and the y-axis the number of responses from that position. Specifically, the bar at -1 (-2) indicates the number of pre-target errors where the response feature reported occurred one position (two positions) before the target’s position. The interpretation of +1 and +2 errors is similar. For each such response distribution, we can calculate a real scalar value called the *Average Position of Intrusions* (API). The API represents the ‘centre of mass’ of the response distribution, and is very useful in characterising it. It is calculated as

$$API = \sum_{i=-n, i \neq 0}^{i=+n} i * \frac{n_i}{\sum_{i=-n, i \neq 0}^{i=+n} n_i} , \quad (1)$$

where  $[-n, +n]$  is the range of response positions around the target (i.e., response positions  $n$  items away from the target position) classified as conjunction errors, and  $n_i$  is the

absolute frequency of responses from position  $i$ . As an example, the API values of the histograms in figure 8 are 0.53 and -0.11, respectively. By comparing API values across related experimental conditions generated by a manipulation, we can quantitatively measure the pre- or post-target *shift* between the distributions resulting from that manipulation.

Given an API for a distribution, we can classify the distribution as one of the following types:

**Post-intrusion pattern** is a response distribution with an  $\text{API} > 0$  (figure 8A).

**Symmetric pattern** is a response distribution with an  $\text{API} = 0$ .

**Pre-intrusion pattern** is a response distribution with an  $\text{API} < 0$  (figure 8B).

Based on this distinction, the response distribution in figure 8A can be classified as a post-intrusion pattern, while that in figure 8B as a pre-intrusion pattern.

With this terminological framework, a large body of behavioural research on temporal binding can be comparatively analysed. Since the early work by Lawrence, many experiments have shown that conjunction errors in time can also be produced using a variety of visual features, including colour, shape and semantic category (Botella & Eriksen, 1992; Botella et al., 1992; Botella, 1992; Botella & Eriksen, 1991; Kikuchi, 1996; Keele, Cohen, Ivry, Liotti, & Yee, 1988; Gathercole & Broadbent, 1984; McLean, Broadbent, & Broadbent, 1983; Broadbent, 1977a). The API values of the response distributions produced in these experiments vary across the spectrum from pre to post. Further, manipulations involving either the key or response feature have produced systematic and predictable shifts in the response distributions (Botella et al., 2001).

### **The Influence of the Attentional Blink on Temporal Binding**

The AB, as introduced in section 2.3, describes the reduction in the ability to perceive a second target (T2) in RSVP, if it is presented 100-500ms after a correctly reported first target (T1). Experiments that have combined the AB with temporal feature binding have found that the response distribution for the T2 is modulated during the AB time window (Vul et al., 2008; Popple & Levi, 2007; Chun, 1997a). Chun (1997a) employed an RSVP paradigm where the key feature was colour and the response feature was letter identity, and found that

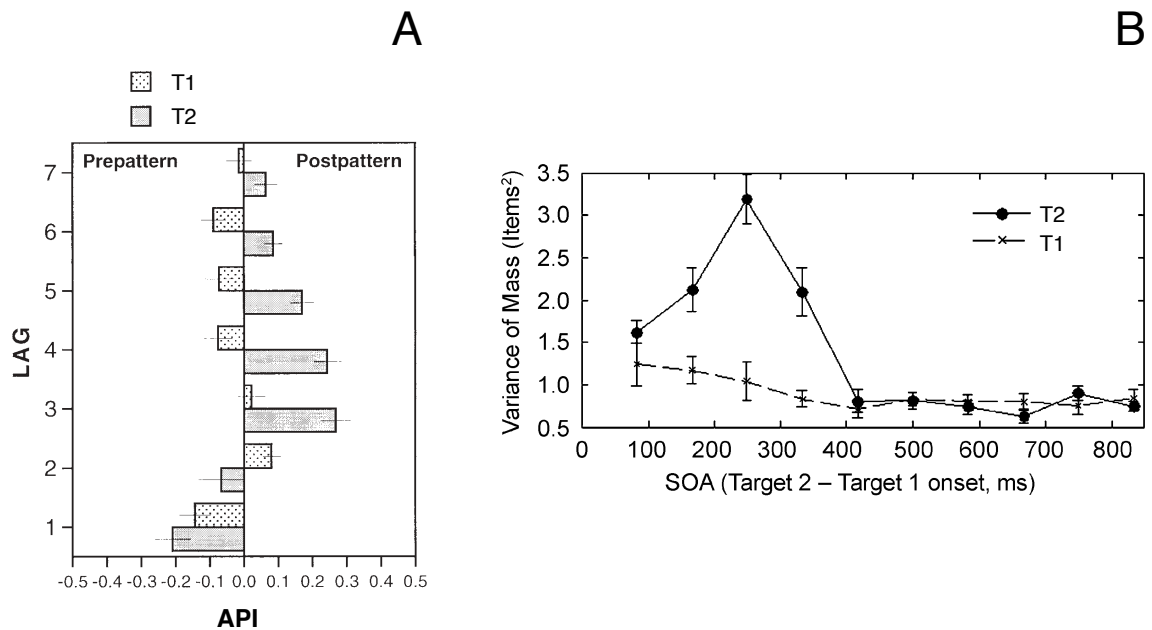


*Figure 9* **Influence of the AB on temporal feature binding.** Panel A: Post-pattern shift in the API of T2’s response distribution during the AB window. Reproduced from Chun (1997a). Panel B: Increased variance in T2’s response distribution during the AB window. Reproduced from Vul et al. (2008).

the response distribution for the T2 had a later API as compared to that for the T1. This is demonstrated in figure 9A. During the window of the AB deficit (from lags 3 to 6), there is a significant post-pattern shift in the API of responses for the T2. However, the post-target shift is absent when a single target (T1) is presented by itself. In another AB experiment, Vul et al. (2008) employ annular rings for the key feature and letter identity for the response. They too find a post-pattern shift in the response distribution for the T2 when presented within the AB window. During this window, they also find a concomitant increase in the variance of T2’s response distribution. As can be seen in figure 9B, participants in Vul et al. (2008) are more likely to select a response feature for the T2 from the distractors surrounding it, when T2 is presented at lags where the AB effect is maximally influential. Further, there are differences in the time-course of these observed effects on temporal binding, potentially deriving from differences in experimental settings like SOA, response settings, etc.

In summary, behavioural research into temporal feature binding has uncovered patterns of data that constrain and inform our theoretical understanding of the underlying mechanisms, and have led to the development of the cognitive modelling work focused on in the

next section.

### **2.5.2 Modelling Temporal Feature Binding**

Since the discovery of the existence of temporal illusory conjunctions in the 70s, many attempts have been made to explain the observed patterns of data. Early theories were proposed by Lawrence (1971), Broadbent (1977b), McLean et al. (1983) and Gathercole and Broadbent (1984). These proposals were based on two-stage serialised mechanisms of perception, where the occurrence of the key feature in the first stage triggered its further processing of response features in a second stage. This theoretical construct was able to explain, to some extent, the occurrence of post-target errors due to occasional processing delays in the first stage. But later findings of large numbers of pre-target errors (Kikuchi, 1996; Botella & Eriksen, 1992; Kanwisher, 1991) are difficult to explain in a serial model. This is because it posited that response features of items in the stream are not analysed till the occurrence of the key feature, precluding the possibility of pre-target errors. In addition, related research found that features processed in parallel can independently drive response selection and decision making (Fournier, Eriksen, & Bowd, 1998; Fournier & Eriksen, 1991). Considered together, these findings provided compelling evidence against serial models of temporal binding.

Consequently, later theoretical explorations of temporal binding have favoured parallel processing of multiple features in early stages of visual processing (Chun & Potter, 1995; Keele & Neill, 1978; Kanwisher, 1991). In these models, collections of features or types are extracted in parallel in an early pre-attentive stage of visual processing. Of these types, those that are deemed relevant for the task being performed are selectively enhanced by top-down attention. Transient attentional enhancement, the exploration of which forms the main focus of this thesis, facilitates response selection and/or the combination of the extracted features into working memory. Further, these theories have proposed that under difficult experimental settings like in RSVP, the fleeting nature of the representations in the early stages leads to confusion in the binding process, resulting in the observed errors in behaviour and the formation of illusory conjunctions.

### The Botella et al. (2001) Model

We now focus our attention on a recent cognitive model of temporal feature binding, proposed by Botella et al. (2001). This two-stage model is an abstract, descriptive one with a formalised mathematical implementation. It draws upon previous models of temporal perception (Chun, 1997b; Chun & Potter, 1995; Shapiro & Raymond, 1994; Kanwisher, 1991; Reeves & Sperling, 1986; Keele & Neill, 1978), and attempts to capture theoretical understanding of temporal visual processing in a high-level yet concrete description. Furthermore, it embodies assumptions about the cognitive architecture and information flow underlying temporal perception. The authors use the model to make behavioural predictions about variations in the response distributions arising from manipulations in temporal binding experiments. Before listing its key predictions, we first briefly summarise the architecture of the model.

As illustrated in figure 10, the model has multiple elements, each of which represents an aspect of processing evoked by items in an RSVP stream. Each element is implemented by a module, the processing within which is computing using formal, parametric equations. The following are the 4 main elements of the model:

**Parallel Module K** labelled (1) in figure 10, continually processes the key feature dimension of items in the RSVP stream, as and when they are presented to the system. It is capable of processing multiple items at the same time. Importantly, for a given experimental setting, it is configured to recognise the occurrence of the target-defining key feature when it comes along. When this occurs at a critical time denoted by  $t_c$ , it triggers the Attentional Focusing module after a certain amount of processing delay dependant on the task setting.

**Parallel Module R** labelled (2) in figure 10, processes the response feature dimension of items, in a manner similar to Module K. Importantly, it starts processing successive response features in the stream before the target-defining key feature has been detected by Module K. Thus, at any given time during the presentation of an RSVP stream, there are likely to be multiple response features being concurrently processed by Module R. Thus, Module K and Module R operate in parallel, with the amount of cognitive resources being made available to each of them being variable across, but constant within, experimental settings.

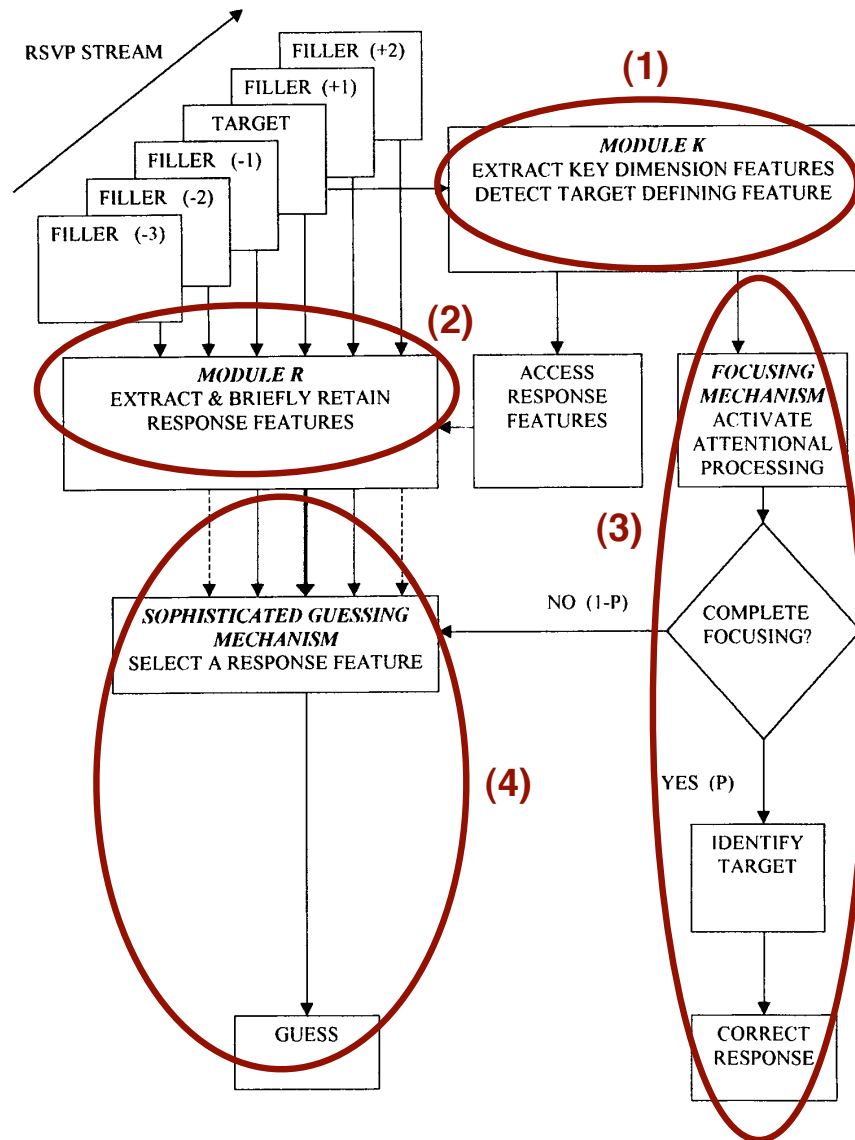


Figure 10 The Botella et al. (2001) model. (1) Module K processes key features in parallel. (2) Module R processes response features in parallel. (3) The deterministic attentional focusing pathway. (4) The probabilistic sophisticated guessing pathway. Reproduced from Botella et al. (2001).

**Binding Route 1: attentional focusing** labelled (3) in figure 10, is triggered after the target is detected by Module K. In everyday circumstances, where stimuli are usually available for around a second or more, this module is triggered when the target is still present in the visual field. But in RSVP, the very short presentation times imply that, contingent on the processing times in Module K, the target might already have been replaced by successive items by the time the Attentional Focusing module is triggered. Thus, depending on the timing of cognitive events, the attentional focusing is successful with a probability of  $p$ , in which case it manages to select from Module R the correct response feature belonging to the target. In RSVP trials in which this happens, feature binding is error-free, this first, deterministic *binding route* is taken and the target is correctly bound and reported.

**Binding Route 2: sophisticated guessing** labelled (4) in figure 10, is the alternative binding route adopted when the Attentional Focusing module fails to get triggered in time to unambiguously identify the target’s response feature. When this happens (with a probability of  $1 - p$ ), the sophisticated guessing mechanism selects one of many response features co-active at time  $t_c$ . These are most likely to be response features of items presented both before and after the target, including that of the target itself. The choice is made probabilistically, with the probability that a particular response feature is chosen being proportional to its level of activation at time  $t_c$ . Thus, over a large number of RSVP trials comprising targets and neighbouring items of varying feature strengths, the outcome of this choice process will be a distribution of probabilities of response feature selection centred around the target position, and including both pre- and post-target errors.

Based on this architecture, the authors of the Botella et al. (2001) model make testable behavioural predictions. It is important to note that the model does not predict any specific response distribution for a given combination of key and response features. Instead, it only predicts changes in the number of correct reports and shifts in the API of response distributions across isolated manipulations of the main elements of the model. These predictions are now summarised below.

**Manipulation of processing time in Module K** In a pair of experimental conditions  $A$  and  $B$ , differing *only* in the processing delay associated with the key feature of items in

Module K (with  $B$  having a greater delay than  $A$ ), the model predicts the following two effects:

1. *The number of correct reports will decrease.* This is because the probability  $p$  with which attentional focusing succeeds (and the first binding route is taken) in condition  $B$  will decrease. This, in turn, happens because the SOA remains the same, but the critical time  $t_c$  at which focusing begins, is delayed. Consequently, it is less likely that the target is still present when attentional focusing finishes and response selection begins.

2. *There will be a post-target shift in the responses.* In other words, the API of the response distribution for condition  $B$  will become more positive. This is because the mean time at which response selection happens is increased, and consequently, response features of items presented after the target are more likely to be selected by the sophisticated guessing mechanism.

**Manipulation of processing time in Module R** In this scenario, the processing delay in Module R is manipulated across a pair of conditions  $A$  and  $B$ , with  $B$  having increased delay compared to  $A$ . In this case, the Botella et al. (2001) model predicts the following:

1. *The number of correct reports will **not** decrease.* The model predicts this because neither the SOA nor the mean processing time in Module K has changed. Consequently, the probability  $p$  of choosing one of the two binding routes remains the same.

2. *There will be a pre-target shift in the responses.* For condition  $B$ , there will be a relative increase in the number of pre-target errors. In other words, the API of the response distribution for this condition will be more negative. This is because, amongst the trials that take the sophisticated guessing route, there will be a greater probability that response features of items presented before the target are still being processed at the time the sophisticated guessing mechanism makes a probabilistic choice.

**Manipulation of probability of successful focusing** In this manipulation, the probability  $p$  of successful focusing in the Attentional Focusing module is reduced across a pair of conditions  $A$  and  $B$ , with  $B$  having a lower value for  $p$  than  $A$ . Relating to this manipulation, the Botella et al. (2001) model has the following predictions:

1. *The number of correct reports will decrease.* This prediction follows directly from the

reduction of  $p$ , as it implies that the number of correct reports via the successful focusing route will decrease.

2. *There will be no shift in the response distribution.* This is because the average time elapsed from target onset till critical time  $t_c$  remains the same across the experimental manipulation. Thus, though the total number of conjunction errors will increase, there will be no pre- or post-target shift in the relative probabilities with which response features are selected. In other words, the model predicts no change in the API of the response distribution.

Of the above predictions, those relating to manipulations of processing times in Modules K and R agree with results from previous temporal binding experiments that separately vary delays in key feature processing (Chun, 1997a; Botella, 1992) and response feature processing (Boucart, Moroni, Fuentes, & Belin, 1998; Kikuchi, 1996). In addition, the authors of Botella et al. (2001) themselves present results from their own experiments (Experiments 1A and 1B for key feature manipulation and Experiment 2 for response feature manipulation), which are also in keeping with these predictions. However, they do not present any results or suggest any experimental techniques that could be used as a test of their predictions relating to the manipulation of the probability of successful focusing.

**Discussion** On the whole, the Botella et al. (2001) model is one of the first concrete, comprehensive attempts at a mechanistic explanation of temporal feature binding. It brings together ideas from many existing theories, and is able to replicate data from and predict variations in response distributions in a large number of behavioural experiments. Nevertheless, it is a “box-and-arrow” model of architecture and dynamics. This limits its descriptive ability, in particular to explain causation by linking cognitive mechanisms to underlying functional neural dynamics.

An important theoretical issue with the Botella et al. (2001) model that we will return to in later chapters of this thesis relates to the existence of two distinct mechanisms for temporal feature binding, implemented by the attentional focusing and the sophisticated guessing routes. Note that these two binding routes are additional to the two parallel pathways posited for processing key and response features, in Module K and Module R, respectively. According to Botella et al. (2001), the adoption of this dual-route approach is necessitated

by a combination of factors. They cite theoretical considerations (Treisman & Gelade, 1980; Treisman & Schmidt, 1982; Prinzmetal, Henderson, & Ivry, 1995; Ashby et al., 1996) which lead them to suggest that the probability of successful attentional focusing depends on exposure time of the target (i.e., SOA). When successful, attentional focusing is thought to lead to a qualitatively and quantitatively distinct outcome, necessitating the existence of a binding route different from that which produces conjunction errors. In addition, they point to complexities in previous behavioural evidence in Botella and Eriksen (1992) and Botella (1992) to argue for a dual-route approach. In particular, reaction time data from Botella (1992) suggests that most correct reports are processed earlier than conjunction errors. To explain this pattern of data, the Botella et al. (2001) model proposes that most correct reports are processed by the deterministic attentional focusing route, which is faster and more efficient than the probabilistic sophisticated guessing route. Conjunction errors, on the other hand, are produced exclusively by the latter binding route, and therefore are slower than correct reports. However, the model leaves unexplained the mechanistic basis for the probabilistic choice of binding route. In other words, in a given trial, it seems to ‘know’ which of the two routes to follow, depending on the SOA and the time taken for processing the target’s key feature. In addition, the model does not specify how the attention focusing route manages to select the correct response feature to bind to the target’s key feature. This is because, as can be seen in figure 10, the attentional focusing route does not receive any input from Module R, which is responsible for the processing of all response features.

On the experimental front, the authors do not suggest an empirical test that could be used to manipulate the probability with which one of these binding routes is chosen during temporal feature binding. Further, they leave open the issue of if and how the two routes might be realised neurally, in particular as to whether they might be more parsimoniously implemented at the level of neural dynamics. Finally, at its current level of abstraction, the model is limited to predictions about behavioural data. Later chapters of this thesis describe the 2f-ST<sup>2</sup> model (an extension to the ST<sup>2</sup> model introduced in the next chapter), which improves upon the Botella et al. (2001) model. The 2f-ST<sup>2</sup> model simulates temporal feature binding using only a single processing route in a neural network architecture. As discussed therein, we show that this single binding route postulated by 2f-ST<sup>2</sup> can more parsimoniously explain data relating to the generation of correct reports and conjunction

errors.

## **2.6 Conclusions**

In this chapter, we have provided a broad overview of the important research techniques, concepts and methodologies relevant to the experimental and theoretical study of temporal attention. The literature discussed here will form the starting point for much of the empirical research described in this thesis. The next chapter continues the review of previous work in the field of temporal attention, but focuses specifically on previous models of temporal attention that have informed and guided the theoretical component of this thesis.

## Chapter 3

# Models of the Temporal Spotlight

This chapter focuses on two computationally explicit models that describe the role of the temporal spotlight of attention in visual information processing. We begin with a description of the  $ST^2$  model of temporal attention and working memory, and move on to the neurocomputational LC-NE model. Both these models attempt to provide a theoretical interpretation of the phenomena associated with the Attentional Blink (AB), and form the basis of the research described in this thesis. In later chapters, we will investigate extensions and explorations involving these models, with the aim of expanding our understanding of temporal attention and its role in conscious perception.

### 3.1 The $ST^2$ Model

The Simultaneous Type, Serial Token ( $ST^2$ ) model of temporal attention, described in detail in Bowman and Wyble (2007), is an abstract neural model of episodic attentional processing. The model incorporates constituent processes of these episodes, which segment and make sense of the continuously evolving visual world along the temporal dimension. These include early visual processing, item identification, attentional selection and encoding into working memory.  $ST^2$  theory as described in Bowman and Wyble (2007) is targeted at modelling the letters-in-digits RSVP task (Chun & Potter, 1995). The model particularly encapsulates the *episodic distinctiveness* hypothesis, suggesting that the AB reflects a system attempting to allocate unique episodic contexts to the target stimuli. The overall architecture of the  $ST^2$  model, or strictly speaking, its neural implementation Neural- $ST^2$ , is shown in figure 11.

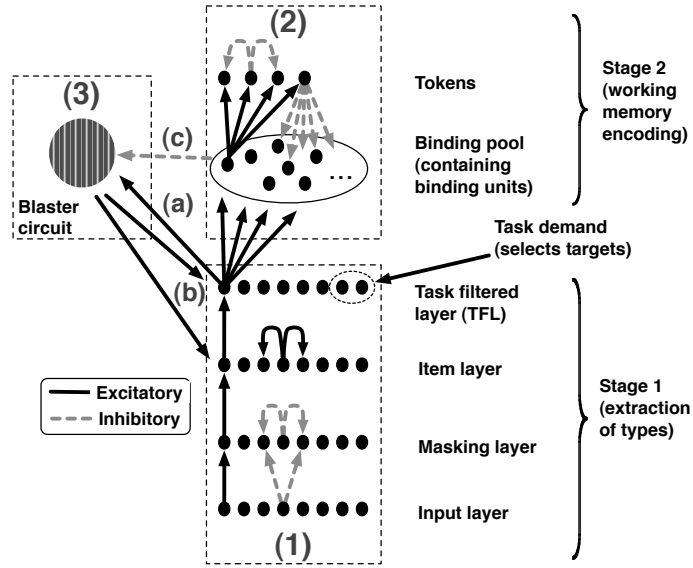


Figure 11 **The Neural-ST<sup>2</sup> model.** The model consists of a parallel Stage 1 and a serial Stage 2. The propagation of activation across these stages is mediated by transient attentional enhancement provided by the blaster. For visual clarity, connections between layers are depicted only for some nodes, but apply to all of them. Reproduced from Craston et al. (2009).

We now discuss an essential distinction underlying ST<sup>2</sup> theory, followed by a description of the model’s components.

### 3.1.1 Types and Tokens

The types-tokens distinction has been considered in the context of a number of temporal attention tasks (Chun, 1997b; Kanwisher, 1987, 1991). The term *type* is used to describe all featural properties associated with an item. This includes both sensory and semantic features. For example, the type representation of the letter K would contain, 1) its semantic features, i.e., that it is in the category of letters and that it follows L in the alphabet, and 2) its visual features, i.e., its shape, constituent line segments, colour, etc.

In contrast, a *token* represents instance specific (or episodic) information about the occurrence of an item. Thus, a token indicates that a particular type has occurred and also, when, relative in time to other items, it occurred. In the ST<sup>2</sup> model, Working Memory (WM) encoding is the process of associating (or binding) a token to a currently active type; we also use the term *tokenisation* to describe this process. In this sense, once bound, tokens act as ‘pointers’, from which the corresponding type can be regenerated when required,

e.g. at retrieval. A token-like mechanism in the brain is likely to be localised in the frontal areas associated with WM (E. K. Miller, Erickson, & Desimone, 1996; Desimone, 1996; Passingham & Sakai, 2004), where neurons have been found to maintain sustained activity following the perception of targets (Marois, Yi, & Chun, 2004; Kranczioch, Debener, Schwarzbach, Goebel, & Engel, 2005).

### 3.1.2 Stage 1 of Neural-ST<sup>2</sup>

Stage 1 of the ST<sup>2</sup> model simulates the functional aspects of cascaded, parallel processing in the ventral visual processing pathway (Rousselet, Thorpe, & Fabre-Thorpe, 2004). Activation fed into the ST<sup>2</sup> model at the *Input* layer propagates through a sequence of layers that abstractly represent the functional steps of visual processing. The *Masking* layer represents inhibitory interactions that generate forward and backward masking effects (Seiffert & Di Lollo, 1997). The transience of item representations arises from these interactions and determines bottom-up trace strength. Thus, activation traces are greatly weaker for stimuli that are followed by another stimulus, as opposed to stimuli followed by a blank (Bowman & Wyble, 2007). Such traces are differentiated by describing them as either strong (followed by a blank) or weak (followed by a stimulus). The simulation of masking in ST<sup>2</sup> is consistent with findings from neurophysiology (Keysers & Perrett, 2002; Rolls, Tovée, & Panzeri, 1999; Kovács, Vogels, & Orban, 1995). Single cell recordings in this context have found clear reductions in the firing rates of neurons in the temporal cortex as a result of masking.

Activation from early visual processing layers in the model feeds into layers that abstractly represent type-oriented processing. The *Item* layer supports temporally sustained but decaying representations of items in the RSVP stream. At this layer, targets and distractors are treated identically. Also, semantic and conceptual features of these items are extracted (Potter, 1993), and priming effects are implemented. The ‘output’ of Stage 1 is the *Task Filtered Layer* (TFL). Each node in the TFL represents the type of an item in the RSVP stream. Such type nodes correspond to neurons at the late stages of ventral visual processing in the IT cortex (E. K. Miller et al., 1996). At the TFL, a *Task Demand* mechanism selectively emphasises processing in nodes corresponding to targets. fMRI studies have found that the ventrolateral prefrontal cortex (VLPFC) performs a similar role within the fronto-parietal network in the brain (Duncan, 2001; E. K. Miller & Cohen, 2001). Neurons

in this region have been found to rapidly adapt and selectively respond only to task-relevant items (Hampshire, Duncan, & Owen, 2007; Hampshire, Thompson, Duncan, & Owen, 2009). In the ST<sup>2</sup> model, task demand effectively filters the items that receive attentional enhancement and proceed to Stage 2.

### 3.1.3 Stage 2 of Neural-ST<sup>2</sup>

Stage 1 of the ST<sup>2</sup> model yields a decaying trace of the visual and semantic features of target items within the TFL. It is parallel in the sense that different items can be simultaneously active at the TFL. In contrast, Stage 2 implements sequential encoding of these items into WM, with this sequentiality emerging from mechanisms that attempt to ensure that items are discretely and unambiguously bound into WM. Types and tokens are bound via a pattern of sustained activation in a set of nodes comprising the *Binding Pool*. In particular, there is no synaptic change involved in this binding mechanism. Further, the binding pool contains one binding node for each combination of type and token (see figure 59B for a pictorial description). In other words, the binding pool is a localist (see O'Reilly & Munakata, 2000 for a definition) activation based memory for type-token associations<sup>1</sup>. The projections into and out of the pool are arranged such that each type-token association is represented by a portion of the pool. Inhibition between tokens ensures only one token is active at any one time, thus enforcing a serialisation of working memory encoding. Effectively, an item is encoded into working memory by connecting its type node in Stage 1 to a working memory token in Stage 2. This process is referred to as *tokenisation*. If at the end of a trial, the type node of a target has a valid connection to a token, the target is successfully 'reported' by the ST<sup>2</sup> model.

### 3.1.4 Transient Attentional Enhancement: the Blaster

ST<sup>2</sup> suggests that when the visual system detects an item that may be task relevant, a Transient Attentional Enhancement (TAE) occurs, which is directed at the location at which that item appears. For a weak (masked) item, the contribution of this enhancement is critical

---

<sup>1</sup>This localist implementation of the binding pool in 2f-ST<sup>2</sup> is not intended to be scalable to the level of complexity represented in the brain. In section 10.3, we will discuss how the binding pool could be implemented with a more neurophysiologically realistic, distributed architecture.

in enabling it to activate a token and thereby be encoded. The TAE is implemented by a mechanism called the blaster (described in greater detail in section 5.2). Above threshold activity in any node of the TFL (which will only happen for targets, because of the task demand filter) excites the blaster through the projection marked (a) in figure 11. The blaster sends a powerful excitatory projection to type nodes in Stage 1 (through the projections marked (b) in figure 11). This causes a generalised, but short lived, feedback excitation of layers in the later part of Stage 1. In the brain, such an attentional mechanism might correspond to the function of the temporo-parietal junction (TPJ) and the ventral frontal cortex (Corbetta & Shulman, 2002; Serences et al., 2005). Further, it might be that that these cortical structures interact with subcortical regions in the thalamus, including the locus coeruleus (Aston-Jones, Rajkowski, & Cohen, 2000; discussed further in section 3.2) and the pulvinar (Arend et al., 2008; Grieve, Acuña, & Cudeiro, 2000).

### 3.1.5 How the Model Blinks - Suppression of TAE

The cause of the blink is inhibition through the projection marked (c) in figure 11. This link ensures that, while binding pool nodes are being allocated, the blaster is held offline. Importantly, this inhibition is not active while an existing encoding is being maintained. As binding pool nodes are in fact *gate-trace* micro-circuits (see appendix A.1.2), the gate is only active during an allocation period; it is the gate of each binding pool node that has an inhibitory projection to the blaster (more details later in section 5.2). Therefore, the general behaviour of the blaster is a brief spike of excitation followed by a period of inactivity until the completion of the current token binding. This is the mechanism by which the model exhibits an AB: unavailability of the blaster protects the integrity of the T1 binding by limiting attentional resources that could cause binding intrusions. This is consistent with our central theoretical position that the blink is the marker of a system that is attempting to allocate distinct episodic contexts. Thus, it ‘deliberately’ sacrifices T2s in order to ensure the episodic integrity of T1, i.e., that it is unambiguously tokenised.

## 3.2 The LC-NE Model

The LC-NE model proposed by Nieuwenhuis, Gilzenrat, et al. (2005) makes an important contribution to understanding the AB; a strength being that the model is framed within the context of a broad neurophysiological theory of attentional function (Aston-Jones & Cohen, 2005; Aston-Jones et al., 2000; Usher, Cohen, Servan-Schreiber, Rajkowski, & Aston-Jones, 1999), based on the function of the *Locus Coeruleus* (LC) brain-stem nucleus, and the neurotransmitter Norepinephrine (NE) released by it. Perhaps of most importance, the LC-NE theory proposes a specific neurophysiological underpinning to the P3 (Nieuwenhuis, Aston-Jones, & Cohen, 2005), which is being extensively used as an ERP correlate of attentional processing in the AB context (Kranczoch et al., 2003; Luck et al., 1996; Martens, Munneke, et al., 2006; Vogel & Luck, 2002; Vogel et al., 1998). On the whole, the LC-NE theory proposes a unified explanation of temporal attention, which reconciles the AB phenomenon, neurophysiology, electrophysiology (in respect of the P3) and neural modelling.

To explain the AB, the LC-NE model depicted in figure 12 is configured such that only task-relevant targets generate a phasic LC response. LC innervation of the cortex ensures that the excitatory response of cortical neurons is amplified. In a visual discrimination task, monkey LC neurons are activated with a temporal profile that seems to match the AB curve, prompting the development of the model. It consists of two main components: the behavioural network and the LC. We discuss these in turn, before considering how the model generates an AB.

### 3.2.1 Behavioural Network

The behavioural network is a simple feed-forward system, with major inter-layer connections being one-to-one. The network comprises three layers: Input, Decision and Detection. In the AB context, a sequence of stimuli is presented at the input layer to simulate the RSVP stream.

The decision layer implements an ongoing competition between three alternatives: the two targets and a single unit abstractly modelling all distractors. Nodes in the decision layer compete through lateral inhibition. Crosstalk connections are also included between input and decision nodes, reflecting feature similarity between stimuli. The decision layer projects

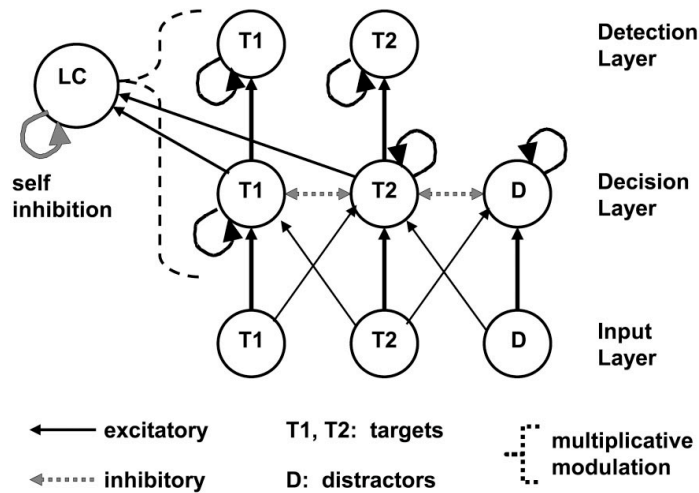


Figure 12 **The LC-NE model.** Crosstalk connections between T1 and D are not shown for visual clarity. Point sizes of arrows indicates weight strength. Reproduced from Nieuwenhuis, Gilzenrat, et al. (2005).

in one-to-one fashion to the detection layer, which serves as the output from the model. On the assumption that only targets are reported, the detection layer does not represent distractors. Finally, excitatory self-loops are included to sustain activation at decision and detection nodes. However, these loops are not strong enough to yield an active memory.

### 3.2.2 The Locus Coeruleus

The Locus Coeruleus (LC) is a minute brain-stem structure (German et al., 1988) that projects widely to the cortex, with a special emphasis on areas involved in attentional processing (Aston-Jones et al., 2000). In the LC-NE model, the LC modulates activity in the behavioural network. Specifically, the LC is excited by detection of a salient stimulus. In the context of the behavioural network, this means that targets fire the LC, as reflected by the fact that target nodes in the decision layer have excitatory projections to the LC. LC activity has a modulatory effect on the behavioural network, by simulating the release of the neurotransmitter Norepinephrine (NE). This release multiplicatively scales the afferent signals to network units, transiently adjusting their gain. Amplification of the multiplicative gain ‘sharpens’ the sigmoidal transfer functions (Aston-Jones & Cohen, 2005) making decision and detection layer units temporarily more responsive.

### 3.2.3 How the Model Blinks - The LC Refractory Period

Following a firing of the LC and the subsequent release of NE, it enters a *refractory period*. This arises because, while NE enhances processing in cortical areas, local NE release within the LC is believed to be autoinhibitory. Thus, following a phasic response, this autoinhibition generates an LC refractory period, during which further LC phasic response is rare. In the LC-NE model, it is unavailability of the LC during its refractory period that causes the blink. That is, the model blinks as a result of the following sequence of events. Firstly, the T1 fires the LC, which provides a window of enhancement lasting around 150ms. Secondly, following this T1-induced firing, the LC enters its refractory period. Thirdly, T2s arriving during this period are unable to immediately re-fire the LC and, consequently, do not benefit from a timely (NE-induced) increase in gain. This leaves T2s arriving during the refractory period at a disadvantage, ensuring that only particularly strong T2s get reported. Blink recovery happens because, if the T2 follows the T1 after a sufficient time interval, the LC will have recovered from its refractory period and the T2 will be able to fire it in short order. Indeed, the LC-NE model suggests that the AB profile will exactly follow the profile of the LC refractory period.

## 3.3 Related Work

In this section, we briefly discuss some other models that simulate the Attentional Blink. In particular, we highlight the mechanisms used in these models to implement the temporal spotlight of attention, and comparatively evaluate them against the blaster and the LC.

### 3.3.1 The Global Workspace Model

The global workspace model (Dehaene, Sergent, & Changeux, 2003) is a general, biologically detailed architecture of neural information processing. It begins at early sensory stages and leads up to a central, global workspace of attentional control and consciousness. In the model, stimuli compete for access to this global workspace and benefit from enhancement due to attentional feedback. In particular, it explains the AB by proposing that when T2 is presented shortly after T1, it fails to enter the global workspace, which is occupied by the processing of T1. However, the model does not explain many of the other findings related

to the AB, including spreading the sparing (see Bowman & Wyble, 2007 for a detailed comparison to the ST<sup>2</sup> model).

### 3.3.2 The CODAM Model

The Corollary Discharge of Attention Movement (CODAM) model is a broad-based mechanism of attentional control, with many links to neurobiology (Taylor & Rogers, 2002). It consists of a bottom-up pathway along which stimuli have to pass, in order to have access to working memory. Importantly, items processed in this pathway require the benefit of an attentional enhancement signal provided by a module called the ‘inverse model controller’ (IMC) to successfully progress into working memory. Fragopanagos, Kockelkoren, and Taylor (2005) simulate the model in an AB setting, in which this attentional control signal is withheld from the T2 when presented in close succession to T1, to ensure that T2 does not interfere with T1 encoding. Though the CODAM model simulates the basic AB curve, it does not generate as broad a range of data as the ST<sup>2</sup> model, and also does not simulate spreading the sparing (see Bowman & Wyble, 2007 for further analysis).

### 3.3.3 The eSTST Model

The eSTST model (Wyble, Bowman, & Nieuwenstein, 2009) is a revision of the ST<sup>2</sup> model that enables it simulate spreading the sparing (Di Lollo et al., 2005; Olivers et al., 2005). As mentioned in section 2.3.2, spreading the sparing is a recent finding that suggests the lag 1 sparing window can be extended to multiple targets, if they are presented in rapid succession after the T1. The eSTST model retains many of the structural aspects of ST<sup>2</sup>; in particular it too has a blaster that is responsible for providing transient attentional enhancement to targets. However, the important difference with respect to ST<sup>2</sup> is that the blaster in eSTST does not have an innate refractory period. Instead, its deployment is controlled by competing inhibitory and excitatory connections from WM encoding and target input, respectively (Wyble, Bowman, & Nieuwenstein, 2009). This implementation allows each target in a string of consecutive targets to generate a recurrent, extended enhancement of attention.

### 3.3.4 The Boost and Bounce Model

The Boost and Bounce model of temporal attention (Olivers & Meeter, 2008) is another recent computational model, which, like the eSTST model explains the AB and spreading the sparing within a common framework. In contrast to the eSTST model however, the Boost and Bounce model emphasises the role of distractor suppression in producing the AB (Raymond et al., 1992). In the model, an attentional ‘gating’ mechanism ‘boosts’ targets and ‘bounces’ (i.e., suppresses) distractors, effectively serving as the temporal spotlight. Once opened by a target, this gate stays open as long as more targets are presented in succession. But a distractor following a target inadvertently benefits from the attentional boost and provokes a prolonged inhibitory bounce response that results in an AB effect.

## 3.4 Conclusions

This chapter has focused on two neural models of temporal visual processing and the AB. These models form the basis of the theoretical explorations in later chapters of this thesis. In particular, the  $ST^2$  model will provide the main modelling platform based on which the experimental results presented in this thesis are interpreted. The characteristics of this model will be comparatively evaluated against the LC-NE model, and a potential extension to the LC-NE model that incorporates concepts from  $ST^2$ . In addition, later chapters of this thesis also elaborate on an extension to the  $ST^2$  model, to enable it to simulate temporal feature binding in vision. The next chapter delves deeper into the mechanisms of the  $ST^2$  model, to elaborate on the methodologies that will be used in this thesis to connect modelling and electrophysiological data.

## Chapter 4

# Connecting Modelling and Electrophysiology

The previous chapters have provided an overview of the experimental and theoretical background related to the research presented in this thesis. Following on from there, a key idea explored in this thesis is how the connection between experiment and theory can be enhanced by EEG data. Here, we provide an overview of the generation of virtual ERPs from the ST<sup>2</sup> model. Beginning with an introduction to the concept, we provide a rationale for the use of virtual ERPs in extending the flow of ideas between models and data. We then go on to describe the methodology for generating specific virtual ERPs from subcomponents of the ST<sup>2</sup> model, which are qualitatively comparable to human ERPs, both at the level of grand averages and single trial dynamics.

### 4.1 Introducing Virtual ERPs

Computational modelling of cognition is commonly focused on the replication of behavioural data. In this regard, they have provided concrete frameworks for expressing and instantiating cognitive theories. These models can then be used to generate experimental predictions. Testing these predictions then feeds back into further refinement of the models they are derived from, thus completing the cycle of theory and experiment.

Within the domain of cognitive models, neural network models of cognition, in addition to replicating behavioural data, embody a hypothesis about underlying structure and function. These models attempt to ‘explain’ behaviour as emerging naturally out of functional structures in the brain and the neural dynamics that these structures support. Often, these structures are inspired by and justified based on research into neural physiology and anatomy. In doing so, neural network modellers hope to understand how specific aspects of cognition are embodied in the brain.

On the empirical front, cognitive science is no longer limited to behavioural research. Recent advances in brain imaging technology allow researchers to monitor the participant’s behaviour at a certain task, and in addition, record ongoing brain activity that is correlated with a particular behaviour. Among the different imaging techniques, EEG provides particularly high temporal resolution, and is well suited to studying the millisecond-scale temporal dynamics of conscious perception. Researchers have been successful in mining EEG data to infer aspects of both subconscious and conscious neural processing. The convergence of behavioural and neuro-imaging research is rapidly changing the insights that can be gained about the neural architecture and processing that underlie behaviour.

Given this background, the natural question that arises is how these two approaches to understand cognition at the neural level can be beneficially combined. A significant part of this thesis has been devoted to this question, previously investigated in Craston et al. (2009) and Craston (2009). Specifically, we are interested in using the Neural-ST<sup>2</sup> model to validate human EEG data. This is possible because cognitive neural networks consist of nodes, which derive from the functional characteristics of real neurons. The activation of nodes in a model can be interpreted as the analogue of the activation of an assembly of neurons in the brain. Consequently, activation traces in a model are comparable to aggregate neural activity expressed in EEG data.

Figure 13 summarises the rationale behind the concept of *virtual ERPs*, and their relationship to human ERPs. As depicted in the illustration, behavioural data for the particular set of experimental observations constrain the development of a neural network model. Drawing on a broad set of behavioural data related to the AB, repetition blindness and RSVP in general, Bowman and Wyble (2007) proposed the ST<sup>2</sup> model, which embodied a two-stage theory of temporal visual processing. As discussed previously in section 3.1, the

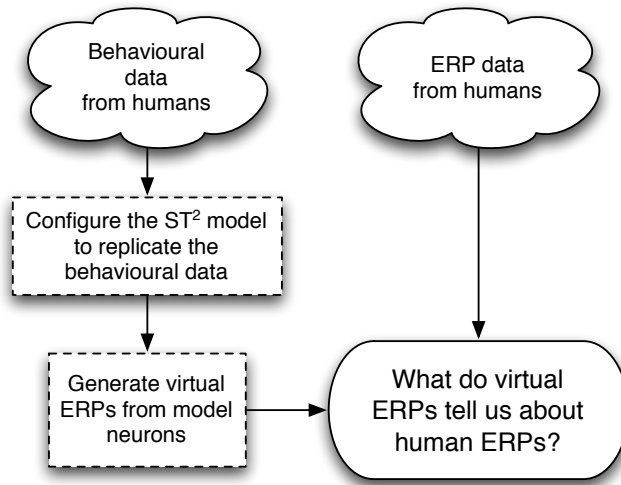


*Figure 13* **The role of virtual ERPs in cognitive science research.** Behavioural data is used to constrain the ST<sup>2</sup> model, virtual ERPs from which are then evaluated against human ERPs.

ST<sup>2</sup> model simulates human behavioural accuracy using its neural network implementation. In parallel, a large amount of electrophysiological data has been collected in the context of the previously stated phenomena. The relevant question explored in this thesis is thus: do virtual activation traces generated from the neural network model represent meaningful patterns that mirror human EEG data, allowing us to replicate, interpret and make predictions about human EEG data in a way similar to that previously used with behavioural data? The rest of this chapter sets down the foundation for this exploration. First, the methodology used to generate virtual ERPs from the model is discussed. This is followed by an overview of the key ERP components that are the focus of study and replication in this thesis.

## 4.2 Generating Virtual ERPs

As illustrated in figure 11, the ST<sup>2</sup> model consists of a number of layers, each containing several nodes. Nodes of one layer are connected to nodes in other layers via excitatory and inhibitory connections. In order to describe the activation dynamics at the individual node level, figure 14 focuses on a single connection between a pair of nodes. The two nodes depicted represent a typical ST<sup>2</sup> node pair in two neighbouring layers. Nodes in the ST<sup>2</sup> model

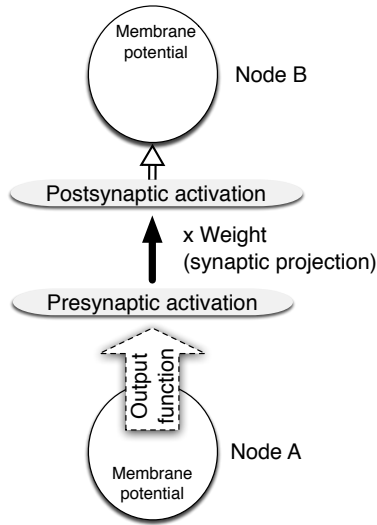


*Figure 14* **Node-level activation dynamics in Neural-ST<sup>2</sup>**. A typical pair of neural network nodes situated in two neighbouring connected layers of the ST<sup>2</sup> model. As shown in the figure, we can extract the membrane potential, presynaptic activation and postsynaptic activation for each node of the Neural-ST<sup>2</sup> model.

receive input from other layers via weighted connections and update their membrane potential according to shunting equations derived from the Hodgkin-Huxley approach (Hodgkin & Huxley, 1952). Once the membrane potential reaches a given threshold, they produce output according to a rate-coding X-over-X+1 function (O’Reilly & Munakata, 2000). In figure 14, the membrane potential describes the activation within the node. The weighted connections between the nodes are assumed to correspond to major synaptic projections in the brain. Within the context of a given weighted synaptic projection outgoing from a node, activation output produced by the node is referred to as presynaptic activation. This activation, when multiplied by the corresponding synaptic weight results in a postsynaptic activation that feeds into the node at which the synaptic projection ends.

In the human brain, the difference in electric charge between the dendrite and the postsynaptic cell body of an active neuron creates an electric dipole. To generate a signal that is strong enough to be registered by the EEG, a population of neurons has to be active together and spatially aligned, which causes the individual dipoles to summate. In our understanding of neural electrophysiology, cortical pyramidal neurons are known to have long-range connections and are aligned perpendicular to the cortex, and are assumed to be a major contributor to EEG activity (Baillet, Mosher, & Leahy, 2001; Luck, 2005). In

addition, pyramidal neurons release glutamate as their neurotransmitter, and therefore have an excitatory effect on networks they participate in.

For generating virtual ERPs, we attempt to keep the methodology as simple as possible, while at the same time approximating the mechanisms that are assumed to occur in the brain. Virtual ERPs are generated by summing over postsynaptic activation values (see figure 14), the rationale being that it is postsynaptic potentials between the dendrite and the cell body that primarily generate the EEG signal recorded at the scalp. In line with pyramidal neurons forming excitatory connections in the brain, the virtual ERP consists of postsynaptic activation values from excitatory connections only. Note that only activation traces from connections between layers (and not self-loops that connect nodes within a layer) are included in the virtual ERP, as these are assumed to be an analogue of the long-range connections from pyramidal neurons that contribute towards the signal measured in the human ERP.

It is obvious that virtual ERPs remain a coarse approximation of the human ERP. Many factors, such as the distortion of the signal by the scalp, are not addressed<sup>1</sup>. In this context, it is important to note that the approach to simulating ERPs employed here is philosophically distinct: in particular, the ST<sup>2</sup> model is not expressly configured to generate virtual ERPs that fit their human counterparts. Rather, the model is first matched to human behavioural data, and the virtual ERPs generated in this configuration are verified for comparability with human ERPs. Consequently, due to these limitations of the virtual ERP technique, one can only expect to obtain a qualitative rather than a quantitative match to the data. Nevertheless, this process allows us to provide a common explanation for a pattern of behavioural and ERP effects, in addition to verifying the internal dynamics of model's architecture. Further, as we shall see in later chapters, virtual ERPs allow us to make qualitative predictions about the pattern of changes in human ERPs across experimental conditions of interest.

---

<sup>1</sup>For an example of an approach to modelling ERPs that is based on a neurobiologically constrained source reconstruction, see the Dynamic Causal Modelling (DCM) technique (David, Harrison, & Friston, 2005; David, Kilner, & Friston, 2006).

### 4.2.1 Grand Average Virtual ERPs

Grand average virtual ERPs, comparable to their human equivalents previously introduced in section 2.4.3, allow for qualitative comparison of traditional ERP components commonly investigated in EEG research. To generate virtual ERPs from a simulated trial, we adopt the straightforward approach and sum over all nodes of a relevant subset of layers from the  $ST^2$  model. In addition, neurophysiological evidence suggests that there is a delay of around 70ms for neural activation related to visual processing to travel from the retina to occipital areas (Schmolesky et al., 1998).  $ST^2$  does not model this aspect of visual processing, and hence to account for this delay, virtual ERPs generated by the model are shifted by 70ms. Finally, to generate the grand average virtual ERP corresponding to an experimental condition, we average across the simulated trials making up that condition.

### 4.2.2 Virtual ERPimages

When generating ERP averages, raw EEG data is collapsed to a one dimensional dataset displaying a sequence of voltage fluctuations over time. The averaging process extracts EEG activity that is time-locked to the stimulus, whereas the rest of the signal is treated as irrelevant background noise. As previously pointed out in section 2.4.4, the problem with this approach is that information that is specific to individual observations is lost. Consequently, ERPimages (Makeig, Debener, et al., 2004; Delorme & Makeig, 2004) have been proposed as a means for visualising single-trial dynamics in EEG data.

This shortcoming of the averaging process also applies to virtual ERPs. A simulation run of the  $ST^2$  model contains a number of trials encompassing a range of target strength values. A grand average virtual ERP illustrates the general time course of activation in chosen layers in the model, but is blind to inter-trial variation that occur because of varying strength values. To address this problem, we generate *virtual ERPimages* from the  $ST^2$  model, using visualisation techniques similar to those used to generate human ERPimages. As we shall see, virtual ERPimages bring out patterns of variation that are not evident in the grand average virtual ERP, and depict the dynamics of the model across individual trials of a simulation run.

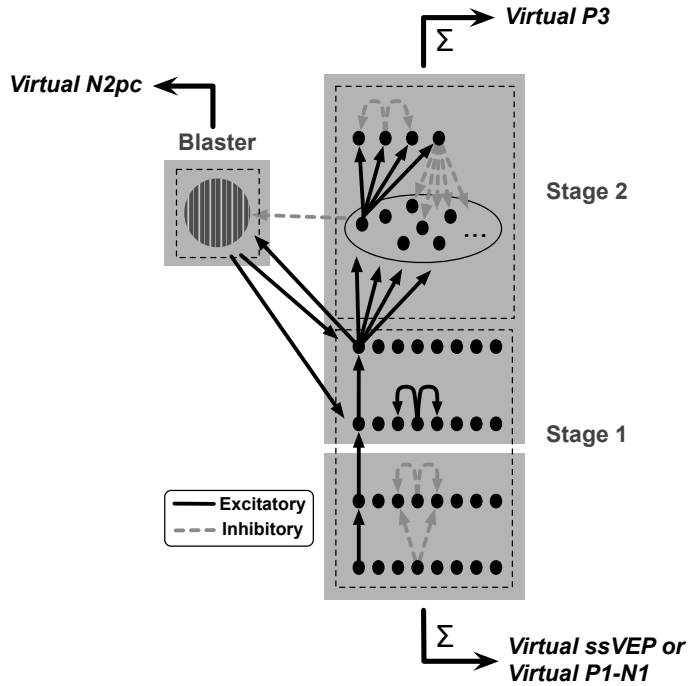


*Figure 15 Virtual ERPs from the ST<sup>2</sup> model.* The virtual ssVEP is generated from the input and masking layers. The virtual P3 is generated from the item, TFL, binding pool and token layers. The virtual N2pc is generated from blaster activation.

### 4.3 Virtual ERP Components

This section focuses on the specific virtual ERP components that are generated from the ST<sup>2</sup> model and compared with human ERP components. A human ERP component is typically recorded from a particular set of electrodes and associated with certain cognitive processes. In the ST<sup>2</sup> model, different layers of the model were designed to correspond to various stages of cognitive processing in the brain. As shown in figure 15, by summing over neural network activation from nodes within specific layers of the ST<sup>2</sup> model, we can extract virtual ERPs related to particular stages of cognitive processing.

#### 4.3.1 Early Visual Processing - The Virtual ssVEP

Correlates of early visual processing in the human ERP are observed at occipital electrode sites. A target presented on its own evokes the well-known N1 and P1 ERP early components, reflecting early perceptual processing of the visual features of the target (see

figure 4A). However, in the context of RSVP, successive items in the stream evoke a sustained ssVEP wave (Di Russo et al., 2003), which oscillates at a frequency equal to the presentation rate of items in the stream (see figure 4B).

In the ST<sup>2</sup> model, targets and distractors in the RSVP stream are ‘presented’ to the input layer. The input layer thus corresponds to very early stages of processing in the brain. At the masking layer, each item is subject to competition from temporally adjacent items in the stream, thus simulating forward and backward masking at early vision. The amount of masking is determined by the bottom-up strength of the neighbouring items. Together, the input and masking layer reflect perceptual processing of stimuli, and thus most closely resemble neural processing in the early visual cortex. Consequently, as in figure 15, activation at these layers is summated to generate the virtual ERP corresponding to early visual processing, and in particular, the *virtual ssVEP*. In chapter 6, we will modify the ST<sup>2</sup> model to simulate the processing of a single target on its own, and generate virtual early P1 and N1 components from it.

### 4.3.2 Transient Attentional Enhancement - The Virtual N2pc

The N2pc ERP component has been associated with attentional selection (Luck & Hillyard, 1994; Eimer, 1996; Hopf et al., 2000) (see figure 4C). It has been observed whenever attention is directed toward a visual stimulus. In the ST<sup>2</sup> model, attention is modelled by the blaster, which is triggered only by targets at the TFL, and provides them with a transient burst of excitation to facilitate working memory encoding. Hence, in order to generate a virtual ERP component that reflects the selective attentional response in the ST<sup>2</sup> model, we average activation from the blaster’s output across multiple trials to generate the virtual N2pc for a particular condition. (see figure 15). However, it should be noted that, unlike the human N2pc, the virtual N2pc is not a lateralised component. This is because the ST<sup>2</sup> model does not simulate hemispheric differences in attentional responses. Further, the virtual N2pc is a positive activation trace from the blaster. In comparison, the human N2pc is a negative-going electrical potential difference. This arises from complexities relating to the neural generators of the human N2pc, and their projections onto the scalp, which are not simulated by the ST<sup>2</sup> model. Despite these differences, variations in blaster activity across conditions of interest are qualitatively comparable to those in the human N2pc.

### 4.3.3 Working Memory Encoding - The Virtual P3

The human P3 ERP component is a broad ERP component spread across a large area of the scalp, most prominent at parietal electrode sites (see figure 4A). It is thought to reflect a global event in the brain, involving interaction between multiple cortical regions. The meaning of the P3 and the cognitive processes that it reflects have been the subject of much debate (see Donchin & Coles, 1988; Verleger, 1988 for an extensive discussion). In almost all RSVP experiments, the P3 is observed to be correlated with conscious perception and working memory consolidation of targets (Donchin, 1981; Vogel et al., 1998; Kranczoch et al., 2003; Sergent, Baillet, & Dehaene, 2005). This notion is supported by the related finding that the P3 is absent for missed targets in RSVP (Kranczoch et al., 2003).

In the ST<sup>2</sup> model, working memory encoding occurs by creating a binding link between types from Stage 1 and tokens from Stage 2, a process referred to as tokenisation (see section 3.1). Tokenisation is initiated by the arrival of a target at the TFL, which triggers the blaster (see figure 11). The blaster responds by generating a transient attentional enhancement, providing a burst of excitation to the item and TFL layers. TFL nodes project to the binding pool, which in turn are connected to the tokens in Stage 2 (see figure 59B). Tokenisation completes when a token node gets bound to the target's type in the TFL via intermediate nodes in the binding pool. Hence, on the whole, the item and TFL layers, the binding pool and the tokens are all involved in encoding an item into working memory. Consequently, as depicted in figure 15, these layers contribute towards the virtual P3 component, which is generated by summing the activation across all constituent nodes.

## 4.4 Conclusions

This chapter has outlined the concept of virtual ERPs, focusing on highlighting the rationale behind virtual ERPs and the general methodology for generating them. In particular, virtual ERPs provide a two-fold benefit: firstly, we can use them to interpret behavioural and ERP data within a common explanatory framework. Secondly, we can use the comparisons between human and virtual ERPs to verify the internal mechanisms of the ST<sup>2</sup> model. The general introduction provided here will be elucidated when specific virtual ERPs from the model are generated and compared to human ERPs across conditions of interest.

## Part II

# Explorations of the Temporal Spotlight

## Chapter 5

# Comparing the ST<sup>2</sup> and the LC-NE models

We begin the main body of this thesis with a theoretical exploration of the ST<sup>2</sup> and LC-NE models. This work comparatively evaluates two complementary neural network models that describe the role of the temporal spotlight in temporal perception and the Attentional Blink. First, we comparatively describe the inner workings of Transient Attentional Enhancement (TAE) as embodied in these two models. This followed by a detailed assessment of how both models fare in terms of explaining the main phenomena that characterise the AB, as previously listed in section 2.3.2. In final section of this chapter, based on our insights into the two models, we introduce a potential extension to the LC-NE model. This extension borrows concepts from ST<sup>2</sup> to expand the explanatory power of the LC-NE model and bridge the levels of explanation they encompass.

### 5.1 Introduction

In addition to the large body of behavioural research relating to the AB described previously in section 2.3, there has been considerable recent interest in identifying neural correlates of the underlying mechanisms (Craston et al., 2009; Martens, Munneke, et al., 2006; Marois, Chun, & Gore, 2000; Rolke, Heil, Streb, & Hennighausen, 2001; Marois et al., 2000; Vogel & Luck, 2002; Vogel et al., 1998). To complement this line of enquiry, there has been

work on developing neurally explicit computational explanations (Bowman & Wyble, 2007; Fragopanagos et al., 2005; Nieuwenhuis, Gilzenrat, et al., 2005; Chartier, Cousineau, & Charbonneau, 2004; Battye, 2003; Dehaene et al., 2003). Amongst these, the ST<sup>2</sup> (Bowman & Wyble, 2007) and the LC-NE (Nieuwenhuis, Gilzenrat, et al., 2005) models, previously introduced in chapter 3, are notable approaches. This is because the former reproduces a broad spectrum of AB phenomena and the latter ties into a concrete neurophysiological substrate. In a sense, the ST<sup>2</sup> model works down from the behavioural data, while the LC-NE model works up from the neurophysiology. Thus, an important research question concerns how these two models relate to one another. In particular, to what extent can the neurophysiological mechanisms highlighted in the LC-NE model be reconciled with the cognitive-level mechanisms inherent in the ST<sup>2</sup> model? This chapter focuses on such issues, and comparatively evaluates the computational implementations of the temporal spotlight in the two models. In this context, we have re-implemented the LC-NE model to better understand the role of attention therein. Additionally, we have worked on extending the model using mechanisms inspired by the ST<sup>2</sup> model to enable it to reproduce a broader spectrum of behavioural data pertaining to the AB. The research in this chapter builds upon the introduction to the ST<sup>2</sup> and LC-NE models provided in chapter 3, and mutually informs the mechanisms that implement the temporal spotlight of attention therein.

A similarity between the LC-NE and ST<sup>2</sup> approaches is that they both assume temporal spotlights that are triggered by detection of a salient stimulus (e.g. a target stimulus) and are short-lived. In ST<sup>2</sup>, the enhancement is the Transient Attentional Enhancement (TAE), which is realised by the blaster, while in the LC-NE model the enhancement arises from the Locus Coeruleus itself. That said, the two enhancements do have somewhat different purposes. ST<sup>2</sup>'s blaster aids detection and WM encoding of weak items, while the LC is assumed to have its affect on decision and response systems, where it optimizes processing in multilayer decision systems (Aston-Jones & Cohen, 2005). However, both approaches assume that it is unavailability of this attentional resource (blaster and LC respectively) that is the direct cause of the blink. The mechanism that causes this unavailability is, though, very different in the two cases. In ST<sup>2</sup>, the blaster is held offline by ongoing working memory encoding. This preserves the integrity of such encoding by preventing a second item from corrupting the episodic integrity of a first item. In the LC-NE model, after

firing, the LC enters an intrinsic refractory period in which it is difficult to re-fire. It is this conceptual difference between the temporal spotlights that is at the heart of the comparison in this chapter.

## 5.2 TAE in the ST<sup>2</sup> Model: The Blaster

In the ST<sup>2</sup> model introduced in section 3.1, the blaster implements transient attentional enhancement. In this role, it mediates the establishment of type-token bindings across a parallel Stage 1 and a serial Stage 2. An item passing the salience filter in the final layer of Stage 1 of the ST<sup>2</sup> model in a strongly active form initiates the blaster, which elevates activation across the later levels of Stage 1. This mechanism is exogenous in character, being triggered externally by the occurrence of a salient stimulus, and highlights a very brief window of time and space that is particularly salient. Specifically, the blaster enhances the activation level of salient items, aiding their encoding into WM. This is particularly important when considering demanding stimulus environments (such as RSVP), as unaided, fleeting representations have insufficient bottom-up activation to facilitate encoding. In this regard, the blaster plays a key role in facilitating type-token binding. The blaster has the following important characteristics:

- Firstly, it is a brief pulse of a fixed duration (around 100ms), irrespective of the exogenous strength of the salient stimulus.
- Secondly, it only fires once per tokenisation. Once a target (T1) triggers the blaster and the process of binding is initiated, it is held offline by inhibition from the binding pool till the process is complete. This inhibition attempts to associate distinct episodic contexts to targets, and prevents a second target (T2) in close temporal proximity to T1 from interfering with its tokenisation. T2 occurring within 200-500ms of T1 must “wait” till the T1 tokenisation is complete for the blaster to fire again. This implies that only T2s with strong bottom up strength have enough activation to “outlive” T1 tokenisation. It is this mechanism, embodying the episodic distinctiveness hypothesis, that enables the ST<sup>2</sup> model to simulate the attentional blink.
- Thirdly, the blaster is spatially specific, but is not featurally selective in its enhancement. That is, it is initiated by detection of features characterising the task set but the

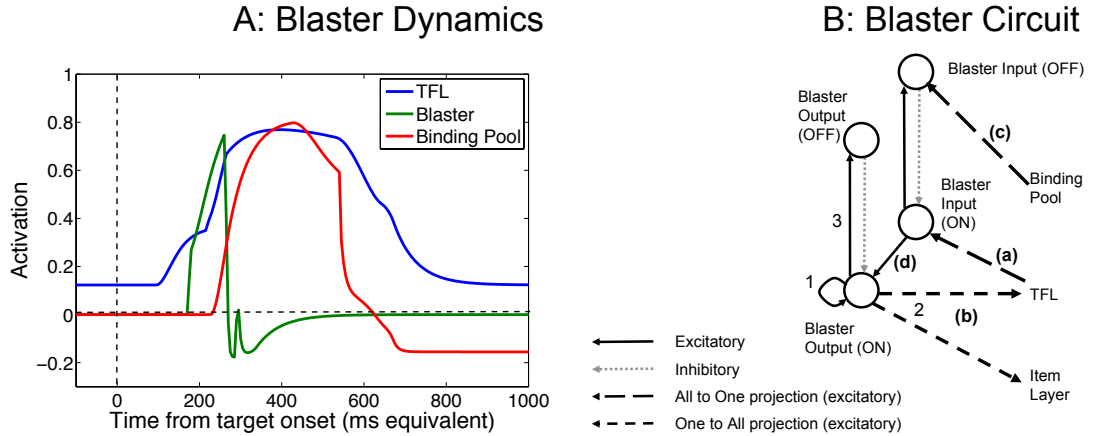


*Figure 16* **The dynamics and circuitry of the blaster in Neural-ST<sup>2</sup>.** Panel A: Dynamics of the blaster as regulated by the TFL and the binding pool. Panel B: Internal circuitry of the blaster. Output connection thresholds emanating from the blaster output on neuron are denoted 1, 2 and 3, with 1 less than 2 less than 3. Reproduced from Bowman and Wyble (2007).

effect of the blaster is not restricted to those features.

Figure 16A depicts the activation dynamics of the blaster and its relationship to input from TFL and inhibition from the binding pool. The presentation of a single target in RSVP excites its corresponding node in TFL, which in turn feeds input to the blaster. Due to the way its internal circuit is configured, the blaster produces a ballistic response to excitation from TFL. This response gets fed back to the TFL, boosting the activation of the target’s TFL node to a value high enough to initiate tokenisation. During tokenisation, the binding pool node connecting the target’s TFL node to the currently active token is excited. As previously described, this excitation is set up to inhibit the blaster. This produces the prolonged suppression in the blaster’s activation seen in figure 16A, preventing it from firing again till tokenisation is complete. Its activation eventually returns to baseline once tokenisation is completed and suppression from the binding pool dies down.

### 5.2.1 Internal Structure

Though not essential for understanding the role of the blaster in the ST<sup>2</sup> model, it is informative to examine the internal circuitry that produces the response characteristics observed in figure 16A. This circuitry is depicted in figure 16B. As all connections in the blaster circuit saturate at a very low level, the nodes making up this circuit display ballistic dynamics. In

other words, when their activation crosses a certain threshold, the output of the nodes very quickly reaches a maximum value, and remains mostly unchanged with further increase in activation. The blaster’s implementation comprises two *on-off* circuits (see section A.1.1), distinguished as blaster input, which governs initiation of the blaster, and blaster output, which governs the blaster’s output effect. Thus, the blaster is initiated by TFL excitation of the blaster input on neuron (via projection (a)). However, the resulting activation is short lived and rapidly curtailed when the blaster input on neuron feeds inhibition back onto the blaster input on neuron (generating the blaster refractory period). Furthermore, this suppression is maintained by ongoing binding, via the projection marked (c)<sup>1</sup>. The resulting brief on neuron activation of the blaster input circuit has the role of instigating blaster output activation through the link marked (d). This Output circuit generates a temporally fixed output to the TFL and Item layer (via the projection marked (b)). This effect is obtained through the blaster output on neuron having different thresholds for outputting along different connections, where threshold (1) is less than (2) is less than (3). When the blaster output on neuron is excited, it begins its self-excitatory cycle with a low threshold (1), causing it to ramp up with a predictable time course. When activation crosses threshold (2), it begins outputting at a fixed level over projection (b). On crossing the third threshold (3), it strongly excites the blaster output on neuron, which in turn inhibits it, ending the blaster’s output at the appropriate time.

### 5.3 TAE in the LC-NE Model: The Locus Coeruleus

The LC-NE model (Nieuwenhuis, Gilzenrat, et al., 2005) is inspired by a broad neurophysiologically grounded theory (Gilzenrat, Holmes, Rajkowski, Aston-Jones, & Cohen, 2002; Aston-Jones & Cohen, 2005; Aston-Jones et al., 2000; Nieuwenhuis, Aston-Jones, & Cohen, 2005; Usher et al., 1999) about the function of the Locus Coeruleus nucleus as a modulator of attentional control. As introduced in section 3.2, the LC-NE theory proposes a unified explanation of temporal attention, which reconciles the AB phenomenon, neurophysiology,

---

<sup>1</sup>Note that this projection is depicted as inhibitory in figure 11. But, in fact, it is realised as an excitatory projection onto the blaster input off neuron, which generates an inhibitory effect of the binding pool onto the blaster input on neuron.

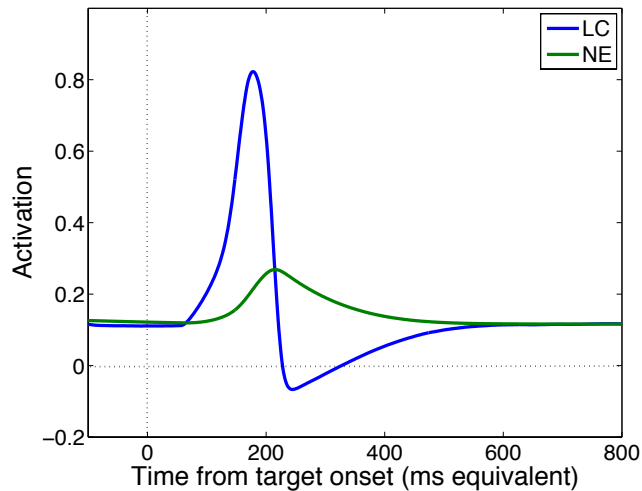


*Figure 17* **Dynamic behaviour of the LC-NE system.** Activation traces plot the response of the LC and NE components of the re-implemented LC-NE model to the presentation of a single target in RSVP.

electrophysiology (with respect to the P3) and neural modelling. The model can be divided into two components: the behavioural network and the LC-NE system. The model hypothesises the LC-NE system to be the component providing the transient attentional enhancement in response to the presentation of task-relevant stimuli to the behavioural network.

As a part of the research leading up to this thesis, the LC-NE model of the AB, as described in Nieuwenhuis, Gilzenrat, et al. (2005) was re-implemented to explore the inner workings of the LC-NE system, and to explore the model’s behaviour with regard to the AB phenomena described in section 2.3.2. This work eventually led to the development of extensions to the LC-NE model, described later in this chapter. The details of this re-implemented LC-NE model are described in appendix A.2. We now draw upon simulations conducted with the re-implemented model to provide an in-depth description of the behaviour and internal details of the LC-NE system.

### 5.3.1 The Locus Coeruleus & Norepinephrine

The LC-NE model explains the AB in terms of the functioning of the Locus Coeruleus (LC) (Nieuwenhuis, Gilzenrat, et al., 2005), a minute brain-stem structure (German et

al., 1988) that projects widely to the cortex, with a special emphasis on areas involved in attentional processing (Aston-Jones et al., 2000). The LC is known to have two modes of operation: in its *phasic* mode, it produces a sharp response to the presentation of a target, but has a low ambient firing rate of 1-2Hz when it is presented with distractors. In the *tonic* mode, it has a higher ambient firing rate of 2-4Hz for distractors, and produces a shallow response to targets (Gilzenrat et al., 2002). In the phasic mode of operation, strong LC innervation of the cortex with the neurotransmitter Norepinephrine (NE) ensures that the excitatory response of cortical neurons is amplified. In a visual discrimination task, LC neurons in monkeys are activated with a temporal profile that seems to match the AB (Aston-Jones et al., 2000). This observation of phasic LC function prompted its application to the AB in the form the LC-NE model previously introduced in section 3.2 and depicted in figure 12 (Nieuwenhuis, Gilzenrat, et al., 2005).

Figure 17 depicts the temporal dynamics of the LC-NE system in its phasic mode of operation. As previously described in section 3.2, this LC component is excited by the detection of task-relevant targets in the decision layer of the behavioural network. Figure 17 depicts how, when perturbed enough from its baseline level because of this excitation, LC activity rapidly increases, producing a characteristic ballistic response to the target. This response causes a much slower increase in the amount of NE produced by the LC. This release of NE has a feedback modulatory effect on the behavioural network of the LC-NE model, as it multiplicatively scales the afferent signals to network units in the decision and detection layers, transiently adjusting their gain and making them more responsive to the activation generated by the target (see section 3.2). However, after firing, the LC enters a *refractory period* evident in figure 17. This arises as, while NE enhances processing in cortical areas, local NE release within the LC is known to be autoinhibitory. Thus, following the excitation of the LC by the decision layer and subsequent release of NE, this autoinhibition generates an LC refractory period, during which further excitation is suppressed by NE release.

### **Internal Structure**

We now describe how the characteristic dynamics of the LC-NE system observed in figure 17 are implemented in the model, though this is not a requirement for understanding its

behaviour. The LC-NE system is realised using an adaptation of the FitzHugh-Nagumo system of equations (Gilzenrat et al., 2002; Fitzhugh, 1969; Nagumo, Arimoto, & Yoshizawa, 1964), which governs the interactions between a pair of coupled activity variables, one simulating the LC and other simulating NE. The FitzHugh-Nagumo system was originally used as simplification of the Hodgkin-Huxley equations for modelling action potentials in individual neurons. It characterises the LC-NE system as a dynamical system controlled by two temporal variables: the first variable,  $v(t)$ , represents LC activity, and is excited by target-related activation in the behavioural network and inhibited by the second variable  $u(t)$ .  $u(t)$  represents NE output, and is influenced by the current level of LC activity. In its standard formulation, the FitzHugh-Nagumo system relates these two variables by a pair of ordinary differential equations (ODE), as described below:

$$\tau_v \frac{dv}{dt} = Av(v-a)(1-v) - u \quad (2)$$

$$\tau_u \frac{du}{dt} = v - \gamma u \quad (3)$$

where  $\tau_v$  and  $\tau_u$  are time constants such that  $\tau_v \ll \tau_u$ , and  $A > 0, 0 < a < 1$  and  $\gamma > 0$ .

Importantly, the time constant associated with LC activity ( $\tau_v$ ) is much smaller than the time constant associated with NE output ( $\tau_u$ ). It is this difference that sets up the dynamics illustrated in figure 17, where LC activity, which is very sensitive to excitatory input, rises rapidly in response to target presentation. In contrast, NE output rises much slower in response to LC activity. But once it does, it has a strong inhibitory effect on the LC, driving it down into the refractory period, from which it recovers only as NE output slowly returns back to baseline.

## 5.4 Assessment of Models

We now assess the ST<sup>2</sup> and LC-NE models against the empirical phenomena relating to the AB, previously discussed in section 2.3.2. This general comparison of the models aims to bring out their similarities as well as their differences, and feeds into the topic of the next section, which discusses a potential extension to the LC-NE model that combines ideas from

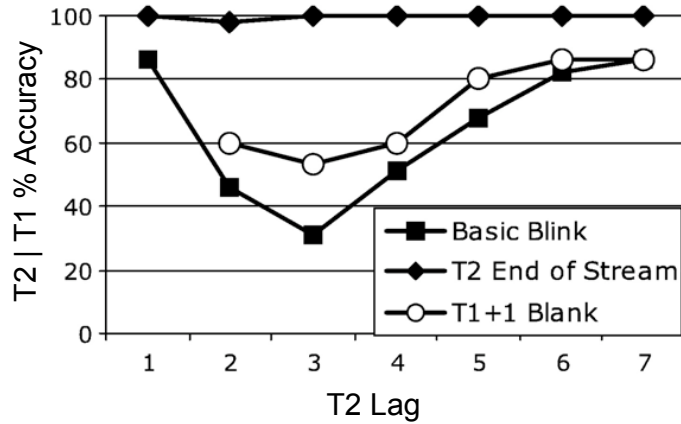


Figure 18 **ST<sup>2</sup> model performance in the AB task.** X-axis denotes lag position of T2, while Y-axis denotes percentage accuracy of T2 report, conditional on the correct report of T1. Note that in the T1+1 Blank condition, there is no lag 1, as that slot is the blank one. Reproduced from Bowman and Wyble (2007).

both approaches.

#### 5.4.1 The ST<sup>2</sup> Model

##### The Basic Blink

The ST<sup>2</sup> model generates a blink because the blaster is suppressed by ongoing T1 tokenisation. T2s at lags 2 and 3 fall at the point of maximum impairment (see figure 18), due to the length of time they have to wait for the blaster to come back online. The impairment decreases monotonically through lags 4, 5 and 6, as it becomes more likely that tokenisation of the T1 finishes before T2 has decayed.

However, at lag 1, the T2 is close enough in time to T1 to take advantage of the (T1-initiated) blaster firing. Thus, the model demonstrates lag 1 sparing (see figure 18). However, although the T2 is typically encoded at lag 1, invariably, this only occurs into the first token, alongside T1.

##### Increased Processing of T1+1 slot

ST<sup>2</sup>'s TAE provides an enhancement that begins shortly after an initiating item (the T1 in an AB setting) and is very brief (lasting around 50ms). Thus, the blaster enhances the

T1 and T1+1 slots. There are a number of phenomena that this mechanism enables the model to exhibit. Firstly, as just discussed, the model generates lag 1 sparing. Secondly, the model’s lag 1 T2 performance has a tendency to be elevated above baseline (i.e. post recovery and single target performance; see Bowman & Wyble, 2007), consistent with findings from Craston et al. (2009). Thirdly, Bowman and Wyble (2007) reproduce the finding by Chua et al. (2001), that a distractor is a more effective prime of a T2 if it is preceded by a T1. Finally, the model is consistent with the finding of labile attention at short T1-T2 SOAs (Potter et al., 2002), in that it allows for a second salient stimulus, T2, to attract processing resources that have already been allocated to an earlier stimulus, T1.

### **Spatial Specificity of Lag 1 Enhancement**

Although the model has not yet been used to simulate spatial phenomena, from a theoretical perspective, the ST<sup>2</sup> blaster is spatially specific. This is consistent with the previous research into this mechanism, viz, transient spatial attention, as identified by Nakayama and Mackeben (1989). As previously discussed, this spatial specificity is consistent with findings in RSVP presentation settings (Visser et al., 1999; Wyble, Bowman, & Potter, 2009).

### **T1-T2 Costs at Lag 1**

ST<sup>2</sup> exhibits T1-T2 costs at lag 1 (see Craston et al., 2009; figure 5B). The loss in T1 accuracy at lag 1 arises because, when T2 is very strong and T1 weak, binding can complete before T1 is strongly active, yielding a successful binding from token 1 to T2 and no binding to T1. Moreover, at lag 1, the model is inaccurate at determining the order of the two targets. At lag 1, often, both T1 and T2 are bound to the first token. This reflects a loss of episodic information: due to the temporal proximity of T1 and T2, the model has failed to allocate discrete episodic contexts for the two targets. These findings of costs at lag 1 are supported by human data (see section 2.3.2).

### **Blink Attenuation with T1+1 Blank**

The model demonstrates the key finding that inserting a blank in the T1+1 slot attenuates the blink. The sequence of events that generates this phenomenon is as follows. Firstly, an

unmasked item yields a strong activation trace. Thus, a T1 followed by a blank generates a higher amplitude trace at the TFL. Secondly, and this is the critical step, tokenisation, both in the sense of binding pool node and token allocation, completes more quickly. This is because, through the gate-trace mechanism (see appendix A.1.2), the model turns activation strength into time to encode, on the principle that stronger evidence for an item (as encapsulated by activation strength) leads to more rapid encoding into WM. Thus, placing a blank after a T1 greatly shortens its tokenisation. Thirdly, tokenisation will be more likely to have finished before the T2 has decayed at the TFL, increasing the probability that the T2 will fire the blaster<sup>2</sup>.

Here, the key principle that blink attenuation with T1+1 blank reflects is that there is a *reciprocal relationship* between bottom-up trace strength and blink depth. This is obtained in ST<sup>2</sup> by tying tokenisation time to trace strength.

### **Blink Attenuation with T2+1 Blank**

We compare the model to data from Giesbrecht and Di Lollo (1998), who examined the effect of placing T2 at the end of the stream (see figure 18). As required, the blink is obliterated. However, the ST<sup>2</sup> model obtains attenuation of the blink with T2 unmasking in a different manner to attenuation with T1 unmasking. Specifically, a T2+1 blank produces strong T2 traces that are more likely to outlive the blink. That is, T2 unmasking does not affect how long the blaster is held offline by T1 tokenisation, but it does make the T2 more ‘resilient’ to this blaster unavailability.

### **Delayed T2 Consolidation**

Following on from above, T2s encoded by ST<sup>2</sup> during the blink typically possess strong activation traces. Variation in activation strength could reflect spontaneous noise or inherent

---

<sup>2</sup>One subtlety of the T1+1 blank data is that performance is particularly elevated at lag 2. The ST<sup>2</sup> model obtains a qualitatively similar pattern at lag 2, as it is the only data point in which T2 is not strongly forward masked. (Although backward masking is far stronger, weak forward masking is also included in ST<sup>2</sup>.) Absence of forward masking increases the bottom-up trace strength of the T2, which gives it a small advantage according to the principles we discuss in the next section. However, it could be that lag 2 sparing in the T1+1 blank condition is actually a reflection of a form of spreading the sparing (see section 2.3.2), because a sequence consisting of a T1 followed by a blank at lag 1 and a T2 at lag 2 is akin to presenting three targets in a row. Consequently, this would explain the quantitatively smaller effect of lag 2 sparing that the ST<sup>2</sup> model currently obtains, as it does not explain spreading the sparing.

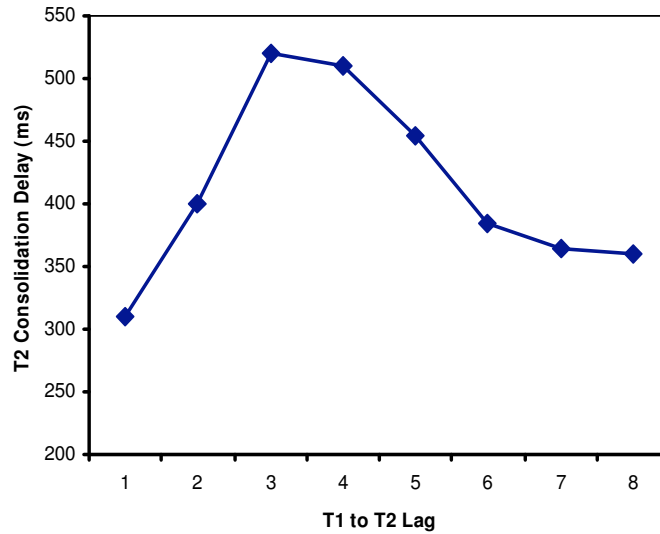


*Figure 19* **T2 consolidation delay by lag for the ST<sup>2</sup> model.** Consolidation delay is measured as the time from target onset to peak amplitude of the TFL unit for that target. At each lag, all seen T2 trials are averaged together. Reproduced from Bowman et al. (2008).

differences in how particular targets stand out (Wyble & Bowman, 2005). Consequently, T2s are often seen during the blink because they outlive blaster unavailability. As a result, in the average, T2s are consolidated later during the blink. Figure 19 shows data from the ST<sup>2</sup> model that encapsulates this effect. T2 consolidation delay qualitatively mirrors the blink curve: T2 consolidation is most delayed when the blink is deepest and un-delayed (i.e. at baseline) post blink recovery. Interestingly, the model suggests that T2 consolidation at lag 1 is accelerated, relative to post recovery baseline, which is consistent with the previously discussed increased processing of the T1+1 slot.

Although a human study that explores the full spectrum of lags is not available, there is considerable evidence from electrophysiology, for delayed T2 P3s during the blink (Martens, Elmallah, London, & Johnson, 2006; Vogel & Luck, 2002) (see section 2.3.2). This provides important support for the ST<sup>2</sup> model.

### Spreading the Sparing

In respect of the parameter settings used in Bowman and Wyble (2007), the ST<sup>2</sup> model does not replicate spreading the sparing. The inhibitory projection from the binding pool to the blaster (marked (c) in figure 11) is sufficiently strong that ongoing tokenisation renders

the blaster unavailable soon after T1 starts to be encoded. Thus, the model exhibits lag 1 sparing, but, in the context of a continuous sequence of targets and a standard SOA of around 100ms, it does not exhibit lag 2 or 3 sparing. This is because, whether interleaved with distractors or not, any target appearing in the 200 to 500ms interval post T1 onset, will not be able to fire the blaster immediately.

A revision of the ST<sup>2</sup> model, in which suppression of the blaster is not absolute and a somewhat more sophisticated token system is used, is described in Wyble, Bowman, and Nieuwenstein (2009). In this revised model, a continuous stream of target-related activity can repeatedly re-fire the blaster, but at the expense of loss of episodic distinctiveness, e.g. order and repetition blindness errors. This revised model also replicates the finding that the blink can be reversed, in the sense that, although a T2 in the sequence T1 D T2 T3 would be blinked, the T3 would not be (Olivers et al., 2005). This is because the T2 overcomes blaster suppression; however, because of the difficulty of re-firing the blaster, T2 misses this benefit, which falls on the T3.

#### **5.4.2 The LC-NE Model**

We now move to an assessment of the LC-NE model. The simulation results that we present are based upon the equations and parameter settings presented in Nieuwenhuis, Gilzenrat, et al. (2005), which was re-implemented for the research described in this chapter. Evidence that we have faithfully replicated the LC-NE model is given by the fact that we generate a blink curve consistent with that found in Nieuwenhuis, Gilzenrat, et al. (2005). (To maintain consistency with the presentation of the ST<sup>2</sup> model and indeed the human behavioural data, we use the conditional measure: T2|T1, instead of the T2 % accuracy measure used by Nieuwenhuis, Gilzenrat, et al. (2005). This change has no qualitative effect on the shape of the basic blink curve.)

#### **The Basic Blink**

The LC-NE model generates a blink curve with lag 1 sparing, as depicted in figure 20. As previously suggested, the blink obtained follows the profile of the LC refractory period and lag 1 is spared, as it benefits from the NE release arising from the T1-induced LC firing.

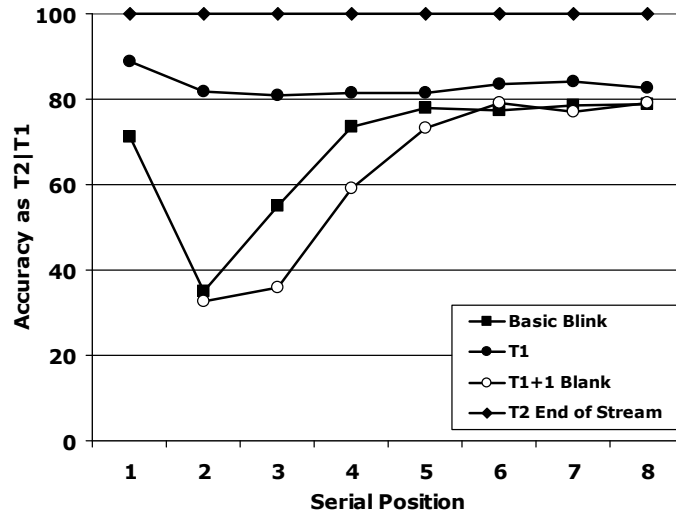


*Figure 20* **Standard blink conditions generated from the re-implemented LC-NE model.** Accuracy is T2|T1 for all conditions except T1. X-axis denotes lag, while Y-axis denotes percentage accuracy of target report. Note that in the T1+1 Blank condition, there is no lag 1, as that slot is the blank one. Reproduced from Bowman et al. (2008).

### Increased Processing of T1+1 Slot

The T1-induced LC firing benefits the T1+1 slot. Furthermore, the enhancement is item non-specific, in the sense that it would also benefit a distractor in the T1+1 slot. Thus, the model should be viewed as consistent with the finding of increased priming from distractors following T1s (Chua et al., 2001). The LC-NE model is also consistent with a temporal, rather than sequential (by-item) interpretation of blink onset. That is, it suggests that the T1-induced enhancement has a minimal extent, which is broadly fixed and is not regulated by intervening distractors. This is supported by a number of findings (see section 2.3.2).

### Spatial Specificity of Lag 1 Enhancement

The LC-NE enhancement is assumed to be completely generalised, both featurally and spatially. That is, any item, whatever its features or spatial location, would be enhanced. In other words, the LC-NE system provides a purely temporal filter. As acknowledged by Nieuwenhuis, Gilzenrat, et al. (2005), this means that the LC-NE model cannot explain the spatial specificity of lag 1 sparing without assuming a further mechanism.

### **T1-T2 Costs at Lag 1**

The LC-NE model does not generate T1-T2 costs at lag 1. Firstly, as can be seen in figure 20, there is no decrement in T1 performance at lag 1. In addition, the model does not encode order information. Thus, the finding of increased order inversions at lag 1 cannot be investigated.

### **Blink Attenuation with T1+1 Blank**

In the LC-NE model, the length of the LC refractory period is not fixed. Rather, stronger LC firings yield a longer refractory period. This raises a problem, as strength of LC firing is determined by the strength of the target that drives it. Thus, greater bottom-up trace strength leads to a longer refractory period. This facet of the model has the consequence that unmasking T1s (i.e., the T1+1 blank condition) deepens and lengthens the blink.

This issue was explored further in simulation runs. As acknowledged by the authors, the LC-NE simulation presented in Nieuwenhuis, Gilzenrat, et al. (2005) does not model masking. Thus, the effects of following a T1 by a 100ms blank instead of a distractor were modelled indirectly. Specifically, an RSVP sequence containing a T1 followed by a blank is modelled as ... D T1 T1 D ..., where a standard (non-blank) T1 is modelled as ... D T1 D D ... (Ds denote arbitrary distractors. See section 5.5 for discussion of the technical issues associated with this manipulation). This approach is consistent with the observation that the after-image of a visual stimulus remains for some hundreds of milliseconds if a masking item does not follow, inferring from the literature on iconic memory (Coltheart, 1983; Sperling, 1960) or single cell recordings of persistence in the visual processing pathway (Keysers & Perrett, 2002; Keysers, Xiao, Földiák, & Perrett, 2005). The results of our simulation of the T1+1 blank condition are shown in figure 20. As predicted, the model shows a deeper and longer blink for this condition, and this is indeed because stronger LC firing (arising from stronger T1s) leads to a longer refractory period. This weakness of the model was acknowledged in Nieuwenhuis, Gilzenrat, et al. (2005).

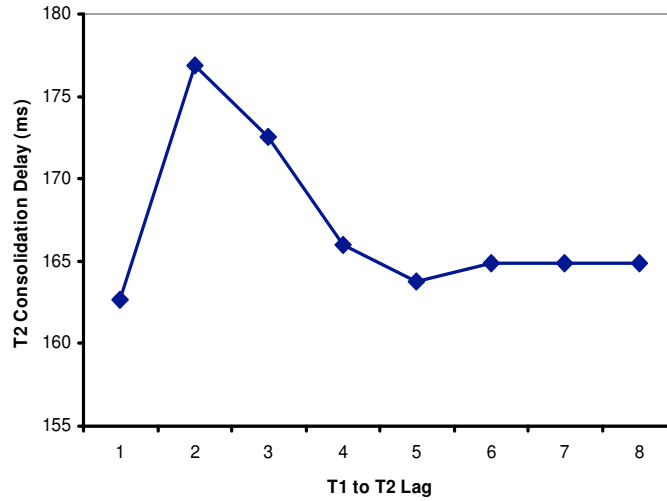


*Figure 21* **T2 consolidation delay by lag for the LC-NE model.** Consolidation delay was measured as the time from target onset to peak amplitude of the detection layer unit for that target. At each lag, all seen T2 trials are averaged together. Reproduced from Bowman et al. (2008).

### Blink Attenuation with T2+1 Blank

The LC-NE model does generate blink attenuation with a T2+1 blank. In order to match T2 end of stream data, a similar manipulation to that just discussed was investigated, but now for T2. Specifically, sequences of the form ... D T1 D D T2 D ... (basic blink, lag 3) were compared with those of the form ... D T1 D D T2 T2 ... (T2 End of Stream, lag 3). As with humans (see figure 2), the model exhibited ceiling performance (see figure 20). Also, as was the case with the ST<sup>2</sup> model, the blink is removed with T2 unmasking, as high amplitude T2s benefit from higher intrinsic strength and a greater ability to outlive the LC refractory period.

### Delayed T2 Consolidation

T2 consolidation latencies are indeed delayed during the blink. This can be seen in figure 21, which shows the results of generating T2 consolidation latencies from our re-implemented LC-NE model. Furthermore, as was the case for ST<sup>2</sup>, the LC-NE model generates accelerated P3 consolidation latencies (relative to recovery baseline) at lag 1. This is again because the lag 1 item benefits from the T1-induced enhancement, which here amounts to NE release generated by the T1-induced LC firing. In fact, the LC-NE model generates the

same qualitative pattern of T2 consolidation latencies by lag as the  $ST^2$  model, which gives strong credence to this particular theoretical prediction. In comparing the T2 consolidation delay produced by the  $ST^2$  and LC-NE models, it should be noted that even though the qualitative match between these two sets of data is very good, quantitatively they are very different, as reflected by them being presented on very different scales (see figures 19 and 21).

### **Spreading the Sparing**

The LC-NE model does not generate spreading the sparing. This is evident in the lag 2 data point of the T1+1 blank condition, see figure 20. As previously discussed, this data point is modelled as a stream of distractors containing the subsequence T1 T1 T2, i.e. a continuous sequence of targets. For this data point, the model performs below the basic blink curve (see figure 20), while humans are almost at baseline performance (see figure 2).

Because of the nature of the LC refractory period, the LC-NE model fails to spread the sparing. This is because, firstly, if a T1 fires the LC, it will go into a refractory period (in this sense it is ballistic) and, secondly, ongoing bottom-up activation to the LC (as generated by a continuous stream of targets) cannot overcome the refractory period. Investigations with the LC-NE model suggest that a continuous stream of particularly strong targets can change the shape of the refractory period, preventing it from being so deep. However, (with the current parameter settings) the length of the refractory period is not shortened by this manipulation. Thus, once it starts, the refractory period has to run to completion.

### **5.4.3 Discussion**

Beyond the realm of specific behavioural phenomena, there are a number of other important differences between the  $ST^2$  and LC-NE approaches. Firstly,  $ST^2$ 's TAE, i.e., the blaster is an additive enhancement, while the LC enhances by increasing the gain of the activation function. Thus, the mechanism in Nieuwenhuis, Gilzenrat, et al. (2005) is multiplicative, which yields a gating aspect that is not present in the blaster.  $ST^2$ 's additive enhancement has the virtue of simplicity; in particular, it does not require any mechanisms that are not present in standard neural network frameworks. However, although the additive bias approach works well in the  $ST^2$  context, in which the enhancement is very brief, we have

had trouble modelling spreading the sparing with this mechanism. Spreading the sparing suggests a more sustained amplification or, at least, a rapid series of pulses of transient attention. In this context, an additive bias is susceptible to pushing even stimuli never presented over threshold, due to the accumulation over time of additive excitation. As a result, our revision of the ST<sup>2</sup> framework to handle spreading the sparing, has moved to a multiplicative gain in further work (Wyble, Bowman, & Nieuwenstein, 2009), which avoids this problem. Thus, in this respect, the ST<sup>2</sup> and LC-NE frameworks seem to be coming together.

Secondly, as acknowledged by the authors (Nieuwenhuis, Gilzenrat, et al., 2005), their approach does not sustain a memory trace to the end of a trial. That is, T1 and T2 activations rise and fall at the detection layer with a time-course in the range of a few hundred milliseconds of simulated time. WM maintenance is viewed as a separate mechanism that is beyond the scope of the LC-NE model. In contrast, the ST<sup>2</sup> model incorporates token micro-circuits that implement durable, activation-based WM maintenance of encoded targets and support their association with types.

Thus far, this chapter has demonstrated that both the ST<sup>2</sup> and LC-NE models generate a number of the key empirical phenomena. However, both have difficulty with spreading the sparing and the LC-NE model additionally has difficulties with blink attenuation with T1+1 blank, T1-T2 costs at lag 1 and requires the assumption of an additional mechanism to explain the spatial specificity of the lag 1 enhancement. A full elaboration on how these models could be extended to explain all these phenomena is beyond the scope of this exploration. Nevertheless, the next section focuses on how the LC-NE model could be extended in order to model an important aspect of the human data, namely the reciprocal relationship between bottom-up trace strength and the AB bottleneck. This extension will provide the additional benefit of adding a WM maintenance mechanism to the model. Furthermore, the implications of such additions for LC neurophysiology are discussed.

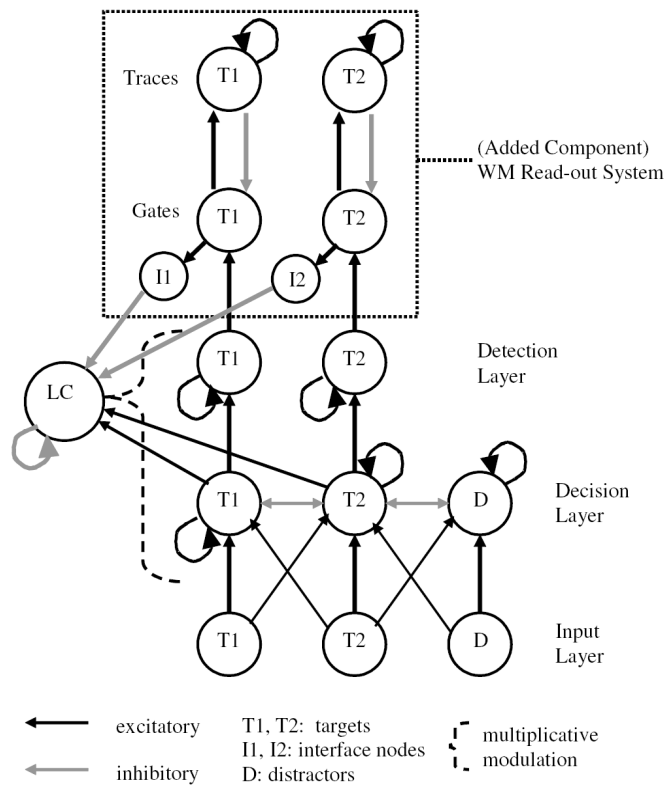


*Figure 22* **The extended LC-NE model.** Crosstalk connections between T1 and D are not shown for visual clarity. Point sizes of arrows indicates weight strength. Interface nodes connect the gate-trace system with the LC, ensuring gradual interactions between them. Reproduced from Bowman et al. (2008).

## 5.5 Extension of the LC-NE Model

This section considers a possible extension of the LC-NE model that would enable it to simulate blink attenuation with T1+1 blank and maintain items in WM beyond encoding. The intent here is not to develop a fully formed alternative AB model. Rather, this section simply considers a possible extension of the LC-NE model that would enable it to simulate blink attenuation with T1+1 blank and maintain items in WM beyond encoding. The mechanisms that considered here are inspired by those already present in ST<sup>2</sup>. This is undertaken as an exploratory exercise that, in particular, could inform further neurophysiological explorations of the LC-NE system, especially of the major projections between the cortex and LC. It thus also clarifies the neurophysiological implications of the cognitive-level mechanisms proposed by ST<sup>2</sup>.

In the LC-NE network, transient representations of decision results arise at the detection layer, which is where the model finishes. However, one could also imagine a WM encoding system that ‘reads out’ from these detection layer activations. Such a system could be based upon the gate-trace mechanisms from the ST<sup>2</sup> context (see appendix A.1.2). This possibility is explored in the context of the LC-NE model. However, it is important to note that in this exploration, the basic LC-NE model remains unchanged; thus, the changes discussed here are a strict extension of the LC-NE model published in Nieuwenhuis, Gilzenrat, et al. (2005). The structure of the extended system is shown in figure 22. Please refer to appendix A.3 for more details on the implementation of the extended LC-NE model.

As is inherent in the gate-trace approach, the trace neurons maintain items in WM, while gate neurons enable items to be encoded into WM, i.e. they gate access to trace neurons. The gate-trace extension to the LC-NE model behaves as follows. Firstly, activation onset of gate neurons mirrors detection node activations, subject to a small time delay. Secondly, active gate neurons drive their corresponding trace neuron until it crosses threshold, at which point encoding is deemed to have completed. As a result, the trace neuron rapidly suppresses its gate and enters a self-sustaining attractor state at which point the target has been successfully encoded into WM.

Thus, the gate-trace extension adds the capacity to hold items in WM once they have been successfully encoded. However, in addition, the extension ties LC suppression to

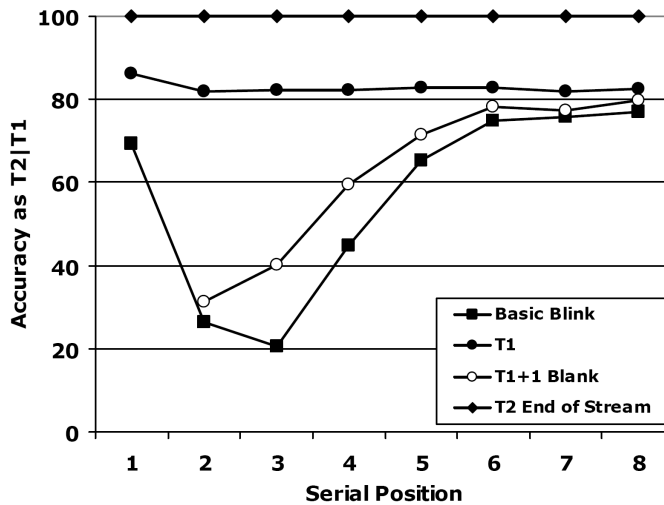


Figure 23 Standard blink conditions generated from the extended LC-NE model. Accuracy is T2|T1 for all conditions except T1. For T1+1, lag 1 is not a valid data point, as it contains the blank. Reproduced from Bowman et al. (2008).

ongoing encoding, in keeping with the ST<sup>2</sup> principle that withholding of the attentional enhancement should be coupled to length of WM encoding. Thus, a projection from gate neurons to the LC has been added. Overall, this has an inhibitory effect on the LC, although it passes through an intermediate node on the way. These intermediate ‘interface’ nodes connect gate neurons with the LC. They are needed to turn the sharp changes in activation that occur at the gates into more gradual effects on the LC. Sharp discontinuities of input to the LC, whether they be excitatory or inhibitory, disrupt the sensitive balance between LC state and NE level, generating spurious, unregulated changes in LC state. This is particularly the case with regard to the offset of activation of the T1 gate, which (due to trace neuron suppression) is very rapid.

### 5.5.1 Performance of the Extended LC-NE Model

The behaviour of the extended LC-NE model with regard to key AB phenomena (see section 2.3.2) is shown in figure 23. In simulations with the extended LC-NE model, a target is considered as ‘seen’ if its corresponding trace neuron is in its attractor state at the end of a trial<sup>3</sup>.

<sup>3</sup>In contrast, the detection unit crossing threshold designates the target as ‘seen’ in the original LC-NE model.

The extended LC-NE model generates an interesting profile of data. Firstly, it generates a longer basic blink curve, which is more consistent with human data. Secondly, attenuation of the blink with T2+1 is preserved. Thirdly, as anticipated, the model obtains blink attenuation with T1+1 blank. The lag 2 data point remains a difficulty with the LC-NE model, as performance can only recover, at best, to the level defined by the refractory period, no matter how rapidly the T1 is encoded. This difficulty would be partially offset by an implementation of weak forward masking, as implemented in the ST<sup>2</sup> model. Furthermore, as suggested previously, the good human performance observed at lag 2 in the T1+1 blank condition could be attributed to a spreading the sparing-like effect. This is because the T1+1 blank is akin to sustaining an iconic representation of T1, yielding a continuous sequence of target-related activity. This effect is not explained by the extended LC-NE model.

Finally, there is the issue of what the neurophysiological implications are for the extensions introduced to the LC-NE model. Firstly, there is nothing controversial about gate-trace circuits, as inhibitory inter-neurons are common-place in the brain (O'Reilly & Munakata, 2000). The central point of uncertainty is the suggested projection from WM encoding areas to the LC, which are posited to have an inhibitory effect. Although it is known that there are major projections from frontal areas (especially orbital frontal cortex and the anterior cingulate) to the LC (Aston-Jones & Cohen, 2005), whether these have the required characteristics to support the extended LC system remains to be answered. For an approach such as that suggested in this section to obtain greater credence, projections such as these would need to be identified in the primate brain.

## 5.6 Final Discussion

The ST<sup>2</sup> model provides a concrete and broad scope theory of the AB, which matches a large spectrum of empirical phenomena. In particular, the model generates a blink curve with lag 1 sparing, increased processing of the T1+1 slot, blink attenuation with T1+1 blank, blink attenuation with T2+1 blank, delayed consolidation for T2s seen during the blink and T1-T2 costs at lag 1. In addition, the mechanisms postulated are consistent with the known spatial specificity of the lag 1 enhancement and a late stage blink bottleneck.

On the other hand, the LC-NE model suggests a compelling theory for the cause of the

AB based on a neurophysiologically prescribed theory of attentional function. The model also generates a number of the key AB phenomena; for example, it generates a blink curve with lag 1 sparing, increased processing of the T1+1 slot, blink attenuation with T2+1 blank and delayed consolidation for T2s seen during the blink. It is also broadly consistent with a late stage bottleneck. However, it does not generate blink attenuation with T1+1 blank, T1-T2 costs at lag 1, and the LC theory does not suggest a spatially specific lag 1 enhancement.

While the ST<sup>2</sup> model is neurophysiologically plausible, in the sense that it is formulated using known neurobiological mechanisms, there is uncertainty concerning the exact localisation of some of ST<sup>2</sup>'s components. Thus, an exploration of the relationship between the LC-NE model's brain-level proposal and the ST<sup>2</sup> model's cognitive-level proposal is potentially valuable, and has been the focus of this chapter. Although it should also be acknowledged that, when comparing the two models, they have somewhat different intent and scope. ST<sup>2</sup> is a more elaborate model than the LC-NE model, containing more layers and components. This reflects ST<sup>2</sup>'s intent to be a relatively broad scope model of temporal attention and WM encoding and maintenance. In contrast, the LC-NE model, as presented in Nieuwenhuis, Gilzenrat, et al. (2005), does not claim to model WM, rather its value lies with the fact that a blink effect is obtained despite only adding a minimal set of additional assumptions to those included in previous LC-NE simulations (Gilzenrat et al., 2002).

### 5.6.1 The Blaster and the LC

The LC enhancement and ST<sup>2</sup>'s blaster have a number of similarities, e.g. both are initiated by detection of a salient stimulus, they are type non-specific and their temporal profiles are similar. However, there are important differences between the two.

Firstly, the blaster is postulated to have its effect on stimulus representations relatively early in the processing pathway, certainly no later than inferotemporal cortex and perhaps actually in visual cortex (Bowman & Wyble, 2007). The hypothesis being that 'blasted' types obtain greater bottom-up trace strength, giving them a tokenisation advantage. Thus, in ST<sup>2</sup>, the attentional gate works by regulating bottom-up trace strength. In contrast, the LC is suggested to have its main effect on decision and response systems (Aston-Jones & Cohen, 2005). Furthermore, LC innervation is not dense in visual cortex (especially

primary visual cortex) (Nieuwenhuis, Aston-Jones, & Cohen, 2005) and LC innervation of the temporal lobes is more focused on the superior temporal gyrus (especially, the Temporoparietal Junction (TPJ)) than the inferior temporal gyrus.

Secondly, the blaster is assumed to be spatially specific; however, the LC enhancement would be expected to be spatially general, as suggested by neuroanatomical studies of the pattern of noradrenergic projections (Nieuwenhuis, Aston-Jones, & Cohen, 2005). The LC-NE approach cannot resolve this difficulty without introducing a further mechanism that enhances specific locations, and that mechanism is likely to be similar to ST<sup>2</sup>'s blaster. One speculative (and perhaps less than parsimonious) explanation could be that the LC provides the temporal profile of a transient form of attention, such as produced by the blaster. One of the candidate areas for locating the blaster is the TPJ (Bowman & Wyble, 2007; Corbetta & Shulman, 2002; Serences et al., 2005) and the LC is known to strongly innervate the TPJ. If one assumed a spatially specific amplifier at the TPJ, then the LC could be 'amplifying the amplifier' in a transient fashion.

### 5.6.2 Correlates of the P3

An important question is how to relate models to the P3. The LC-NE theory suggests a specific neural substrate for the P3 (Nieuwenhuis, Aston-Jones, & Cohen, 2005). The link from activation traces in the LC-NE model to the P3 though is not as clear cut. In particular, all the target-induced activations in the LC-NE model peak and indeed finish a good deal earlier than the known time-course of the P3, as is evident in figure 21. Thus, these target-induced activations are not direct analogues of the P3. This leaves the possibility that the P3 is an indirect (delayed) consequence of these target-induced activations; that is, that there is a latency offset between model activation traces and what is observed as the P3. However, a judgement of the validity of this explanation awaits a concrete proposal for the mechanics of this further latency offset. Although not perfect, the time-course of ST<sup>2</sup> target activation (especially at the TFL) is more consistent with that of the P3, which, in an RSVP setting, peaks between 400 and 450ms after the onset of the eliciting stimulus. Indeed, as introduced in chapter 4 and discussed in later chapters, the ST<sup>2</sup> model has been successfully used to generate virtual ERP components, which are compared with human ERPs (Craston et al., 2009; Chennu, Craston, Wyble, & Bowman, 2008), including the P3.

## 5.7 Conclusions

The comparative evaluation of the ST<sup>2</sup> and LC-NE models in this chapter has described the implementation of TAE in both models, and assessed their ability to explain the main AB phenomena. In doing so, we have gained key insights into how the behaviour and neurophysiology of temporal attention and the AB could be related. In addition, the proposed extension to the LC-NE model has attempted to combine ideas from both models and bridge across their levels of explanation. The following chapter shifts focus to explore a different aspect of the temporal spotlight, namely the influence of target discriminability on its temporal dynamics.

## Chapter 6

# Target Discriminability and Temporal Perception

How does the discriminability of targets from distractors affect the temporal dynamics of visual perception? This is the question investigated in this chapter. This issue is explored using evidence from EEG data, and complementary neural network modelling. Specifically, we describe an experiment that manipulates the discriminability of targets in RSVP between two contrasting conditions, one in which targets are discernible by their visual onset, and another in which a categorical discrimination must be made to distinguish targets. We then examine the effect of this on the evoked EEG activity, and attempt to explain the pattern of changes by simulations involving the ST<sup>2</sup> model. As we shall see, this exercise adds to our understanding of how the process of target discrimination influences the latency of attentional deployment, in addition to informing issues related to the equivalence of previous AB experiments.

### 6.1 Introduction

The deployment of endogenous attention allows the visual system to selectively enhance the neural representations of task-relevant features in the environment. Our understanding of the neurophysiology of vision in monkeys suggests that focal attention can modulate neural activity very early in the visual processing pathway. Studies of neural firing patterns in

spatial selection tasks report correlates of endogenous attention in the extrastriate visual cortex, when a salient feature must be discriminated and selectively enhanced in the presence of competing spatial distractors (Reynolds, Chelazzi, & Desimone, 1999; Luck et al., 1997; Chelazzi, Miller, Duncan, & Desimone, 2001). In humans, ERP studies of selective spatial attention have found that stimulus features at attended locations are enhanced as early as 70-80ms after onset (Hillyard & Anllo-Vento, 1998). But how does selective attention operate in time? Specifically, when the visual system is rapidly presented with successive fleeting stimuli at an already attended spatial location, how quickly can it discriminate a target embedded in a sequence of distractors, and generate a transient attentional enhancement? In this regard, previous behavioural research has found that the extent to which irrelevant distractors temporally interfere with target processing critically depends on how effectively the visual system is configured to distinguish between featural characteristics of targets and distractors (Visser et al., 2004).

Visser et al. (2004) use two variants of a sequential stimulus presentation paradigm, previously used by Ward et al. (1997) to study the Attentional Blink. In the typical RSVP variant, targets are inserted in a sequential stream of distractors presented at the same spatial location. In the second variation, referred to in this chapter as *Onset* (termed the ‘Skeletal’ task by Ward et al. (1997)), no stream of distractors is used. Instead, targets are briefly presented and are followed by a backward visual mask. See figure 60 in appendix B.2 for samples streams from the Onset and RSVP conditions.

The Attentional Blink deficit is found in many previous studies employing Onset presentation (Ward et al., 1997; McLaughlin et al., 2001; Visser et al., 2004; Rolke et al., 2007). The AB curves obtained therein are shown in figure 24. However, Visser et al. (2004) have found that the presence of distractors in RSVP nevertheless influences the difficulty of target selection during the AB. In addition to the reduction in behavioural accuracy, another common finding observed with RSVP is lag 1 sparing, which is missing with Onset presentation<sup>1</sup>.

---

<sup>1</sup>An exception to this pattern is data reported by Visser et al. (2004) (see figure 24C), which suggests a small amount of lag 1 sparing even with Onset presentation.

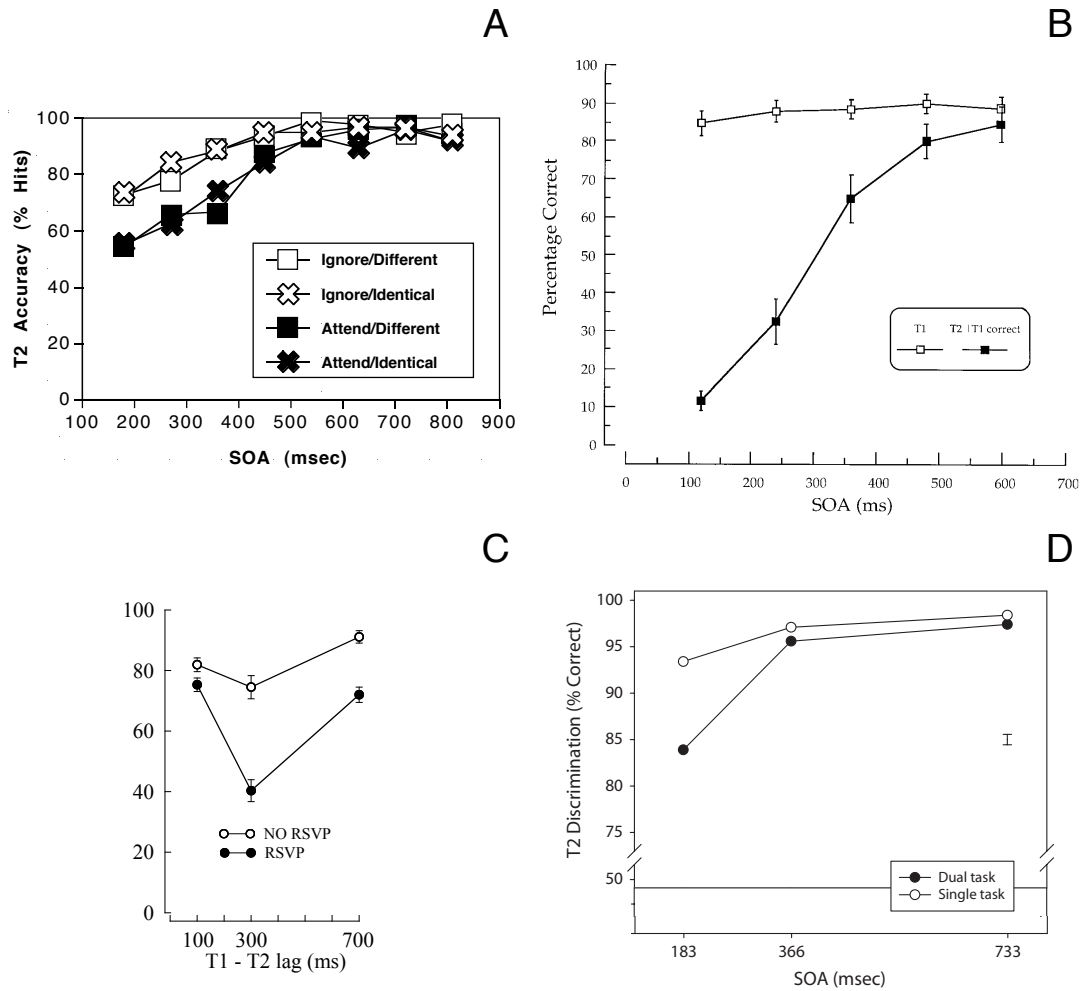


*Figure 24* **Behavioural accuracy scores from AB studies using Onset presentation.** Panel A: Reproduced from Ward et al. (1997). The ‘Attend/Different’ and ‘Attend/Identical’ conditions represent Onset presentation with two different and identical targets, respectively. The ‘Ignore/Different’ and ‘Ignore/Identical’ conditions were similar, but participants were required to ignore the first target. Panel B: Reproduced from McLaughlin et al. (2001). White squares show T1 accuracy per lag. Black squares indicate T2 accuracy per lag conditional on T1 being correct. Panel C: Reproduced from Visser et al. (2004). The ‘No RSVP’ condition represents Onset presentation. Panel D: Reproduced from Rolke et al. (2007). White circles (Single task) show T2 accuracy per lag when subjects were instructed to ignore T1 and report T2. Black circles (Dual task) show T2 accuracy per lag when subjects were instructed to report both T1 and T2 per lag.

### 6.1.1 Motivation and Overview

Taken together, previous behavioural research clearly shows that when distractors are featurally similar to targets, accuracy of target identification is reduced. This chapter builds upon this finding, and investigates how the time course of target processing is affected by target discriminability. Adapting an experimental paradigm similar to that used by Visser et al. (2004), we record EEG data in an experiment that aims to compare the temporal dynamics of the underlying neural processing evoked by a single target presented in the Onset and RSVP conditions. We choose a simple one-target setup for our experiment to keep its design simple, to avoid potential confounds arising from multiple targets, and to allow us to focus on specific questions relating to EEG dynamics. Importantly, we complement the analysis of the data from our experiment with a theoretical exploration. Specifically, we compare the differences in the ERP signatures evoked by targets presented in the above conditions, and propose an explanation of these differences within the context of the ST<sup>2</sup> model. To this end, we take the ST<sup>2</sup> model as described in section 3.1, and by performing a sequence of theoretically sound changes to its configuration, we enable it to simulate the Onset condition. The modifications are validated by comparing virtual ERP traces generated from the model to human ERP traces. As we shall see, the model provides a convincing explanation of the pattern of experimental results, in addition to informing questions about the cognitive equivalence of target processing in masking and RSVP experiments.

## 6.2 The Single Target Experiment

This chapter analyses behavioural and EEG data from Experiment 1, which employed a blocked design with two conditions of interest: trials in the RSVP condition had single letter targets embedded within a centrally presented RSVP stream of digit distractors presented at a rate of 47.1ms. In comparison, the Onset condition consisted of single letter targets presented on their own, and followed by a digit mask immediately after, both presented for 47.1ms. Participants were required to report the identity of the letter at the end of each trial. The P3 ERPs analysed below were recorded at the P7 and P8 electrodes. Please refer to appendix B.1 for a detailed overview of the experimental method.

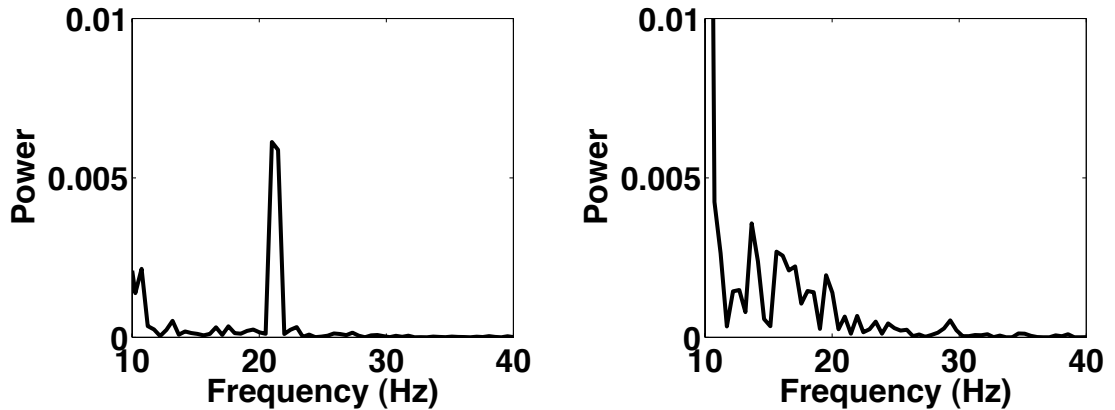


*Figure 25* Fast fourier transforms (FFT) of the ERPs for the RSVP (left) and Onset (right) conditions. The ERPs are averaged across the P7 and P8 electrode locations. The RSVP condition shows a peak in the FFT plot at the frequency of target presentation (approx. 21Hz), which is not present for Onset presentation. Reproduced from Chennu et al. (2009b).

### 6.3 Target Processing in Onset Presentation

We first present the behavioural and electrophysiological results for targets in Onset presentation and targets in RSVP. Following this, we elaborate on how the ST<sup>2</sup> model can be modified in order to simulate Onset presentation and conclude this section with a theoretical discussion.

#### 6.3.1 Behaviour

Overall, when compared to RSVP, Onset presentation makes targets easier to detect. Participants report 76% of targets correctly if they are embedded in a regular RSVP stream, whereas in the Onset condition target accuracy is 86%. This difference is statistically significant:  $F(1,16) = 7.87$ ,  $MSE < 0.01$ ,  $p = 0.01$ , and corroborates a similar finding by Visser et al. (2004).

#### 6.3.2 Early Components

Whether a target is presented in Onset presentation or RSVP has a strong effect on early processing. Figure 26 illustrates a highly significant difference in the P1 and N1 ERP early components between targets in RSVP and Onset presentation. The mean absolute value in the area from 0-200ms after target presentation is  $3.3\mu V$  for targets in Onset streams and

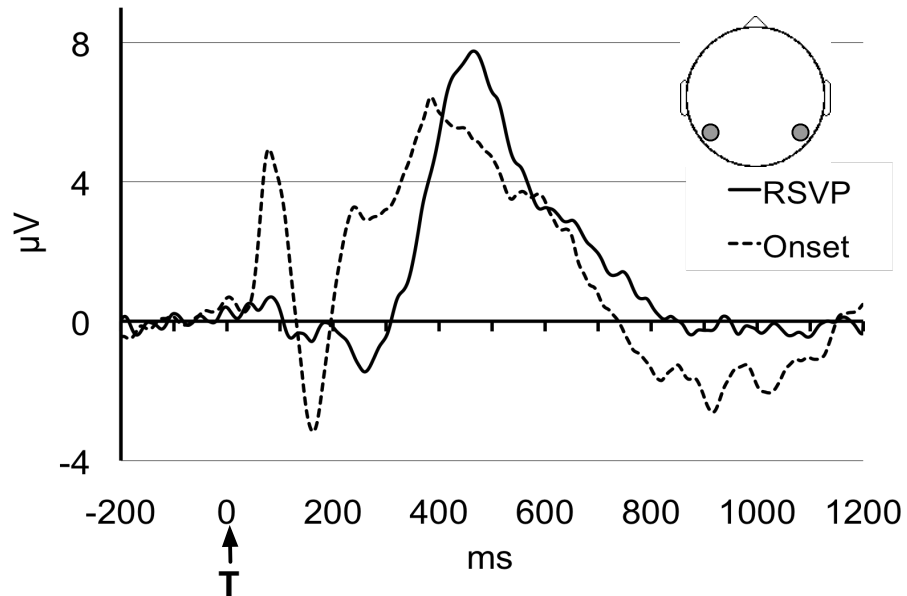


*Figure 26* **Human P3 for targets in RSVP and Onset presentation.** The ERPs are averaged across the P7 and P8 electrode locations. ERPs are time-locked to target presentation time ‘T’. Reproduced from Chennu et al. (2009b).

1.02 $\mu$ V for targets in RSVP ( $F(1,16) = 91.93$ ,  $MSE = 0.479$ ,  $p < 0.001$ ).

Instead of evoking the P1/N1 complex of early components, RSVP targets produce an ssVEP (steady state Visual Evoked Potential) wave (Di Russo et al., 2003) oscillating at the same frequency as the presentation rate of items in the RSVP stream. As seen in Figure 25, each item is presented for 47.1ms (corresponding to the RSVP rate of roughly 20 items per second), resulting in a peak at approx. 21Hz in the FFT plot for the RSVP condition.

### 6.3.3 The P3

The P3 component, which is depicted in Figure 26, temporally overlaps with the ssVEP evoked by the sequence of distractors preceding and following the target, and shows a different profile for Onset compared to RSVP targets. The 50% area latency (Luck & Hillyard, 1990) of the P3 in the 200-800ms window is shorter for Onset (mean 452.59) than RSVP targets (mean 518.53ms). This difference is marginally significant;  $F(1,16) = 4.16$ ,  $MSE = 8885.97$ ,  $p = 0.06$ . However, the difference in the mean or peak amplitude of the P3 in the 200-800ms window is not significant.

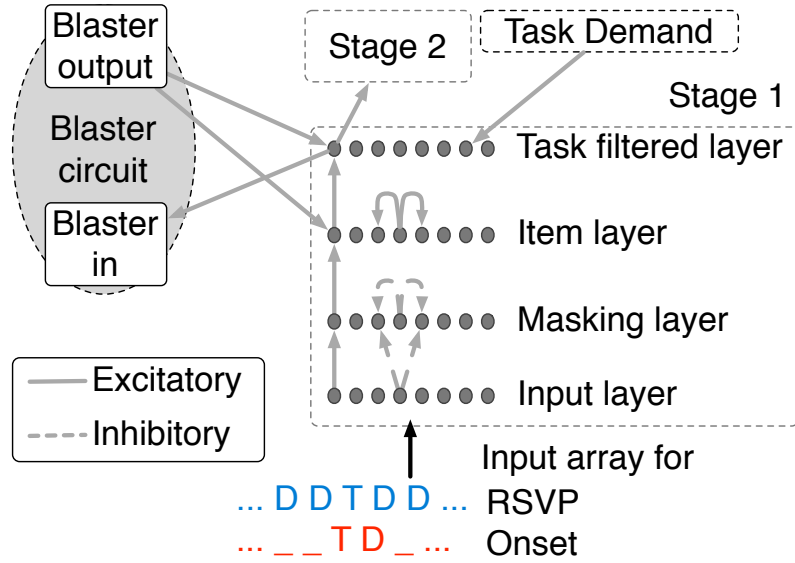


Figure 27 **Step 1 of simulating Onset presentation.** As indicated in the figure, the input array to the model is modified by removing distractors.

## 6.4 Modelling Onset Presentation with the ST<sup>2</sup> Model

The ST<sup>2</sup> model as published in Bowman and Wyble (2007) and described in Section 3.1 cannot simulate Onset presentation. In the following, we will show how, by making a number of theoretically justified changes to the architecture of the model, we can replicate our experimental results with respect to Onset presentation, with respect to both behavioural and EEG data. Please refer to appendix B.1 for more details of the model configuration.

### 6.4.1 Step 1: Simulating Early Components

#### Manipulation

In Onset presentation, the stream contains just the target and the distractor following the target. All other distractors are replaced by blank intervals. In order to simulate such a stream in the ST<sup>2</sup> model, we modify the array of values that serve as input to the model. As depicted in figure 27, all distractors - except the one following the target - are set to a value of zero, equivalent to no activation.

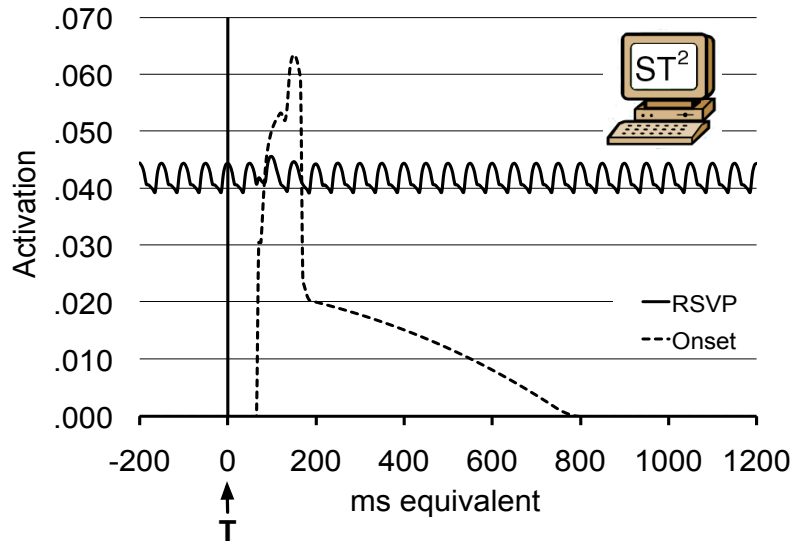


Figure 28 **Virtual ssVEP wave for the RSVP and early components for the Onset conditions.** The virtual ERPs are recorded from the input and masking layers of the ST<sup>2</sup> model. ‘T’ indicates the presentation of the target. ERPs are time-locked to presentation of the target. Reproduced from Chennu et al. (2009b).

## Results

The modification of the input array has a strong effect on virtual ERP traces resembling early visual processing. For targets in RSVP, the model shows a continuous *virtual ssVEP* wave oscillating at the frequency of target presentation (figure 28), replicating the pattern of human data observed in figure 25. The first item of the RSVP stream causes an increase of activation in early layers of the model, and subsequent stimuli excite early layers and suppress previous stimuli due to masking, producing a sustained oscillation that lasts until the end of the RSVP stream. In effect, the cumulative effect of early visual processing in the model manifests as the virtual ssVEP, instead of as distinctive early virtual ERP components. Note that the average activation in the virtual ssVEP in figure 28 is constantly above zero, because of continual input from the RSVP stream. However, the actual value of this activation has no particular significance. In human EEG data, baseline corrections ensure that the mean amplitude over time of the human ssVEP is close to zero.

In contrast, in Onset presentation, there are no distractors and hence there is no activation preceding the target. Presentation of the target creates a strong burst of activation at early layers of the ST<sup>2</sup> model. As there is no forward masking, the activation evoked by

the Onset target at early layers is higher than in regular RSVP. The distractor following the target in Onset presentation then produces a second large burst of activation, as it is not constrained by backward masking. All of this activation at early layers occurs between the model equivalent of 100 and 200ms following target presentation.

Overall, there is a general qualitative match between the observed changes in the virtual ERPs (figure 28) and the human early ERP components (figure 26), comparing across the RSVP and Onset conditions. Virtual ERP activation associated with early visual processing shows a distinct activation for Onset targets and an oscillatory pattern for RSVP targets. However, it is evident that there are considerable differences between the virtual ERP for the Onset condition and the P1/N1 complex observed in the human ERP. This is because the ST<sup>2</sup> model does not incorporate much of the complexity of early visual processing that underlies this complex. Furthermore, many factors, such as the distortion of the signal by the scalp, are not simulated<sup>2</sup>. Nevertheless, by matching the model to human behaviour and comparing the consequently generated virtual ERPs again their human counterparts, we have attempted to provide an common explanation for patterns of change in the behavioural and EEG data.

## 6.4.2 Step 2: Simulating the P3

### Manipulation

Replication of behavioural accuracy and the virtual P3 component requires theoretically justified changes to the architecture of the ST<sup>2</sup> model. Onset targets appear on a previously blank screen, whereas in RSVP, the target has to be selected from a continuous stream of distractors. In terms of the ST<sup>2</sup> model, we hypothesise that the difference between target detection in these conditions influences the way in which the blaster is triggered:

- In RSVP, the system cannot distinguish targets from distractors until they have reached the TFL. There, the task demand mechanism acts as a filter, selectively enhancing targets and inhibiting distractors.
- In Onset presentation, there are no distractors preceding the target, hence, the system

---

<sup>2</sup>See the Dynamic Causal Modelling (DCM) technique (David et al., 2005, 2006) for an example of an approach to modelling ERPs that is based on a neurobiologically constrained source reconstruction.

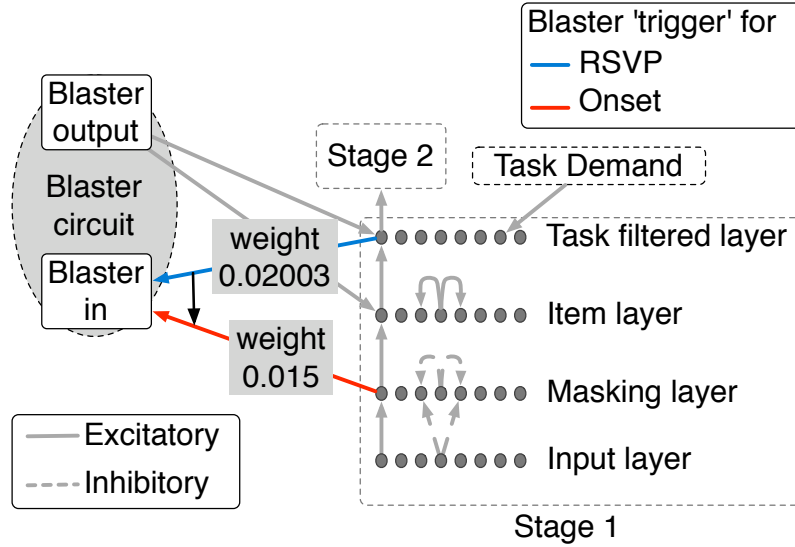


*Figure 29 Step 2 of simulating Onset presentation.* The connection from Stage 1 that triggers the blaster is moved from the task filtered layer to the masking layer. Reproduced from Chennu et al. (2009b).

can assume that the first item that is ‘presented’ to the input layer is the target. Accordingly and as seen in Figure 29, we propose that in Onset presentation, the blaster is triggered as soon as activation reaches the masking layer<sup>3</sup>. Moving this connection from the TFL to the masking layer also requires a modification of the weight value of that connection (see Figure 29), because activation levels in the TFL and masking layers differ<sup>4</sup>.

## Results

Activation propagates through the ST<sup>2</sup> model with a temporal lag from one layer to the next. Hence, if the blaster is triggered from the masking layer, the blaster fires at an earlier timepoint relative to target onset than if activation has to propagate to the TFL before the blaster can be triggered. Consequently, the blaster’s output is also shifted earlier in

<sup>3</sup>For the purpose of simulating Onset presentation, our manipulation produces the desired effect. However, our modification of the model architecture would have to be reconsidered in order to simulate a slightly different stream setup, for instance, if the target was also preceded by distractor items (e.g. a stream of the type ‘D D T D’). Under these circumstances, the distractors can potentially also fire the blaster, as task demand does not operate until the TFL and, hence, the system cannot distinguish targets from distractors at the masking layer. Note, however, that although distractors can fire the blaster in Onset presentation, task demand at the TFL will prevent distractors from being tokenised.

<sup>4</sup>Compared to the TFL, activation values at the masking layer are higher in absolute terms. Hence, we reduce the weight values between masking layer and blaster, to prevent the blaster circuit from being overcharged by the input from the masking layer.

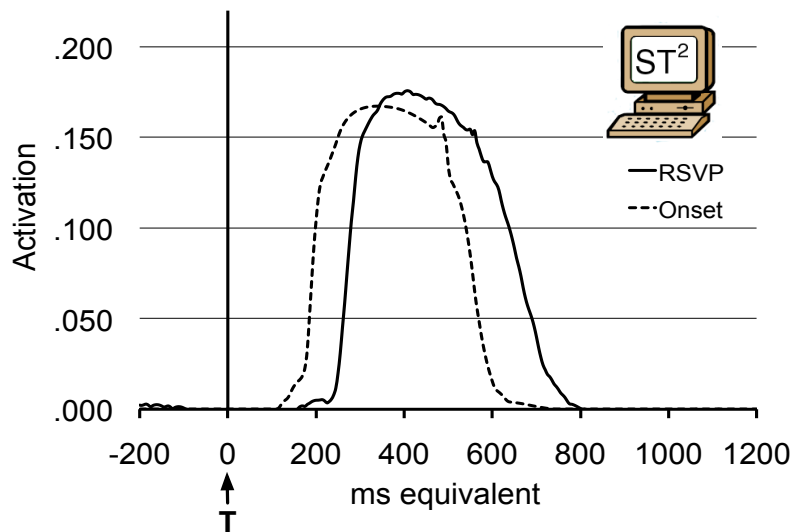


*Figure 30* **After Step 2: Virtual P3 for the RSVP and Onset conditions.** The RSVP virtual ERP is baseline corrected to -200 to 0ms with respect to target onset to account for distractor related activity, which is absent in the Onset condition. ERPs are time-locked to target presentation time ‘T’. Reproduced from Chennu et al. (2009b).

time. The first consequence of this change is a shift in latency of the virtual P3 for Onset compared to RSVP targets, as seen in Figure 30. With the change in model architecture to reflect processing of Onset targets, the blaster is triggered earlier, and thus initiates the target’s tokenisation and virtual P3 earlier than in the RSVP condition.

The change in model architecture means that the blaster now fires for all Onset targets. This correctly increases the accuracy of the ST<sup>2</sup> model at encoding Onset targets relative to RSVP targets (100% vs 77%). Furthermore, the same change in the model that simulated the behavioural effect also produces a latency difference in the virtual P3: the 50% area latency of the virtual P3 in the 200-600ms window is shorter for Onset (365ms) than for RSVP targets (430ms). This pattern replicates the significant latency difference observed in human P3 data.

Although behavioural accuracy in the Onset condition should indeed be above RSVP accuracy, this is not a very good replication of the human behavioural performance for detecting Onset targets, which is below ceiling. A further modification of the weight value between masking layer and blaster does not have the desired effect on simulated accuracy

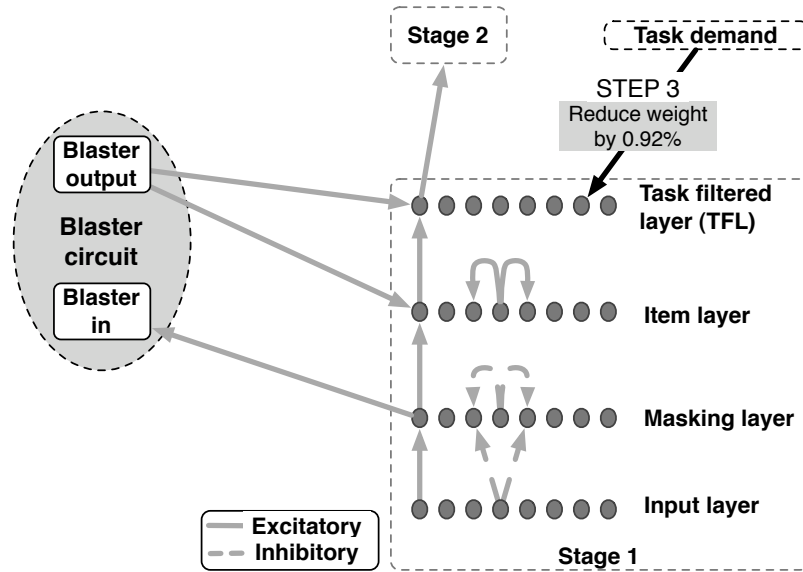


Figure 31 **Step 3 of simulating Onset presentation.** The weight of the connection from task demand to target nodes in the TFL is reduced by 0.92%.

and virtual P3 for Onset targets. This is due to the blaster ‘trigger’ functioning in an ‘all-or-none’ fashion, hence, the weight value would have to be reduced to close to zero before there is any further effect on the target’s tokenisation process. Reducing the weight to close to zero, however, has a counterproductive effect as, in this case, the blaster can only be triggered by those targets with the highest strength values. Consequently, only a few targets are tokenised and all other targets are not ‘detected’ by the model. This reduces the simulated accuracy in the Onset condition to below that for RSVP targets, which is obviously not a desirable replication of the human data either. Consequently, we need to perform one additional modification to the architecture of the ST<sup>2</sup> model, as described in the next section, in order to accurately simulate Onset presentation.

### 6.4.3 Step 3: Simulating Behavioural Accuracy

#### Manipulation

An RSVP stream consists of one or more targets embedded in a stream of distractors. In Onset presentation, however, the stream contains only the target and the following distractor. When an RSVP target arrives at the TFL, the task demand mechanism plays a vital role in selecting the target from simultaneously active distractors. In Onset presentation,

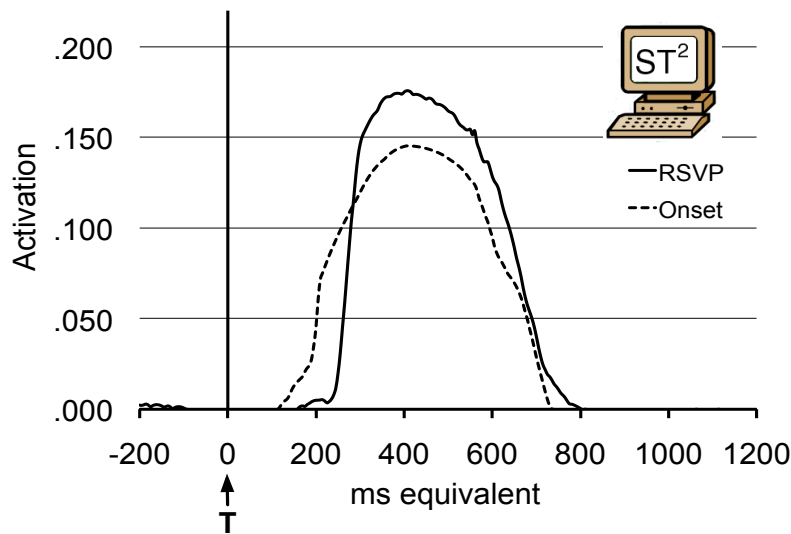


*Figure 32* **After Step 3: Virtual P3 for the RSVP and Onset conditions.** The RSVP virtual ERP is baseline corrected to -200 to 0ms with respect to target onset to account for distractor related activity, which is absent in the Onset condition. ‘T’ indicates the presentation of the target and ERPs time-locked to presentation of the target.

however, the target competes with only one other distractor at the TFL and hence there is no need for the task demand mechanism to be as strong. Conceptually, in Onset presentation, the focus of selection moves earlier and reducing the strength of the task filter reflects this adjustment of focus. In other words, as the system can select earlier with Onset presentation, its later selection mechanism (at the TFL) can be more liberal. Consequently, we reduce the weight from task demand to target nodes in the TFL by 0.92% of the original value (see Figure 31).

## Results

The reduction in task demand for Onset presentation means that target nodes have less activation at the TFL. Relatively strong targets can nevertheless initiate a tokenisation process despite lower activation levels. Weak targets, however, fail to overcome the threshold for tokenisation and cannot proceed into Stage 2 for working memory encoding. After this modification to the model’s architecture, weak Onset targets have too little activation for tokenisation and are ‘missed’. The ST<sup>2</sup> model now generates a simulated accuracy of 85% for Onset targets, which replicates the human behavioural accuracy for Onset targets.

Simulated RSVP accuracy from the model obviously remains unchanged at 77%.

The decreased task demand also causes a change in the virtual P3 evoked in the Onset condition. As can be seen in figure 32, there is a reduction in its mean amplitude compared to the RSVP condition. This reduction is in addition to the latency shift produced in it after Step 2 (figure 30), and is produced because the reduction in task demand means that target nodes in the TFL receive less positive bias. Consequently, in comparison to the RSVP condition, target nodes in the Onset condition have relatively lesser activation going into Stage 2 and evoke a weaker virtual P3 during the tokenisation process. This pattern of differences between the virtual P3s bears qualitative correspondence to the visual differences observed in the human P3s in figure 26. As can be seen therein, the human P3 for the RSVP condition has a higher grand average peak amplitude in the RSVP condition than in the Onset condition, though this could not be verified statistically.

## 6.5 Discussion

After making the described changes to the ST<sup>2</sup> model, we have enabled it to simulate the Onset condition in terms of its qualitative relationships to the RSVP condition, with respect to both behavioural and EEG data. Comparing these to the simulation of target presentation in RSVP provides us a potential explanation of the mechanisms underlying the observed differences in behavioural and EEG data.

### 6.5.1 Early Components vs. the ssVEP

Consistent with previous findings, individually presented items in Onset presentation produce the P1/N1 complex, whereas repeatedly presented items in RSVP evoke an ssVEP wave oscillating at the frequency of stimulus presentation (Mueller & Hillyard, 2000). In RSVP, the virtual ssVEP oscillation is caused by the stream of distractors and targets feeding into the model. Each item is presented at the input layer and propagates to the masking layer where the item experiences weak inhibition from previous items (forward masking). The item generates a short-lived peak of activation in the virtual ssVEP, before it is subject to stronger suppression from the following item in the RSVP stream (backward masking). This process repeats itself for each item in the RSVP stream and causes the oscillatory

pattern that can be observed in the virtual ssVEP wave.

In Onset presentation, the target is not forward masked, hence its activation at early layers of the  $ST^2$  model is immediately larger than the activation of a target in RSVP. The following distractor inhibits the target, which causes a very transient reduction in activation. Following this, the distractor's activation causes a large spike in the virtual ERP, as it is not backward masked. Although visually quite different to the P1/N1 complex in the human ERP, the virtual ERP representing early processing in the  $ST^2$  model has a corresponding time course and is a qualitative fit to the human data.

### 6.5.2 Lag 1 Sparing and Onset Presentation

After modifying the  $ST^2$  model, we are able to simulate Onset presentation and can qualitatively replicate the human data in our single target paradigm in terms of behavioural accuracy and virtual ERPs. Our change to the model architecture also suggests a prediction about lag 1 sparing in two target paradigms investigating the AB.

In the regular RSVP, targets are embedded in a continuous stream of distractors. If two targets are presented in immediate succession, and they are backward masked by at least one distractor, T2 accuracy is quite high. In fact, T2 accuracy is often higher than that of single target detection. This is the lag 1 sparing effect (see section 2.3.2). In an AB experiment using Onset presentation, however, we would expect there to be no such second target advantage.

According to the  $ST^2$  model, this is because in a regular RSVP stream, T1 triggers the blaster when it reaches the TFL. However, there is some temporal delay between the blaster being triggered and the timepoint of its full effect on the item layer and the TFL. In regular RSVP, this means that a T2 appearing at the TFL shortly after T1 will get much of the benefit of T1's blaster response. This results in the increased accuracy at detecting T2, manifesting as lag 1 sparing.

In Onset presentation however, T1 triggers the blaster at an earlier timepoint, i.e. as soon as T1 reaches the masking layer. Despite there being some temporal delay until the blaster becomes fully active, the blaster will have its major effect by the time T1's activation has reached the item layer and the TFL. As Onset presentation causes the whole activation profile of the blaster to be earlier in time, the blaster is no longer active when T2 arrives,

as it is already being suppressed by T1's tokenisation. Hence, the  $ST^2$  model predicts low accuracy for T2 at lag 1 in Onset presentation.

Turning to the evidence from human data, we know that in the regular RSVP condition, if T2 is presented immediately following T1, its accuracy is high, i.e. we observe clear lag 1 sparing (see section 2.3.2). In comparison, behavioural data from AB studies employing Onset presentation (see figure 24) suggest that the evidence for lag 1 sparing is weak. Indeed, with the exception of findings by Visser et al. (2004), most of the previous studies employing Onset presentation (Ward et al., 1997; McLaughlin et al., 2001; Rolke et al., 2007) find that T2 accuracy is lowest at lag 1.

### 6.5.3 Is Onset Presentation an Equal Substitute for RSVP?

Despite its common application in experiments designed to study temporal visual processing, the RSVP paradigm has a number of practical disadvantages. Due to the fast presentation rate, RSVP streams contain a large number of distractors, and have a typical duration of 2-3 seconds. Furthermore, the rapid presentation of items is often taxing for participants, especially in long experiments. This situation arises when conducting EEG or Magnetoencephalography (MEG) experiments, where, in order to increase the signal-to-noise ratio by averaging, each condition is presented several times. Hence, as experimental time in an EEG/MEG laboratory is costly, there is a major incentive to minimise the duration of the experiment.

In comparison, the Onset task 'minimises demands both on selective attentional processing and on location switching mechanisms' (Ward et al., 1997), while nevertheless seeming to reveal the attentional limitations underlying the AB. Thus, due to simpler and shorter experiments, the Onset condition seems ideal for studies employing MEG or EEG to study the AB. Indeed, as a previous study investigating the AB by means of MEG and the Onset condition states: 'an AB effect is observed whether targets are embedded in a 20-item RSVP stream or just presented on their own followed by masks. In order to save measurement time, we decided to employ this abbreviated version for our study' (Kessler et al., 2005). However, from the results presented in this chapter, we argue that there are considerable differences in target processing between Onset presentation and RSVP. Though our experiment employed only a single target, we believe that these results inform and are directly relevant to dual

target RSVP studies. Consequently, direct comparisons between EEG/MEG data collected using these two paradigms should be interpreted with caution.

## 6.6 Conclusions

This chapter has investigated the influence of target discriminability on temporal dynamics of visual perception using electrophysiology. In addition, by making systematic and justifiable changes to the ST<sup>2</sup> model, we have enabled it to simulate Onset presentation of targets. The comparison between the performance of this modified version to the original one has allowed us to propose an explanation to the observed differences in the human EEG between the RSVP and Onset conditions, on the basis of how target discriminability affects the latency of attentional deployment. Further, this exercise has informed questions about the experimental equivalence of these paradigms, at the level of neural dynamics, for the study of the Attentional Blink phenomenon.

## Chapter 7

# The Temporal Precision of Attention

In this chapter, we continue our exploration of the temporal spotlight, and investigate its role in providing perception with temporal precision. Using the Attentional Blink (AB) as a modulatory mechanism and EEG as an index of temporal dynamics, we will show how impairing the temporal spotlight adversely affects conscious perception. We describe data from an EEG experiment, which is used to compare the temporal precision of perception outside and inside the AB window. In this process, we begin with an analysis of average ERPs, and then delve deeper into time-frequency analysis of single trial EEG data to provide a more fine-grained test of our hypothesis. We then interpret our findings from this analysis using virtual ERP simulations from the ST<sup>2</sup> model, to propose an explanation based on variation in the temporal precision of attention.

### 7.1 Introduction

This chapter investigates the hypothesis that diminished attentional control increases the *temporal jitter* in the latency of a target's working memory consolidation. The Attentional Blink (AB) provides us with a suitable phenomenon with which to test our hypothesis: we propose that the reduced availability of attention during the AB increases the temporal noise in visual attention. To investigate this issue, we compare the ERPs evoked by targets outside vs. inside the AB. In doing so, we determine whether there is an increase in the inter-trial variability of the latency of target consolidation inside the AB. EEG has the advantage of excellent temporal resolution, allowing us to study short-lived cognitive events that evoke

changes in ongoing EEG activity. To test for increased temporal jitter, we analyse the N2pc and P3 ERP components, commonly associated with selective attention (Eimer, 1996) and working memory (Kok, 2001; Vogel et al., 1998), respectively.

In addition to presenting and analysing human EEG data, we use the ST<sup>2</sup> model’s neural network implementation to generate *virtual* ERPs (see chapter 4). For each of the experimental conditions, virtual ERPs are contrasted with human ERPs, both at the level of grand averages and single trials. This comparative evaluation allows us to validate the ST<sup>2</sup> model and propose explanations for the human ERP effects.

### 7.1.1 Attentional Precision and the ST<sup>2</sup> Model

Before delving into the EEG data, we summarise the predictions of the ST<sup>2</sup> model about temporal variability in target processing. The model suggests that working memory encoding involves creating a binding between the *type* of a stimulus (which can include its visual features and semantic attributes) and a *token* (an episodic representation specific to a particular occurrence of an item) (Kanwisher, 1987; Mozer, 1989). In the ST<sup>2</sup> model, a Transient Attentional Enhancement (TAE) from the blaster amplifies the *type* representation of a salient (i.e., task relevant) stimulus to assist in its binding to a token, in a process referred to as *tokenisation*. This TAE can serve as an attentional gate, which can be temporarily deactivated to allow one target encoding to be completed before a second is begun.

From the perspective of the ST<sup>2</sup> model, the AB is an artefact of the visual system attempting to assign unique tokens to targets (Wyble, Bowman, & Nieuwenstein, 2009)<sup>1</sup>. More specifically, the process of encoding T1 into working memory is triggered by TAE, and TAE itself is subsequently suppressed until T1 encoding has completed. The period of TAE unavailability varies from trial to trial depending on how long it takes to tokenise T1, which in turn depends on its bottom-up strength. As pointed out previously in this thesis, the ST<sup>2</sup> model suggests that there is a reciprocal relationship between T1 strength and the duration of its tokenisation process (see chapter 5 and Bowman et al., 2008). Thus,

---

<sup>1</sup>In order to explain findings relating to the AB, the definition of an episode is extended in Wyble, Bowman, and Nieuwenstein (2009) to include multiple tokens. Nevertheless, for the purposes of this chapter, each token corresponds to an episodic context in working memory.

in an RSVP stream, if a T2 is presented 100-600ms after a perceived T1 (as is the case during the AB), its processing outcome depends on multiple factors. T2's own strength determines its dependence on TAE, as highly salient T2s might potentially 'break-through' the AB (Anderson, 2005) and get encoded relatively early. T2s with strength values slightly lower in the range 'outlive' the AB (and thus the unavailability of TAE), and hence are indirectly influenced by T1 strength. Overall, the variability in the temporal dynamics of T2's encoding process is influenced both by T1 and T2 strengths. Hence, over all possible strengths, the ST<sup>2</sup> model proposes that there should be increased variance in processing latency for targets seen during the AB. With this initial prediction from the ST<sup>2</sup> model, we now proceed to describe results from an EEG experiment that serves to test it.

## 7.2 The Two Target Experiment

This chapter analyses behavioural and EEG data from Experiment 2. The experiment consisted of RSVP trials with two bilateral streams, presented at a rate of 105.9ms per item. Each trial had two letter targets, T1 and T2, embedded among digit distractors. T2 was presented at lags 1, 3 and 8 following the T1. EEG was recorded from participants while the streams were being presented, and later correlated with their behavioural responses. The N2pc ERPs analysed in this section were recorded at the P7, P8, O1 and O2 electrodes, while the P3 ERP was recorded at the Pz electrode. Please refer to appendix B.2 for a detailed overview of the experimental method.

## 7.3 Behavioural Analysis

The mean human accuracy for T1 identification in Experiment 2 is 82%. The accuracy of T2 identification (conditional on correct report of T1) is 83% at lag 1, 54% at lag 3, and 74% at lag 8. There is a significant effect of lag on accuracy ( $F(1.48,12.58) = 15.58$ ,  $MSE = 0.03$ ,  $p < 0.001$ , after applying a Greenhouse-Geisser correction on the degrees of freedom). Additionally, in pairwise comparisons, T2 accuracy is significantly lower at lag 3 compared to lag 8 ( $F(1,17) = 11.66$ ,  $MSE = .03$ ,  $p < 0.01$ ) and lag 1 ( $F(1,17) = 60.88$ ,  $MSE = 0.01$ ,  $p < 0.001$ ). Consequently, the paradigm employed evokes a reliable AB effect.

## 7.4 ERP Analysis

Figure 33A depicts the grand average human N2pc ERPs evoked by targets presented outside (*all T1s followed by T2s at lag 8*) and inside (*all T2s at lag 3 following a seen T1*) the AB. A standard one-way repeated measures ANOVA reveals that there is no significant difference across subjects, in the mean/peak amplitude of the N2pc ERPs within the 130-260ms window indicated in the figure ( $F < 1$ ). Further, analysis of the onset latency of the N2pc using jackknife analysis (with an onset criterion of 50% of peak amplitude; see J. Miller, Patterson, & Ulrich, 1998) did not find any differences ( $t < 1$ ). The lack of any difference in mean N2pc amplitude stands in contrast to results reported by Jolicoeur, Sessa, Dell'Acqua, and Robitaille (2006), who found that the N2pc evoked by targets presented inside the AB was significantly smaller than that evoked by targets presented outside it (see Jolicoeur et al., 2006; figure 3). In our data, as evident in figure 33A, we find that the N2pc evoked by targets presented inside the AB has a comparatively less well-defined onset and offset, and increased horizontal spread<sup>2</sup>.

The human P3 ERPs for targets presented outside and inside the AB is depicted in figure 33B. As suggested by the large reduction of amplitude in the figure, there is a significant reduction in P3 amplitude for targets inside the AB within the 300-700ms window indicated therein: targets presented outside the AB have a mean P3 amplitude of  $3.68\mu\text{V}$ , while targets presented inside the AB have a mean amplitude of  $2.22\mu\text{V}$  ( $F(1,17) = 11.61$ ,  $\text{MSE} = 1.65$ ,  $p < 0.01$ ). However, there is no suggestion of a latency difference between the P3s, as measured by subject-wise 50% area latency analysis (Luck & Hillyard, 1990) ( $F < 1$ ).

The comparative analysis of ERPs performed above is confounded by the variation in behavioural accuracy across the conditions, occurring as a natural consequence of the AB effect. In other words, the ERPs for targets presented inside the AB include a much greater number of trials in which targets were completely missed or partially processed, but failed to

---

<sup>2</sup>Findings by Jolicoeur et al. (2006) also suggest that the N2pcs for seen T2s at lag 3 might be temporally coincident with the Sustained Posterior Contralateral Negativity (SPCN) component evoked by the seen T1 preceding it. This is because, in their data, the SPCN component occurred in the 300-500ms window following target onset (Jolicoeur et al., 2006; figure 3). However, no such component is evident in our data, either for targets presented outside or inside the AB. Specifically, in figure 33A, there is no statistically significant negativity in the 300-500ms window following target onset.

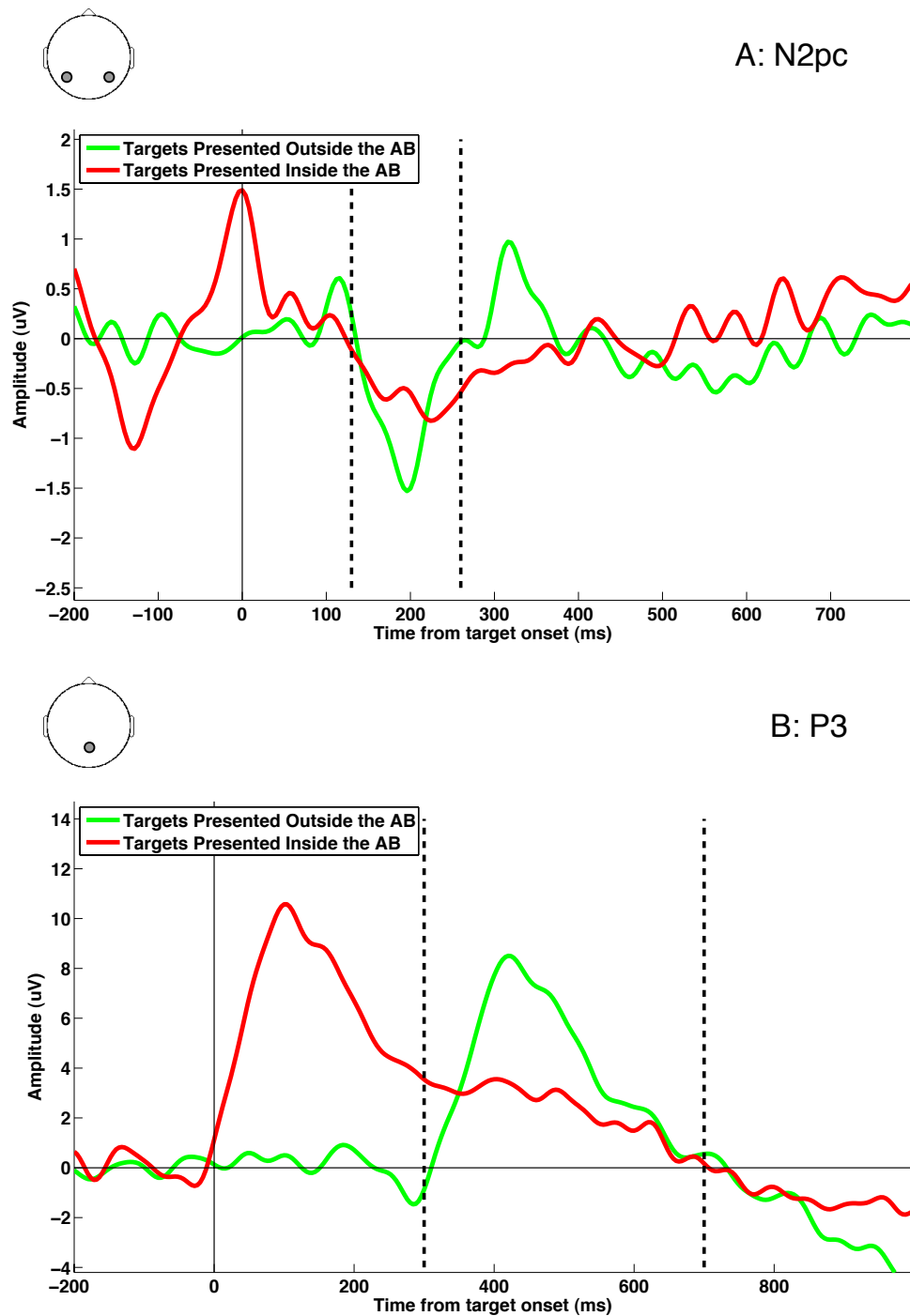


*Figure 33* Human ERPs for targets presented outside and inside the AB. Panel A: Grand average N2pc. Panel B: Grand average P3. Dashed lines indicate the window used for statistical analysis.

be correctly reported. Such targets are unlikely to evoke a clear P3, as has been previously reported (Kranzloch et al., 2003; Vogel et al., 1998). Consequently, the process of averaging over trials with varying behavioural responses in the above conditions could have resulted in a differential attenuation of the ERPs for targets presented inside the AB. To address this issue, we investigate the N2pc and P3 evoked only by correctly reported or *seen* targets, and evaluate our EEG data against our hypothesis of increased temporal variability.

Figure 34A depicts the N2pc evoked by targets seen outside (T1 Lag 8: *seen T1s followed by T2s at lag 8*) and inside (T2 Lag 3: *seen T2s at lag 3 following a seen T1*) the AB. The pattern of variation observed here is similar to that in figure 33A: the N2pc evoked by targets seen inside the AB appears to be more attenuated and spread out in the grand average. But as before, there is no statistically significant difference between the N2pc ERPs in terms of mean/peak amplitude ( $F < 1$ ) within the 130-260ms window indicated in the figure. A comparison of jackknife latency (with an onset criterion of 50% of peak amplitude) suggests a small difference: the N2pc for targets seen inside the AB is later (195.12ms) than that for targets seen outside the AB (164.68ms). However, this difference does not reach significance ( $t(1,17) = 1.19$ ,  $p = 0.13$ ).

With the P3, as before, we observe significant differences (figure 34B), with targets seen inside the AB evoking an attenuated P3 in the 300-700ms window: targets seen outside the AB have a mean amplitude of  $4.08\mu\text{V}$ , while targets seen inside the AB have a mean amplitude of  $2.69\mu\text{V}$  ( $F(1,17) = 9.09$ ,  $\text{MSE} = 1.92$ ,  $p < 0.01$ ). In addition, a 50% area latency analysis reveals that targets seen inside the AB evoke a significantly delayed P3 (483.78ms) compared to targets seen outside the AB (455.78ms):  $F(1,17) = 6.33$ ,  $\text{MSE} = 1115.31$ ,  $p = 0.02$ . This finding agrees with results reported by Martens, Elmallah, et al. (2006) and Vogel and Luck (2002), who have found that target consolidation is delayed during the AB.

On the whole, these findings suggest that, even for targets that are seen inside the AB, there might exist key differences in the dynamics of temporal visual processing, as compared to targets seen outside the AB. Indeed, as is evident in figure 34A (and in figure 33A), the N2pc ERPs evoked by targets outside and inside the AB appear to have very different temporal profiles. However, these differences are not very well suited to the application of the average ERP analysis techniques we have employed in this section. In particular, the

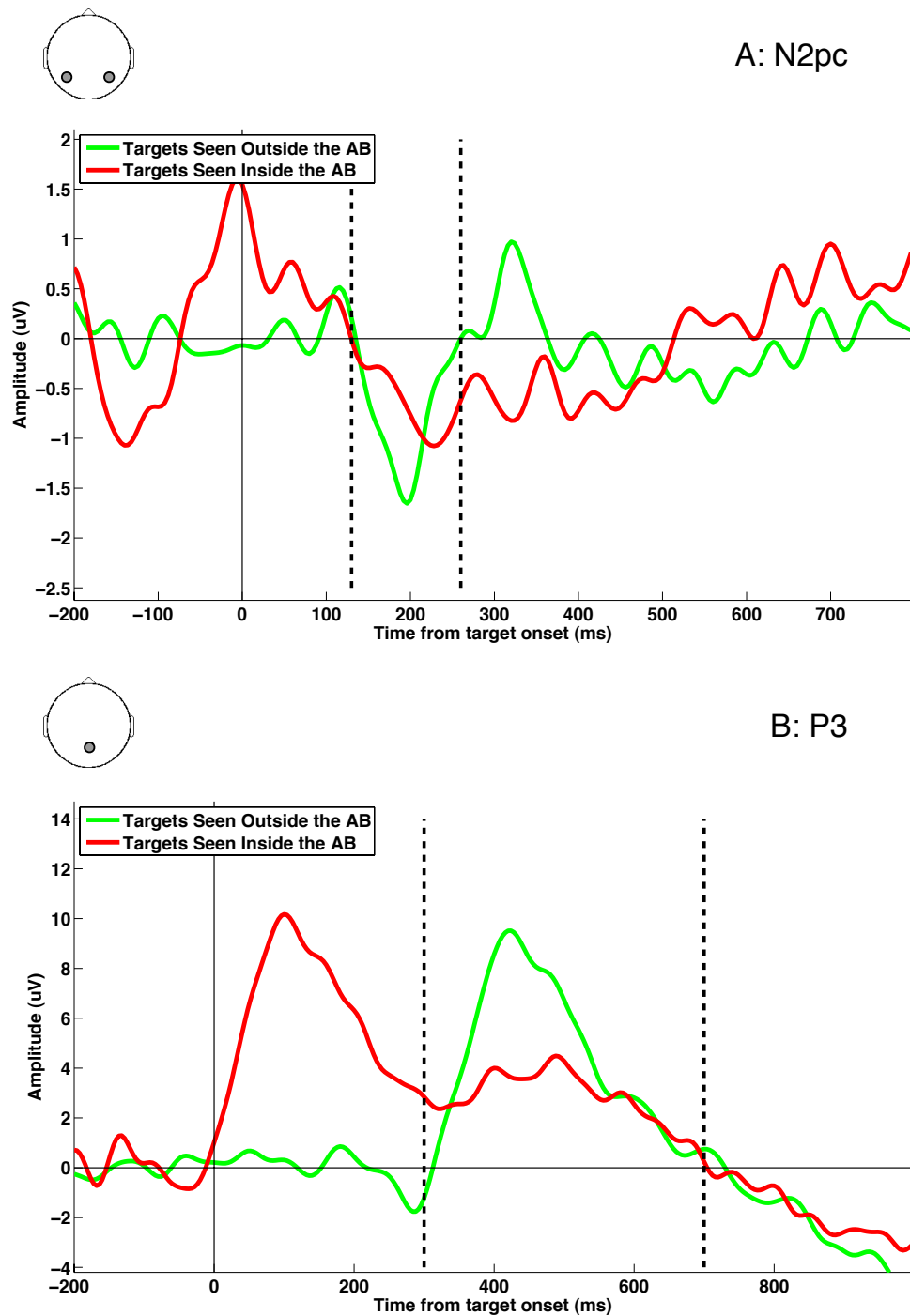


Figure 34 Human ERPs for targets seen outside and inside the AB. Panel A: Grand average N2pc. Panel B: Grand average P3. Dashed lines indicate the window used for statistical analysis.

statistical results produced by mean/peak amplitude analysis, jackknife analysis, etc. are sensitive to the choice of the time window used to define the ERP component. Owing to the temporal characteristics of the N2pc evoked by targets inside the AB, the appropriate choice of this window is difficult, and has to be based on unreliable visual estimates. In the next section, we circumvent these problems and go beyond the analysis of average ERPs. Instead, we enquire into differences in the temporal dynamics of target processing outside and inside the AB at the level of single EEG trials.

## 7.5 Single-Trial Analysis

We now go beyond an analysis of averaged ERP components, as such methods cannot directly inform our hypothesis of reduced attentional precision during the AB. This is because the averaging collapses across and hence discards information about temporal fluctuations in the individual EEG trials contributing to the ERP. Given a set of trials that are averaged together, both decreases in amplitude and increases in latency variation within that set will attenuate the mean amplitude of the ERP. Hence, examining the average does not directly provide the necessary information to decide which of the two sources of variation in the individual trials (amplitude or latency) caused the reduction in ERP amplitude. Further, measures like 50% area latency analysis (Luck & Hillyard, 1990) cannot be used to measure latencies in single trials, due to the levels of irrelevant noise activity. Consequently, we employ time-frequency analysis techniques that provide alternative measures to investigate single trial dynamics underlying grand average ERPs. These methods enable us to perform a more fine-grained analysis of EEG data, and test our hypothesis using both qualitative and quantitative means.

### 7.5.1 Analysis of ITC and ERSP

To begin our investigation of the single-trial dynamics latent in the N2pc and the P3 ERPs, we characterise their time-frequency signatures by calculating *Inter-Trial phase Coherence analysis* (ITC) and Event-Related Spectral Perturbation (ERSP) (Delorme & Makeig, 2004; Tallon-Baudry, Bertrand, Delpuech, & Pernier, 1996). ITC provides an index of the amount of inter-trial variability in the latency of EEG activity. Here, latency is estimated by the

*phase* of the EEG signal, calculated using wavelet-based time-frequency analysis (see appendix B.2 for details). From these phase values, ITC is calculated as a dimensionless scalar normalised to a value between 0 and 1. It measures the extent to which the phase of stimulus-locked EEG activity at a particular frequency is correlated across a set of trials. Time-frequency maps of ITC values allow us to visualise the amount of phase synchronisation in different time windows and frequency bands. The other measure we are interested in, ERSP, estimates stimulus-related power changes, measured in decibels. In parallel with ITC, ERSP time-frequency plots depict how the stimulus-related power fluctuates over time and across frequencies.

In the following analysis, we are interested in investigating the ITC underlying the N2pc and P3 ERP components. Consequently, we measure and comparatively evaluate the temporal variation in ITC within the time and frequency windows where the power of these ERP components is located. At a given time-frequency point, an ITC value of 0 indicates a complete lack of phase coherence across the set of trials being analysed, whereas an ITC value of 1 signifies that the phase is perfectly time-locked to the stimulus. ITC values can hence be visualised in a time-frequency colourmap with time relative to stimulus onset along one dimension, and frequency along another. Each data point in the plot is coloured according to the amount of ITC observed at a particular time and frequency across all trials in an experimental condition. Please refer to appendix B.2 for further details about the ITC analysis parameters.

Figure 35 shows the ITC plots for the N2pc and P3 components. Each of the time-frequency plots in the figure is a colour map depicting ITC effects time-locked to the presentation of the target, which occurs at timepoint zero. As indicated by the colour scale to the right, increased ‘redness’ represents a larger ITC value, and thus more phase synchronisation across the trials making up the corresponding grand averages in figure 34. ITC significance for each data point in these plots is calculated using a two-tailed bootstrap significance test with a significance criterion of 0.01 (Delorme & Makeig, 2004). Non-significant data points are coloured green. In this regard, it is important to note that bootstrap analysis does not correct for multiple comparisons at the time-frequency data points. However, in practice, neighbouring data points calculated by time-frequency decomposition are not

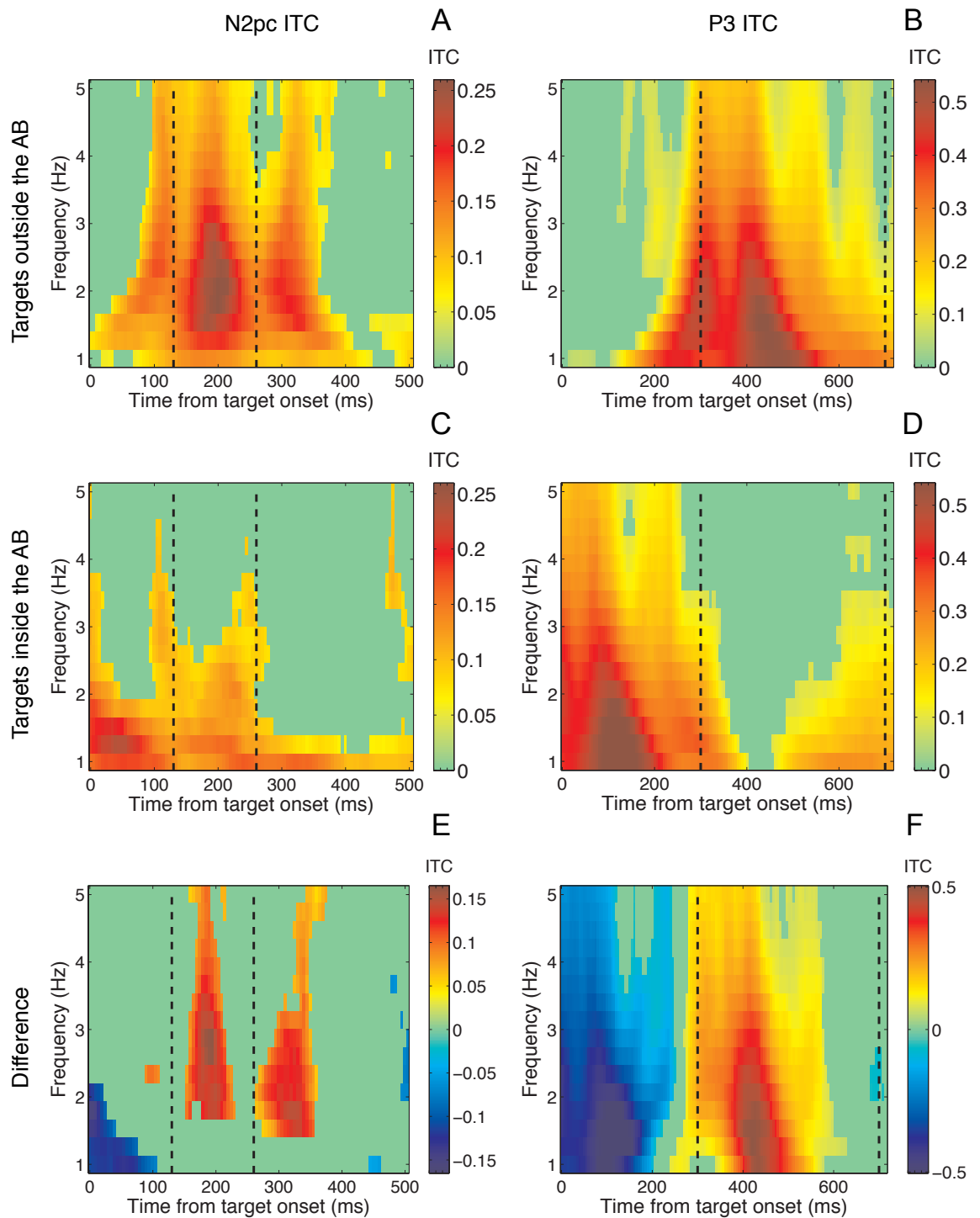


*Figure 35* **Inter-trial Coherence produced in the N2pc and the P3 evoked by targets inside and outside the AB.** The left column shows ITC time-frequency plots for the N2pc, while the right column shows those for the P3. Targets outside the AB are plotted on the first row, and targets inside the AB on the second row. The final row contains a difference plot between the two conditions. Dashed lines indicate time window of interest for the ERP in question.

independent, and are highly correlated<sup>3</sup>. We avoid the multiple comparisons problem by basing our analysis on an a priori hypothesis of expected differences in ITC. Specifically, we compare the ITC evoked by targets outside and inside the AB only within the time windows defined by the grand average ERPs in figure 34 (130-260ms for the N2pc and 300-700ms for the P3). The corresponding windows are indicated by dashed lines in the ITC plots in figure 35. Further, we focus only on the 1-5Hz frequency window, where the power of the N2pc and P3 are located. According to our hypothesis, the relative decrease in temporal precision for targets inside the AB should produce a corresponding reduction in ITC evoked by the N2pc/P3 within this time-frequency window. Hence, a smaller ITC value for targets inside the AB (compared to targets outside the AB) would argue for increased temporal jitter across the single-trial ERPs evoked in this condition.

In figure 35, the first row depicts ITC effects for targets outside the AB and the second row depicts the ITC for targets inside the AB. The third row shows differences in ITC between the previous two plots. As apparent from the altered colour scale for these difference plots, a positive data point coloured red indicates a significantly greater ITC in the former (target outside the AB) condition, whereas a negative data point coloured blue indicates a significantly greater ITC in the latter (target inside the AB) condition.

The left column of figure 35 depicts the ITC plots of EEG activity underlying the N2pc ERP component. A visual comparison of the relevant time windows within the plots in figures 35A and 35C suggests that the N2pc for targets inside the AB does indeed produce lesser ITC than targets outside the AB. The difference plot in figure 35E corroborates this, as it registers an increased amount of ITC in figure 35A than in figure 35C, within the N2pc time window.

Turning to the P3 ITC plots in the right column, it is evident that the P3 evoked by targets inside the AB produces much lesser ITC than targets outside the AB (figures 35B and 35D). Further, the large positive region within the P3 time window in the difference plot in figure 35F, along with its wider colour scale, clearly shows that there is much more ITC in figure 35B than in figure 35D.

---

<sup>3</sup>Consequently, the standard bonferroni correction for multiple comparisons is too conservative in this context, and more specialised correction methods are required (Tanji, Suzuki, Delorme, Shamoto, & Nakasato, 2005).

The ITC differences in figures 35E and 35F are located in a single cluster of data points within the expected time-frequency window. They agree with our previously stated hypothesis, and make it highly improbable that these differences were produced by random effects. However, in the comparisons of the ITC difference plots, it is clear that the P3 registers much larger differences in temporal variability than the N2pc. This is most likely due to relatively small N2pc amplitudes at the single trial level. Nevertheless, the qualitative similarity of the pattern observed in the ITC plots for the N2pc and the P3 suggest that the AB affects both ERP components in the same way, albeit with differences in the measurable strength of the effect.

To complement the ITC plots, figure 36 plots event-related power changes, or Event-Related Spectral Perturbation (ERSP; Delorme & Makeig, 2004) for the same 6 conditions. Each of the time-frequency plots in figure 36 is a colour map depicting power fluctuations time-locked to the target, in the trials making up the corresponding grand averages in figure 34. Importantly, these fluctuations are measured relative to a spectral baseline window of -500ms to -300ms preceding target presentation. Consequently, as indicated by the colour scale to the right, ‘redness’ implies increase in power, while ‘blueness’ reflects decrease, relative to the mean power in this baseline window. As with the ITC plots, ERSP significance for each data point is calculated using a two-tailed bootstrap significance test with a significance criterion of 0.01. Non-significant data points are coloured green. Please refer to appendix B.2 for further details about the ERSP analysis parameters.

As can be seen by comparing the difference plots in figures 35E and 35F with those in figures 36E and 36F, it is evident that the changes in ITC are concomitant with changes in ERSP. Specifically, the reduced ITC evoked by targets inside the AB is associated with a reduction in the amount of ERSP associated with the ERPs. This highlights a potential confound in the ITC analysis: it is possible (though unlikely) that the observed reduction in ITC could be solely explained by the reduction in ERSP, rather than by any underlying reduction in temporal precision. This confound arises because the relative reduction in power could have diminished the accuracy of ITC calculation. In a later section, we solve this problem by directly analysing the phase distributions underlying the ITC analysis after correcting for the influence of changes in ERP power during the AB.

To reiterate our central hypothesis in this chapter, if there is indeed a reduction in the

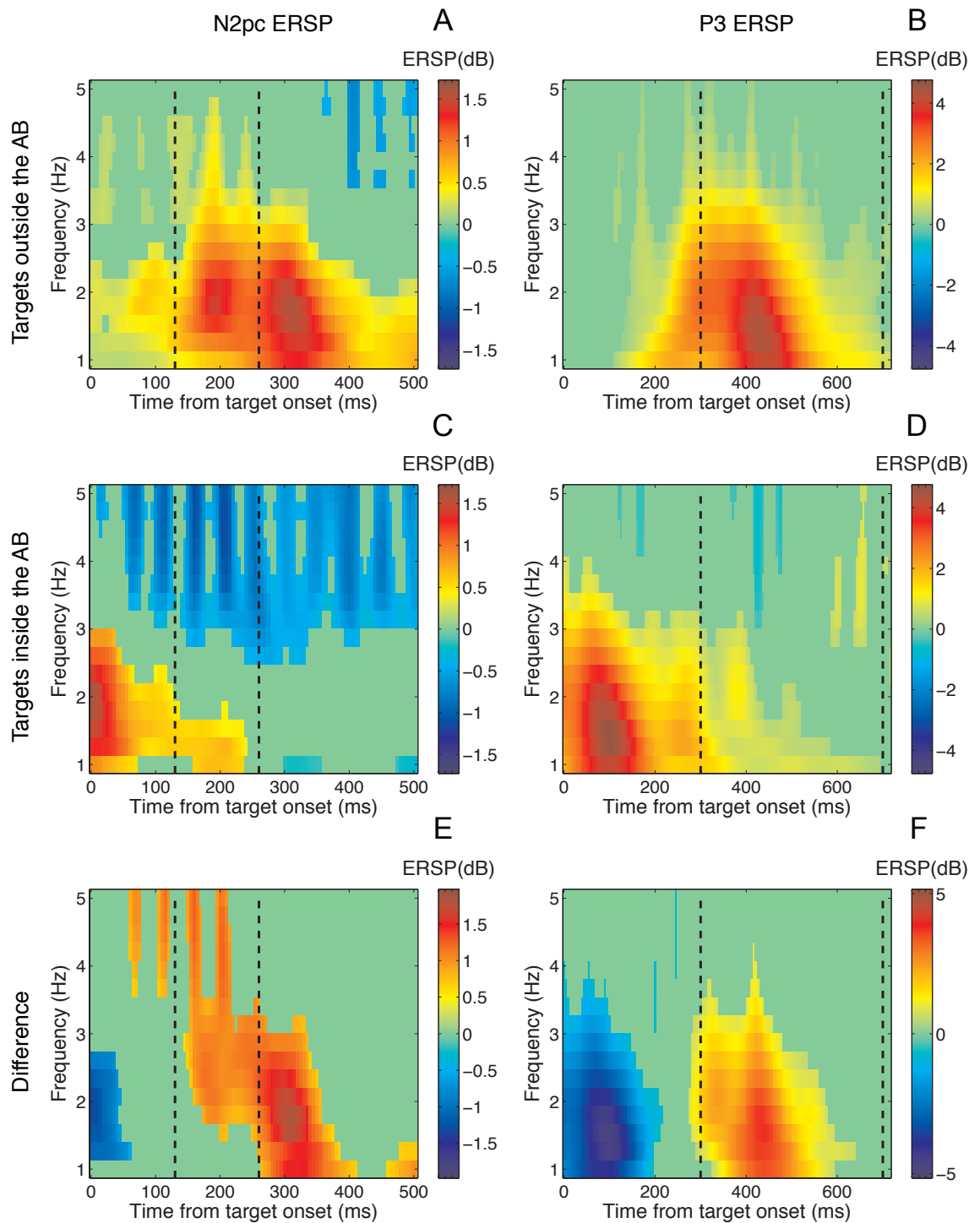


*Figure 36* **Event-related Spectral Perturbation produced in the N2pc and the P3 evoked by targets inside and outside the AB.** The left column shows ERSP time-frequency plots for the N2pc, while the right column shows those for the P3. Targets outside the AB are plotted on the first row, and targets inside the AB on the second row. The final row contains a difference plot between the two conditions. Dashed lines indicate time window of interest for the ERP in question.

precision of the deployment of attention in response to targets during the AB, we would expect this to indirectly affect the temporal variability of the related ERP components. The ITC analysis above provides support for our hypothesis. However, there exist an important problem with the interpretation of the ITC plots. This is the potential confound that the observed ITC changes could be explained by the ERSP changes. In the next sections, we address this issue by directly visualising and analysing the phase distributions of the ERPs.

### 7.5.2 Analysis of ERPimages

The ERPimages (Delorme & Makeig, 2004) in figures 37 and 38 compare the N2pc and the P3, respectively, evoked by targets seen outside and inside the AB. They allow us to visualise the EEG trials underlying the grand average ERPs (figures 34A and 34B). These ERPimages represent time with respect to target onset along the X-axis, individual trials along the Y-axis, and the single-trial EEG amplitude using a colour scale. The trials in these images are time-locked to the onset of the corresponding target. Further, they have been sorted from bottom to top by descending order of the phase angle of the single-trial N2pc/P3 at the timepoint indicated by the dashed line, which is set to the peak latency of the corresponding grand average N2pc/P3. This phase-sorting method effectively attempts to order the trials according to the approximate latency of the phasic N2pc/P3 response to a target. Here again, single-trial ERP latency is estimated by EEG phase, calculated using a wavelet-based analysis similar to that employed for calculating ITC and ERSP (see appendix B.2 for more details). Further, the frequency at which these N2pc/P3 phase angles are estimated is that at which the corresponding ITC is maximally different between the conditions of interest. This choice of frequency aims to maximise the observable difference in the phase distributions of the N2pc/P3 between targets outside and inside the AB. This frequency, identified by the peaks of the difference plots within the time windows indicated in figures 35E and 35F, is 2.45Hz for the N2pc and 1.53Hz for the P3, respectively. Phase-sorted ERPimages are then plotted for each condition, with trials having longer latency N2pc/P3 being placed at the bottom, and trials with shorter latency N2pc/P3 at the top. These ERPimages have been vertically smoothed to improve visual clarity, using a sliding window of 50 trials. Following from our hypothesis, for targets inside the AB, we expect to observe an increased “slope” in the blue “smear” representing the N2pc, and/or the red

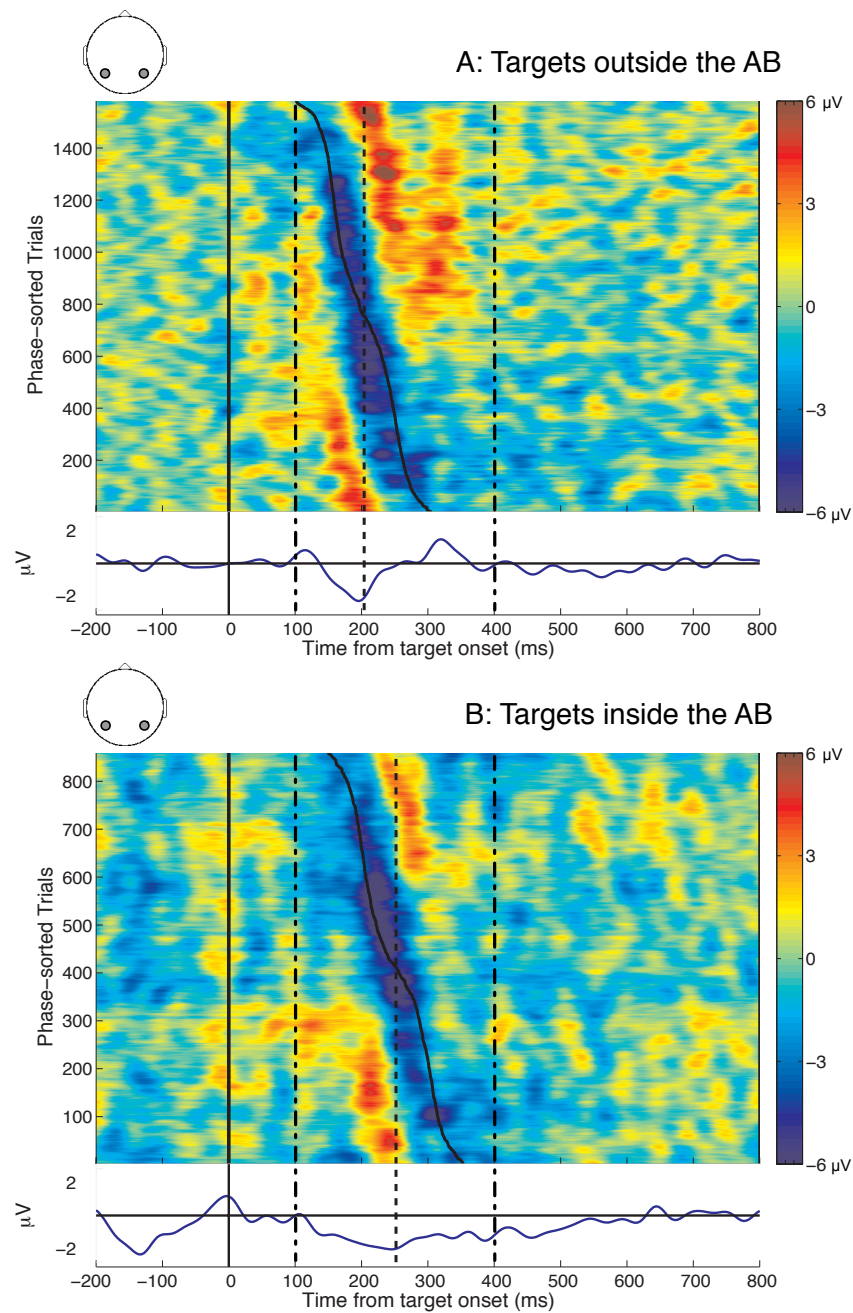


*Figure 37* **Human N2pc ERP images for targets seen outside and inside the AB.** The ERP images are time-locked to target presentation. Trials are sorted by phase at the peak latency of the grand average N2pc (indicated by the dashed line). The diagonal solid line running across the ERP image illustrates the variation in phase, and is plotted by mapping the circular range of phase values onto the linear range of timepoints encompassed by the wavelet. Dashed-dotted lines indicate the time window used to measure subject-wise peak latencies.

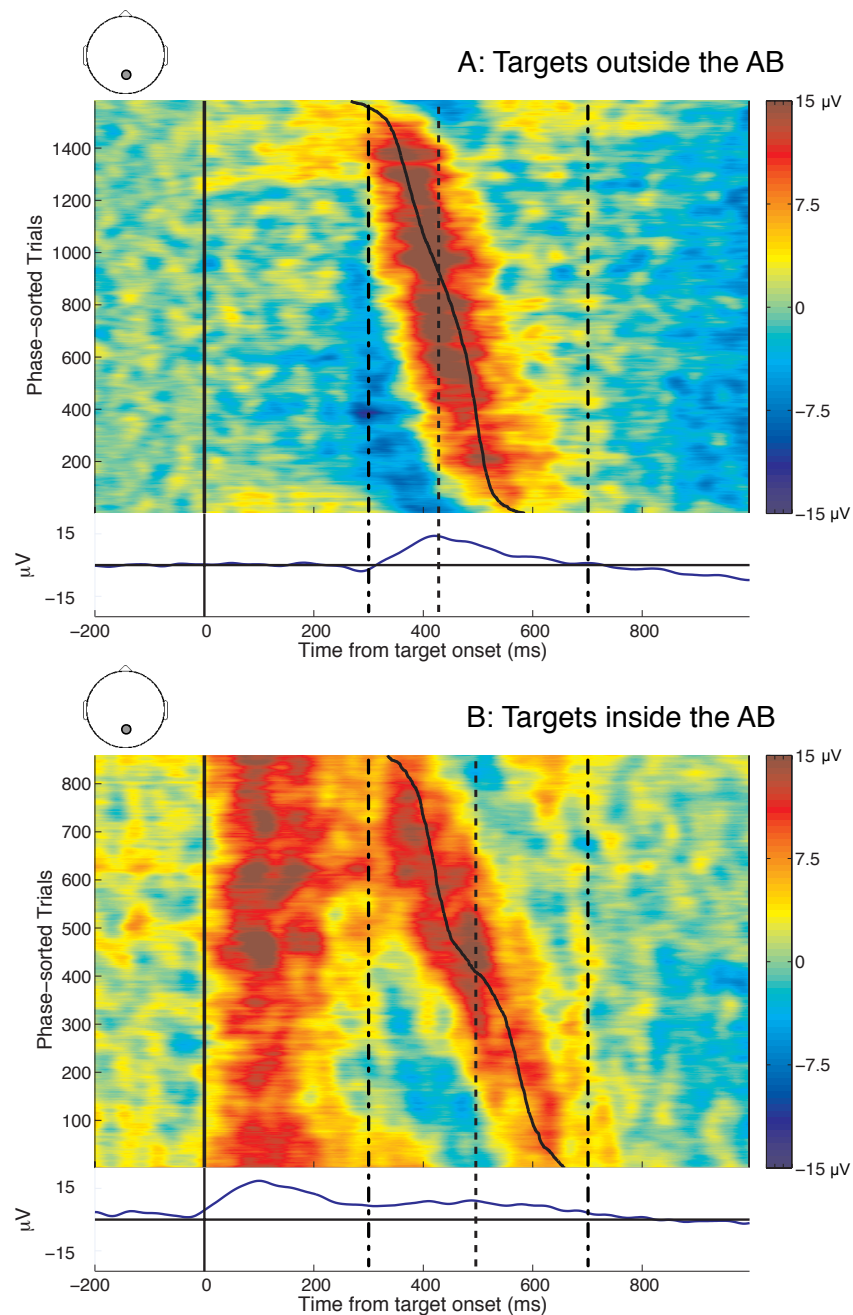


*Figure 38* **Human P3 ERP images for targets seen outside and inside the AB.** The ERP images are time-locked to target presentation. Trials are sorted by phase at the peak latency of the grand average P3 (indicated by the dashed line). The diagonal solid line running across the ERP image illustrates the variation in phase, and is plotted by mapping the circular range of phase values onto the linear range of timepoints encompassed by the wavelet. Dashed-dotted lines indicate the time window used to measure subject-wise peak latencies.

“smear” representing the P3. This would indicate that these targets suffer greater temporal variance compared to targets outside the AB.

Comparing the human N2pc ERP images in figure 37, there is a weak suggestion of increased inter-trial temporal variance for targets inside the AB. This lack of a strong difference is possibly because the N2pc is a relatively small fluctuation in single trials, and does not produce a large amount of measurable latency variation. In comparison, the human P3 ERP images in figure 38 suggest much more strongly, that the P3 for targets inside the AB suffers from increased temporal jitter: in comparison to the P3 evoked by targets outside the AB, the P3 evoked by targets inside the AB seems to exhibit increased inter-trial variance in latency around the peak of the corresponding grand average. This is because the P3 has a relatively large amplitude at the single trial level, and mirrors the larger differences in P3-related ITC in the previous section. It is relevant in this context to note that we did not find a correlation in the phase of the N2pc and the P3 from trial to trial, either for targets seen outside or inside the AB. This might possibly be due to the fact that latency variation in the single-trial N2pc is smaller compared to the P3, and is affected by higher levels of noise. Consequently, the ability of phase analysis to accurately estimate the latency of the single-trial N2pc could be diminished, effectively obscuring a weak correlation. Later in this chapter, we will discuss this issue with respect to predictions from the ST<sup>2</sup> model.

### 7.5.3 Analysis of Phases

In this section, we back up the comparisons from previous sections and directly analyse the phase estimates generated by time-frequency decomposition of ERP data. This method of analysing phase distributions allows us to statistically test whether the observed reduction in temporal precision during the AB is consistent across subjects. It delves deeper than the ITC analysis in section 7.5.1, and provides a more specific estimate of the magnitude of the difference in the temporal precision of the N2pc/P3. In addition, as we shall see, this method of phase analysis allows us to correct for the potential power-related confound highlighted in the previous section.

In the previous section, we used the phase values estimated at the peak latency of grand average ERPs to sort the trials plotted in the ERP images. Here, we adapt this technique to subject-wise analysis of phases. We group the trials in each condition by subject. For each

group, we select the phase angles estimated at the peak latency of the individual subject averages<sup>4</sup>. However, the frequencies used to estimate these phase angles remain the same as those used in the previous section. The time windows within which the peak latencies of the subject averages are measured are based on the maximal temporal extents of the phase-sorted single-trial ERPs seen in the ERPimages. As indicated in figures 37 and 38, the time windows used are 100-400ms for the N2pc and 300-700ms for the P3. The phase angles thus selected form a circular distribution (Mardia & Jupp, 2000) of angular data values that effectively represent the temporal latency of the single trial ERP. By comparing across subjects the variance in the distributions of phase angles for targets outside and inside the AB, we can test whether the visual differences observed in the ERPimages are statistically significant.

To calculate variance, the subject-wise N2pc/P3 phase distributions are modelled as von Mises distributions (Mardia & Jupp, 2000). For each of them, a concentration parameter  $\kappa$  is calculated using maximum likelihood estimation. The  $\kappa$  parameter of a distribution is a measure of its density around its mean value, and is an analogue of the inverse of its variance. The larger the  $\kappa$  value of a circular distribution, the more concentrated it is around the mean. Importantly,  $\kappa$  is a linear parameter, and can be compared using conventional statistical tools. Hence, in order to test whether targets inside the AB suffer from increased temporal jitter, we compare  $\kappa$  values of subject-wise N2pc/P3 phase distributions evoked by targets outside and inside the AB, using a standard one-way repeated-measures ANOVA. The results of the ANOVA validate what the visual differences observed in the ERPimages clearly indicate: the  $\kappa$  of the phase distribution for the N2pc for targets outside the AB is statistically larger than that for targets inside the AB: mean  $\kappa$  for targets outside the AB is 0.46, whereas mean  $\kappa$  for targets inside the AB is 0.32 ( $F(1,17) = 6.14$ ,  $MSE = 0.03$ ,  $p = 0.02$ ). The  $\kappa$  values of the phase distributions for the P3 show a similar pattern: mean  $\kappa$  for targets outside the AB is 0.98, whereas mean  $\kappa$  for targets inside the AB is 0.56 ( $F(1,17) = 13.09$ ,  $MSE = 0.12$ ,  $p < 0.01$ ). Hence, both the N2pc and the P3 have reduced temporal precision during the AB. However, as is evident from the magnitude of the mean  $\kappa$  values and the results of the ANOVAs, the effect is stronger in the P3.

---

<sup>4</sup>Note that the phase angles used to sort the ERPimages in the previous section were estimated at peak latency of the grand average.

## The Potential Confound of Reduced Amplitude

A potential confound in our time-frequency analysis arises from a comparative reduction in the amplitude of the N2pc/P3 during the AB. This reduction can be observed in the grand average ERPs in figure 34. This also agrees with previous reports of reduced amplitude of the N2pc (Jolicoeur et al., 2006) and P3 (Craston et al., 2009; Sessa, Luria, Verleger, & Dell'Acqua, 2006; Kranczioch et al., 2003; Vogel et al., 1998) for targets presented during the AB. In addition, as pointed out previously with ITC-ERSP analysis, the ERSP difference plots in figures 36E and 36F highlight the reduction in stimulus-related power during the AB. It could hence be argued that the increased variation in the onset latency of the ERPs for targets inside the AB is due to its reduced amplitude. This issue arises because the reduction in power can effectively diminish the ability of the time-frequency analysis to calculate the phase of the single-trial ERP. In other words, given a pair of N2pc/P3 datasets, one with reduced power compared to the other, the counter-argument to our interpretation would have claimed to explain the statistical differences in the phase distributions by a reduction in power during the AB.

To address this claim, we discount the influence of differences in power by redoing our statistical comparison of N2pc/P3 phase angles for targets outside and inside the AB. But this time, before comparing the phase distributions, we first reject trials from the *outside the AB* condition with the highest power, within the 100-400ms window for the N2pc and the 300-700ms window for the P3. This has the effect of reducing the mean power of the N2pc/P3 for targets outside the AB, now consisting only of the remaining trials. In performing this step, we discount any influence of the amplitude of the N2pc/P3 on the phase calculations. Indeed, we reject a sufficiently large number of trials so as to reduce the mean power for targets outside the AB to a value significantly smaller than that of the mean power for targets inside the AB. Specifically, before trial rejection (i.e., including all trials in the condition) the mean N2pc power for targets outside the AB is 3.98dB<sup>5</sup>. This value is statistically greater than the mean N2pc power for targets inside the AB: 3.63dB

---

<sup>5</sup>ERP power is estimated using a procedure different from that used to estimate ERSP. Consequently, the actual power values reported here differ from corresponding ERSP values in figure 36. However, the qualitative relationship between ERP power for targets outside and inside the AB is the same as that observed in the ERSP.

( $F(1,17) = 17.19$ ,  $MSE = 0.06$ ,  $p < 0.001$ ). After rejecting 223 trials with the highest N2pc power, the mean N2pc power for targets outside the AB is reduced to 3.50dB over 1358 trials. This diminished power is now statistically *lesser* than that for targets inside the AB ( $F(1,17) = 5.49$ ,  $MSE = 0.01$ ,  $p = 0.03$ ). But in confirmation of our hypothesis, we find that the difference between the  $\kappa$  values of the subject-wise N2pc phase distributions for targets outside the AB after trial rejection and targets inside the AB is still marginally significant: mean  $\kappa$  for targets outside the AB after trial rejection is reduced to 0.44; mean  $\kappa$  for targets inside the AB remains unchanged at 0.32 ( $F(1,17) = 4.35$ ,  $MSE = 0.03$ ,  $p = 0.05$ ).

The above procedure produces similar results with the P3. Before trial rejection, mean P3 power for targets outside the AB is 8.42dB. This value is statistically greater than the mean P3 power for targets inside the AB: 6.65dB ( $F(1,17) = 38.51$ ,  $MSE = 0.73$ ,  $p < 0.001$ ). After rejecting 598 trials with the highest P3 power, the mean P3 power for targets outside the AB is reduced to 6.39dB over 983 trials. This diminished power is statistically lesser than that for targets inside the AB ( $F(1,17) = 6.91$ ,  $MSE = 0.089$ ,  $p = 0.02$ ). However, the difference in the  $\kappa$  values of the P3 phase distributions for targets outside the AB after trial rejection and targets inside the AB is still significantly different: mean  $\kappa$  for targets outside the AB after trial rejection is reduced to 0.80; mean  $\kappa$  for targets inside the AB remains unchanged at 0.53 ( $F(1,17) = 7.37$ ,  $MSE = 0.07$ ,  $p = 0.01$ ).

These results address the potential confound associated with the reduction in power during the AB. Specifically, they confirm that the differences observed in the N2pc/P3 phase distributions reflect underlying differences in the corresponding temporal dynamics, which cannot be explained away by differences in amplitude or power.

### **Phase distributions for T2s at Lag 8 and T1s at Lag 3**

In order to further elucidate the statistical comparisons presented above, we extend them to include two complementary conditions: T2 Lag 8 (*seen T2s at lag 8 following a seen T1*), and T1 Lag 3 (*seen T1s followed by seen T2s at lag 3*). For the sake of brevity, we restrict ourselves to the analysis of the P3 data. As observed in the previous analyses, the pattern of differences produced by the AB in the N2pc and P3 ERPs are qualitatively similar, and the P3 registers a much stronger effect that is easier to measure. We compare the P3 phase distributions for the T2 Lag 8 and T1 Lag 3 conditions with those for targets seen outside

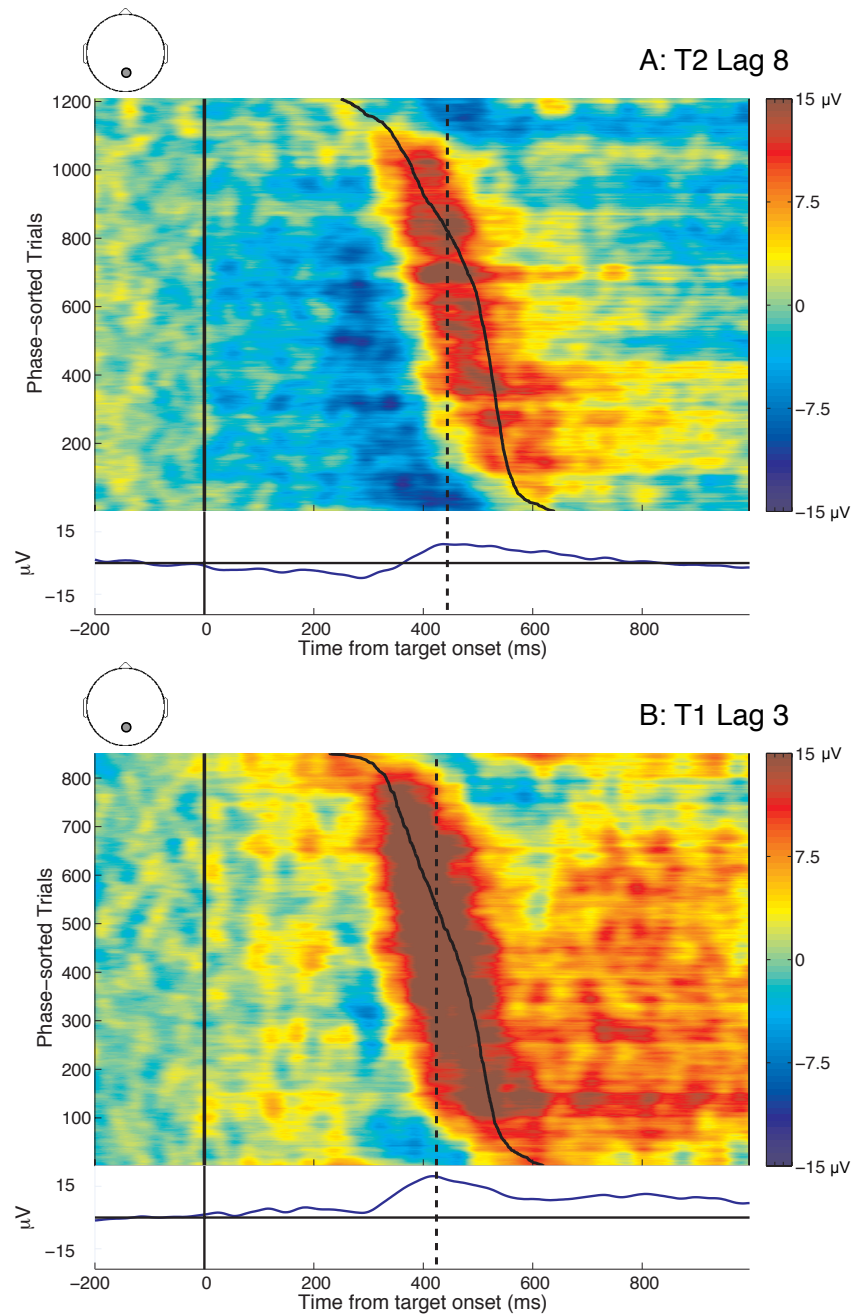


*Figure 39* **Human P3 ERPimages for the T2 Lag 8 and T1 Lag 3 conditions.** Trials are sorted by phase at the peak latency of the grand average P3 (indicated by the dashed line). The diagonal solid line running across the ERPimage illustrates the variation in phase, and is plotted by mapping the circular range of phase values onto the linear range of timepoints encompassed by the wavelet.

(T1 Lag 8: *seen T1s followed by T2s at lag 8*) and inside (T2 Lag 3: *seen T2s at lag 3 following a seen T1*) the AB. The ERPimages in figure 39 depict the phase-sorted P3s for these two conditions<sup>6</sup>.

First, in order to confirm the methodological validity of our time-frequency analysis, we check for whether the proximity of the T1 and T2 P3s at lag 3 adversely affects the estimation of phases. Specifically, it could be that the preceding T1 P3 interferes with the wavelet analysis of the T2 P3 (despite the short wavelet length) and artificially increases the variance of its phase distribution<sup>7</sup>. To test for this, we compare the subject-wise phase distributions for the T1 Lag 8 P3 (figure 38A) and the T1 Lag 3 P3 (figure 39B) conditions<sup>8</sup>. If the wavelet analysis is indeed confounded, we would expect a comparative increase in the variance of the phase distribution (and concomitant decrease in  $\kappa$ ) of the T1 Lag 3 P3. But instead, we find that the T1 Lag 3 P3 has a slightly *higher* mean  $\kappa$  of 1.01 than the T1 Lag 8 P3 with a mean  $\kappa$  of 0.98. This difference is not significant. ( $F < 1$ ). Thus, the T1 Lag 3 P3 has a relatively high  $\kappa$  value despite its proximity to the T2 Lag 3 P3. Overall, this suggests that the wavelet analysis is not confounded by this proximity, and is indeed capturing the EEG activity associated with the P3 being analysed.

The finding of increased temporal variance in T2 processing during the AB leads us to the question of the influence of variance in T1 processing thereupon. Towards answering this question, we compare the differential effect of T1 on T2, across its presentation outside and inside the AB. We find that there are no visual differences apparent in the temporal variability of the T1 Lag 8 P3 (figure 38A) and the T2 Lag 8 P3 (figure 39A). In keeping with this observation, the  $\kappa$  values of the corresponding phase distributions, 0.98 for the T1 Lag 8 P3 and 0.89 for the T2 Lag 8 P3, are not statistically distinguishable ( $F < 1$ ). In contrast, the visual comparison between the T1 Lag 3 P3 (figure 39B) and the T2 Lag 3 P3 (figure 38B) suggests that the former has higher temporal precision. Also, the  $\kappa$  of the phase distribution for the T1 Lag 3 P3 ( $\kappa = 1.01$ ) is statistically greater than that for the

---

<sup>6</sup>The phase angles used to sort these ERPimages are estimated at the peak latencies of the corresponding grand averages, and at the frequencies at which the ITC values for the corresponding conditions are maximal (1.27Hz for both T2 Lag 8 and T1 Lag 3).

<sup>7</sup>Note that this question does not arise with the N2pc, as the T1 Lag 3 and T2 Lag 3 N2pc ERPs are temporally disjoint (see figure 37).

<sup>8</sup>The phase angles used for the statistical comparisons in this section are estimated at the peak latencies of the subject-wise grand averages for each condition, and at the frequencies at which the ITC values for the corresponding conditions are maximal.

T2 Lag 3 P3 ( $\kappa = 0.55$ ):  $F(1,17) = 12.67$ ,  $MSE = 0.15$ ,  $p < 0.01$ . Taken together, these findings lead to an important conclusion: T1's influence on T2 jitter is temporally limited, i.e., T1 significantly increases T2 jitter *only* when T2 is presented within the AB window.

Following on from these findings, we are interested in whether there exist a direct relationship between the latencies of individual T1 and T2 P3s during the AB, as reflected by their phase values. However, a trial-by-trial circular correlation of phase values of the T1 and T2 P3s at lag 3 fails to find any relationship between the phases. This lack of an effect agrees with visual inferences from figure 38B, which suggest that sorting by the phase of the T2 Lag 3 P3 does not result in any evident sorting of the T1 P3 preceding it. In the same vein, sorting by the phase of the T1 Lag 3 P3 in figure 39B does not produce any sorting of the T2 P3 following it. Later in this chapter, we will look at implications of this finding for the  $ST^2$  model, and suggest a possible explanation for it within our experimental context.

## 7.6 Explaining Temporal Precision using the $ST^2$ Model

In order to validate the  $ST^2$  model, we now use it to generate virtual ERPs. In analogy to human ERP components, we can generate virtual ERP components for targets outside and inside the AB. This approach, in addition to allowing us to validate the internal dynamics of the  $ST^2$  model, provides theoretical explanations for the human EEG effects observed in the previous section. Please refer to appendix B.2 for more details on how virtual ERPs and ERPimages specific to this analysis are generated.

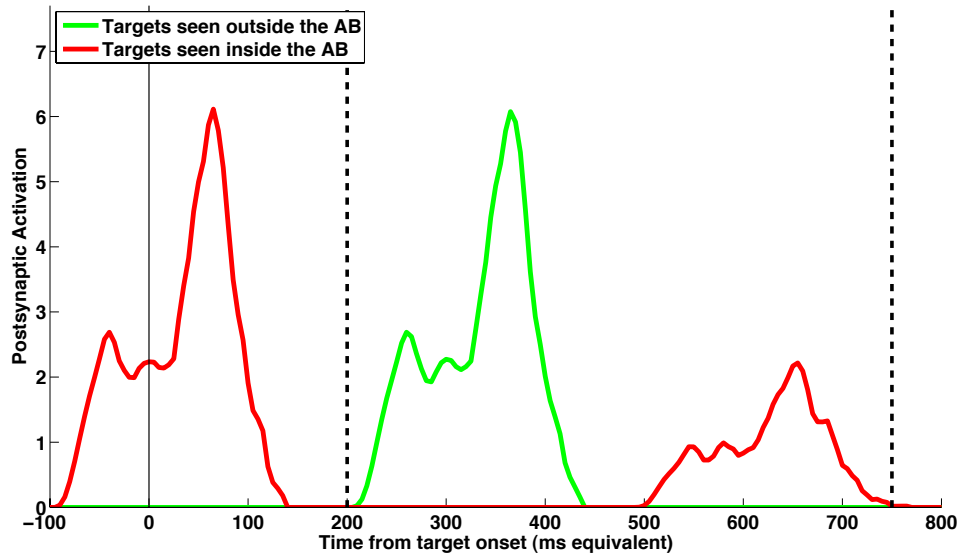
### 7.6.1 Simulated Behavioural Accuracy

The simulated behavioural accuracy from the  $ST^2$  model is 85% for targets outside the AB and 31% for targets inside the AB. The  $ST^2$  model thus qualitatively replicates the human behavioural data.

## 7.7 Virtual ERPs

Human ERPs and ERPimages unavoidably include inter-subject variability, occurring naturally in the neural dynamics across the subject pool. Hence, in this section, in order to

A: N2pc



B: P3

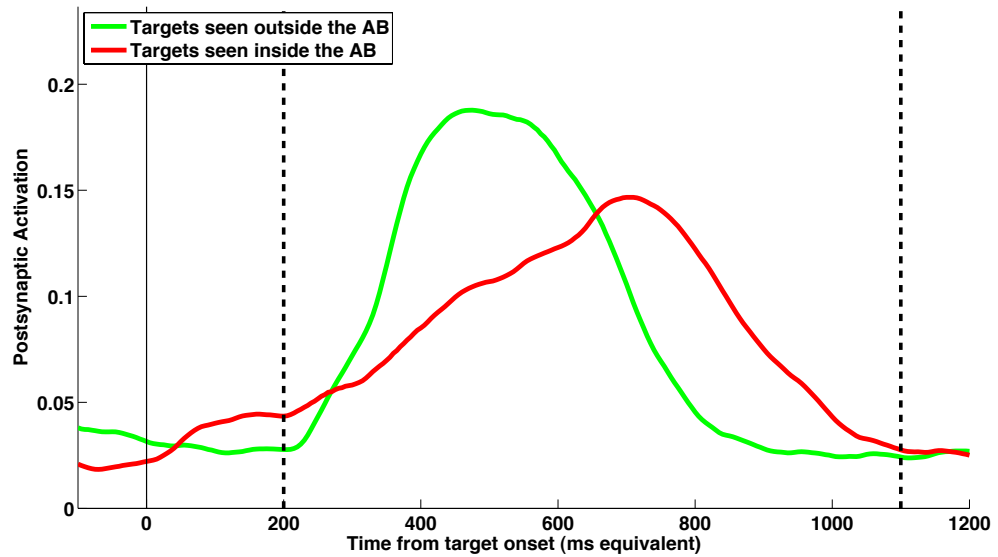


Figure 40 Virtual ERPs for targets seen outside and inside the AB. Panel A: The virtual N2pc. Panel B: The virtual P3. The virtual P3s only depict simulated activity evoked by the target in question.

generate comparable virtual ERPs and ERPimages, we simulate inter-subject variability by introducing a small, random subject-wise delay in the processing of all stimuli in the model (see appendix B.2 for more details). For each such ‘simulated’ subject with a particular delay value, we execute a complete run of the model. This procedure is then repeated as many times as there are experimental subjects. In this way, we generate multiple datasets of simulated trials, one per subject and condition, which can then be statistically analysed. Further, by combining trials across all simulated subjects, we generate virtual ERPs and ERPimages that capture some of the complexity present in their human counterparts.

Figure 40 depicts the average virtual N2pc and P3 ERPs evoked by targets seen outside (*seen T1s followed by T2s at lag 8*) and inside (*seen T2s at lag 3 following a seen T1*) the AB. Note that in contrast to the human P3 ERPs in figure 34B, the corresponding virtual P3 ERPs in figure 40B only depict simulated activity evoked by the target in question. This has been done for visual clarity, and is possible because we can isolate and selectively plot the dynamics associated with the consolidation of a specific target in the ST<sup>2</sup> model. However, this is not possible with the virtual N2pc, as it only consists of activation from the blaster.

Comparing figures 40A and 34A, it is obvious that there exist many differences between the virtual and human N2pc ERPs. As pointed out earlier in section 4.3, the visual differences between the virtual and human N2pc arise due to neurophysiological factors. However, more importantly, the virtual N2pc is considerably delayed for targets inside the AB. This prediction could not be fully confirmed in the human N2pc ERPs (figure 34A); but as pointed out in section 7.4, there is a suggestion of a latency difference that is weakly significant. Thus, there might indeed be a small delay in the latency of the human N2pc for targets inside the AB, which is obscured by the effect of noise. In figure 40A, the model also predicts that the virtual N2pc for targets inside the AB is comparatively attenuated. In addition, there is also a relative increase in its temporal ‘spread’, though this is not easily discernible in the average. In the next section, we will elaborate on and explore the underlying causes of these differences by analysing single-trial virtual ERPs.

Turning to the virtual P3 ERPs in figure 40B, it is evident that the model exaggerates the delay of the virtual P3 for targets inside the AB. Nevertheless, this predicted increase in latency with respect to the virtual P3 for targets outside the AB agrees with similar

differences in the human P3s (figure 34B). As pointed out in section 7.4, there is a significant increase in the 50% area latency of the human P3 during the AB. This replication of the human ERP data by the model effectively follows from the delayed consolidation of targets during the AB. However, as can be seen in figure 40B, the model also predicts that the virtual P3 is relatively attenuated and more temporally spread out during the AB. We will explore these differences further in the next section, using virtual ERPimages.

This section has highlighted the main qualitative similarities between the virtual and human ERPs evoked by targets outside and inside the AB. However, there are many differences between the virtual and human N2pc/P3, in terms of shape and temporal characteristics. This is a consequence of the fact that virtual ERPs do not represent much of the complex neural dynamics underlying the human ERPs. Hence, any comparison between the human and virtual ERPs should be considered at a level of abstraction that the ST<sup>2</sup> is capable of. Hence, the focus of the evaluation of model vs. data in this context is on the relative variation in these ERPs across conditions of interest. Importantly, the virtual N2pc/P3 for targets inside the AB show a comparative attenuation, increase in overall latency and horizontal spread, similar to their human counterparts. Following on from these observations, we delve further into the underlying causes of the observed variation in the virtual ERPs, at the level of single trials.

### 7.7.1 Virtual ERPimages

As with the analysis of human ERPs, grand average virtual ERPs are ‘blind’ to underlying trial-by-trial fluctuations, and cannot be used to dissociate potential sources of aggregate effects. Hence we investigate the correspondence between model and human ERP data at the level of individual trials. This is done by generating *virtual ERPimages* from the ST<sup>2</sup> model. Similar to their human counterparts, virtual ERPimages illustrate the activation profiles of simulated trials making up a particular condition of interest.

Figures 41 and 42 depict the virtual N2pc and P3 ERPimages for targets seen outside and inside the AB. Trials in these ERPimages are sorted by 50% area latency (Luck & Hillyard, 1990) within the windows indicated in the figures<sup>9</sup>. In addition, these virtual ERPimages

---

<sup>9</sup>Note that, unlike with human ERPs, we can use the 50% area latency measure with single virtual ERP traces, as they are free from noise.

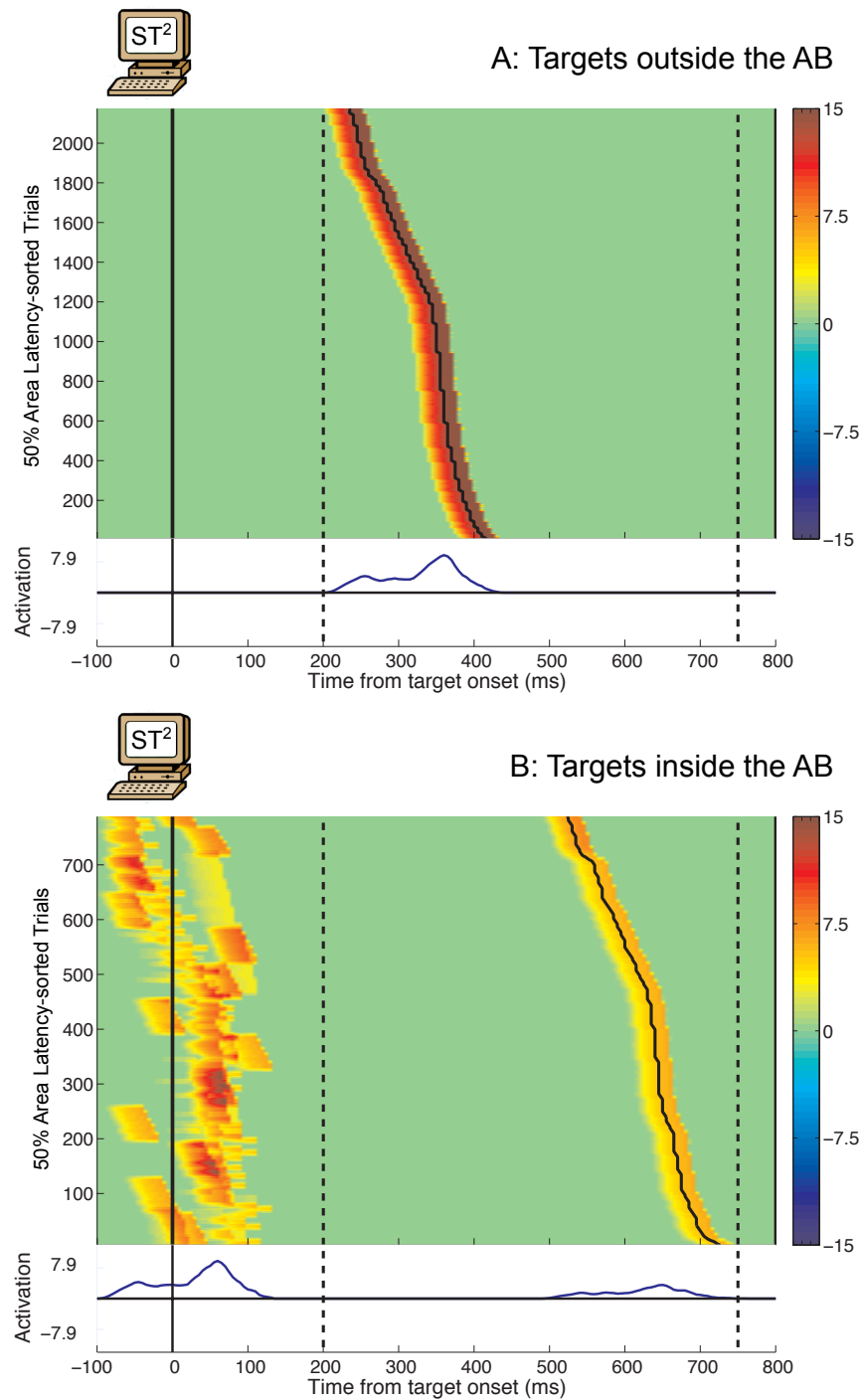


*Figure 41* 50% area latency-sorted virtual N2pc ERP images for targets seen outside and inside the AB. The virtual ERP images are time-locked to presentation of the target of interest, and are plotted with respect to model time equivalent to milliseconds. The dashed lines indicate the window within which the 50% area latency of the virtual N2pc was identified. The solid line indicates the 50% area latency of the virtual N2pc in each trial.

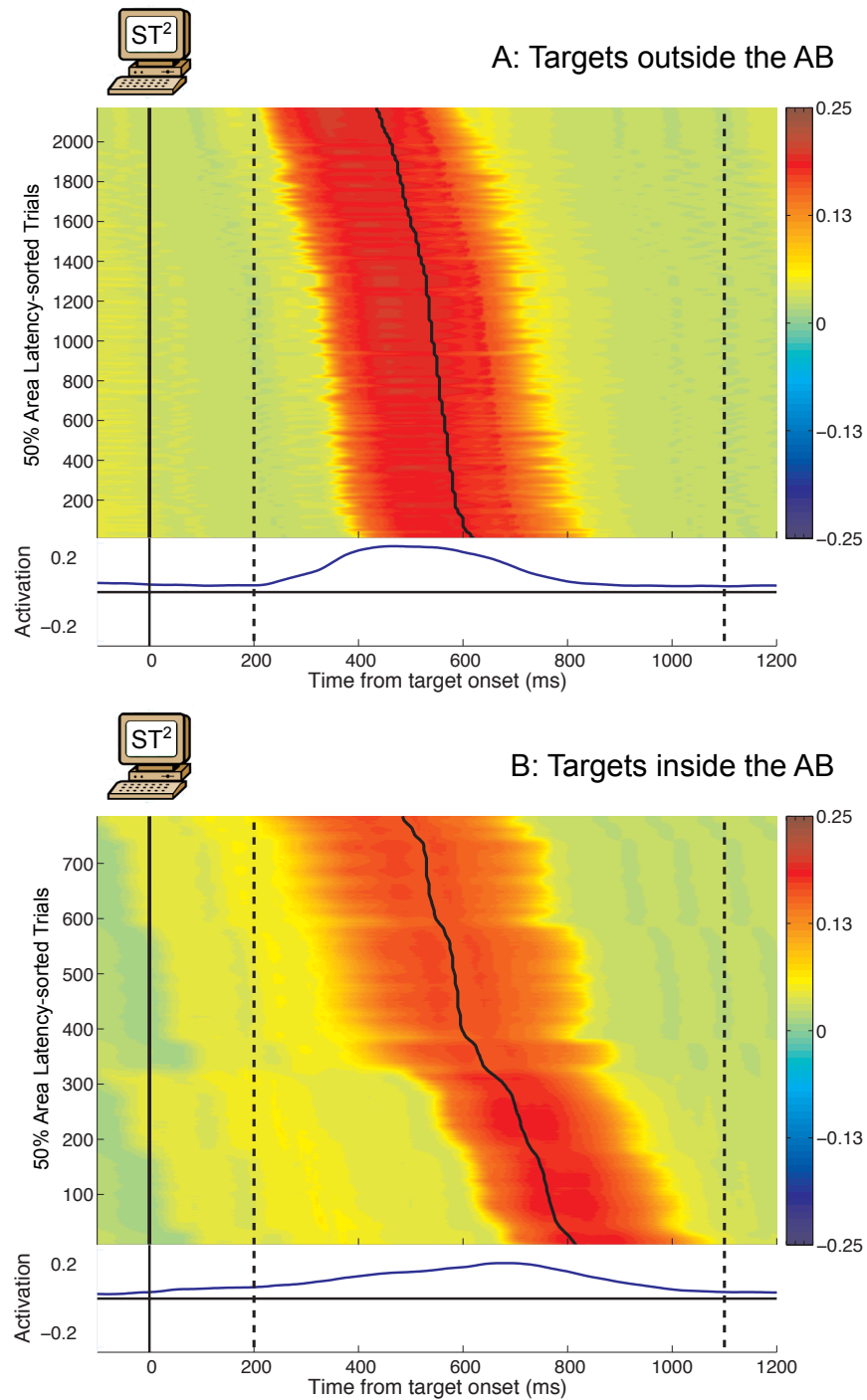


*Figure 42* **50% area latency-sorted virtual P3 ERP images for targets outside and targets inside the AB.** The virtual ERP images are time-locked to presentation of the target of interest, and are plotted with respect to model time equivalent to milliseconds. The dashed lines indicate the window within which the 50% area latency of the virtual P3 was identified. The solid line indicates the 50% area latency of the virtual P3 in each trial. They only depict simulated activity evoked by the target in question.

have been vertically smoothed to improve visual clarity, using a sliding window of 10 trials. Note that in contrast to the human ERPimages in figure 38, the corresponding virtual ERPimages in figure 42 only depict simulated activity evoked by the target in question. As in figure 40B, this has been done for visual clarity, and is possible because we can isolate and selectively plot the dynamics associated with the consolidation of a specific target in the ST<sup>2</sup> model. However, this is not possible with the virtual N2pc ERPimages in figure 41, as they only depict activation from the blaster.

In the next sections, we compare the virtual ERPimages to their human counterparts using qualitative and quantitative methods. As we shall see, this process sheds light on the dynamics of the model at the single-trial level, and provides an in-depth explanation of increased temporal variability during the AB.

### **Qualitative Comparisons to Human ERPimages**

The virtual ERPimages in figure 41 depict the single-trial virtual N2pcs evoked by targets seen outside and inside the AB. These are the same trials that went into the grand averages plotted in figure 40A. Trials in these virtual ERPimages have been sorted by 50% area latency (Luck & Hillyard, 1990) of the appropriate virtual N2pc within 200-750ms after target onset (indicated by dashed lines) in each trial.

As can be seen in figure 41A, a strong virtual N2pc is evoked by all targets seen outside the AB. The latency of the virtual N2pc in this condition is influenced only by variation in T1 strength. For targets inside the AB (figure 41B), the single-trial virtual N2pcs appears to be relatively weaker. This is because, trials in figure 41B fall into one of two types. There are trials in which T2 is strong enough to ‘break-through’ the AB, and gets encoded early despite getting no enhancement from the blaster. Consequently, there is no virtual N2pc in such trials. However, there are many trials in which T2 is not quite strong enough to break-through, but manages to ‘outlive’ the suppression of the blaster and get encoded relatively late. In these trials, the blaster does fire for the T2 after T1 tokenisation is complete, producing a late virtual N2pc. Further, in such trials, the firing latency of the blaster varies more from trial to trial than it does for targets outside the AB, because of the combined influence of variation in T1 and T2 strengths. As a consequence, the virtual N2pc evoked by targets inside the AB has slightly more temporal variability in its latency. This is

not immediately evident in comparing virtual N2pc ERPimages. In the next section we will demonstrate this difference using a quantitative comparison. In figure 41B, this mixture of ‘break-through’ and ‘outlive’ trials, along with vertical smoothing in the ERPimage, reduces the apparent amplitude of the single-trial N2pc. As a result, the corresponding average in figure 40A is relatively delayed and attenuated. This is because though it averages over both types of trials, only ‘outlive’ trials evoke a visible virtual N2pc. Furthermore, as can be inferred from figure 41B, the mixture of these two trial types means that the model does not predict a strong correlation between the latency of the virtual N2pc evoked by a T2 seen during the AB and the T1 preceding it.

The difference between the virtual N2pc ERPimages qualitatively matches the pattern of differences in the human N2pc ERPimages (figure 37). Specifically, as will be shown quantitatively in the next section, the virtual N2pc for targets inside the AB, when it is evoked, has increased temporal variability than the virtual N2pc for targets outside the AB. In addition, the model suggests that the human N2pc might consist of a mixture of ‘break-through’ and ‘outlive’ scenarios, across which its amplitude is very different. However, as with the virtual N2pc ERPimage (figure 41B), these two types of trials might be intermixed in the human ERPimage (figure 37B). This is because the phase-sorting of human ERPimages in section 7.5.2 does not separate trials based on the amplitude of the N2pc. Hence, it is difficult to definitively determine the existence of these two types of trials in the human N2pc for targets inside the AB. Nevertheless, the relative attenuation, increase in latency and temporal spread observed in both the virtual (figure 40A) and human (figure 34A) average N2pc for targets inside the AB lend support to the model’s interpretation of the data.

Figure 42 depicts the single-trial virtual P3s evoked by targets seen outside and inside the AB. These are the same trials that went into the grand averages plotted in figure 40B. Also, trials in these virtual ERPimages have been sorted by 50% area latency of the virtual P3 within 200-1100ms after target onset.

The ERPimages for the virtual P3 show that the simulated EEG activity for targets outside the AB (figure 42A) is relatively more well aligned with target onset. In comparison, the virtual P3s for targets inside the AB (figure 42A) have visibly more inter-trial temporal variability. As with the virtual N2pc, this is because the virtual P3 is only influenced by T1

strength variation. In comparison, the virtual P3 for targets inside the AB (figure 42B) has a wider range of latencies. This increase in variation arises due to the combination of effects influencing T2's encoding process. Very strong T2s break-through the AB and produce an early virtual P3. T2s with mid-range strengths outlive the AB, and evoke a late virtual P3 whose dynamics depend on both T1 and T2 strengths. Consequently, its latency varies considerably from trial to trial. Taken together, the combination of these effects produces comparatively increased temporal jitter in the virtual P3 for targets inside the AB, as seen in the virtual P3 ERPimage (figure 42B). Also, it explains the relative attenuation, increased delay and temporal spread in the virtual P3 average for targets inside the AB, in figure 40B. Further, it also implies that the model does not predict a strong correlation between the latency of the virtual P3 for a T2 seen inside the AB and the T1 preceding it.

On the whole, the differences between the virtual P3 ERPimages for targets outside and inside the AB are a qualitative replication of those in the corresponding human P3 ERPimages (figure 38). The increased temporal variability in the P3 during the AB, evident in both the human and virtual ERPimages, is explained by the model as arising due to the combined influence of target strengths. In the next section, we extend our analysis of single-trial virtual ERPs, and verify the qualitative differences depicted here using statistical analysis of latencies across simulated subjects.

### **Quantitative Comparisons to Human ERPimages**

We now quantitatively test the observed differences in the virtual ERPimages, by comparing across simulated subjects the latencies of the virtual N2pc and P3. To do so, the 50% area latency values that were used to sort the virtual ERPimages in the previous section are grouped by subject. The subject-wise distributions thus generated are then compared using conventional statistical methods. This analysis follows on from the qualitative comparison of the virtual ERPimages, and mirrors the statistical analysis of the human N2pc and P3 phase distributions.

We find that the virtual N2pc evoked by targets outside the AB has a significantly earlier mean 50% area latency (329.82ms) than targets inside the AB (624.44ms)<sup>10</sup>: ( $F(1,17) > 100$ ,

---

<sup>10</sup>For targets seen inside the AB, only trials that evoked a virtual N2pc were included in the analysis.

MSE < 0.001,  $p < 0.001$ ). Importantly, the latency of the virtual N2pc evoked by targets outside the AB has a smaller standard deviation (SD): mean SD values for virtual N2pc latency are 6.98ms and 17.57ms outside and inside the AB, respectively. This difference is highly significant ( $F(1,17) > 100$ , MSE < 0.001,  $p < 0.001$ ). This result provides confirmation that the virtual N2pc does indeed suffer from comparatively increased temporal variability during the AB, as suggested by the virtual ERPimage in figure 41B.

We obtain similar results when analysing the virtual P3. Targets outside the AB have significantly earlier mean 50% area latency (514.20ms) than targets inside the AB (635.44ms):  $F(1,17) > 100$ , MSE = 6.69,  $p < 0.001$ . Further, virtual P3s evoked by targets outside the AB have much smaller standard deviation in their latencies (mean SD = 45.56ms) than those evoked by targets inside the AB (mean SD = 94.54ms). This difference is highly significant:  $F(1,17) > 100$ , MSE = 0.052,  $p < 0.001$ . Again, this result agrees with the qualitative differences in the virtual ERPimages, demonstrating that the P3 evoked by targets inside the AB is more temporally jittered.

On the whole, the results in this section argue that the effect of increased temporal jitter for targets inside the AB is statistically significant across simulated subjects, and affects both the virtual N2pc and P3. Indeed, to some extent, the differences reported here are entirely expected. This is because the model does not incorporate any noise at the single-trial level, and hence inter-trial differences are necessarily significant. However, the statistical comparisons performed here ensure that these differences are not affected by the addition of inter-subject variability.

## 7.8 Discussion

Our qualitative and quantitative comparisons of human ERPimages support the notion of increased temporal variance in target processing during the AB. Further, we have shown that the observed differences in the phase distributions of targets seen outside and inside the AB are indeed real, and cannot be explained by differences in amplitude or any methodological limitations. Finally, our analysis also suggests that T1 processing significantly influences the variance in T2 processing during the AB window, though this could not be confirmed by a trial-by-trial correlation of T1 and T2 phases. At the end of this section, we interpret

this finding in relation to predictions from the ST<sup>2</sup> model.

The virtual ERPs and ERPimages have provided a means for visualising the theory underlying the ST<sup>2</sup> model, at a fine-grained level of detail. Using this novel methodology of comparing model and data both at the level of averages and single-trials, we have shown that, in line with the ST<sup>2</sup> model's hypothesis, activation traces of attentional response and consequent working memory encoding show decreased temporal precision for targets inside the AB compared to targets outside it. However, it is clear from the virtual ERPimages that the virtual N2pc/P3 for targets inside the AB is exaggerated in terms of its delay and duration. This is because the model overemphasises the duration of TAE suppression during T1 encoding. But it does not affect the qualitative comparisons with the human ERPimages, or the conclusions we have drawn therefrom.

To explicate the causes of temporal variability in the ST<sup>2</sup> model, we now summarise the underlying mechanisms that produce it. In the model, transient attentional enhancement (TAE) is evoked by detection of a target, and this attention triggers the encoding of that target into working memory by binding its type representation to a working memory token, which results in this target being correctly reported at the end of the trial. For targets presented outside the AB, the TAE mechanism (i.e. the blaster circuit) is readily available. It fires as soon as an item is classified as a target, and encoding is thus tightly time-locked to the target onset. Thus, there is relatively lesser variation in the tokenisation delay and consequently the latency of the virtual N2pc and P3. Also, because attention is immediately deployed, the model's behavioural accuracy at detecting targets outside the AB is high.

However, as described previously, the processing of a target presented during the AB is complicated by multiple factors. Firstly, T1's strength determines the period of unavailability of the blaster, because of the reciprocal relationship between T1 strength and the duration of its tokenisation process. In addition, T2's own strength determines its dependence on the blaster, as highly salient T2s (at upper end of the range of target strength) can break-through the AB and get encoded early. T2s with slightly lower strength values can outlive the AB, but require the blaster's enhancement. Quite a few T2s, however, have insufficient strength to survive the delay in the blaster response and are missed, producing an AB. This complex relationship between T1 and T2 at lag 3 increases temporal variability in the latency of T2's virtual N2pc/P3. Also, as pointed out earlier, it implies that the model

does not predict a strong, direct correlation between the N2pc/P3 latencies of targets seen outside vs. inside the AB. A possible reason for the lack of any such correlation between the corresponding human N2pc/P3 phase distributions could be insufficient variation in T1 strength in Experiment 2, combined with noise obscuring a weak effect. With sufficient variation in T1 strength (for example, when comparing across T1 masked vs. unmasked) the dynamics of the ST<sup>2</sup> model propose a stronger relationship between the *duration* of the T1 P3 and the latency of the T2 N2pc/P3 during the AB. Indeed, as pointed out before, the model suggests that there should be a reciprocal influence of T1 strength on its encoding duration (Bowman et al., 2008), which would in turn have implications for T2 N2pc/P3 latency. Testing for such a relationship would be informative, but a detailed exploration of this topic is beyond the scope of this thesis (see section 10.3 for a discussion). However, the ST<sup>2</sup> model does predict that there should be a strong correlation between the latency of the N2pc and P3 evoked by a particular target, whether it is seen outside or inside the AB. However, no clear correlation was found in the human data. As pointed out previously, this might possibly be due to the fact that latency variation in the single-trial N2pc is relatively small compared to the P3, and is affected by higher levels of noise. Consequently, the ability of phase analysis to accurately estimate the latency of the single-trial N2pc might be relatively diminished, effectively obscuring a weak correlation.

## 7.9 Related Work

Our experimental results and theoretical explorations complement and inform previous research on temporal selection and the AB. We now discuss these findings and propose interpretations in terms of the ST<sup>2</sup> model.

### 7.9.1 Chun (1997), Popple and Levi (2007)

Chun (1997a) provides initial evidence regarding the effect of the AB on temporal binding. Employing an RSVP paradigm consisting of letters enclosed in coloured boxes and target letters marked by a distinctively coloured box, he investigates the distribution of responses made by participants when either one or two targets are presented. He calculates the centre of mass of this distribution for targets outside and inside the AB, and finds that for targets

outside the AB, the distribution is roughly symmetrical around the target position. But for targets inside the AB, he observes a significant shift in the response distribution toward items presented after the target. In addition, behavioural data presented in Chun (1997a) shows that the variance of the response distribution for T2 report increases when it is presented inside the AB. Popple and Levi (2007) present additional behavioural evidence consistent with findings from Chun (1997a). Using a colour-marked RSVP paradigm where each item had two features (colour and identity), they find that incorrect reports mostly come from the distractor items that are presented close to, and generally following the T2. In addition, they observe that this distribution of responses for T2 shows a pronounced increase in its spread compared to T1.

These findings are well explained by the  $ST^2$  model. In  $ST^2$ , the inhibition of the blaster delays the deployment of attention to a T2 presented during the AB. Consequently, distractors presented right after the T2 are more likely to be tokenised when the second stage becomes available, resulting in the observed shift in the response distribution. Also, as explained in the previous section, due to a combination of factors influenced by T1 and T2 strengths, there is increased temporal variability in T2's encoding process. This in turn leads to increased variation in the behavioural response for T2s presented inside the AB.

### 7.9.2 Vul, Nieuwenstein and Kanwisher (2008)

Vul et al. (2008) propose that temporal selection is modulated along multiple dimensions by the AB. They employ an RSVP paradigm consisting of letters, with targets delineated by simultaneously presented annular cues. Their behavioural analysis suggests that target selection is affected by the AB in one or more of three externally dissociable dimensions discussed below: suppression, delay, diffusion. However, with the  $ST^2$  model, we demonstrate that all three can result from the suppression of attention.

- *Suppression* refers to the reduction in the effectiveness of temporal selection during the AB, and a concomitant increase in random guesses. Vul et al. (2008) measured this effect in the form of a decrease in the mean probability of selecting a proximal response (from  $\pm 3$  item positions) around the target, when it occurs during the AB. In contrast to results in Popple and Levi (2007), they find a significant decrease in this value for T2s during the AB. In the  $ST^2$  model, suppression can be explained by a reduction in the probability of

a target triggering the blaster. During the AB, a relatively large percentage of T2s fail to fire the blaster and do not have enough bottom-up strength to be tokenised. The model would hence predict the suppression observed by Vul et al. (2008), because the percentage of trials in which the blaster fires in response to a T2 would be reduced during the AB. Furthermore, as participants are forced to indicate a response for both targets in Vul et al. (2008), this reduction would translate to an increase in the number of random guesses for the T2. Finally, as one would expect, the time course of suppression follows the time course of the AB as simulated by the  $ST^2$  model.

- *Delay* refers to a systematic post-target shift in the locus of responses chosen for T2 when compared to T1. Vul et al. (2008) quantified delay as the centre of mass of the distribution of responses for each target, calculated similarly to the API (Average Position of Intrusions) measure in Botella et al. (2001) and the intrusion index score in Chun (1997a). This notion of an increase in the latency of attentional selection is reflected in the  $ST^2$  model. Specifically, suppression of the blaster during T1 encoding results in an increase in the latency of its response to a T2 during the AB (see Bowman et al., 2008 for more details on delayed T2 consolidation in the  $ST^2$  model). As a result, in an RSVP paradigm like that used by Vul et al. (2008), items presented after T2 are more likely to get the benefit of the blaster and get chosen as responses, resulting in the observed shift in the response distribution. However, this shift in the locus of responses observed by Vul et al. (2008) seems to persist at late T2 lag positions well beyond the duration of the AB, and is somewhat more puzzling. This finding could perhaps be attributed to the cognitive load associated with holding T1 in working memory.

- *Diffusion* refers to a decrease in the precision of temporal selection, corresponding to an increase in the overall spread in the distribution of responses during the AB. Vul et al. (2008) estimate diffusion by comparing the variance around the centre of mass of the response distributions for T1 and T2, and find that it is significantly increased for T2s during the AB. This observation is explained by the  $ST^2$  model as follows: in the context of the paradigm in Vul et al. (2008), there would be increased temporal variation in T2 encoding because of the influence of T1 processing. Hence, due to the influence of both T1 and T2 strengths on response selection, erroneous responses further away from the target position would get selected for tokenisation, producing increased variance in the distribution

of responses. Again, the time course of diffusion is similar to that of suppression, and is in keeping with the window of the AB predicted by the ST<sup>2</sup> model.

In summary, we think that a single underlying mechanism of variation in the temporal dynamics of attention from trial to trial could potentially explain the three effects observed in Vul et al. (2008). An explicit computational account of these three dimensions in terms of the ST<sup>2</sup> model is beyond the scope of this thesis. Nevertheless, the explanation proposed above highlights the role that the temporal dynamics of transient attention would play in explaining these effects.

### 7.9.3 Sergent, Baillet and Dehaene (2005)

Sergent et al. (2005) combine behaviour and EEG to investigate the timing of brain events underlying access to consciousness during the AB. They analyse early and late ERP components evoked by a pair of targets, a T1 followed by a T2 either at a short lag (equivalent to our *inside the AB* condition) or at a long lag (equivalent to our *outside the AB* condition). They plot unsorted ERPimages to visualise the inter-trial variation in the EEG activity, and find that when T2 is presented within the AB, T1's P3 influences the temporal dynamics of the ERP components correlated with conscious access to T2. In particular, the ERPimage depicting their T1 and T2 P3s clearly shows that even when T2 is seen during the AB window, it evokes a more 'smeared out' P3 as compared to the T1. However, the analysis of single-trial data in Sergent et al. (2005) presents ERPimages that are not sorted (unlike the phase sorting we have performed in this chapter), thus limiting their interpretation. Further, they do not compare temporal variability of targets seen outside and inside the AB. Despite these differences, their data agrees with ours, and supports our hypothesis of reduced temporal precision during the AB. This is because we would expect increased inter-trial variability in the P3 evoked by a T2 inside the AB to result in a 'smearing out' effect in its ERPimage, when trials are plotted after smoothing, but without sorting by phase.

## 7.10 Conclusions

In this chapter, we have presented human ERP evidence in favour of a reduction in the temporal precision of transient attention during the AB. The AB provides us with a suitable

phenomenon with which to investigate the interplay between attention and perception. The interplay between these tightly linked cognitive processes is adversely affected during the AB, producing the reduction in precision observed in behavioural and EEG data.

Using ERPimages, we have provided qualitative evidence for differences in temporal variability in the N2pc and P3 evoked by targets seen outside vs. inside the AB. This evidence is supported quantitatively, by a combination of ITC analysis and direct statistical comparison of phase distributions. These analyses suggest that there is significantly increased temporal jitter in the ERP activity evoked by targets inside the AB. This finding is consistent with the theoretical framework of the ST<sup>2</sup> model. Specifically, we have used the ST<sup>2</sup> model's neural implementation to generate both virtual ERPs and ERPimages, which we have then compared to their human counterparts. We believe that correlating model and electrophysiological data in this way provides a two-fold benefit. Firstly, it has provided a sufficient explanation for the modulatory effects of the AB on the temporal precision of visual processing. Secondly, it has allowed us to instantiate and test the model at the level of single-trial dynamics. In doing so, we have shown that the theoretical assumptions about the nature of temporal visual processing embodied in ST<sup>2</sup> can be validated using EEG data. We believe that the combination of experimental and theoretical analyses presented in this chapter contributes to converging evidence for the notion that the AB results in a reduction in the temporal acuity of selective attention.

The last chapter of this thesis will return to the general idea of comparing human and virtual ERPs. But before that, the next chapter shifts focus to discuss a significant extension to the ST<sup>2</sup> model, which extends its capabilities to the domain of feature binding in time.

## Chapter 8

# Attention and Temporal Feature Binding

In this chapter, we describe the  $2f\text{-ST}^2$  neural network model of temporal feature binding. Beginning with a rationale for its development, we describe its neural network architecture and dynamics. We then generate behavioural predictions from the model relating to experimental manipulations, and validate them using data from previous studies. In this process, we will highlight how the  $2f\text{-ST}^2$  model improves over the Botella et al. (2001) model, and provides a more parsimonious description of temporal binding. Following on from this, we describe behavioural data from our temporal binding experiment. This data refutes a prediction of the Botella et al. (2001) model and confirms an alternative one by the  $2f\text{-ST}^2$  model, demonstrating that  $2f\text{-ST}^2$  can explain a potentially broader set of data.

### 8.1 Introduction

The empirical and theoretical work discussed thus far in this thesis has investigated various aspects of the temporal visual processing where targets had only one task-relevant feature dimension. In other words, in such experimental contexts, a target is distinguishable from distractors based on a distinguishing characteristic that participants are asked to detect, identify and later report. In conjunction, the original  $\text{ST}^2$  model described in section 3.1 and published in Bowman and Wyble (2007) simulates the temporal processing of targets with a

single feature dimension, i.e., semantic identity, and the subsequent encoding of this identity into working memory. The research in this chapter extends beyond such paradigms, and investigates the binding of arbitrarily selected pairs of feature dimensions in time, referred to in this thesis as *temporal feature binding*<sup>1</sup>. This is the process by which arbitrarily specified categories of visual/semantic features are ‘bound’ together into working memory, under tight temporal constraints. We present the *2f-ST<sup>2</sup>* model of temporal feature binding and the role of the temporal spotlight therein. This theoretical research draws upon and extends beyond the ST<sup>2</sup> and Botella et al. (2001) models, in addition to previous behavioural research into temporal feature binding (see section 2.5 for a detailed introduction).

## 8.2 The Two-Feature Extension to ST<sup>2</sup>: The 2f-ST<sup>2</sup> Model

The *2f-ST<sup>2</sup>* model has been designed to simulate temporal feature binding in RSVP experiments. In the kind of paradigms we will refer to in this and the next chapter, RSVP streams contain sequences of target items and distractor items. Each such item has a constituent pair of features relevant to the task, which we refer to as the *key* and *response* feature of the item. Over the items in the stream, these features vary along orthogonal and independent dimensions (see section 2.5 for formal definitions of these terms). The 2f-ST<sup>2</sup> model simulates the initial parallel processing of these features and the detection of a target item defined by its task-relevant key feature. Further, it highlights the role of the temporal spotlight in binding a pair of concurrent key and response features into working memory. In the sections below, we highlight the rationale behind the development of this model, and describe its neural network architecture in detail.

### 8.2.1 Rationale

The main proposal of the 2f-ST<sup>2</sup> model is a neurophysiologically inspired mechanism describing the process of temporal feature binding in vision. It draws upon previous models (Keele & Neill, 1978; Chun & Potter, 1995; Botella et al., 2001), and provides a deeper level of elucidation of the experimental findings. and in particular, improves upon the high level

---

<sup>1</sup>As pointed out in section 2.5, the term ‘feature’ here (and in the literature) is used in a general sense, to include both basic visual features and high-level semantic representations.

model proposed by Botella et al. (2001) (see section 2.5.2). Highlighted below are the main advantages of the 2f-ST<sup>2</sup> model, which we will revisit later in this and the next chapter.

**Depth** As 2f-ST<sup>2</sup> is a neural network model, it explains the causation of behavioural outcomes and cognitive events at the level of neural dynamics. In this sense, the model allows for a level of explanation that is lower than that provided by Botella et al. (2001), whose ‘box-and-arrow’ model is limited to a description of abstract information processing constructs.

**Breadth** Another key theoretical advantage of the 2f-ST<sup>2</sup> model is that its explanatory powers extend beyond behavioural research relating to temporal feature binding. As it is based on the original ST<sup>2</sup> model, it preserves the ability to explain behavioural and EEG findings relating to other phenomena like Attentional Blink, Repetition Blindness, etc. 2f-ST<sup>2</sup> subsumes these phenomena within a relatively broad framework describing temporal visual processing. In comparison, Botella et al. (2001) restrict themselves to an explanation of correct reports and the formation of illusory conjunctions in temporal feature binding.

**Parsimony** In their model, Botella et al. (2001) propose two distinct mechanisms for temporal feature binding, implemented by the attentional focusing and sophisticated guessing routes. Their arguments for the existence of two different binding routes are based on theoretical and empirical grounds (please refer to the discussion in section 2.5.2 for details). However, the Botella et al. (2001) model leaves unclear the mechanistic basis upon which one of the two hypothesised routes is chosen in a given situation. Critically, the model hypothesises an unspecified mechanism by which it knows how to switch between the attentional focusing route (and bind the correct response feature) and the sophisticated guessing route (and probabilistically select a response feature). In this sense, the Botella et al. (2001) model is non-parsimonious in its proposition.

In contrast, as we shall see, the 2f-ST<sup>2</sup> model explains how common underlying neural network constructs could lead to different dynamics and consequent processing outcomes at the behavioural level. Importantly, the process of temporal feature binding in 2f-ST<sup>2</sup> does not have any knowledge of the ‘correct’ response feature. Rather, correct responses and conjunction errors are all generated by the same underlying architecture, due to variation

in activation dynamics from trial to trial. Importantly, this common architecture explains previous reaction time data (Botella, 1992) that led Botella et al. (2001) to propose a dual-route approach in their model (see the discussion in section 2.5.2 for more details). Thus, the 2f-ST<sup>2</sup> model is more parsimonious in its assumption of required mechanisms, and provides a common framework for interpreting qualitative differences in behaviour. As described in the next section, the 2f-ST<sup>2</sup> model includes two parallel *pathways* for processing key and response features of items, but only one common binding mechanism for binding a pair of such features into working memory. In contrast, the Botella et al. (2001) model, in addition to having two parallel modules (Module K and R) to process key and response features, also suggests that there are two distinct *routes* for completing feature binding.

**Verification** As we have shown in previous chapters, the ST<sup>2</sup> model has been used to generate virtual ERPs, which have been beneficially compared to human ERPs from different experiments studying temporal perception. The 2f-ST<sup>2</sup> model provides the same benefit in the context of temporal feature binding. The generation of virtual ERPs from the 2f-ST<sup>2</sup> model, and the evaluation of these predictions in the light of human ERPs relating to temporal binding form the basis of the next chapter. In this regard, 2f-ST<sup>2</sup> extends beyond the Botella et al. (2001) model in two ways: firstly, it allows for interpretation of ERP data, in addition to explaining behaviour using a common theoretical framework. Secondly, ERP data can then also be used as an additional source of informing and constraining the model (see chapter 4 for a general introduction to model-data comparisons at the level of ERPs).

## 8.2.2 Architecture

Figure 43 depicts the neural architecture of the 2f-ST<sup>2</sup> model. As is evident from the comparison to the architecture of the original ST<sup>2</sup> model in figure 11, 2f-ST<sup>2</sup> borrows from and extends beyond it, introducing some important additions described below. For technical details on the configuration of the 2f-ST<sup>2</sup> model, please refer to appendix A.4.

Broadly speaking, the architecture of the 2f-ST<sup>2</sup> model can be divided into two stages of processing. Stage 1 is responsible for the processing of the features of items, and building their type representations. 2f-ST<sup>2</sup> proposes that, in Stage 1, the key and response features (see section 2.5) of items in RSVP are processed separately and concurrently, within two

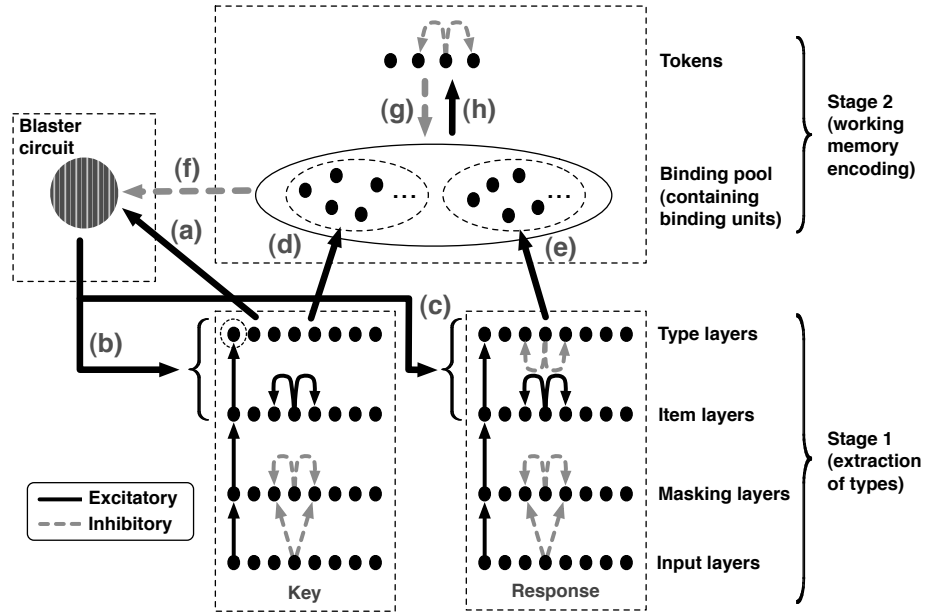


Figure 43 **The 2f-ST<sup>2</sup> model.** Task demand is indicated by the dashed ellipse around the target’s key pathway type node. In comparison to ST<sup>2</sup>, 2f-ST<sup>2</sup> includes a parallel response feature processing pathway in Stage 1, in addition to an extended binding pool and token mechanism in Stage 2.

distinct, parallel pathways. To some extent, these two pathways share functional similarity with Module K and Module R of the Botella et al. (2001) model. In 2f-ST<sup>2</sup>, the *key feature processing pathway* and the *response feature processing pathway*, each consist of 4 layers, namely *Input*, *Masking*, *Item* and *Type*. Thus, for each item in an RSVP stream, each layer in the key/response pathway has a node responsible for processing the corresponding feature of the item. Functionally speaking, these layers in the key and response pathways of 2f-ST<sup>2</sup> have roles similar to their counterparts in the original ST<sup>2</sup> model, but with some important technical and conceptual differences, discussed further in the sections below.

Stage 2 of the 2f-ST<sup>2</sup> model consists of the binding pool and a set of tokens. The binding pool mediates the establishment of an association between a pair of type nodes in the Type layers of the two pathways in Stage 1 with a working memory token. Tokens create in the model a notion of serial order, and provide it with an episodic memory of previous bindings. In order to create and maintain such bindings between a pair of key and response types with a token, the binding pool contains multiple nodes that are selectively activated during the binding process. Importantly, this binding process is supported by the deployment of Transient Attentional Enhancement (TAE) from the blaster. This positive

feedback from the blaster ensures that the key and response features to be bound have enough activation strength to get consolidated into a token via the binding pool. On the whole, feature binding in 2f-ST<sup>2</sup> involves the temporal interplay between concurrently active key and response types, the blaster and the binding pool.

### **The Key Feature Processing Pathway**

As defined previously in section 2.5, the key feature dimension of RSVP items in temporal binding experiments is that which participants are required to monitor for the occurrence of the target item. Thus, the key feature dimension could be a basic visual property of the items, like colour, shape, orientation, etc., or a semantic property, like identity. The target item in the stream is defined by its unique key feature, which participants are required to detect. In 2f-ST<sup>2</sup>, the constituent key features of items in RSVP are processed in the key feature processing pathway. In terms of its architecture and internal connectivity between layers, the key feature processing pathway of 2f-ST<sup>2</sup> is effectively the same as the processing pathway in Stage 1 of the original ST<sup>2</sup> model (see section 3.1). Hence, the key pathway is responsible for processing key features of items in a cascaded fashion, and eventually generating type representations at its Type layer.

At the Type layer of the key pathway, a task demand mechanism operates to enhance type representations of key features belonging to a target, and suppress those belonging to distractors. Hence, by definition, distractors are RSVP items that do not have the target-defining key feature. The role of the task demand here, similar to that in ST<sup>2</sup>, is to ensure that only the activation of key features of a target at the key pathway Type layer can trigger the blaster, through the connection labelled (a) in figure 43.

### **The Blaster**

The blaster in 2f-ST<sup>2</sup> is internally implemented identically to that in the ST<sup>2</sup> model. However, here it is only triggered by activation feeding in from target type nodes at the Type layer in the key pathway. Once activated, the blaster produces its characteristic ballistic response, to provide a non-specific, short-lived burst of attentional enhancement to all Item and Type layer nodes in *both* key and response pathways, through the connections marked (b) and (c) in figure 43. This boost provides the maximally active key and response types

enough activation to initiate a combined binding process in the binding pool. As we shall see later, the temporal relationship of the blaster’s firing to feature processing times effectively determines the dynamics and behaviour of 2f-ST<sup>2</sup>.

### **The Response Feature Processing Pathway**

As pointed out earlier, RSVP items in temporal feature binding experiments typically have a pair of orthogonal and independent feature dimensions (see section 2.5 for an introduction). The key feature dimension identifies a target in the stream, while the response feature dimension specifies features that are available to be bound to the key feature of the target for later report. Within Stage 1 of 2f-ST<sup>2</sup>, response features of successive items in RSVP are processed independently of their key features, in a separate, parallel response feature processing pathway. This response pathway has a hierarchy of layers similar to the key pathway described earlier. However, there are some important differences in its architecture and connectivity, as described below.

**Task Demand** In 2f-ST<sup>2</sup>, the task demand mechanism does *not* operate at the Type layer of the response pathway. This is because, by definition, a target in RSVP is differentiated and selectively enhanced due to its unique key feature. Hence, task demand operates, as with the ST<sup>2</sup> model, at the Type layer of the key pathway, selectively emphasising the type node of the target and suppressing those of distractors. However, at the Type layer of the response pathway, there is no task demand mechanism. In other words, all response features, including that of the target, are treated equally. In contrast to the Botella et al. (2001) model (specifically, the attentional focusing route therein), the 2f-ST<sup>2</sup> model does not have any knowledge of the ‘correct’ response feature. At the response pathway Type layer, response types of distractors presented in temporally proximal (i.e., -2, -1, +1 and +2) positions relative to target can be co-active with the response type of the target. Hence, any of these response types can be bound with the key type of the target. But in order to generate a binding, the potential conflict between multiple co-active response type nodes needs to be resolved. This requirement leads to the second important difference in the response pathway, lateral inhibition, described next.

**Response Competition** Type representations of co-active response features compete with each other, because of the weak lateral inhibition that is introduced between type nodes in the response pathway Type layer. This ensures that, under normal circumstances, only strongly active response types can initiate the feature binding process. During the tokenisation of a target, depending on the relative timing of the blaster firing and the strengths of the co-active response types, the response type of the target or a temporally proximal distractor can win this competition. This competitive interaction between type nodes in the response pathway Type layer hence produces different possible binding outcomes and eventual behavioural responses, including correct reports and conjunction errors. In addition, the lateral inhibition also makes it unlikely that multiple response types have enough strength to get bound simultaneously with the same key type.

### The Binding Pool

The binding pool in 2f-ST<sup>2</sup> maintains associations between tokens and key and response types at the corresponding Type layers in the two pathways in Stage 1. It consists of a set of nodes, which are implemented identically to those in the binding pool of the ST<sup>2</sup> model. In the current localist implementation<sup>2</sup> of the binding pool in 2f-ST<sup>2</sup>, its nodes can be grouped into two disjoint subsets. The first subset is responsible for maintaining associations between key types and the tokens. Hence, it has one node for each combination of key type and token<sup>3</sup>. Consequently, these binding pool nodes receive activation from their corresponding target type nodes in the key pathway Type layer, via the connection labelled (d) in figure 43. Internally, this connectivity is implemented like in the ST<sup>2</sup> model (see figure 59B). The second subset of binding pool nodes maintains associations between response types and the tokens, and has one binding pool node for each combination of response type and token. Thus, nodes in this subset receive activation from their corresponding type nodes in the response pathway Type layer, via the connection labelled (e) in figure 43.

Given this architecture, for a target with a pair of (key and response) features, creating a

---

<sup>2</sup>This localist implementation of the binding pool in 2f-ST<sup>2</sup> is not intended to be scalable to the level of complexity represented in the brain. In chapter 10.3, we will discuss how the binding pool could be implemented with a more neurophysiologically realistic, distributed architecture.

<sup>3</sup>Note that key type nodes of distractors are suppressed at the Type layer by the task demand mechanism, and do not participate in binding.

successful binding involves two binding pool nodes, one in each of the above subsets. Because of activation feeding in from the two pathways, these nodes are activated to associate a token with two type nodes, one in the key pathway Type layer and the other in the response pathway Type layer<sup>4</sup>.

An important consequence of this combined binding pool is the resulting functional distinction between the 2f-ST<sup>2</sup> model and the Botella et al. (2001) model. The latter model proposes two distinct binding routes for temporal feature binding, where most correct reports come from the attentional focusing route, while conjunction errors occur in the sophisticated guessing route. The 2f-ST<sup>2</sup> model suggests a mechanism where these different kinds of responses lie on the same spectrum of possible binding outcomes, despite qualitative differences in behaviour. Here, the binding of both correct reports and conjunction errors proceeds through the same processing sequence over a common neural network architecture. However, differences in the temporal dynamics lead to different behavioural outcomes. Later in this chapter, by simulating reaction times with the 2f-ST<sup>2</sup> model, we will describe how this single mechanism could potentially explain previous data that was used to justify the dual-route approach adopted in the Botella et al. (2001) model.

## **Tokens**

The 2f-ST<sup>2</sup> model has a set of tokens that provide it an episodic memory of previous bindings. Tokens in 2f-ST<sup>2</sup> have an internal architecture like those in the ST<sup>2</sup> model. They are activated in serial order, and the currently active token inhibits all binding pool nodes of other tokens via the connection labelled (g) in figure 43. However, during binding in 2f-ST<sup>2</sup>, a token receives activation from a pair of binding pool nodes, via the connection labelled (h) in figure 43. These binding pool nodes are in turn excited by a pair of type nodes, one in the key pathway Type layer and the other in the response pathway Type layer. Thus, the successful completion of the binding process results in an association being established between the active token, a pair of binding pool nodes, a key type and a response type. Later, the model can retrieve a previously established binding recorded in a token,

---

<sup>4</sup>Under occasional circumstances, if multiple response type nodes have enough activation in the response pathway Type layer, they can both activate their corresponding binding pool nodes and get bound with a key type into the same token. However, the probability of such ‘multiple bindings’ is low, and is specified for specific simulation configurations in the appendix.

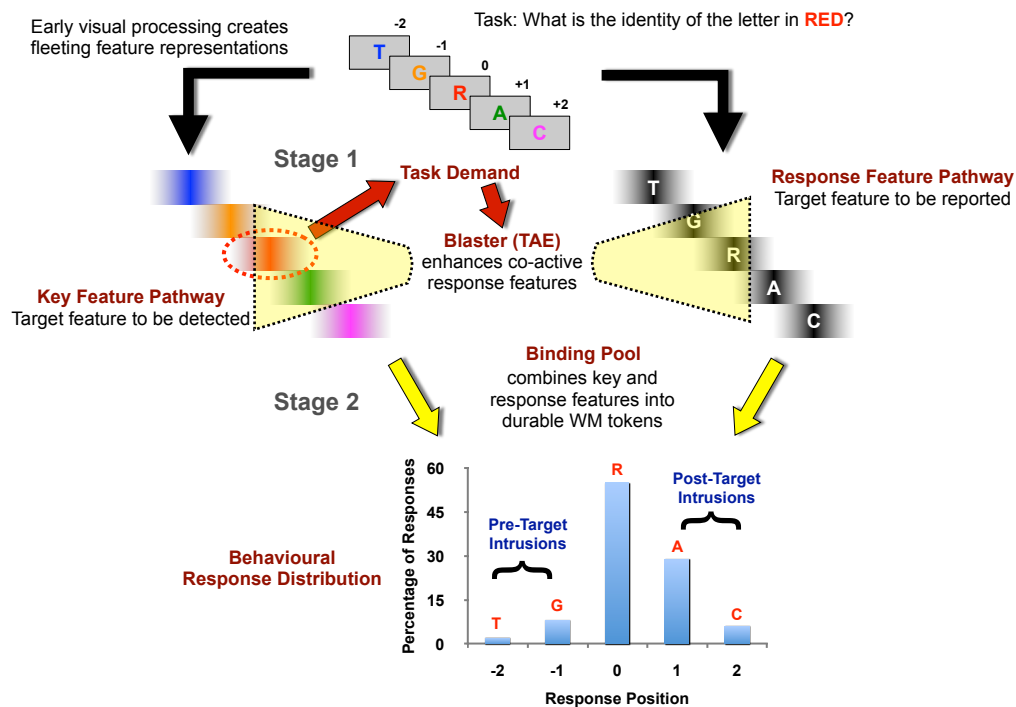


Figure 44 **Temporal feature binding in the 2f-ST<sup>2</sup> model.** Key and response features of successive items in an RSVP stream are processed in parallel, and get bound together into tokens via the extended binding pool. The range of different possible binding outcomes produces a behavioural response distribution shown at the bottom.

by following in reverse the path of activation used to establish it, to identify the key and response types that are bound to it via the binding pool.

### 8.2.3 Dynamics

We now describe how the architecture of the 2f-ST<sup>2</sup> model simulates the temporal binding of key and response features in a typical RSVP setting. At a conceptual level, figure 44 illustrates the process by which this happens in the model, using the example of an RSVP paradigm consisting of coloured letters. A typical task instruction in such an experimental context would be “Identify the letter presented in the colour Red” (the letter ‘R’ in the sample trial shown in figure 44). The key and response features (colour and identity, respectively, in the example paradigm) of successive items in the RSVP stream are processed in parallel, within the corresponding pathways in Stage 1. Importantly, response features of items are processed all the way up to the Type layer, well before the target item actually occurs

within the stream. The occurrence of the target is detected by the appropriately tuned task demand filter in the key pathway at the end of Stage 1. In this example paradigm, the task demand is tuned to look for the colour red. Upon the activation of the corresponding type node, it triggers the blaster.

The feedback enhancement provided by the blaster in 2f-ST<sup>2</sup> is non-specific, and provides a short-lived burst of enhancement to all nodes in the Item and Type layers in both pathways. At the key pathway Type layer, only the key feature of the target derives practical benefit from this enhancement, as key features of distractors are suppressed by the task demand mechanism. In case of the example in figure 44, the target's key feature is the colour red. Hence, as with single target encoding in the ST<sup>2</sup> model, the corresponding key pathway Type layer node is the only one that has enough activation to feed into a binding pool node. However, in the response pathway, there is no such suppression in operation. Thus, any response features currently active at the time of the blaster firing benefit from its enhancement. In everyday circumstances, this would typically be the response feature of the target. But in an RSVP setting, where featural representations of items in the stream are fleeting and overlap in time, multiple response features (letter identities in the example) are likely to be co-active at any given time. Further, these co-active responses compete with each other, due to the lateral inhibition at the response Type layer. Because of the blaster's enhancement, the maximally active response has enough strength to feed activation into a binding pool node. This then initiates the chain of events to trigger its binding into the token that is being bound in parallel with the key feature. At end of a typical binding process, a token in WM is bound to a pair of type nodes, one in each of the Type layers of the two pathways, through a pair of binding pool nodes. In effect, it is the *temporally concurrent* activation of a pair of (key and response) features that results in them being bound together. Further, this mechanism is common to all the possible behavioural outcomes the model can produce, including correct reports, pre-target and post-target errors. Also, it is this mechanism that is the major point of contrast between 2f-ST<sup>2</sup> and the Botella et al. (2001) model, which proposes two conceptually different binding routes for correct reports and conjunction errors. In particular, the (Botella et al., 2001) model leaves unspecified how the choice between its two binding routes is implemented. The dynamics outlined above describe how the need for choosing between different behavioural outcomes is unnecessary

in the 2f-ST<sup>2</sup> model. Here, these apparently different binding routes are parsimoniously realised by a single underlying mechanism.

As can be inferred from this description of 2f-ST<sup>2</sup> dynamics, the relative times for feature processing in the two pathways plays an important role in determining the pattern of bindings produced over a range of key and response feature strengths. This is because, in any given trial, the relative amounts of time taken to process key and response features of items determines which response feature benefits most from the blaster's enhancement and gets encoded. This in turn depends not only on the strengths of the features themselves (which vary from trial to trial), but also on the configuration of processing times in the two pathways. Over a large number of simulated trials encompassing a variety of feature strengths, the model produces a range of binding outcomes, making up a response distribution, depicted as a histogram at the bottom of figure 44. This histogram plots the relative probabilities with which the model produces correct reports, pre-target and post-target errors. In a majority of trials with normal model configuration, the response feature of the target is the maximally active one at the time of blaster firing. Hence it receives most of the TAE, and successfully gets bound into a token. But on quite a few trials, response features of items before (in the -1 or -2 positions) or after (in the +1 or +2 positions) the target can be more active at the time of blaster firing, and subsequently get encoded. This can happen due to a combination of factors, including systematic variation in feature strengths, random trial-to-trial variation in processing delay in the pathways, and additive systematic manipulations of this delay (described further in the next section). In such circumstances, the model produces a conjunction error or an illusory conjunction, in the form of a pre-target or a post-target intrusion (see section 2.5 for formal definitions of these terms). Of course, the relative probability of occurrence of these different responses depends on the specific configuration of the model. As we shall see in the next section, systematic manipulations in its configuration allow the 2f-ST<sup>2</sup> model to simulate different response distributions observed in previous behavioural experiments.

#### 8.2.4 Configuration

As a neural network model, the 2f-ST<sup>2</sup> model has many parameters that control its operation (see appendix A.4 for details). These include local parameters that affect the dynamics in

a particular layer, and global parameters that affect the model as a whole. However, for all the simulations described in this and the next chapter, the model’s configuration as defined by these parameters is kept mostly unchanged. In these simulations, the parameters of interest are the following:

$\tau_D$  is a random, *variable* +ve/-ve delay added to the processing of features in both pathways, within a trial. Importantly,  $\tau_D$  is repeatedly sampled within each trial run, once per item in the stream, from a gaussian distribution with mean of 0 and standard deviation of 15ms, and is added to both key and response pathways<sup>5</sup>. For a particular item in a trial, the value of  $\tau_D$  introduced in the processing of its key and response features is the same. However, the bottom-up input strengths of these features are varied independently from trial to trial (see appendix A.4). Consequently, the parallel processing of these features in Stage 1 is not perfectly synchronous. The addition of  $\tau_D$  effectively introduces temporal noise in this processing, and allows the model to generate larger numbers of conjunction errors and broader response distributions.

$\tau_K$  adds a *fixed* +ve/-ve delay to the processing of all features in the key pathway. Note that, unlike  $\tau_D$ ,  $\tau_K$  is not sampled from a gaussian distribution. Rather, it is kept the same for all trials within a complete simulation run. In this thesis,  $\tau_K$  is altered across a pair of simulation runs, to model experimental conditions involving systematic manipulations of key feature processing.

$\tau_R$  is similar to  $\tau_K$ , except that it adds a fixed +ve/-ve delay to the processing of all features in the response pathway instead. In this thesis,  $\tau_R$  is altered across a pair of simulation runs, to model experimental conditions involving systematic manipulations of response feature processing.

With this understanding of the 2f-ST<sup>2</sup> model’s architecture, dynamics and configuration, we now proceed to generate predictions from it. These predictions are generated by reconfiguring the  $\tau_K$  and  $\tau_R$  parameters described above, while keeping all other parameters unchanged.

---

<sup>5</sup>These settings for  $\tau_D$  are kept the same in all the simulations described in this thesis.

### 8.3 Behavioural Predictions of the 2f-ST<sup>2</sup> Model

Behavioural research has investigated isolated manipulations in the times of feature processing in the key or response pathway, and measured the subsequent effect on the pattern of responses (Botella et al., 2001; Botella, 1992; Kikuchi, 1996; Boucart et al., 1998). These manipulations have involved changes to a variety of different stimulus characteristics, from low-level psychophysical aspects (like colour) to high-level lexical contexts (like word frequency). Behaviourally, the main consequence of these manipulations is a measurable change in the number of correct reports, and a shift in the locus of responses relative to the target. This shift is visible in the response distribution, and can be quantified and statistically compared using metrics like the Average Position of Intrusions (API) ( Botella et al., 2001; also see section 2.5).

The 2f-ST<sup>2</sup> model described above is capable of simulating the generation of correct reports, pre-target and post-target errors in temporal binding tasks. Further, it can simulate the effect of manipulations in the relative processing delays of features in the key or response pathway. Specifically, as pointed out in the previous section, the model has a parameter for each pathway, which, for all trials within a complete simulation run, adds a fixed delay in the processing of all features in that pathway. This delay parameter is referred to as  $\tau_K$  in the key feature pathway and  $\tau_R$  in the response feature pathway. In the ‘default’ configuration of the model,  $\tau_K$  and  $\tau_R$  are set to 0. This setting effectively means that there is no overall difference in the processing times of features in the two pathways. In order to simulate an isolated increase in the processing time in one pathway, the corresponding delay parameter,  $\tau_K$  or  $\tau_R$ , is set appropriately. With this fixed delay, and with all other parameters remaining unchanged, a complete simulation run of the model is executed, encompassing multiple trials over a range of feature strength combinations in both pathways (See appendix A.4 for details of strength variation in the model). The simulated trials thus generated are used to plot response distributions and virtual ERPs.

This method for simulating the effect of key and response feature manipulations abstracts away from the particulars of the experimental techniques used in previous studies to create similar manipulations. The advantage offered by this method is that it involves the reconfiguration of a single generic parameter (either  $\tau_K$  or  $\tau_R$ ) in the model. With

this change, the model can simulate data from a potentially large number of studies, which produce shifts in the response distributions, albeit using different experimental techniques. Like the Botella et al. (2001) model, 2f-ST<sup>2</sup> does not make any quantitative predictions about the response distribution produced in an experimental condition. Rather, it makes qualitative predictions about shifts in the response distributions produced in experimental conditions that differ only in the relative processing times of either the key or the response feature. Consequently, the value of the delay introduced in a pathway to simulate a particular condition is arbitrarily chosen. But the direction of the difference between the delay values required to simulate a pair of conditions is significant. In the same sense, the actual API values and correct report percentages generated by the model are not matched to behavioural data. Instead, the direction of the change in these values across a pair of simulated conditions is compared with human data.

### 8.3.1 Manipulation of the Key Feature Pathway

According to the 2f-ST<sup>2</sup> model, increasing the processing delay in the key pathway, while keeping all other model settings constant, should increase the relative proportion of post-target errors. In other words, given a pair of conditions  $A$  and  $B$ , where  $B$  has a greater  $\tau_K$  than  $A$ , the response distribution for condition  $B$  should have a more positive API. This is because an isolated increase in the processing delay in the key pathway implies that activation reaches the key Type layer later in condition  $B$ , in turn delaying the firing of the blaster. It is thus more probable that response features of items presented after the target in the RSVP stream are more active at the time of blaster firing. They consequently benefit more from its enhancement and get bound to the key feature. Over the entire range of target strengths, the competitive interactions of response features with different target strengths produce a response distribution with a range of different outcomes. Across all trials, the distribution for condition  $B$  will consist of more post-target errors than that for condition  $A$ .

Conceptually speaking, this manipulation is, in part, similarly described by the 2f-ST<sup>2</sup> and Botella et al. (2001) models. The Botella et al. (2001) model also predicts a post-target shift in the response distribution if the mean processing time in Module K is increased in isolation. However, an important distinction between the two models relates to correct

reports. The Botella et al. (2001) model predicts that the number of correct reports will *always* decrease along with an increase in the API of the response distribution (see section 2.5.2). This seemingly implausible prediction arises because their model posits a dual-route binding mechanism, where increasing the processing delay in Module K results in fewer trials binding via the attentional focusing route, and consequently reduced accuracy. Indeed, to quote Botella et al. (2001),

*If we make an experimental manipulation involving an increase in mean processing time per element in Module K while the other mechanisms of the model are held constant, two things will occur. The first is that the number of correct responses produced through successful attentional focusing will decrease. The reason is that SOA is held constant and the moment at which the focusing process begins is delayed, the probability of completing it in time decreases. The second is that the response features selected will tend to come from elements presented later, given that the mean time elapsed before the triggering of the selection mechanism will be greater in the condition with longer processing time. Thus, on increasing mean processing time in Module K we can predict a reduction in the number of correct responses and a later API.*

In contrast, the 2f-ST<sup>2</sup> model does not mandate a reduction in the number of correct reports alongside a post-target shift. Whether the number of correct reports increases, decreases or remains unchanged along with a post-target shift depends on the pair of conditions being compared. Going from a condition with a strongly pre-target response distribution to one with a relatively more symmetric distribution, 2f-ST<sup>2</sup> predicts that the number of correct reports should increase. However, going from a condition with a relatively symmetric response distribution to one with a strongly post-target distribution, the model predicts that the number of correct reports should decrease. These predictions arise because binding in 2f-ST<sup>2</sup> occurs over the same architecture for all responses. In other words, correct reports and conjunction errors are qualitatively similar in terms of the neural dynamics leading up to them. Thus, depending on the model's configuration for a pair of conditions, the number of correct reports can either increase, decrease or remain unchanged along with a post-target shift. Later in this chapter, we will present behavioural data from our experiment, which

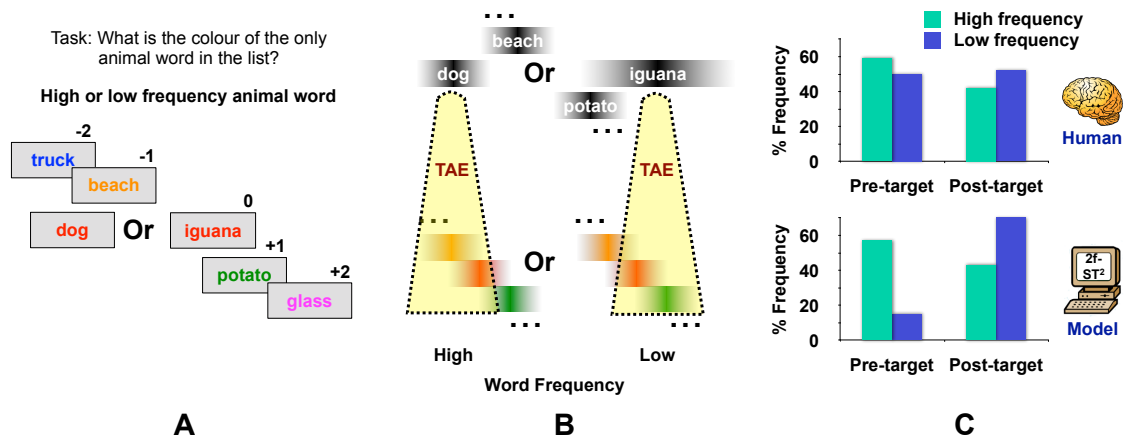


Figure 45 **Key feature manipulation in Botella et al. (2001) simulated by the 2f-ST<sup>2</sup> model.** Panel A: Pair of task conditions in Experiment 1A of Botella et al. (2001). Panel B: Variation in 2f-ST<sup>2</sup> model dynamics across the task conditions. Panel C: Response distributions generated by humans and the 2f-ST<sup>2</sup> model in the task conditions.

validates the 2f-ST<sup>2</sup> model and refutes the Botella et al. (2001) model.

To test these predictions from the 2f-ST<sup>2</sup> model, we focus on Experiment 1A from Botella et al. (2001), as it provides an isolated manipulation of key feature processing time in an RSVP task. In this experiment, participants viewed a sequence of coloured words presented in an RSVP setting, and were asked to identify the colour of the only animal word in an RSVP stream of coloured words. Hence word identity was the key feature, and colour the response feature. Figure 45A depicts an example trial from the experiment. The processing delay for the key feature was manipulated by altering the frequency of the word in language use: high-frequency words corresponded to key features that could be processed quickly (i.e., with lesser delay) than low frequency words. As in the example, the animal word could either be a high-frequency animal word (say, ‘dog’) or a low-frequency animal word (say, ‘iguana’). In confirmation of the assumption that low-frequency word identities are processed slower, Botella et al. (2001) report a significant post-target shift in the response distribution for low-frequency words in comparison to high-frequency words. This shift is evident in the histogram plotted at the top of figure 45C, which depicts the relative percentages of pre-target and post-target errors reported in the two conditions from Experiment

1A<sup>6</sup>. Further, it is supported by a significantly later API for the low frequency condition (API = .043) than the high frequency condition (API = -0.306):  $t(1,12) = 4.18$ ,  $p < 0.001$ . In addition, Botella et al. (2001) also find a significant reduction in the number of correct reports, going from the high-frequency word condition with 77.6% correct reports, to the low-frequency word condition with 29.2% correct reports:  $t(1,12) = 15.697$ ,  $p < 0.001$ <sup>7</sup>.

Figure 45B conceptually illustrates how the 2f-ST<sup>2</sup> model simulates this pattern of data. The  $\tau_K$  parameter is set to 0ms and 40ms for the high-frequency and low-frequency word conditions, respectively<sup>8</sup>. This difference reflects the fact that key feature processing is presumed to take longer in the low-frequency word condition. All other model parameters are kept constant (see appendix A.4 for more details). This manipulation effectively delays the average blaster firing latency for the low frequency condition, leading to a increased probability that it enhances response features following the target. Across an entire simulation run involving a range of key and response feature strengths, it eventually produces a distribution of responses that has a later (i.e., more positive) API in the low-frequency word condition.

The lower histogram in Figure 45C depicts the relative percentages of pre-target and post-target errors produced by the 2f-ST<sup>2</sup> model for the  $\tau_K$  values corresponding to the high-frequency and low-frequency word conditions. A clear post-target shift can be seen therein, and is mirrored by the corresponding simulated API values of -0.11 and 0.78 for the high-frequency and low-frequency word conditions, respectively. In addition, the model generates more (62%) correct reports in the high-frequency condition, compared to that (55%) in the low-frequency condition. Taken together, the post-target shift and the reduction in the number of correct reports produced by the 2f-ST<sup>2</sup> model are a replication of the pattern seen in the human data in Experiment 1A from Botella et al. (2001). It is important to note that the actual API and accuracy values generated by the model are not important. Rather, it is the relative change in the values across the high-frequency and low-frequency word conditions that demonstrates the model's replication of the data.

---

<sup>6</sup>The histograms in figure 45C only compare pre-target errors to post-target errors, as Botella et al. (2001) do not report separate values for error rates at individual response positions.

<sup>7</sup>All values reported are from Botella et al. (2001).

<sup>8</sup>Note that for the high-frequency condition, the model is effectively in its default configuration.

### 8.3.2 Manipulation of the Response Feature Pathway

The complementary manipulation to that described in the previous section involves changing the processing delay in the response pathway of the 2f-ST<sup>2</sup> model. For a pair of conditions  $A$  and  $B$ , with  $B$  having a greater value for  $\tau_R$  than  $A$ , the response distribution for condition  $B$  should have an earlier, more negative API. This is because an isolated increase in the processing delay in the response pathway means that response features are slower to get processed. Hence, all else being equal, in condition  $B$ , at the time the target's key feature reaches the key pathway's Type layer, response features from items presented before the target are more likely to be getting processed at the response pathway's Type layer. Consequently, they benefit more often from the blaster's enhancement and get bound to a token, producing an overall response distribution with a greater proportion of pre-target errors.

The above prediction of the 2f-ST<sup>2</sup> model is similar to that from the Botella et al. (2001) model. But as in the previous section, the two models differ in terms of their prediction regarding changes in the number of correct reports. The Botella et al. (2001) model places a restriction on the number of correct reports, and predicts that they remain unchanged when the response pathway is manipulated, as the relative proportion of trials processed via the attentional focusing and the sophisticated guessing pathways remains the same. As per Botella et al. (2001),

*Suppose now that we experimentally manipulate the mean processing time in Module R, maintaining constant the other mechanisms of the model. Because neither SOA nor mean processing time in Module K are altered, the proportion of trials completed by means of focusing will not change. In contrast, in the trials completed through the sophisticated guessing mechanism, there will be changes in the intrusion pattern. In the condition with greater mean processing time in Module R, the API will be earlier because the development of the representations is more incipient. The balance between pre- and posttarget intrusions will be more favorable for the pretarget intrusions as the average processing time increases in Module R. This could also lead to a small change in the correct response rate because, although correct responses produced by the focusing system will remain*

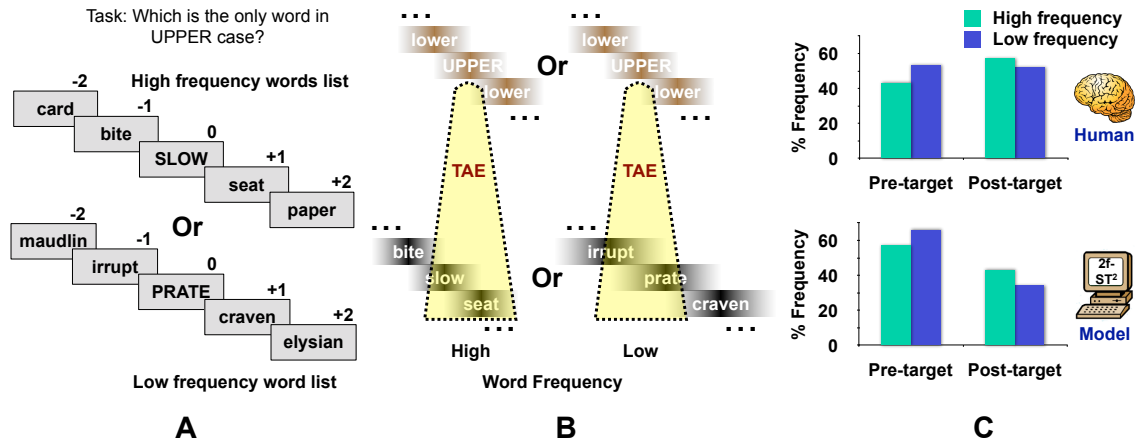


Figure 46 **Response feature manipulation in Botella et al. (2001) simulated by the 2f-ST<sup>2</sup> model.** Panel A: Pair of task conditions in Experiment 2 of Botella et al. (2001). Panel B: Variation in 2f-ST<sup>2</sup> model dynamics across the task conditions. Panel C: Response distributions generated by humans and the 2f-ST<sup>2</sup> model in the task conditions.

*the same, there can be changes in the frequency of fortunate conjunctions.*

The 2f-ST<sup>2</sup> model, however, does not require that correct reports remain the same or change only by a small amount. The rationale for this is similar to that pointed out in the previous section: in contrast to the Botella et al. (2001) model, all correct reports and conjunction errors are processed by the same neural network hierarchy in 2f-ST<sup>2</sup>. Consequently, the model predicts that sufficiently large manipulations in the response pathway will produce a significant change (either increase or decrease, depending on the configuration) in the number of correct reports, in conjunction with pre-target shifts.

Experiment 2 from Botella et al. (2001) provides behavioural data to test these predictions from the 2f-ST<sup>2</sup> model. It describes an isolated response feature manipulation involving words, where target words were presented in uppercase, amongst an RSVP stream of distractor words in lowercase. This experimental design, a sample trial from which is shown in figure 46A, is based on initial experiments by Lawrence (1971). Participants were asked to identify the only word in uppercase. Thus, “uppercaseness” was the key feature to be detected, and word identity was the key feature to be reported. An isolated manipulation of the processing delay of the response features of items was obtained by using low or high frequency words. With the assumption that low frequency word identities (e.g., ‘PRATE’)

were associated with a relative increase in processing time in the response pathway, they were expected to produce more pre-target errors than high-frequency word identities (e.g., 'SLOW'). The upper histogram in figure 46C illustrates the observed shift in the relative distribution of pre-target and post-target errors in the two conditions <sup>9</sup>. In confirmation of their expectations, Botella et al. (2001) report a pre-target shift in the response distribution, going from the high-frequency word condition to the low-frequency word condition. This was concomitant with a relatively small but significant API shift from 0.131 for high-frequency words to -0.034 for low frequency words:  $t(1,9) = 2.763$ ,  $p < 0.03$ . However, no significant change was found in the number of correct reports, which were 30.7% and 31.5% for the high and low frequency conditions, respectively ( $t(1,9) = 0.556$ ,  $p < 0.6$ ) <sup>10</sup>.

As shown in figure 46B, the 2f-ST<sup>2</sup> model simulates this pattern of data using a method similar to that employed in the previous section.  $\tau_R$ , the parameter controlling the fixed amount of processing delay in the response pathway is set to a higher value (10ms) in the low-frequency word condition as compared to the high-frequency word condition (0ms)<sup>11</sup>. This choice is based on the same logic as that applied in the previous section: low-frequency words take longer to get processed in the response pathway compared to high-frequency words. All other model parameters are kept constant (see appendix A.4 for more details). Consequently, response features of items take longer to reach the Type layer in the low-frequency condition, and those of distractors presented before the target are more likely to have higher activation at the moment the blaster is triggered by the occurrence of the target-defining feature in the key pathway. Hence, over a complete simulation run, the larger  $\tau_R$  value produces a distribution of responses that has a earlier (i.e., more negative) API in the low-frequency word condition.

The lower histogram in Figure 46C depicts the relative percentages of pre-target and post-target errors produced by the 2f-ST<sup>2</sup> model for the  $\tau_R$  values corresponding to the high-frequency and low-frequency word conditions. A pre-target shift can be seen therein, and is mirrored by the corresponding simulated API values of -0.11 and -0.31 for the high-frequency and low-frequency word conditions, respectively. In addition, the model produces the same

---

<sup>9</sup>The histograms in figure 46C only compare pre-target errors to post-target errors, as Botella et al. (2001) do not report separate values for error rates at individual response positions.

<sup>10</sup>All values reported are from Botella et al. (2001).

<sup>11</sup>Note that for the high-frequency condition, the model is effectively in its default configuration.

number of correct reports (62%) in the two conditions. Taken together, these results from the model are a replication of findings in Experiment 2 from Botella et al. (2001). Firstly, the API shift produced by the model is in keeping with the weakly significant pre-target shift seen in the human response distributions. Secondly, the constancy in the number of correct reports agrees with the similar lack of a significant difference in the human data. However, it should be noted that this constancy in the number of correct reports predicted by the 2f-ST<sup>2</sup> model arises due to the relatively small change in  $\tau_R$ . With a big enough manipulation in the response feature pathway, the model would predict a larger pre-target shift, accompanied by a significant change in the number of correct reports.

### 8.3.3 Summary

The previous two sections have described how the 2f-ST<sup>2</sup> model simulates behavioural data relating to temporal feature binding, involving a representative set of experimental conditions. By following a method of model reconfiguration based on only single parameter changes, we have enabled it to simulate the effects observed in a pair of experiments from Botella et al. (2001), involving systematic, isolated manipulations of key and response feature processing times. Importantly, the method employed for simulating these manipulations abstracts away from the specifics of the experimental configuration being simulated. This gives the 2f-ST<sup>2</sup> model a broad applicability and explanatory power that is extensible to many other behavioural studies that investigate temporal feature binding (Botella, 1992; Kikuchi, 1996; Boucart et al., 1998). This is because, though these studies have used a variety of techniques for producing key and response feature manipulations, they effectively generate shifts in response distributions and changes in the number of correct reports similar to those seen in the previous sections. Indeed, later in this chapter, we will apply the 2f-ST<sup>2</sup> model and the reconfiguration method used above to interpret new behavioural data from our own experiment.

## 8.4 Reaction Times for Response Positions

In the previous section, we have used the 2f-ST<sup>2</sup> model to replicate response distributions from Botella et al. (2001). The model proposed by Botella et al. (2001) also explains these

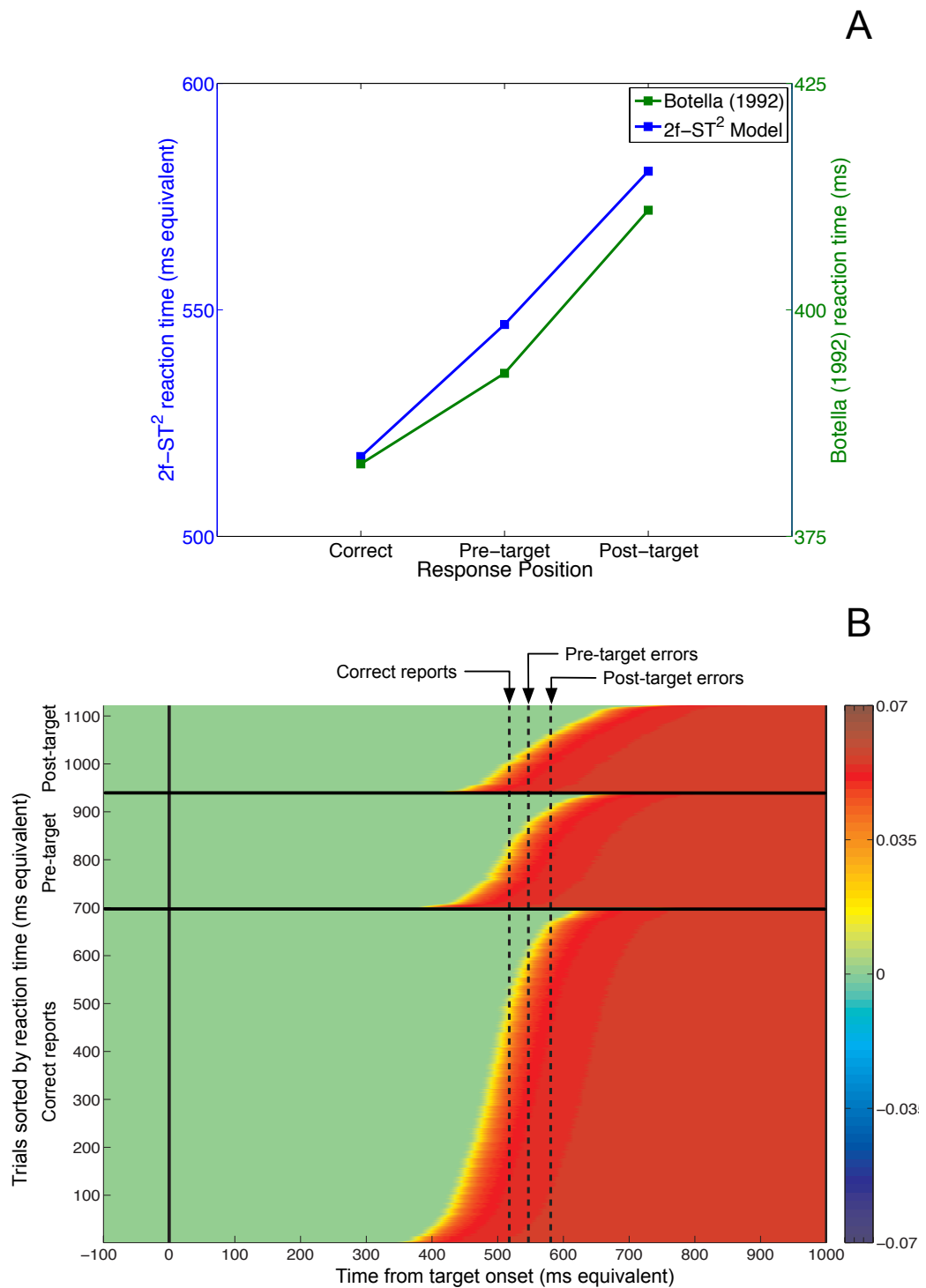


*Figure 47* **Reaction time data from Botella (1992) explained by the 2f-ST<sup>2</sup> model.** Panel A: Average reaction times from Botella (1992) and the 2f-ST<sup>2</sup> model for the three response positions. Panel B: Virtual ERP image depicting the activation dynamics of token trace neurons, grouped by response position and sorted by reaction time within each group. Dashed lines indicate the mean reaction time for each response position.

distributions; but we argue that it proposes a non-parsimonious dual-route approach to do so. As pointed out in section 2.5.2, Botella et al. (2001) proposed two distinct binding routes for producing correct reports and conjunction errors, partly in order to explain reaction time data from Botella (1992). In this section, we generate reaction times from the 2f-ST<sup>2</sup> model and show that it can replicate this data using its common binding mechanism, thereby removing the need for a dual-route approach.

In Botella (1992), participants were required to detect the colour of a digit target embedded in an RSVP sequence of coloured letters, and make a speeded response to this detection. Trials belonged to one of two conditions: in the target-specified condition, the identity of the digit was pre-specified, whereas in the target-categorised condition, participants only knew that the target could be any digit. Botella (1992) measured reaction times of participants when they produced correct reports and conjunction errors, and found the same pattern in both conditions: correct reports were associated with the earliest reaction times, followed by pre-target errors and post-target errors. This can be seen in figure 47A, which plots reaction times for the three response positions, averaged across the target-specified and target-categorised conditions. Further, according to Botella et al. (2001), there was large variability in the reaction times for correct reports. Specifically, correct report trials were made up of two types, ‘fast’ ones with short reaction times, and ‘slow’ ones with relatively longer reaction times. Combining these patterns in the reaction time data, Botella et al. (2001) justified the existence of two binding routes: the fast, deterministic attentional focusing route and the slower, probabilistic sophisticated guessing route. They hypothesised that ‘fast’ correct reports take the attentional focusing route, while ‘slow’ correct reports, along with pre-target and post-target errors, take the sophisticated guessing route.

In 2f-ST<sup>2</sup>, reaction times are modelled by the time at which the token completes binding to a pair of key and response pathway Type layer nodes. This event is indexed by the trace neuron<sup>12</sup> of the active token reaching 75% of its maximal postsynaptic activation<sup>13</sup>. In the model, this threshold marks the completion of target consolidation into WM, and its earliest availability for conscious report. Hence, in each trial, we define the reaction time measure produced by the model as the simulation time at which this threshold is reached by the

---

<sup>12</sup>Tokens are made up of gate-trace pairs (see appendix A.1.2).

<sup>13</sup>In both the ST<sup>2</sup> and 2f-ST<sup>2</sup> models, tokenisation proceeds to completion if this threshold is reached.

token trace neuron. To generate reaction time distributions comparable to human data, trials from a complete simulation run of the model in its default configuration ( $\tau_K = 0$  and  $\tau_R = 0$ ) are grouped according to response position (i.e., correct reports, pre-target or post-target errors). Within each group, reaction times measured as above are averaged together. These average reaction times for the three response positions are plotted in figure 47A. As can be seen, the model produces the same pattern of data as reported by Botella (1992). However, it is evident from comparing the scales on the y-axis that the model overestimates the actual reaction time values. Nevertheless, it replicates the relative qualitative differences between the reaction times observed in the human data.

To understand and further explore the pattern of reaction times produced by the 2f-ST<sup>2</sup> model, it is useful to examine the activation dynamics of the trace neuron of the active token in each trial. Figure 47B plots these dynamics as a virtual ERP image, grouping trials based on the response position. Within each group, trials have been sorted by the reaction time measured as described above. The dashed lines indicate the mean reaction time for each response position. As can be seen, correct reports have the earliest mean, followed by pre-target and post-target errors, in that order. However, there is also considerable variation and overlap in the distributions of reaction times for these response positions. This gaussian variation arises naturally due to the inter-trial variability set up in the 2f-ST<sup>2</sup> model (see section 8.2.4 and appendix A.4). We explain how this variation influences the distributions, by first focusing on the reaction times for correct reports. As can be seen at the bottom of figure 47B, there are some correct reports that complete tokenisation earlier than any errors; but many others are tokenised later than the mean reaction times for pre-target and post-target errors. For the early correct reports, the blaster fires early. Further, it fires temporally close to the peak of the activation of a strongly active response type node. This is because an early blaster firing for a strong target key type node, produced by a negative  $\tau_D$  value for the target item, will be correlated with a correspondingly early and strong target response type node. In this situation, this node maximally benefits from the blaster's enhancement, quickly wins the competition between co-active response types, and hence initiates tokenisation relatively early. For the late correct reports with a more positive value of  $\tau_D$ , the blaster fires later, and enhances the activation of a less strong response type. In such situations, it takes longer for the response type to overcome the lateral inhibition and

initiate tokenisation. Together, these trials make up the variation in the simulated reaction times for correctly reported targets. This variation in 2f-ST<sup>2</sup> dynamics explains similar observations of ‘fast’ and ‘slow’ correct reports in the human data (Botella et al., 2001).

Conjunction errors occur in trials in which the target’s key and response features are relatively weak and occur later (due to a more positive  $\tau_D$ ). Because of this, the blaster fires relatively later. Among such trials, there are those in which the response feature of a proximal distractor before the target is relatively stronger. The corresponding response type node hence benefits more from the blaster’s enhancement and wins the competition, producing a pre-target error. In other trials, a stronger response feature of a proximal distractor after the target is enhanced by the blaster, resulting in a post-target error. For both types of conjunction errors, the blaster’s enhancement occurs temporally further away from the peak of the activation of the response type node that eventually gets bound. These type nodes take longer to overcome the lateral inhibition at the Type layer of the response pathway. As a result, tokenisation takes longer on average, and contributes to the increases in mean reaction times for conjunction errors. Further, this mean is naturally later for post-target errors than for pre-target errors. This is because post-target errors are correlated with late blaster firing and delayed activation of the response type that benefits from it. In addition, as can be seen in figure 47B, there is increased inter-trial variability in the tokenisation time for conjunction errors. This is because, overall, they are associated with an increased amount of variation in feature strength and  $\tau_D$ .

The dynamics described above produce the pattern of reaction time data depicted in figure 47. Importantly, using a common binding mechanism for correct reports and conjunction errors, the 2f-ST<sup>2</sup> model replicates human reaction time data reported by Botella (1992). In doing so, it provides a more parsimonious and in-depth explanation of the temporal dynamics of feature binding than the Botella et al. (2001) model. In the next section, we go further, and demonstrate that the 2f-ST<sup>2</sup> model also explains a wider range of data than the Botella et al. (2001) model.

## 8.5 The Temporal Binding Experiment

In this section, we describe and analyse behavioural data from an EEG experiment that investigates the neural dynamics of temporal binding. This data refutes a prediction from the Botella et al. (2001) model, relating to the influence of an isolated key feature manipulation on the number of correct reports. Further, we demonstrate that the 2f-ST<sup>2</sup> model can be configured to replicate this data.

The analysis below focuses on behavioural data from Experiment 3. It consisted of coloured letter and symbol targets embedded within bilateral RSVP streams of digit distractors presented at a rate of 94ms per item. The key feature in the blocked design was target identity (letter or symbol), and the response feature was colour. Please refer to appendix B.3 for a detailed description of the experimental method.

Figure 56A depicts the response distributions generated by the letter and symbol target conditions in Experiment 3. As is evident, due to the high presentation rate, participants produced a large number of errors in both conditions, centred around the relative position of the target in the RSVP stream. We calculate the API of these distributions to provide a scalar estimate of mean location of the responses in the two conditions. The API value for letter targets is 0.18, and that for symbol targets is 0.31. This difference is significant ( $F(1,13) = 9.7$ ,  $MSE = 0.01$ ,  $p < 0.01$ ). In addition, the number of correct reports (i.e., at position '0') varies significantly across the two conditions: 29% for letter and 35% for symbols, with a marginally significant difference ( $F(1,13) = 3.24$ ,  $MSE = 65.9$ ,  $p = 0.09$ ). Based on these results, the letter and symbol target conditions can be considered as an isolated experimental manipulation of key feature processing. This is because, across these two conditions, only the average delay involved in the processing of the target-defining key feature, i.e., its identity, is varied. The average delay in the processing of the response feature (i.e., colour) remains the same. Further, going from the letter condition to the symbol condition, the delay in the processing of key features increases. This is corroborated by the fact that there is a post-target shift in the response distributions, as characterised by their API values.

The interesting finding in this data is that the post-target shift is concomitant with an increase in the number of correct reports, even if this increase is only marginally significant.

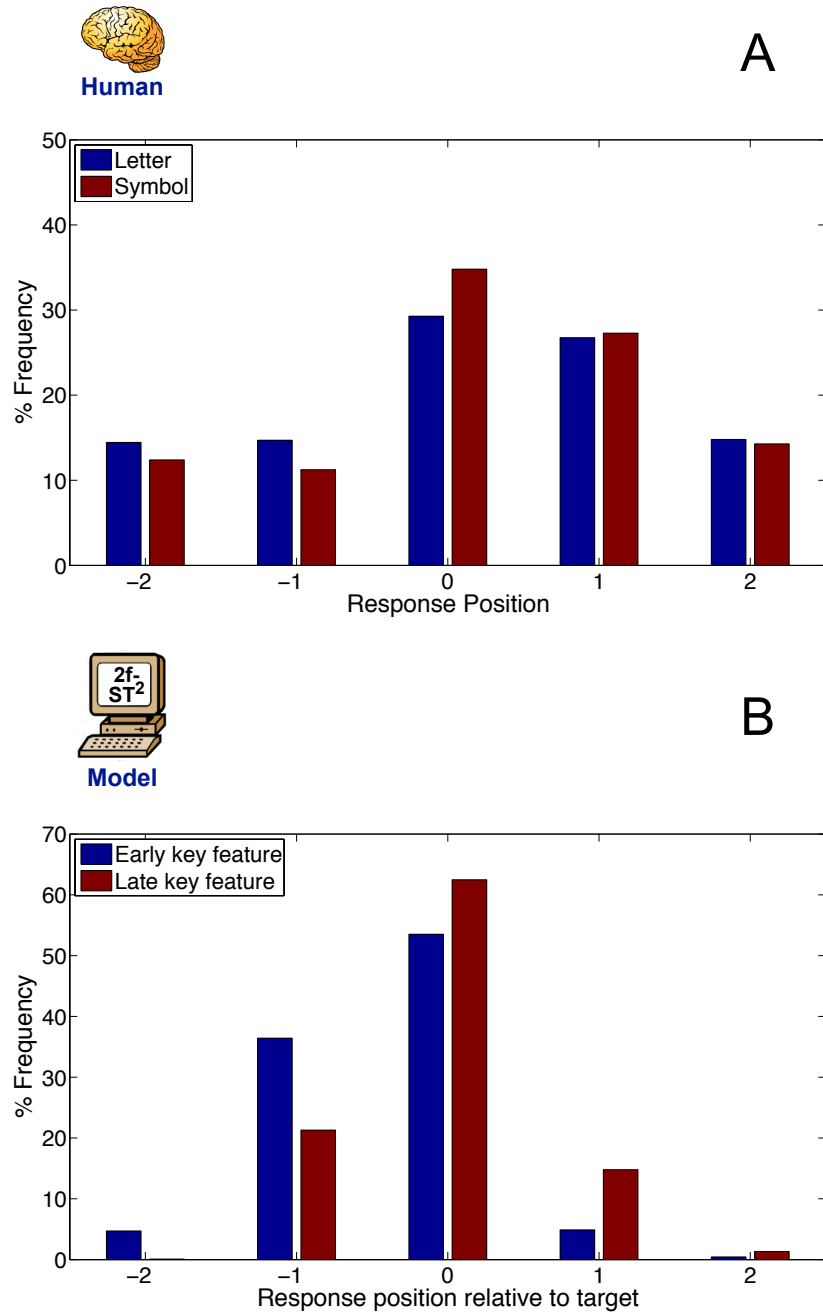


*Figure 48* **Simulation of behavioural data from Experiment 3 by the 2f-ST<sup>2</sup> model.** Panel A: Response distributions for the letter (API = 0.18) and symbol (API = 0.31) conditions. Panel B: Response distributions for the early key feature (API = -0.86) and late key feature (API = -0.11) conditions.

This directly contradicts the prediction of the Botella et al. (2001) model (see section 2.5.2). Contrary to the pattern in the data, it posits that post-target shifts in response distributions induced by an isolated manipulation of the key feature are associated with a decrease in the number of correct reports<sup>14</sup>. This prediction derives from the dual-route approach to temporal binding in the model. Hence, our data casts doubt on this aspect of Botella et al. (2001) model, and the mechanisms in the model that lead to this falsified prediction.

We now test whether the 2f-ST<sup>2</sup> model can replicate this pattern of data. In order to generate a pair of conditions involving an isolated manipulation of the key pathway, we execute two complete simulation runs of the model, differing only in the amount of fixed additional delay  $\tau_K$  introduced in the processing of all features in the key pathway for one condition. This technique is similar to that used to simulate the response distribution shifts in section 8.3.1. Here, we employ it to generate a pair of conditions, *early key feature* and *late key feature*, with  $\tau_K$  values of -40ms and 0ms, respectively, while keeping all other model parameters constant (see appendix B.3 for details)<sup>15</sup>.

Figure 48B depicts the response distributions generated by the 2f-ST<sup>2</sup> model in the early and late key feature conditions. The early key feature condition has an API of -0.86, while the late key feature condition has an API of -0.11. Also, the number of correct reports increases from 54% to 62%. The increase in API between the two conditions corresponds to the large post-target shift<sup>14</sup> seen in the response distributions. Importantly, this post-target shift is associated with an increase in the number of correct reports. It is worth noting that this prediction of an increase is different from the prediction in section 8.3.1. Therein, owing to a different configuration of  $\tau_K$ , the model had predicted a *decrease* in the number of correct reports alongside a post-target shift. This change in the model's prediction reiterates the point previously highlighted in that section: as all behavioural outcomes share a common binding mechanism, correct reports can increase or decrease in the model along with pre-target or post-target shifts, depending on the actual values of  $\tau_K$  and  $\tau_R$ .

The pattern of changes going from the early key feature to the late key feature condition

---

<sup>14</sup>Note that even if the statistical difference between the number of correct reports in the letter and symbol conditions is taken to be insignificant, it still contradicts the prediction from Botella et al. (2001).

<sup>15</sup>Note that for the late key feature condition, the model is effectively in its default configuration.

are qualitatively equivalent with those observed in the human data, going from the letter to the symbol condition (figure 48A). There are, of course, many differences between model and data in this regard, in terms of the actual API values and the number of correct reports. However, as pointed out earlier, the focus of the comparisons here is the ability of the model to replicate patterns in the human data using a systematic manipulation of a single parameter.

In this section, we have explained new behavioural data relating to temporal feature binding using the 2f-ST<sup>2</sup> model. Importantly, we have shown that this data verifies the earlier prediction from the model, that the number of correct reports can increase (or stay the same), along with a post-target shift in the response distribution. This data is in opposition to the predictions of the Botella et al. (2001) model, which always predicts a reduction in the number of correct reports. The falsification of this prediction brings into question the underlying mechanisms in the model, and in particular existence of two distinct routes for temporal feature binding in the brain. In contrast, the ability of the 2f-ST<sup>2</sup> model to explain this data provides support for its assumption of a common binding mechanism for correct reports and conjunction errors.

## 8.6 Conclusions

The 2f-ST<sup>2</sup> model has been the main focus of this chapter. Starting with a justification for building it, we have described its neural network architecture and unified binding mechanism. Following that, we have conducted a series of explorations with the model. Overall, these explorations, in addition to highlighting the capabilities of the 2f-ST<sup>2</sup> model, have also critiqued many aspects of the Botella et al. (2001) model. We have shown that though the 2f-ST<sup>2</sup> model draws upon aspects of the high-level structure of the Botella et al. (2001) model, it makes some important new contributions, mainly in terms of depth, breadth and parsimony.

Firstly, the model provides an in-depth explanation of temporal feature binding and the role of attentional enhancement therein. The sub-symbolic level of description afforded by 2f-ST<sup>2</sup> goes beyond the symbolic level of explanation afforded by the Botella et al. (2001) model. This is because, using a neurophysiologically inspired architecture, it is possible

to describe how cognitive differences in the binding process might be realised using neural network dynamics. Further, as we shall see in the next chapter, the 2f-ST<sup>2</sup> model allows us to make predictions about the electrophysiology of temporal feature binding.

Secondly, using 2f-ST<sup>2</sup>, we have described a generic methodology for simulating experimental manipulations of key and response feature processing. Further, we have used the model to generate specific, testable predictions relating to such manipulations. These predictions have been comparatively evaluated against those from the Botella et al. (2001) model, and consequently verified using previous behavioural data. Further, new data from our experiment has generated evidence that confirms predictions from 2f-ST<sup>2</sup>, and refutes those from the Botella et al. (2001) model. This comparative evaluation has demonstrated that the 2f-ST<sup>2</sup> model has greater explanatory breadth than the Botella et al. (2001) model.

Finally, in addition to simulating response distributions, we have employed the 2f-ST<sup>2</sup> model in this chapter to model behavioural reaction times. With this ability, we have shown that the model can more parsimoniously explain previous data about reaction times associated with correct reports and conjunction errors. This effort has provided support for the common binding mechanism employed in 2f-ST<sup>2</sup> for generating correct reports and conjunction errors, and effectively argued against the dual-route approach proposed by the Botella et al. (2001) model.

In the next chapter, we continue further with explorations using the 2f-ST<sup>2</sup> model. Therein, we tap into the capabilities of the model's neural network implementation and generate ERP predictions from it. In conjunction, we describe new ERP data from Experiment 3 and compare them to virtual ERPs from the 2f-ST<sup>2</sup> model.

## Chapter 9

# Neural Dynamics of Temporal Feature Binding

In the previous chapter, we have described and modelled behavioural data relating to temporal feature binding. Specifically, previous experiments have investigated how participants respond in RSVP tasks involving the temporal binding of pairs of features, and characterised their response distributions under different conditions. In this context, we have introduced the 2f-ST<sup>2</sup> neural network model of temporal binding, and shown that it can explain behavioural data from a variety of previous experiments. In this chapter, we take the model further, and employ it to make a range of testable predictions about the EEG responses evoked during temporal binding in RSVP. We then describe results from our EEG experiment into temporal feature binding. To our knowledge, this experiment is the first EEG study of temporal feature binding in RSVP. We have used the behavioural data from this experiment in the previous chapter to verify predictions from the 2f-ST<sup>2</sup> model. Here, we use the EEG data therefrom to test some of the main ERP predictions of the 2f-ST<sup>2</sup> model.

### 9.1 Virtual ERPs from 2f-ST<sup>2</sup>

The neural network architecture of the 2f-ST<sup>2</sup> model allows us to make qualitative predictions of systematic patterns of change in ERPs reflecting temporal feature binding. Indeed,

this ability of the model is one of its important strengths, as it allows us to connect behaviour and EEG data within one explanatory framework. However, it is important to note that the 2f-ST<sup>2</sup> model is not explicitly reconfigured to generate virtual ERPs that fit their human counterparts. Rather, the model is first qualitatively matched to human behavioural data, and the virtual ERPs generated in this configuration are verified for comparability with human ERPs. In this sense, the process of generating virtual ERPs from 2f-ST<sup>2</sup> is similar to that used with the ST<sup>2</sup> model (see chapter 4). Consequently, one can only expect to obtain a qualitative match to the data. Nevertheless, this process allows us to provide a common explanation for a pattern of behavioural and ERP effects, in addition to verifying the internal dynamics of the model's architecture.

Following from the behavioural predictions generated in the previous chapter, we will focus on ERP predictions relating to effects of manipulations of processing time in the key and response feature pathways. Some of these will later be tested using human EEG data from our experiment. But first, we describe the virtual ERP components that serve to explicate the predictions from the 2f-ST<sup>2</sup> model (please see chapter 4 for an introduction to the virtual ERP technique).

The two main virtual ERPs we are interested in generating from the 2f-ST<sup>2</sup> model and comparing with their human counterparts are the virtual N2pc and virtual P3.

**The Virtual N2pc** is essentially the same as in the original ST<sup>2</sup> model, and is introduced in section 4.3. As shown in figure 49, it is generated by averaging the activation traces from the blaster in the 2f-ST<sup>2</sup> model over the simulated trials comprising a condition of interest.

**The Virtual P3** is enlarged in its definition compared to the ST<sup>2</sup> model, to now summate over the Item and Type layers of both key and response feature pathways, in addition to the extended binding pool and the tokens (see figure 49). This is because, in the 2f-ST<sup>2</sup> model, the process of binding a pair of key and response features into a WM token involves activation of all these layers. Consequently, their combined activation is considered to represent the process of target consolidation.

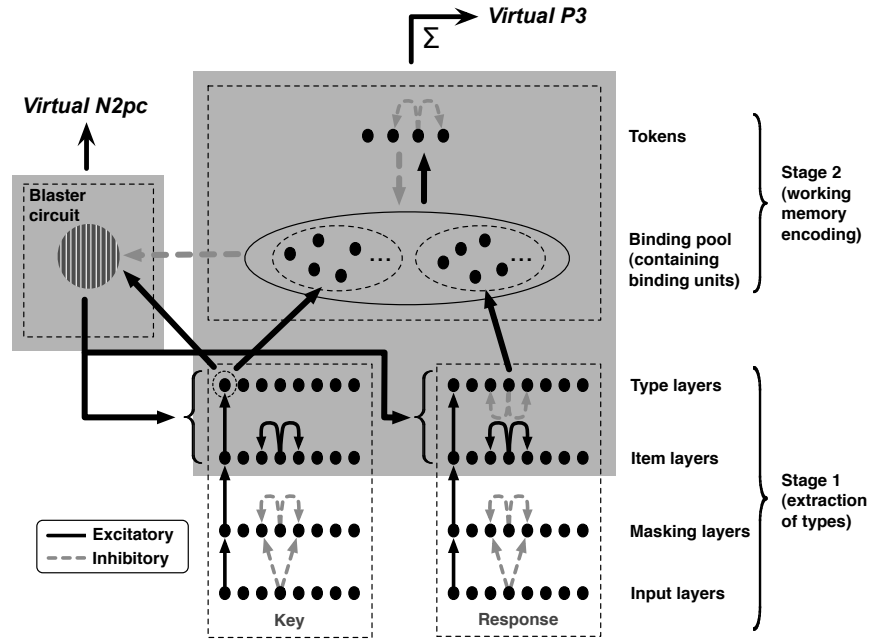


Figure 49 Virtual ERPs from the 2f-ST<sup>2</sup> model. The virtual P3 is generated from the item, Type, binding pool and token layers of both key and response feature pathways. The virtual N2pc is generated from blaster activation.

## 9.2 Determinants of the P3

Previous empirical research has investigated the influence of stimulus processing and response generation on the human P3 (Verleger, Jaskowski, & Wascher, 2005; Falkenstein, Hohnsbein, & Hoormann, 1994; Falkenstein, Hohnsbein, Hoormann, & Blanke, 1991). In these experiments, participants are typically required to detect the occurrence of a task-relevant stimulus and also respond to it in a speeded fashion. It has been found that the P3 reflects a combination of influences from both stimulus and response related processing. In other words, the temporal dynamics of the P3 depend in part, on the updating of cognitive context by the target, and on the preparation of a response to it ('stimulus updating' and 'response updating'; see Rösler, Borgstedt, & Sojka, 1985). In particular, Verleger et al. (2005) argued that the P3 in their task was influenced by stimulus and response in equal measure. To do so, they produced two P3 averages, one time-locked to the presentation of the target stimulus (*stimulus-locked*), and the other time-locked to the production of an overt response to it (*response-locked*). To them, the finding that the amplitude of the P3 was reliably equal in both these averages suggested that the P3 was influenced similarly

by stimulus and response related processes. Verleger et al. (2005) based this conclusion on the hypothesis that if the P3 was more influenced by temporal characteristics of stimulus processing, it would have a relatively higher amplitude in the stimulus-locked average. Conversely, if the P3 were more influenced by the temporal characteristics of response processing, this would show up as a higher amplitude in the response-locked average.

In this chapter, we inform and extend this empirical research into the nature of the P3, by combining theoretical explorations using the 2f-ST<sup>2</sup> model with analysis of human EEG data. The virtual P3 in the model is produced by a combination of dynamics of key and response feature processing, in addition to the binding pool and the tokens. Hence an interesting question that we explore here is how the processing in the key and response pathways determines the dynamics of the virtual P3. A related question also addressed in this context is how the virtual P3 is affected by systematic manipulations of processing delay in these pathways, similar to those performed in the previous chapter.

Despite the conceptual similarities between our analysis and that conducted by Verleger et al. (2005), it is important to note that there are some important differences. Firstly, there is a fundamental distinction between their notion of ‘stimulus’ and ‘response’ processing and our definition of ‘key’ and ‘response’ feature processing. A potential source of confusion here relates to the common use of the term ‘response’, which in the context of Verleger et al. (2005) means the production of a speeded response to a stimulus. In contrast, in the 2f-ST<sup>2</sup> setting, ‘response’ refers to the processing of response features of stimuli presented in RSVP, which are concurrently processed with key features and eventually integrated with the target’s key feature into WM tokens during the binding process. Hence, for each trial in which a token is bound to a pair of feature types, we generate virtual ERPs time-locked to presentation of the key and the response feature in that trial. These are referred to as *key-locked* and *response-locked* virtual ERPs, respectively.

Another crucial divergence between the analysis in Verleger et al. (2005) and the analysis here relates to the issue of temporal variability: as acknowledged by Verleger et al. (2005), an important assumption in their analysis is that there is no appreciable difference in the relative amounts of temporal variability in the dynamics of stimulus and response processing contributing to the P3. With this assumption, they view differences between the stimulus-locked and response-locked averages as indicative of the relative extent to which the P3 is

driven by these two processes. In contrast, we do not assume that the effective amounts of temporal variability in key and response feature processing reflected in the virtual P3 are equal. In the absence of this assumption, differences in our key-locked and response-locked averages could be explained by differences in the relative amounts of temporal variability manifested in the key and response pathways. For example, higher virtual P3 amplitude in the key-locked average compared to the response-locked average could mean that the amount of temporal variability in key feature processing is lower than that in response feature processing. This is likely to be the case in 2f-ST<sup>2</sup>: over a complete simulation run, temporal variability in activation dynamics at the Type layer of the key pathway is determined by  $\tau_D$  and the strength of the target’s key feature. The key feature strengths of distractors are kept constant (see appendix A.4 for details). However, in the response pathway, in addition to  $\tau_D$ , the strengths of pairs of response features are varied over all possible combinations. This sets up competition between the corresponding types at the Type layer of the response pathway. Consequently, the effective amount of temporal variability in the activation dynamics within the response pathway is greater. Indeed, it is this variability that allows the model to simulate different behavioural outcomes, including correct reports, pre-target and post-target errors.

In this chapter, we extend the analysis of the determinants of the P3 beyond that conducted by Verleger et al. (2005). This is because by examining P3 differences produced by time-locking, Verleger et al. (2005) could only make claims about *synchronicity* of the P3 to stimulus or response processing. To elaborate, by finding that the P3 had equal amplitude in the stimulus-locked and response-locked averages, they effectively showed that it was equally *synchronised* to the onset time of the stimulus and the response. However, this synchronicity reflects an *extrinsic* property of the P3 relating to time-locking, and does not fully address the issue of what *intrinsic* effect the temporal dynamics of stimulus and response processing have on the P3.

Towards informing this issue, we employ the 2f-ST<sup>2</sup> model to ‘look inside’, at the intrinsic determinants of the virtual N2pc/P3. In the following sections, we use key-locked and response-locked averages to show that the N2pc/P3 is determined by feature processing in two ways: it is intrinsically *driven* by (or *caused* by) activation dynamics in the key pathway, but is also *sensitive* to (or *correlated* with) the behavioural outcome of competitive

processing in the response pathway. In this regard, our claim that the P3 is driven by key feature processing is stronger than the claim by Verleger et al. (2005) that the P3 is synchronised to stimulus processing. This is because the former demonstrates causation, while the latter only demonstrates a temporal correlation. As we shall see, these theoretical explorations provide us with a deeper understanding of the temporal dynamics of 2f-ST<sup>2</sup>, and the determinants of the N2pc/P3. In addition, we complement these explorations with empirical analysis to test the model’s predictions. To do so, we comparatively evaluate our virtual ERPs against human ERPs from Experiment 3.

## 9.3 ERP Predictions of the 2f-ST<sup>2</sup> Model

### 9.3.1 Combined Key-locked and Response-locked Averages

We begin our explorations of ERP predictions from the 2f-ST<sup>2</sup> model with an investigation of integrative aspects of processing reflected in key-locked and response-locked virtual ERPs. From the description of the 2f-ST<sup>2</sup> model in the previous chapter (see section 8.2.3), it is clear that it is the occurrence of the target’s key feature in the key pathway Type layer that triggers the blaster’s attentional response and the consequent binding process. The aggregate dynamics of these processes drive the virtual N2pc and P3, respectively. Further, as pointed out in the previous section, there is effectively more temporal variability in the response pathway than the key pathway. In this scenario, we expect that response-locking (as compared to key-locking) would produce relatively more temporal variance in the single-trial virtual ERP. In turn, this implies that the response-locked average virtual ERP is expected to be broader and have a lower amplitude. This is because the response-locked average combines trials across all response positions (i.e., correct reports, pre-target and post-target errors). Effectively, it averages over the temporal variability in the response pathway that produces these different behavioural outcomes.

To test this intuition, we compare the virtual ERPs produced by the 2f-ST<sup>2</sup> model in its default configuration. With  $\tau_K$  and  $\tau_R$  both set to zero, a complete simulation run of the model is executed. This produces the response distribution plotted in figure 50A, which allows us to group trials based on behavioural outcome. We then plot the mean virtual N2pc and P3, averaged across all trials in which a successful binding was completed. Figures 50B

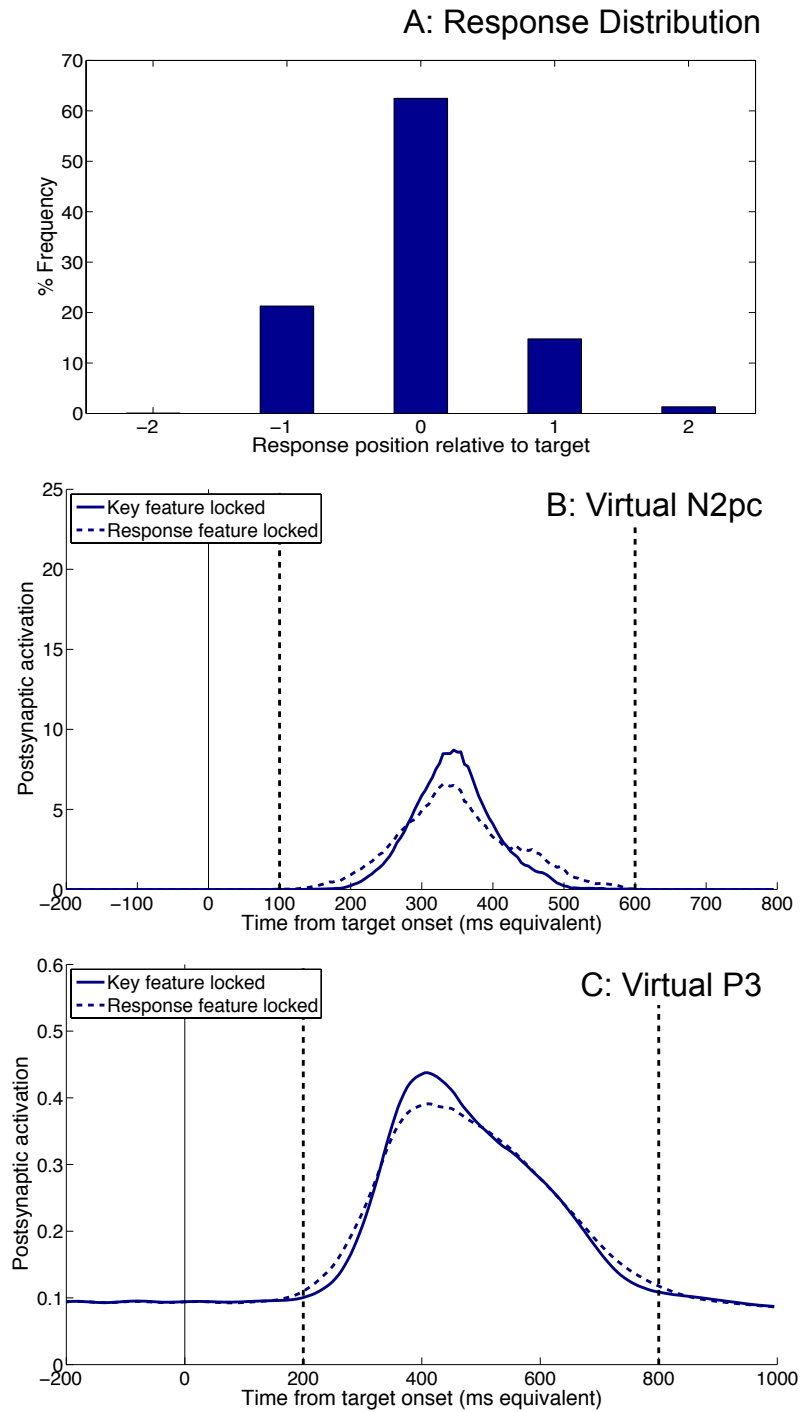


*Figure 50* Virtual ERPs from the 2f-ST<sup>2</sup> model combining across all response positions, time-locked to the key feature and response feature in each trial. Panel A: The response distribution produced by the 2f-ST<sup>2</sup> model in its default configuration. Panel B: Average key-locked and response-locked virtual N2pc generated by the model in its default configuration. Panel C: Average key-locked and response-locked virtual P3 generated by the model in its default configuration. Dashed lines indicate the window used for measuring peak activation and 50% area latency.

and 50C depict these average virtual ERPs. In both figures, the trials comprising the averages plotted with solid lines are *key-locked*, i.e., time-locked to the time of presentation of the target's key feature. In other words, timepoint '0' represents the time at which the target's key feature was presented at the input layer of the key pathway in the model. The trials in the averages plotted with dashed lines are *response-locked*, i.e., time-locked to the time of presentation of the target's response feature. In these trials, timepoint '0' represents the time at which the response feature that eventually got bound with the target's key feature was initially presented at the input layer of the response pathway.

It is evident from comparing the virtual N2pc ERPs in figure 50B that the peak amplitude decreases and the temporal 'spread' increases, going from the key-locked to the response-locked average. Specifically, the peak postsynaptic activation of the virtual N2pc within the 100-600ms window is 8.71 in the key-locked average, and 6.58 in the response-locked average. Also, there is a difference in the 50% area latency (Luck & Hillyard, 1990) between the two averages, which is 346.97ms and 350.98ms in the key-locked and response-locked averages, respectively. A similar pattern of reduction in peak amplitude and increase in temporal spread emerges with the virtual P3 ERPs in figure 50C. The peak postsynaptic activation within the 200-800ms window is 0.44 and 0.39 in the key-locked and response-locked averages, respectively. In addition, there is a relatively small shift, from 466.59ms (key-locked) to 470.03ms (response-locked), in 50% area latency.

The comparisons between the key-locked and response-locked ERPs support our intuition that there is more temporal variability in the activation dynamics of the response pathway. However, it does not fully answer the question of exactly how this variability affects the virtual N2pc and P3. Specifically, the averages plotted in figure 50B and 50C combine across behavioural responses (i.e., correct reports, pre-target and post-target errors). Consequently, they do not allow us to visualise in what way the virtual ERPs are sensitive to the behavioural outcome of competitive processing in the response pathway. To elaborate, though the virtual N2pc and P3 are strongly driven by the key pathway<sup>1</sup>, it is not fully clear in what way they are sensitive to the temporal variability in the response pathway that produces different behavioural responses. To address these issues, in the next section

---

<sup>1</sup>Indeed, as the blaster's firing depends only on key feature processing, the virtual N2pc is driven *entirely* by the key pathway.

we investigate differences in the virtual ERPs produced by correct reports, pre-target and post-target errors.

### 9.3.2 Correct Reports, Pre-target Errors and Post-target Errors

Figure 51 compares the key-locked and response-locked virtual N2pc and P3 generated by the 2f-ST<sup>2</sup> model for correct reports, pre-target errors and post-target errors. A comparison of the key-locked virtual N2pc averages in figure 51A (plotted using solid lines) shows that the latency of the virtual N2pc within the 100-600ms window is indeed correlated with the behavioural outcome. Specifically, correct reports are associated with the earliest virtual N2pc, with a 50% area latency of 334.62ms. They are followed by pre-target and post-target errors, with latencies of 356.50ms and 382.15ms respectively. The peak postsynaptic activation for these 3 conditions are 9.25, 10.09 and 7.66, respectively. The latency differences observed in the key-locked virtual N2pc ERPs are mirrored in the corresponding virtual P3 ERPs in figure 51B (plotted using solid lines). Virtual P3s generated by correct reports, pre-target and post-target errors have average 50% area latencies (within the 200-800ms window) of 455.17ms, 474.42ms and 500.41ms, respectively. The corresponding peak postsynaptic activations are 0.46, 0.43 and 0.41.

On the whole, the differences in the key-locked virtual N2pc and P3 averages suggest that both ERPs are indeed influenced by the processing in the key pathway. Importantly, the pattern of differences produced shows that correct reports are associated with the lowest latencies, followed by pre-target and post-target errors. This counterintuitive prediction from the 2f-ST<sup>2</sup> model runs contrary to a simplistic notion that the blaster fires the earliest for pre-target errors, followed by correct reports and post-target errors. Such a notion suggests that the virtual N2pc/P3 associated with pre-target errors would have the lowest latencies. The alternative pattern produced by the model suggests more complex dynamics, and in fact agrees with behavioural reaction time data from Botella and Eriksen (1992). Indeed, this pattern underlies 2f-ST<sup>2</sup>'s previous replication of this reaction time data in section 8.4. As pointed out therein, the model suggests that, for many correct reports, the blaster fires early, resulting in a relatively early virtual N2pc. Further, it fires temporally close to the peak of the activation of a strongly active response type node. This is because an early blaster firing for a strong target key type node, produced by a negative  $\tau_D$  value for

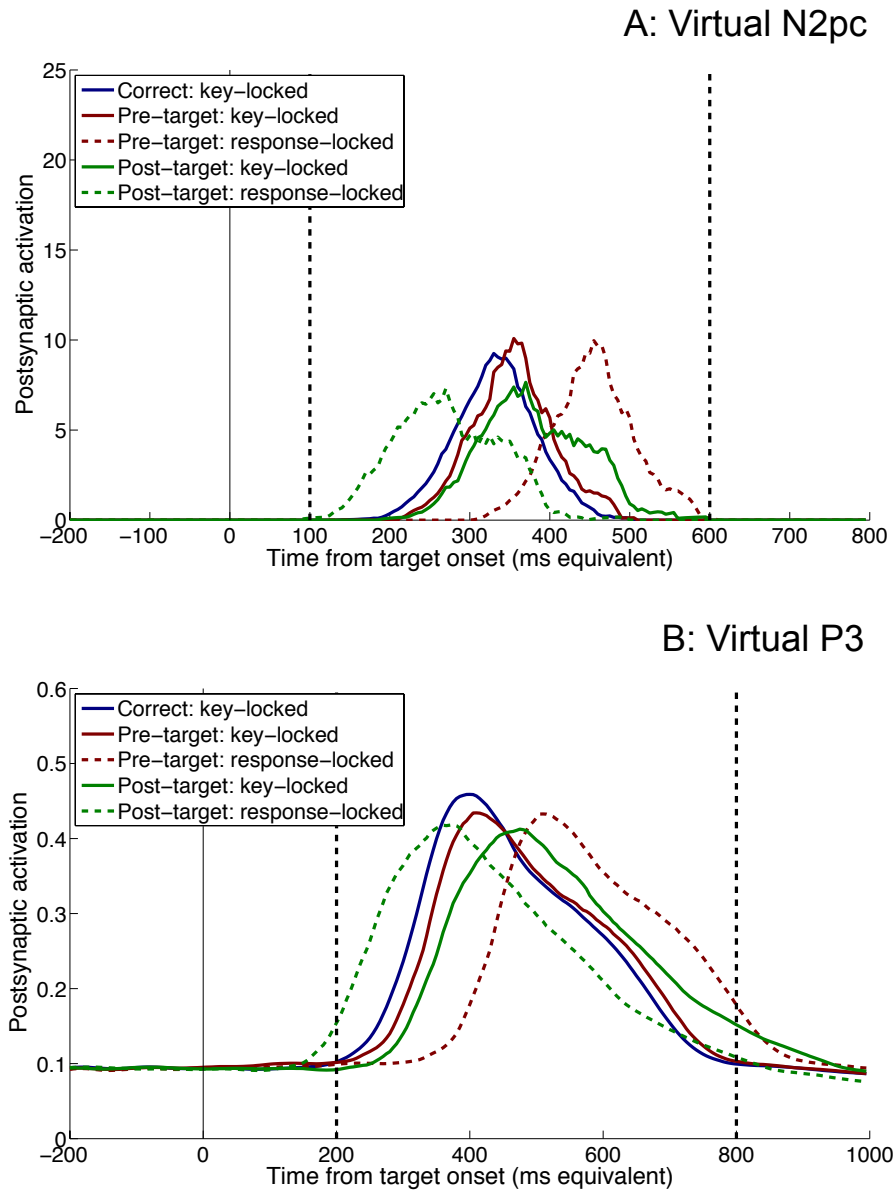


*Figure 51* **Key-locked and response-locked virtual ERPs from the 2f-ST<sup>2</sup> model for correct reports, pre-target and post-target errors.** Panel A: Virtual N2pc. Panel B: Virtual P3. Note that the response-locked virtual ERP averages for correct reports are the same as the key-locked averages. Dashed lines indicate the window used for measuring peak activation and 50% area latency.

the target item, will be correlated with a correspondingly early and strong target response type node. In this situation, this response type node maximally benefits from the blaster's enhancement, and quickly wins the competition between co-active response types. Consequently, tokenisation is initiated relatively early, producing an early virtual P3. Conjunction errors, on the other hand, occur in trials in which the target's key and response features are relatively weak and are activated later (due to a more positive  $\tau_D$ ). In this situation, the blaster fires relatively later on average, producing a later virtual N2pc. Among such trials, there are those in which the response feature of a proximal distractor before/after the target is relatively stronger, producing a pre-target/post-target error. For both types of conjunction errors, the blaster's enhancement occurs temporally further away from the peak of the activation of the response type node that eventually gets bound. These type nodes take longer to overcome the lateral inhibition at the Type layer of the response pathway. As a result, tokenisation takes longer on average for conjunction errors, and produces later virtual P3s. Further, this mean is naturally later for post-target errors than for pre-target errors. This is because post-target errors are correlated with late blaster firing and delayed activation of the response type that benefits from it.

Turning to the response-locked averages in figure 51 (plotted using dashed lines), we see that the virtual N2pc/P3 for pre-target errors are shifted later in time, whereas those for post-target errors are shifted earlier in time<sup>2</sup>. Furthermore, the latency differences between the response-locked averages are much larger than those between the key-locked averages. These shifts demonstrate that the response-locked virtual ERPs are correlated with differences in processing outcomes in the response pathway. In other words, though the virtual N2pc/P3 is *driven* by the key pathway, it is *sensitive* to the effectively greater temporal variability in the response pathway that produces different behavioural outcomes (i.e. correct reports, pre-target and post-target errors). The consequently large variation in the latencies of the response-locked virtual ERPs in figures 51A and 51B produces the reduction in amplitude and increased temporal spread seen in the corresponding combined response-locked averages (see figures 50B and 50C).

---

<sup>2</sup>Note that, as would be expected, the response-locked ERP average for correct reports is the same as the key-locked average.

### 9.3.3 Manipulation of the Key Feature Pathway

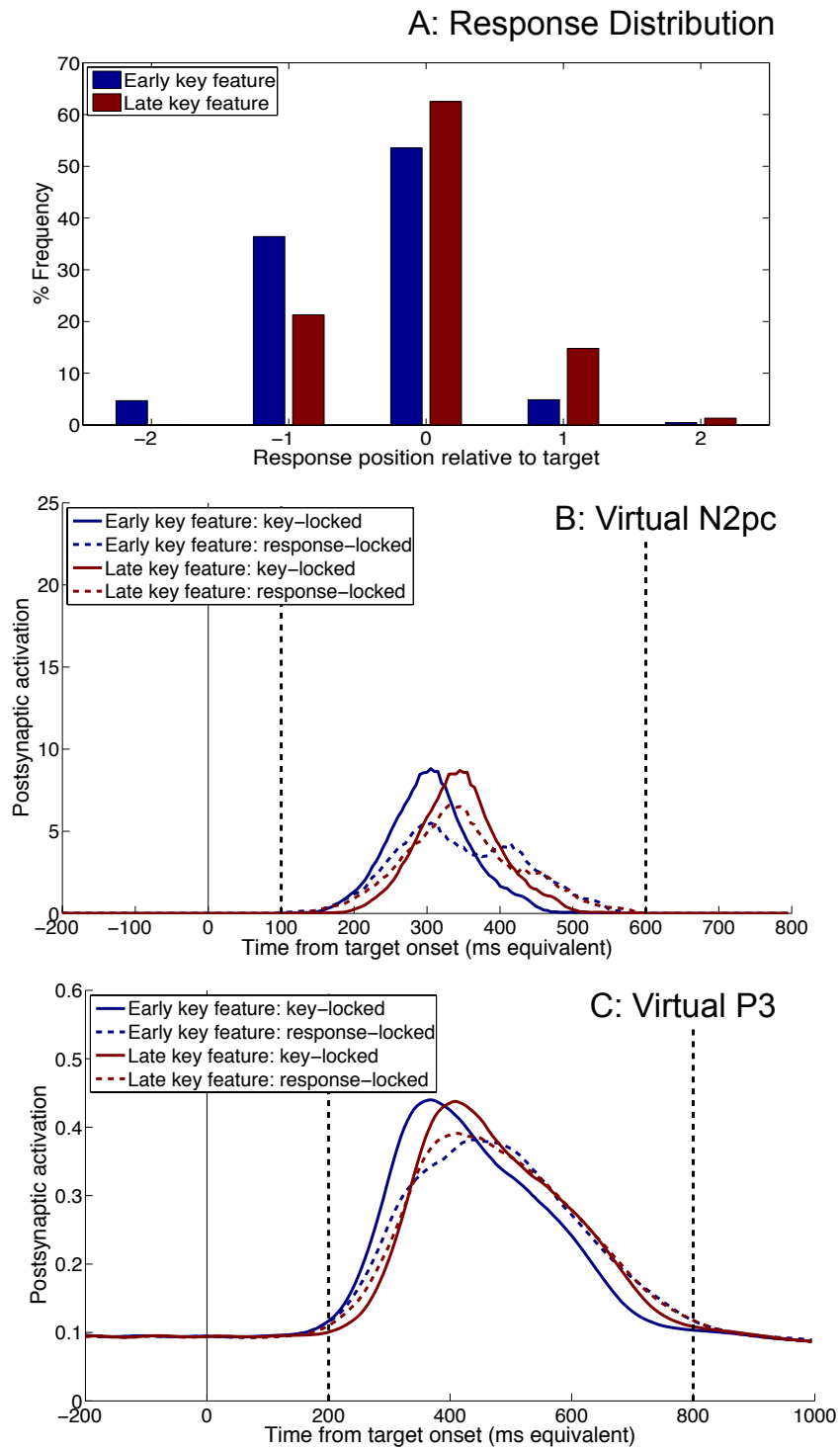
In this section, we look at the ERP predictions of the 2f-ST<sup>2</sup> model in the context of manipulation in processing delay in the key pathway. In order to compare virtual ERPs across a pair of conditions involving an isolated manipulation of the key pathway, we execute two complete simulation runs of the model. These conditions differ only in the amount of fixed additional delay  $\tau_K$  introduced in the processing of all features in the key pathway for one condition. In the previous chapter, we used such a manipulation to replicate shifts in response distributions in data from Botella et al. (2001) (see section 8.3.1) and from Experiment 3 (see section 8.5). Here, we employ the pair of conditions, *early key feature* and *late key feature* (with  $\tau_K$  values of -40ms and 0ms, respectively), the same as the ones previously generated in section 8.5<sup>3</sup> (see appendix B.3 for details). In that section, this configuration of the model allowed us to simulate response distributions that were comparable to behavioural data from Experiment 3. Here, we investigate the virtual ERPs for the same pair of conditions. Later in this chapter, we will compare them to their human counterparts, using the EEG data from the same experiment.

Figure 52 depicts the behavioural and virtual ERP output of the model for the early and late key feature conditions. As is evident from the distributions in figure 52A, the model produces a post-target shift in the responses, reflected by an increase in the API across the early (API = -0.86) and late key feature (API = -0.11) conditions. In conjunction with this post-target shift, we intuitively expect a concomitant increase in the latency of the key-locked virtual ERPs. This is because the increase in  $\tau_K$  used to produce this shift would effectively delay the activation of the target's key type node. In turn, this would increase the average latency of blaster firing in the late key feature condition, producing a relatively later virtual N2pc and P3.

The key-locked (plotted using solid lines) and response-locked (plotted using dashed lines) virtual N2pc and P3 averages evoked in the early and late key feature conditions are shown in figures 52B and 52C. For each condition, these averages include all trials in which a token was bound, combining across all response positions (i.e., correct reports, pre-target and post-target errors). In keeping with intuition, the key-locked virtual N2pc is

---

<sup>3</sup>Note that for the late key feature condition, the model is effectively in its default configuration.



*Figure 52* **Early and late key feature conditions from the 2f-ST<sup>2</sup> model.** Panel A: Behavioural response distributions. Panel B: Key-locked and response-locked virtual N2pc averages. Panel C: Key-locked and response-locked virtual P3 averages. Dashed lines indicate the window used for measuring peak activation and 50% area latency.

later in the late key feature condition. The visual difference is confirmed by the mean 50% area latencies (Luck & Hillyard, 1990) within the 100-600ms window in the two conditions: 307.18ms in the early key feature condition and 346.97ms in the late key feature condition. In comparison, there is not much difference in their peak postsynaptic activations, which are 8.82 and 8.71 respectively. The key-locked virtual P3 in figure 52C (plotted using solid lines) is also relatively later in the late key feature condition: the 50% area latencies of the virtual P3 (within the 200-800ms window) in the early and late key feature conditions are 437.62ms and 466.59ms, respectively. The peak activation is the same (0.44) in both cases.

On the whole, the latency shifts observed in the key-locked virtual N2pc and P3 ERPs follow naturally from the increase in processing delay in the key pathway. However, these key-locked ERPs are in contrast to their response-locked counterparts. As can be seen in figure 52B, the peak activations of the response-locked virtual N2pc ERPs are markedly lower than those of the corresponding key-locked averages. Specifically, the peak activation of the response-locked virtual N2pc is 5.51 in the early key feature condition and 6.58 in the late key feature condition. Similarly, the peak activation of the virtual P3 is also reduced in the response locked averages in figure 52C: 0.38 and 0.39 in the early and late key feature conditions, respectively. This decrease in peak activation of the response-locked averages is similar to that seen in figure 50, and is explained by the fact that there is effectively more temporal variability in the response pathway. Hence, response-locking increases the latency differences in the virtual ERPs associated with correct reports, pre-target and post-target errors (see figure 51). This increase in turn reduces the peak activation and increases the breadth of the combined response-locked average.

Finally, in comparing the virtual ERPs in figures 52B and 52C, it is interesting to note that the clear latency shift in the key-locked ERP averages are reduced by response locking. Indeed, the 50% area latencies of the response-locked virtual N2pc ERPs in figure 52B are similar: 347.25ms and 350.98ms in the early and late key feature conditions, respectively. The corresponding latencies of response-locked virtual P3 ERPs in figure 52C are also similar (467.51ms and 470.03ms). This absence of a latency difference in the response-locked averages reflects the fact that the response pathway is not affected by the manipulation of processing delay in the key pathway. Response locking produces a compensatory effect that cancels out the latency differences seen in the key-locked averages. To elaborate, in both

the early and late key feature conditions, the response-locked average for correct reports has the same latency as the corresponding key-locked average. However, the latency of the response-locked average for pre-target errors in the early key feature condition is *later* than the corresponding average in the late key feature condition. This is because, in the early key feature condition, there are more trials that result in pre-target errors. Across these trials, the relatively earlier firing of the blaster in the key-locked average is compensated for in the response-locked average, by the earlier presentation of the response feature that gets bound. Consequently, in the early key feature condition, the response-locked virtual N2pc/P3 for pre-target errors is more delayed with respect to the presentation time of the response feature being time-locked to<sup>4</sup>. Following an analogous logic, the response-locked average for post-target errors in the late key feature condition is *earlier* than the corresponding average in the early key feature condition. Here again, there is a compensatory effect of increased number of post-target error trials in the late key feature condition. Hence, the response-locked virtual N2pc/P3 in these trials is advanced with respect to the relatively later presentation time of the response feature that gets bound therein. This pair of effects produced by response locking means that the latency difference between the combined key-locked averages in the early and late key feature conditions is cancelled out in the response-locked averages.

### 9.3.4 Manipulation of the Response Feature Pathway

In this section, we shift focus to a comparative evaluation of virtual ERPs generated by the model across a pair of conditions involving a manipulation in the response pathway of the 2f-ST<sup>2</sup> model. This exploration complements and contrasts that in the previous section, which focused on a manipulation in the key pathway. Therein, we established that an increase in processing delay in the key pathway was associated with a concomitant increase in the latency of the key-locked virtual N2pc and P3. This is in agreement with the architecture and dynamics of temporal feature binding in 2f-ST<sup>2</sup>, which is strongly influenced by the key pathway. However, we have also previously shown in section 9.3.2 that the virtual N2pc/P3 are sensitive to response feature processing, in terms of the latency differences between

---

<sup>4</sup>These delayed virtual N2pcs for pre-target errors in the early key feature condition produce the second, late peak in the corresponding response-locked average plotted in figure 52B.

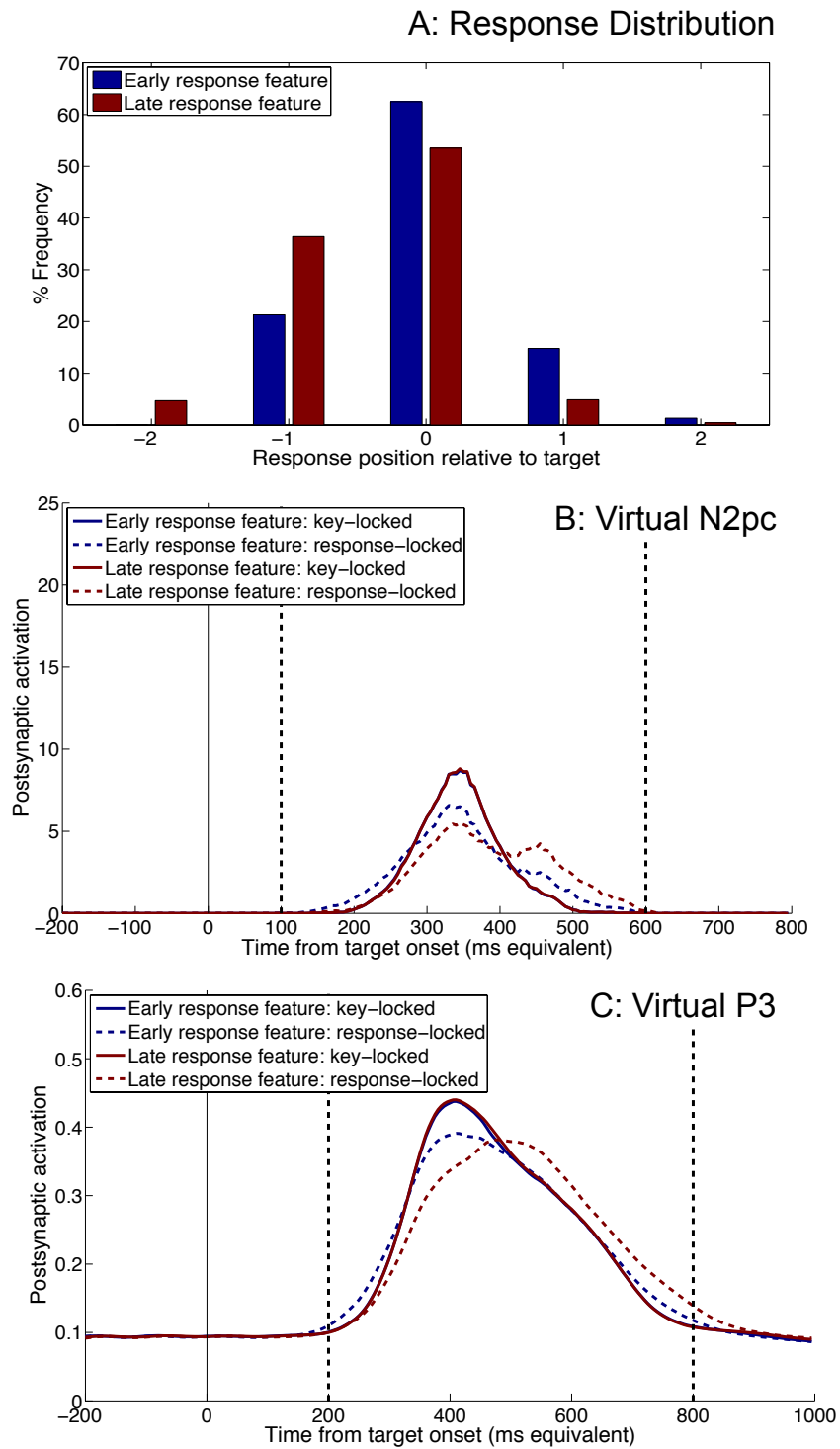


*Figure 53* **Early and late response feature conditions from the 2f-ST<sup>2</sup> model.** Panel A: Behavioural response distributions. Panel B: Key-locked and response-locked virtual N2pc averages. Panel C: Key-locked and response-locked virtual P3 averages. Dashed lines indicate the window used for measuring peak activation and 50% area latency.

the ERPs for different response positions (see figure 51). Following on from that, in this section, we elaborate on how these differences are affected by a systematic manipulation of processing delay in the response pathway.

An isolated manipulation of the processing time in the response pathway is generated in a similar fashion to that previously described in section 8.3.2. A fixed additional delay  $\tau_R$  is introduced in the processing of all features in the response pathway, to generate a pair of conditions termed *early response feature* with  $\tau_R$  of 0ms and *late response feature* with  $\tau_R$  of 40ms<sup>5</sup>. All other model parameters are kept unchanged (see appendix B.3 for details).

Figure 53A depicts the response distributions for the early and late response feature conditions. A clear pre-target shift is evident, going from the early to the late response feature condition, also reflected in the API values corresponding to the two distributions: -0.11 and -0.86 respectively. In addition, there is a considerable reduction in the number of correct reports, from 62% in the early response feature condition to 54% in the late response feature condition<sup>6</sup>. In section 8.3.2, we obtained a similar but weaker pre-target shift in the response distributions by a smaller increase in  $\tau_R$ . As explained therein, the increase in processing delay within the response pathway means that at the time of blaster firing, response types of RSVP items presented before the target are likely to be more active. Consequently, they benefit from its enhancement, and proceed to get bound to the target's key feature. Across a complete simulation run, this results in a predilection towards pre-target errors, resulting in an observed shift in the response distribution. However, in section 8.3.2, we did not obtain a change in the number of correct reports. But as pointed out therein, the 2f-ST<sup>2</sup> model predicts that, with a large enough manipulation of processing delay in the response pathway, the number of correct reports would change significantly. Hence, the reduction obtained by the manipulation of  $\tau_R$  performed in this section explicates

---

<sup>5</sup>Note that for the early response feature condition, the model is effectively in its default configuration.

<sup>6</sup>In comparing the response distributions in figure 53A to those in figure 52A, it is worth noting that the distributions for the early and late response feature conditions are identical to distributions for the late and early key feature conditions, respectively. This happens to be the case because of the  $\tau_K$  and  $\tau_R$  values used to generate the conditions. Both the early response and late key feature conditions have been generated by running the 2f-ST<sup>2</sup> model in its default configuration ( $\tau_K = 0$  and  $\tau_R = 0$ ). As a result, the virtual ERPs for these two conditions are also identical. In addition, the early key feature condition has been generated with  $\tau_K = -40$ ms and  $\tau_R = 0$ ms, while the late response feature condition has been generated with  $\tau_K = 0$ ms and  $\tau_R = 40$ ms. However, despite the behavioural equivalence of these conditions, the virtual ERPs for these two conditions are different.

that prediction.

Figure 53B and 53C depict the key-locked (plotted using solid lines) and response-locked (plotted using dashed lines) virtual N2pc and P3 averages for the early and late response feature conditions. For each condition, these averages include all trials in which a token was bound, combining across all response positions (i.e., correct reports, pre-target and post-target errors). As is evident, there is no difference in either pair of key-locked averages across the two conditions. For the key-locked virtual N2pc, the 50% area latencies are 346.97ms and 347.18ms, and the peak activations are 8.71 and 8.82 (within the 100-600ms window) in the early and late response feature conditions, respectively. For the key-locked virtual P3, the 50% area latencies (466.59ms) and peak activations (0.48) within the 200-800ms window are the same in both conditions.

In the previous section, an increase in the processing delay within the key pathway produced concomitant increases in latency of the key-locked virtual ERPs. In contrast, an increase in processing delay within the response pathway produces no such latency differences in the key-locked virtual ERPs. In case of the virtual N2pc, this is because it is entirely *driven* by blaster firing, which in turn depends on processing in the key feature pathway. As the processing delay in the key pathway remains unchanged, the activation of the target's key type node has the same average latency across the early and late response feature conditions. This translates into identical firing times for the blaster, reflected in the virtual N2pc. In addition, the virtual P3 reflects the fact that, irrespective of the response type that gets bound to the target's key type, the binding process has the same temporal profile in both conditions. However, the pre-target shift in the response distribution arises because, in the late response feature condition, the blaster's enhancement more frequently benefits response types active before that of the target. Thus, though the key-locked virtual ERP averages do not change in any way, the relative proportion of correct reports, pre-target errors and post-target errors making up these averages differ considerably.

Turning to the response-locked averages in figures 53B and 53C, a clear increase is evident in the latency of the virtual ERPs in the late response condition. Further, the response-locked virtual N2pc and P3 have lower peak activation in both conditions, compared to their key-locked counterparts. Specifically, the 50% area latencies of the response-locked virtual

N2pc are 350.98ms and 387.22ms in the early and late response feature conditions, respectively. The corresponding peak activations are 6.58 and 5.51. Also, the 50% area latencies of the response-locked virtual P3 are 470.03ms and 496.05ms, and the peak activations are 0.39 and 0.38, in the early and late response feature conditions, respectively.

The relative increase in the latency of the response-locked virtual ERPs in the late response feature condition derives from underlying shifts in the latencies of pre-target and post-target errors. Specifically, there are more pre-target errors in the late response feature condition (see figure 53A). Hence, the response-locked ERP for such errors in this condition constitutes relatively more trials time-locked to a timepoint well in advance of target onset. As the virtual N2pc and P3 are driven by the key pathway but are sensitive to the response pathway, this relatively earlier time-locking delays them in the response-locked average for pre-target errors<sup>7</sup>. Alongside, there are more post-target errors in the early response feature condition (see figure 53A). As a result, the response-locked ERP for such errors in this condition includes relatively more trials time-locked to a timepoint well after target onset. Again, as the virtual N2pc and P3 are driven by the key pathway, this relatively later time-locking effectively produces an earlier virtual ERP in the response-locked average for post-target errors in the early response feature condition. In other words, the corresponding average is earlier in the late response feature condition. On the whole, a combination of delayed pre-target errors in the late response feature condition and advanced post-target errors in the early response feature condition produce the relative shift in the combined response-locked averages, as seen in figures 53B and 53C<sup>8</sup>.

The above sections have discussed a series of explorations with the 2f-ST<sup>2</sup> model. In these explorations, we have explicated a series of qualitative predictions, generated using conditions simulated with the model. These predictions specify the pattern of changes we expect to see in human ERPs for corresponding experimental conditions. In the following section, we turn to new EEG data from Experiment 3, which allows us to test many of these predictions.

---

<sup>7</sup>These delayed virtual N2pcs for pre-target errors in the late response feature condition produce the second, late peak in the corresponding response-locked average plotted in figure 53B.

<sup>8</sup>Taken together, the pattern of differences between the key-locked and response-locked virtual ERPs for the early and late response feature conditions can be seen as inversion of the pattern observed with the virtual ERPs for the early and late key feature conditions (see figures 52B and 52C). This is effectively because, as pointed out earlier, these conditions are simulated by an inversion of the  $\tau_K$  and  $\tau_R$  parameters.

## 9.4 The Temporal Binding Experiment

In this section we shift focus to an analysis of EEG data from Experiment 3. In the previous chapter, we analysed the behavioural data from this experiment (see section 8.5). As pointed out therein, it consisted of coloured letter and symbol targets embedded within bilateral RSVP streams of digit distractors presented at a rate of 94ms per item. The key feature in the blocked design was target identity (letter or symbol), and the response feature was colour. Also, EEG was recorded at the P7, P8, O1 and O2 electrodes for the N2pc and at the Pz electrode for the P3. This data was later correlated with the behavioural responses of the participants. Please refer to appendix B.3 for a detailed description of the experimental method.

### 9.4.1 Combined Key-locked and Response-locked Averages

In line with the sequence of explorations conducted with the 2f-ST<sup>2</sup> model, we begin our analysis of the ERP data by comparing the key-locked and response-locked averages of the human N2pc and P3. To generate these averages, we combine trials across the letter and symbol conditions, selecting trials in which participants made a correct report, pre-target or post-target error. The overall response distribution produced is shown in figure 54A. The API of this distribution is 0.25.

Figures 54B and 54C depict the key-locked (plotted using solid lines) and response-locked (plotted using dashed lines) N2pc and P3 grand average ERPs. These averages combine the same correct report, pre-target and post-target error trials across the letter and symbol conditions. The only difference between the averages is in terms of time-locking. The key-locked averages are time-locked to the presentation time of the target's key feature in each trial. In contrast, the response-locked averages are time-locked to the presentation time of the response feature that was eventually reported in that trial.

From the figures, it is evident that response locking reduces the amplitude of both the N2pc and the P3. The peak amplitude of the key-locked N2pc within the 130-330ms window is  $-1.3\mu V$ , while that of the response-locked N2pc is  $-0.99\mu V$ . This difference is marginally significant across subjects:  $F(1,13) = 3.83$ ,  $MSE = 0.17$ ,  $p = 0.07$ . In addition, there is a small but significant difference in the jackknife latency (with an onset criterion of 50%

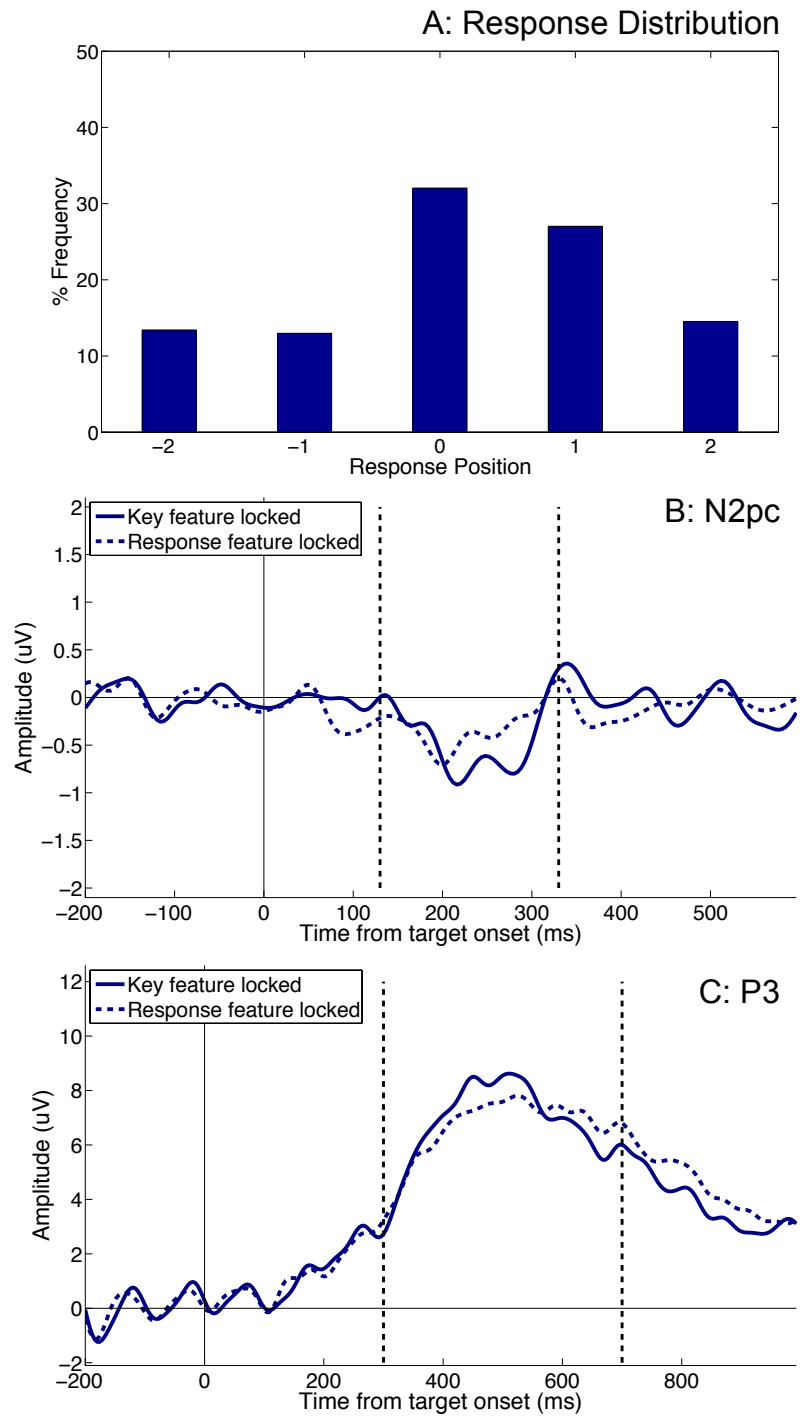


*Figure 54* **Behaviour and ERPs from Experiment 3.** Panel A: Response distribution. Panel B: Key-locked and response-locked N2pc grand average ERPs. Panel C: Key-locked and response-locked P3 grand average ERPs. Dashed lines in the ERP plots indicate the window used for statistical analysis. All figures combine trials across the letter and symbol conditions.

of peak amplitude; see J. Miller et al., 1998) between the two averages: 193.89ms in the key-locked average and 172.52ms in the response locked average ( $t(1,13) = 2.4$ ,  $p < 0.05$ ).

The difference in peak amplitude between the key-locked and response-locked P3s in figure 54C exhibits a similar pattern to the N2pcs. The peak amplitudes of the key-locked and response-locked averages are  $10.07\mu\text{V}$  and  $8.94\mu\text{V}$  respectively. This difference is significant:  $F(1,13) = 13.92$ ,  $\text{MSE} = 0.65$ ,  $p < 0.01$ . In addition, there is a significant difference in the 50% area latencies between the two averages: 498.57ms and 590.43ms in the key-locked and response-locked average, respectively ( $F(1,13) = 8.66$ ,  $\text{MSE} = 95.3$ ,  $p < 0.05$ ).

The peak amplitude differences between the key-locked and response-locked N2pc and P3 averages in figures 54B and 54C match the peak activation differences predicted in the virtual ERPs generated by the 2f-ST<sup>2</sup> model (see figures 50B and 50C). Specifically, as there is less temporal variability in the key pathway than the response pathway, the model predicted that the key-locked average N2pc/P3 would have a larger peak activation than the response-locked averages (see section 9.3.1). This prediction is validated by the corresponding human ERPs. In addition, the latency difference predicted between the key-locked and response-locked virtual P3 is also in agreement with the human P3 ERPs in figure 54C. However, in case of the human N2pc, the direction of the small latency shift across the two averages in figure 54B is opposite to that predicted by the model. This difference is possibly because the N2pc is a relatively small ERP component, and is considerably attenuated in the response-locked average. As with the virtual N2pc, this is due to increased temporal variation in the response-locked ERPs. As a result, correct estimation of latency is difficult. In contrast, the P3 is a much larger component, and allows for a more reliable calculation of 50% area latency.

#### **9.4.2 Correct Reports, Pre-target Errors and Post-target Errors**

Following on from the comparison between combined key-locked and response-locked averages, we now investigate differences between the ERPs associated with correct reports, pre-target and post-target errors. This investigation parallels the comparison between corresponding virtual ERPs in section 9.3.2. Therein, we had found that even though the virtual N2pc and P3 were driven by the key pathway, they were sensitive to the temporal variability in the response pathway that produced behavioural differences. Specifically,

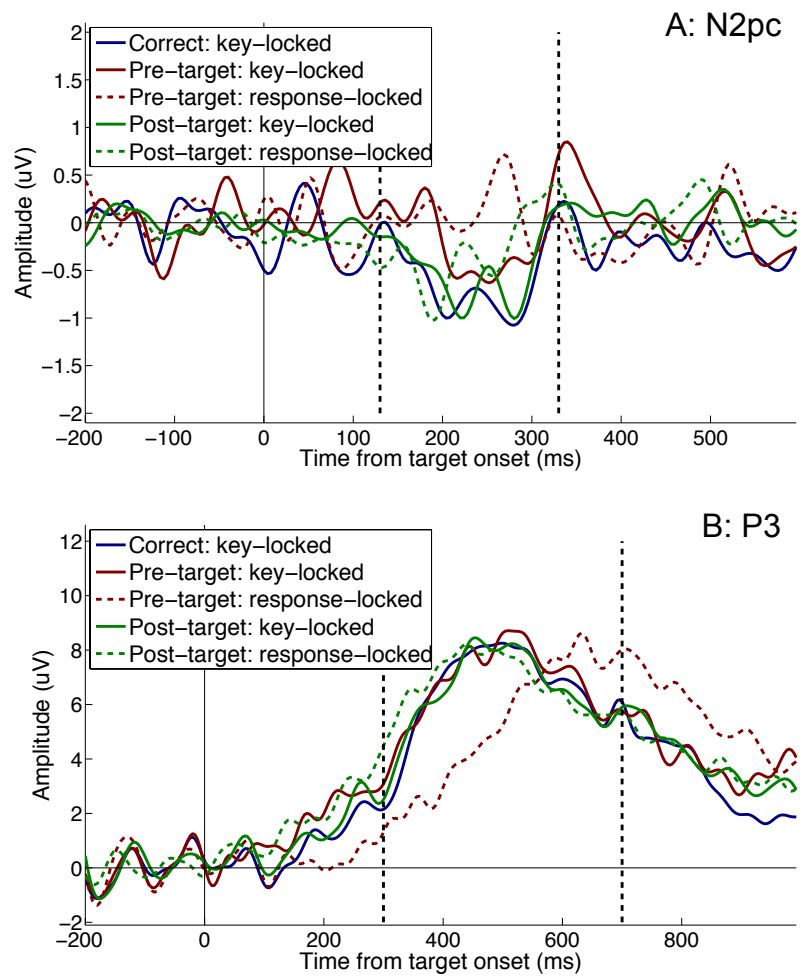


*Figure 55* ERPs evoked by correct reports, pre-target errors and post-target errors. Panel A: Key-locked and response-locked N2pc grand average ERPs. Panel B: Key-locked and response-locked P3 grand average ERPs. Note that the response-locked ERP averages for correct reports are the same as the key-locked averages. Dashed lines indicate the window used for statistical analysis.

correct reports had the earliest key-locked virtual N2pc and P3 latencies, followed by pre-target and post-target errors. In addition, we found that with the response-locked ERPs, the order of latencies was markedly different: post-target errors were the earliest, followed by correct reports and pre-target errors (see figure 9.3.2). This was explained by reasoning that, though the virtual ERPs were driven by the key pathway, they were sensitive to the temporal variability in the response pathway that eventually produced behavioural differences. Consequently, the response-locked ERPs for pre-target errors were delayed and those for post-target errors were advanced, relative to the presentation time of the erroneous response feature that got bound.

Figure 55 depicts the key-locked (plotted using solid lines) and response-locked (plotted using dashed lines) grand average N2pc and P3 ERPs evoked by the three response positions, combining trials across the letter and symbol conditions. As can be seen in figure 55A, the key-locked N2pc for correct reports and post-target errors are identical, while that for pre-target errors appears to be affected by a slight baseline shift relative to the other two conditions. However, pairwise comparisons between the conditions did not yield any significant differences in peak amplitude ( $F < 1$ ) or jackknife (with an onset criterion of 50% of peak amplitude) latency ( $t < 1$ ) within the 130-330ms window. This lack of any differences between the N2pc is consistent with the pattern seen in the key-locked P3 ERPs. As can be seen in figure 55B, the key-locked P3 evoked by correct reports, pre-target and post-target errors are effectively identical, with no suggestion of any visual differences. In keeping with this, a pairwise statistical comparison within the 300-700ms window did not reveal any variation in 50% latency ( $F < 1$ ) or peak amplitude ( $F < 1$ ) across the three response positions.

Turning to the response-locked N2pc and P3 ERPs in figure 55, clear differences are visible when comparing them to their key-locked counterparts<sup>9</sup>. First, we compare the response-locked N2pc for correct reports and pre-target errors: we find that correct reports have an earlier jackknife (with an onset criterion of 50% of peak amplitude) latency (179.28ms) than pre-target errors (286.9ms). This difference is not significant ( $t(1,13) = 1.39, p = 0.09$ ). This lack of an effect is due to the obvious attenuation of the response-locked

---

<sup>9</sup>Note that, as would be expected, the response-locked ERP for correct reports is the same as the key-locked ERP.

ERP (see figure 55A). In turn, this is because the N2pc is a relatively small component, and the increased latency variation between the response-locked ERPs for the -1 and -2 positions greatly reduces the amplitude of the pre-target error average ERP, which combines trials from these two positions. This attenuation is confirmed by a significant difference in the peak amplitude ( $F(1,13) = 7.61$ ,  $MSE = 1.09$ ,  $p = 0.01$ ) between the response-locked N2pc for correct reports ( $-2.28\mu V$ ) and pre-target errors ( $-1.15\mu V$ ). The next comparison of interest is between the response-locked N2pc for correct reports and post-target errors. There is a visual suggestion of a latency difference between the ERPs, confirmed by an estimation of their jackknife latencies (with an onset criterion of 50% of peak amplitude): post-target errors have a slightly earlier latency (164.73ms) than correct reports (194.8ms), but this difference is not significant ( $t < 1$ ). Again, this lack of an effect is most likely due to the attenuation of the N2pc average caused by response locking, which combines ERPs across the +1 and +2 positions. Because of this attenuation, the peak amplitude for post-target errors ( $-1.48\mu V$ ) is marginally lower than that for correct reports ( $-2.28\mu V$ ) ( $F = 4.16$ ,  $MSE = 1.01$ ,  $p = 0.06$ ).

The pattern of differences between the response-locked ERPs are clearer in the P3 averages in figure 55B, due to the relatively large amplitude of the P3. The first comparison is between the response-locked P3s for correct reports and pre-target errors. As is clearly evident, the P3 for pre-target errors is significantly later than that for correct reports. This is supported by a highly significant difference in 50% area latency of the P3, which is 504.92ms for correct reports and 567.69ms for pre-target errors ( $F(1,13) = 48.83$ ,  $MSE = 524.52$ ,  $p < 0.001$ ). Also, there is a small, expected reduction in peak amplitude between the averages (which is not significant):  $11.23\mu V$  for correct reports and  $10.04\mu V$  for pre-target errors ( $F(1,13) = 1.98$ ,  $MSE = 4.67$ ,  $p = 0.2$ ). The next comparison, between the response-locked P3s for correct reports and post-target errors, also suggests a latency difference: the 50% area latency of the P3 evoked by post-target errors is earlier (486.15ms) than that evoked by correct reports (504.92ms). This difference is not significant:  $F(1,13) = 1.8$ ,  $MSE = 1295.17$ ,  $p = 0.2$ . However, a jackknife analysis (with an onset criterion of 50% of peak amplitude) of P3 latencies within the 250-700ms window suggests a weakly significant effect ( $t(1,13) = 2.08$ ,  $p = 0.03$ ), with post-target errors having an earlier latency (298.5ms) than correct reports (337.91ms). There is no suggestion of a difference in peak amplitude between the

two P3s ( $F < 1$ ).

The differences between the key-locked and response-locked human ERPs are worth comparing to the corresponding virtual ERPs. The key-locked virtual ERPs in figure 51 show small but clear differences in latency and amplitude. In particular, the model predicts that correct reports are associated with the earliest key-locked ERPs, followed by those for pre-target errors and post-target errors (see section 9.3.2). However, the statistical tests performed above on the key-locked human N2pc and P3 ERPs in figure 55 do not suggest any differences in latency or amplitude. This finding is in contradiction to the predictions of the 2f-ST<sup>2</sup> model<sup>10</sup>. This divergence between model and data could be due to implicit assumptions in our simulations with the 2f-ST<sup>2</sup> model, which might not be valid in our experiment. In particular, for simplicity, we assume that the amount of random delay introduced to the processing of items, as controlled by the  $\tau_D$  parameter (see section 8.2.4), is the same in the key and response pathways. It is possible that in our experiment, the temporal variability in the processing of key (letter, digits and symbols) and response features (colours) are markedly different. Indeed, to test this possibility, we conducted further simulations with the model, with reduced temporal variability in the key pathway relative to the response pathway. To do so, for all trials in a simulation run, the  $\tau_D$  parameter was fixed at 0ms in the key pathway (i.e., key features of items were not randomly delayed or advanced). In the response pathway, as before,  $\tau_D$  was randomly sampled for each item in a trial, from a gaussian distribution with a mean of 0ms and a standard deviation of 15ms. All other model parameters were the same as in its default configuration. We found that, in this altered configuration of the model, the latency and amplitude differences between the key-locked averages for correct reports, pre-target and post-target errors (figure 51) were eliminated. However, the latency differences between the corresponding response-locked averages remained qualitatively unchanged. Thus, the model produced a pattern of virtual ERPs similar to their human counterparts in figure 55. Based on this simulation, we propose that in our setup in Experiment 3, there might be much less temporal variability in the processing of key features.

---

<sup>10</sup>In fact, the lack of any difference in the latencies of the key-locked ERPs for correct reports, pre-target and post-target errors also contradicts reaction time data reported by Botella (1992). However, this difference might be due to the fact that our experimental setup did not involve a speeded reaction time task.

The differences between the response-locked virtual ERPs in figure 51 show a clear correspondence with the human ERPs in figure 55. As there is more temporal variability in the response pathway, response locking increases the amount of latency variation between the virtual N2pc and P3 associated with correct reports, pre-target and post-target errors. Specifically, the model predicts that post-target errors have the earliest response-locked virtual ERPs, followed by correct reports and pre-target errors. The statistical differences between the response-locked human ERPs corroborate this ERP prediction from the model, though the effects are weak with the human N2pc in particular. Nevertheless, the qualitative pattern of differences between the response-locked human ERPs are similar to those between the virtual ERPs from the 2f-ST<sup>2</sup> model. This similarity lends support to the dynamics in the model that produce these differences. Further, it suggests that the human N2pc/P3, though driven by key feature processing, is sensitive to temporal variability in the temporal dynamics of response feature processing.

### 9.4.3 Manipulation of the Key Feature Pathway

In this section, we focus on the influence of an isolated manipulation of key feature processing on the human N2pc and P3 ERPs. As pointed out previously in section 8.5, the letter and symbol conditions in Experiment 3 constitute a pair of conditions involving a relative delay in the processing of key features (in the symbol condition). This is seen in the post-target shift between the response distributions for the two conditions, plotted in figure 56A. The API of the distribution for the letter condition is 0.18, and that for the symbol condition is 0.31. Further, this difference is significant ( $F(1,13) = 9.7$ ,  $MSE = 0.01$ ,  $p < 0.01$ ). Following on from this behavioural difference, we now compare the N2pc and P3 ERPs evoked by letter and symbol targets.

Figures 56B and 56C depict the key-locked (plotted using solid lines) and response-locked (plotted using dashed lines) N2pc and P3 ERPs evoked by letter and symbol targets. Each of these ERPs include all trials in which the key feature of the target was correctly reported, and average across all response positions (i.e., correct reports, pre-target and post-target errors). The first comparison is between the key-locked N2pc evoked by letter and symbol targets. As can be seen in figure 56B, symbol targets evoke a later key-locked N2pc. Statistically, a jackknife analysis (with an onset criterion of 50% of peak amplitude) of the

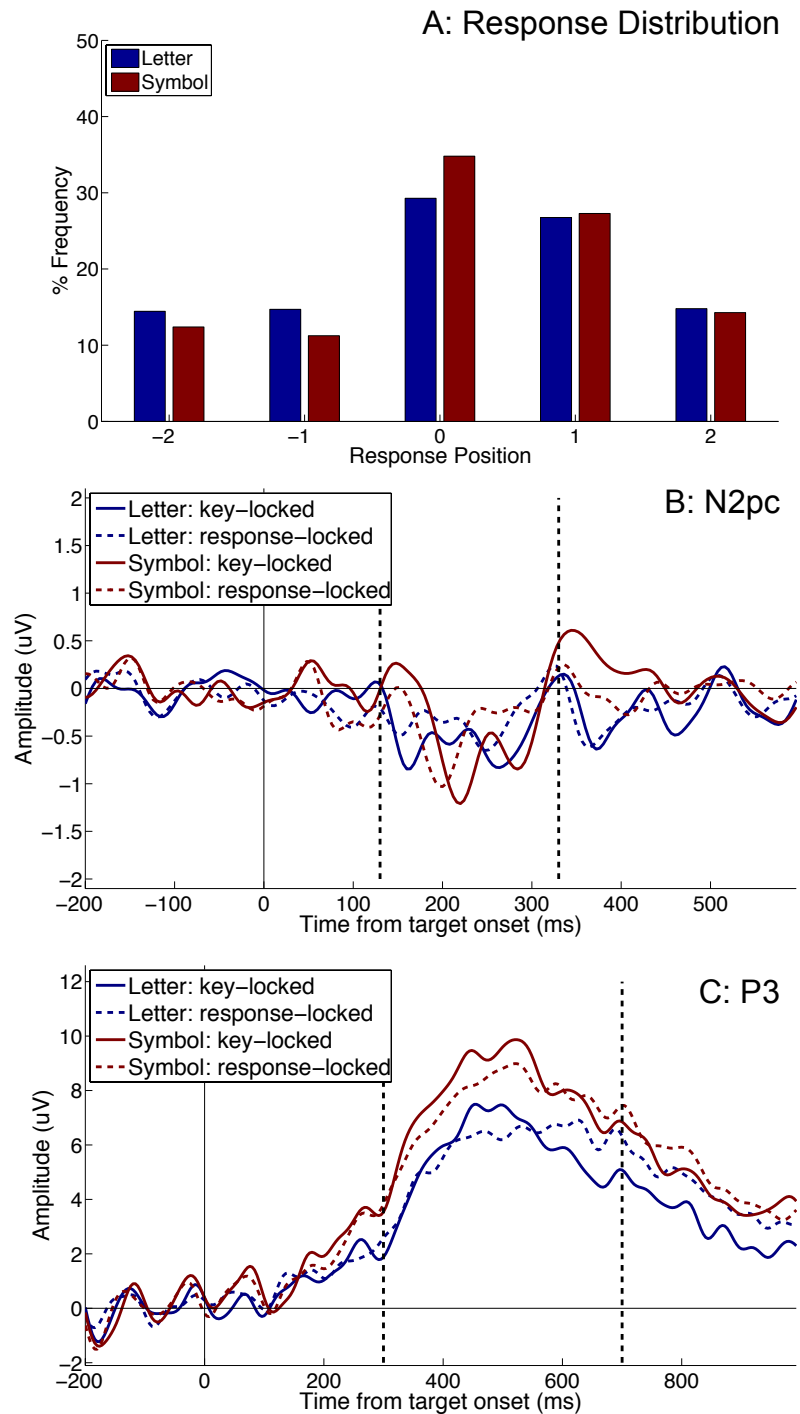


*Figure 56* **Behaviour and ERPs for the letter and symbol conditions.** Panel A: Response distributions. Panel B: Key-locked and response-locked N2pc grand average ERPs. Panel C: Key-locked and response-locked P3 grand average ERPs. Dashed lines in the ERP plots indicate the window used for statistical analysis.

visual difference in latency (within the 130-330ms window) shows a significant effect: letter targets have a mean jackknife latency of 147.56ms, whereas symbol targets have a latency of 197.92ms. ( $t(1,13) = 6.26$ ,  $p < 0.001$ ). However, there is no evidence for a difference in peak amplitude ( $F < 1$ ). Next, we compare the key-locked P3 for letter and symbol targets, shown in figure 56C. The main visual difference between the key-locked P3 ERPs is their amplitude. The peak amplitude of the P3 within the 300-700ms window is  $9.41\mu\text{V}$  for letter targets and  $11.44\mu\text{V}$  for symbol targets. This difference is significant:  $F(1,13) = 6.68$ ,  $\text{MSE} = 4.3$ ,  $p = 0.02$ . However, though the peak latencies of the key-locked grand average P3s differ considerably (456ms for letter targets and 524ms for symbol targets), this difference is not statistically significant across subjects ( $F < 1$ ). Similarly, there is no indication of a significant difference in the 50% area latencies (Luck & Hillyard, 1990) across the two conditions ( $F < 1$ ).

We now move to comparisons between the response-locked ERPs in figure 56. A comparison of the response-locked N2pc ERPs for letter and symbol targets in figure 56B to their key-locked counterparts shows that they are relatively attenuated by the process of response locking. This pattern, essentially the same as that described in section 9.4.1 (see figure 54B), arises because of the significant latency variation between the response-locked N2pcs for the different response positions. This in turn reduces the amplitude of the combined average. With a small ERP component like the N2pc, this attenuation considerably obscures the component in the grand average. We find that there is no statistical difference between the peak amplitudes of the response-locked N2pc ERPs for letter and symbol targets ( $F < 1$ ). Also, a jackknife analysis (with an onset criterion of 50% of peak amplitude) of the latencies of these response-locked N2pc ERPs fails to find a statistical difference.

Finally, we compare the response-locked P3 ERPs evoked by letter and symbol targets in figure 56C. There is no significant difference in the 50% area latencies ( $F < 1$ ). The peak amplitudes of the response-locked P3 for letter and symbol targets are  $8.6\mu\text{V}$  and  $10.02\mu\text{V}$  respectively. This difference is not significant:  $F(1,13) = 3.0$ ,  $\text{MSE} = 4.67$ ,  $p = 0.1$ . As with the N2pc, the response locking clearly reduces the peak amplitude of the P3, due to reasons previously highlighted in section 9.4.1 (see figure 54C).

The ERP results presented above exhibit a complex pattern of effects in terms of changes

in amplitude and latency across the conditions of interest. The 2f-ST<sup>2</sup> model offers a qualitative explanation for some important effects, with the aid of the virtual ERPs described earlier in section 9.3.3. Therein, we compared the key-locked and response-locked virtual ERPs generated by the model in the early and late key feature conditions. As established in the previous chapter (see section 8.5), these two conditions in the model are behaviourally comparable to the letter and symbol conditions, respectively. Following on from that, we can compare the virtual ERPs in figure 52 to those described in this section. However, it is worth noting that, as can be seen in the response distributions in figure 56A, the number of post-target errors does not change much between the letter and symbol conditions. Consequently, the magnitude of the differences between the human ERPs for these conditions are likely to be smaller than those between the corresponding virtual ERPs for the early and late key feature conditions.

In particular, the key-locked human N2pc ERP in figure 56B shows a shift in latency between letter and symbol target conditions, which is consistent with the latency shift between the virtual N2pc for early and late key feature conditions (see figure 52B). In addition, a similar shift is also evident in the key-locked virtual P3 generated by the model for these two conditions (see figure 52C). This derives directly from the fact that target consolidation in 2f-ST<sup>2</sup>, as reflected by the virtual P3, is driven strongly by the blaster activity reflected in the virtual N2pc. However, this prediction from the model could not be verified in the key-locked human P3 ERPs (figure 56C). This could possibly be due to a weak effect obscured by noise. Also, the main effect observed in the human P3 (in both the key-locked and response-locked averages), i.e., the reduction in amplitude of the letter P3, could potentially be due to aspects of the experimental design. Previous research has shown that the P3 is sensitive to a variety of experimental factors (see Kok (2001) for a review). It has been found that changes in task difficulty interact with changes in processing strategy and stimulus characteristics across experimental blocks to affect the size of the P3. As a consequence, it is possible that the relatively large difference in P3 amplitude produced by the blocking of letter and symbol targets obscured smaller differences in P3 latency predicted by the 2f-ST<sup>2</sup> model.

In the context of differences between key-locked P3s, it is interesting to note that the

latency shift predicted by the model (across a pair of conditions involving an isolated manipulation of the key feature) is indeed observed in previous ERP data reported by Polich and Donchin (1988). In their lexical decision experiment, Polich and Donchin (1988) found that low-frequency words (equivalent to the late key feature condition) evoked P3s that were generally later than those evoked by high-frequency words (equivalent to the early key feature condition)<sup>11</sup>. Importantly, in their experiment, trials were not blocked by word frequency, i.e., participants did not know whether the target in a given trial would be a low-frequency or high-frequency word. This is in contrast to the design in Experiment 3, where letter and symbol targets were presented in separate blocks. Consequently, participants knew beforehand as to whether the target would be a letter or a symbol. For this reason, it could be that our P3 data was additionally influenced by differences associated with ‘cognitive effort’ employed by the participants in the two blocks. This potential confound did not exist in the experimental setup employed by Polich and Donchin (1988). As a result, their data provides us with a clearer test of the 2f-ST<sup>2</sup> model’s predictions, which are indeed confirmed by the pattern of P3 latency differences reported by them.

As pointed out previously in section 9.4.1, the response-locked N2pc and P3 in the human data suffer an attenuation similar to that observed in the response-locked virtual ERPs in figure 52. In the case of the model, this attenuation derives from the increased latency variation in the response pathway. Hence, we see a qualitative equivalence of the response-locked human ERPs to their model equivalents, for both the letter and symbol conditions. This corroboration provides important empirical support for the architecture and dynamics of the 2f-ST<sup>2</sup> model.

#### 9.4.4 Manipulation of the Response Feature Pathway

In section 9.3.4, we discussed the ERP predictions from the 2f-ST<sup>2</sup> model relating to a manipulation of processing delay in the response pathway (see figure 53). However, these predictions could not be directly tested with human EEG data from Experiment 3. This was because Experiment 3 did not incorporate a manipulation of response feature processing, either a priori or post-hoc. As a result, the ERP predictions of the model relating to an

---

<sup>11</sup>See figures 1 and 2 in Polich and Donchin (1988).

isolated response feature manipulation could not be directly tested. However, as pointed out in section 9.3.4, the late key feature and the early response feature conditions are the same, in that they both represent the output of the 2f-ST<sup>2</sup> model simulated in its default configuration. Further, the early key feature and late response feature conditions are mutual inversions, as the former is simulated with  $\tau_K = -40\text{ms}$  and  $\tau_R = 0\text{ms}$ , while the latter is simulated with  $\tau_K = 0\text{ms}$  and  $\tau_R = 40\text{ms}$ .

In the previous section, we have used the human EEG data to test the model's ERP predictions for the early and late key feature conditions. Hence, due to the correspondence between the early/late key feature and the late/early response feature conditions, respectively, we have indirectly tested the model's predictions for the latter pair of conditions. Indeed, this equivalence does not obviate the need for direct verification of the model's predictions in the early and late response feature conditions. Nevertheless, it mitigates the seriousness of the limitation imposed by the unavailability of comparable human EEG data.

#### 9.4.5 Summary

We now summarise the outcomes of the comparisons between the virtual ERPs from the 2f-ST<sup>2</sup> model and the human ERPs from Experiment 3. In section 9.4.1, we began with a comparison of key-locked and response-locked ERPs combining across the letter and symbol conditions, and across all response positions. The main prediction of the model in this regard was that the amplitude of the response-locked average would be lower than the key-locked average (figure 50). This prediction was confirmed in the corresponding human ERPs (figure 54).

Next, in section 9.4.2, we separated the key-locked and response-locked human ERPs for correct reports, pre-target and post-target errors. For the key-locked ERPs, the 2f-ST<sup>2</sup> model predicted a pattern where correct reports had the earliest latency, followed by pre-target and post-target errors (figure 51). However, we found that there was no difference in the latency or amplitude of the corresponding human ERPs (figure 55). As discussed therein, with a further reduction in the amount of effective temporal variability in the key pathway, the model was better able to predict the pattern observed in the key-locked human ERPs. Alongside, the model was able to qualitatively replicate the pattern of latency differences observed in the response-locked ERPs for the three response positions. It predicted that

the response-locked ERPs for post-target errors would be the earliest, followed by correct reports and pre-target errors (figure 51). This pattern was also seen in the human data, though it was not significant in the N2pc due to its diminished amplitude (figure 55).

Finally, in section 9.4.3, we analysed the key-locked and response-locked ERPs for the letter and symbol conditions. As highlighted in section 8.5, these conditions were behaviourally equivalent to the early and late key feature conditions simulated by the 2f-ST<sup>2</sup> model. The model predicted that, concomitant with the post-target shift in the response distributions, symbol targets should produce key-locked ERPs that were later than those produced by letter targets (figure 52). Though this pattern was verified in the key-locked human N2pc ERPs, it was not seen in the P3 ERPs (figure 56). As discussed in section 9.4.3, this might have been due to methodological confounds in our experimental setup, which produced other systematic differences in the key-locked human P3s. Further, we pointed out that P3 data from Polich and Donchin (1988) provides a clearer test of the model's predictions in this regard, and is in agreement with them. As for the response-locked virtual ERPs, the model predicted a relative attenuation due to response locking (figure 52). This attenuation was confirmed in the response-locked human N2pc and P3 for both the letter and symbol conditions (figure 56).

## 9.5 Conclusions

This chapter has extended the capabilities of the 2f-ST<sup>2</sup> model beyond the behavioural domain, and highlighted its ability to make testable predictions relating to human ERPs. This is an important strength of the model, as it allows us to interpret behavioural and EEG data using a common explanatory framework. We began the chapter with a series of explorations that explicated the ERP predictions from the model. Exploring the 2f-ST<sup>2</sup> model at this greater level of detail has allowed us to provide in-depth explanations of how it simulates high-level behaviour, building up from the level of neural network dynamics. In particular, we have described how the model produces a counterintuitive pattern that replicates reaction time data reported by Botella and Eriksen (1992). In addition, the explorations have drawn upon results from current empirical research into the influence

of stimulus and response related processing on the P3. The comparisons between key-locked and response-locked averages in these explorations have informed this research, and highlighted the model's predictions in each case.

In addition, we have used EEG data from our temporal binding experiment to verify some of the main ERP predictions from the model. In particular, we have compared key-locked and response-locked averages in our EEG data and compared them with virtual ERPs from the 2f-ST<sup>2</sup> model. Further, we have described in our data a pair of experimental conditions involving a systematic manipulation of delay in key feature processing. The ERPs generated in these conditions have also been tested against virtual ERPs from the model. However, as pointed out previously in chapter 4, limitations in the virtual ERP technique imply that the match between human and virtual ERPs can only be qualitative. In addition, limitations deriving from experimental methodology have meant that not all the predictions from the model could be fully tested with our EEG data. Nevertheless, the comparative evaluations conducted here have allowed us to verify important internal mechanisms implemented in the 2f-ST<sup>2</sup> model. In summary, this combination of theory and experiment has contributed to our understanding of the temporal dynamics of feature binding and the role of the temporal spotlight therein.

## Part III

# Discussion

## Chapter 10

# Conclusions, Contributions and Outlook

Over the previous chapters, we have described research involving a collection of theoretical and experimental explorations into the dynamics of temporal attention and perception. In this chapter, we take stock, to bring together the ideas explored therein and highlight how they have addressed the central hypotheses of this thesis. Following that, we discuss how this work informs the current state of research in its field, and directions in which it could be taken forward.

### 10.1 Conclusions

In this section, we return to the central hypotheses of this thesis, outlined in section 1.2. We highlight how the research described in this thesis has addressed the proposals made therein, and discuss issues that remain to be resolved.

#### **The Existence of TAE**

We hypothesised in section 1.2 that there exists in human cognition a mechanism that provides transient attentional enhancement (TAE), thereby functioning like a temporal spotlight. In this thesis, we have highlighted a large body of experimental research that points to the existence of such a mechanism. The evidence therefrom, drawing on both behaviour

and electrophysiology, suggests this TAE functions like an attentional gate, providing an enhancement that is short-lived and non-specific. Further, the incorporation of such a TAE in the ST<sup>2</sup>, 2f-ST<sup>2</sup> and other cognitive models, as described in chapters 5 and 8, have enabled them to sufficiently explain a broad spectrum of empirical evidence. In particular, the profile of blaster unavailability during ongoing encoding explains the temporal characteristics of the Attentional Blink (AB) deficit. In addition, the finding of lag 1 sparing agrees with the time course and generality of the blaster's enhancement. Further, as demonstrated in chapters 7 and 9, the human N2pc, thought to reflect attentional selection, shows a qualitative correspondence to the blaster's activation reflected in the virtual N2pc. Together, these sources of evidence provide support for the notion that a TAE-like mechanism might indeed exist in the brain.

However, though we have speculated on the neurophysiological underpinnings of TAE, this line of investigation has not been focused on here. It might be that TAE is actually a emergent product of the collective interaction of many different brain regions and systems. Further research in this direction might shed more light on the inter-connectivity and dynamics of these systems. Indeed, this knowledge would inform our interpretation of existing behavioural and EEG data, and the architectural assumptions of the ST<sup>2</sup> and 2f-ST<sup>2</sup> models.

### **The Task Relevance of Stimuli and TAE**

Another hypothesis in section 1.2 was that the detection of task relevant stimuli selectively activates TAE, and that this can happen earlier or later in time relative to stimulus presentation. In chapter 6 we focused on this issue, and explored how the discriminability of targets from distractors affects temporal perception. The chapter described results from our EEG experiment that directly investigated how the neural dynamics of perception varied across a pair of conditions that differed maximally in the discriminability of targets. In particular, we compared changes in early visual processing and the P3 ERP across this manipulation. Therein, we showed that the latency of the P3 was clearly affected by how quickly targets could be identified. Furthermore, we followed up this empirical research with a theoretical elucidation based on the ST<sup>2</sup> model. By making a sequence of justifiable changes to its architecture, we enabled the model to replicate the pattern of effects observed in our data.

With this exploration, we explained how target discriminability might be influencing the deployment latency of TAE, thereby producing observable changes in temporal perception and consequent behaviour.

### **Suppression of TAE by Working Memory Encoding**

Next, we suggested that TAE is suppressed by ongoing consolidation. Further, the duration of this suppression is dependant on the strength of the mental representations generated by the target. To support this claim, in chapter 5 we pointed to behavioural evidence relating to the AB, which suggests that the AB is attenuated when T1 strength is increased (for example, by presenting a blank after it). In addition, we demonstrated how the reciprocal relationship between target strength and AB duration implemented by the ST<sup>2</sup> model explains this pattern of data. As described in chapter 3, the ST<sup>2</sup> model implements the suppression of TAE during binding. Because of the reciprocal relationship, stronger targets produce shorter windows of TAE suppression, thereby producing the observed attenuation of the AB. Further, chapter 5 also focused on the neurophysiologically inspired LC-NE model of temporal attention. We pointed out that, in its published form, it could not explain the behavioural evidence for the reciprocal relationship. However, we proposed and implemented an extension to the LC-NE model based on ST<sup>2</sup> concepts. This extension enabled it to replicate the reciprocal relationship between target strength and the suppression of the LC-NE system.

### **The Influence of TAE on the Temporal Precision of Perception**

In section 1.2, we proposed that the unimpaired availability of TAE ensures the temporal precision of perception. In contrast, impairment of TAE results in increased temporal uncertainty and error rates. This proposal was focused on in chapter 7, using a combination of experimental and theoretical techniques. For the experimental aspect, we employed data from our experiment that recorded EEG activity evoked by target processing outside and inside the AB window. With this data, we applied a methodology that used ERP images and time-frequency analysis of single-trial N2pc and P3 responses to test the hypothesis that the neural dynamics of target perception inside the AB were more temporally variable.

Based on this methodology, a combination of qualitative and quantitative techniques was employed to show that impairment of TAE (during the AB window) temporally ‘jittered’ the processing reflected by the ERPs. To complement this empirical approach, we employed the ST<sup>2</sup> model to interpret our data at the level of single-trial dynamics. Using complementary virtual ERPs and ERPimages, we showed that T1 processing affected the precision of TAE deployment for T2, thereby adversely affecting its consolidation into working memory. Correlating data and model at this level not only allowed us to propose a sufficient explanation for the pattern of EEG data, but also to validate the architecture and dynamics of the ST<sup>2</sup> model in greater detail. Finally, we tied in our research with existing literature, and interpreted reports of increased binding errors and temporal inaccuracy during the AB in terms of our hypothesis.

### **The Role of TAE in Temporal Feature Binding**

The last hypothesis in section 1.2 was that TAE plays an important role in the process of temporal feature binding. We suggested that TAE determines the dynamics of the process by which concurrently active mental representations of task-relevant features are bound into working memory. Chapters 8 and 9 instantiated this hypothesis in the form of the 2f-ST<sup>2</sup> model. In chapter 8, we described how 2f-ST<sup>2</sup> provides a sub-symbolic description of the role of TAE in binding co-active stimulus features into working memory. We generated behavioural predictions from the model, which were verified using data from previous experiments, in addition to our own. In particular, it showed how the dynamics of TAE deployment affected behavioural outcomes (i.e., correct reports and illusory conjunctions) and associated reaction times, producing patterns of variation that agreed with behavioural data. This validation demonstrated that 2f-ST<sup>2</sup> improves upon previous modelling approaches, by providing a description of temporal feature binding that is more in-depth, broad-based and parsimonious.

The research in chapter 8 laid the groundwork for generating EEG predictions from 2f-ST<sup>2</sup> in chapter 9. There, we focused on virtual ERPs from the model, to gain deeper insights into the temporal dynamics of attention and perception embodied therein. Over a sequence of explorations, we generated virtual N2pc and P3 traces from 2f-ST<sup>2</sup> to provide predictions about human EEG data relating to temporal feature binding. Specifically, these

predictions embodied the model’s claims about the interaction between TAE, temporal perception and behavioural outcomes. To test these claims, we turned to EEG data from our experiment. The findings therefrom successfully verified some of the main ERP predictions of the model. In particular, we demonstrated that, as predicted by 2f-ST<sup>2</sup>, the dynamics of TAE deployment and temporal perception were driven by key feature processing. These dynamics formed the basis of the model’s ability to replicate a counterintuitive pattern of reaction time data. However, not all the ERP predictions from 2f-ST<sup>2</sup> could be verified, due to limitations of experimental methodology and theoretical assumptions. Nevertheless, the comparative evaluations between model and data allowed us to validate the model’s main internal mechanisms. Finally, to return to our hypothesis, this combination of theory and experiment elucidated the influence of TAE in mediating temporal feature binding.

## 10.2 Contributions

This section broadens the scope of the discussion to highlight the main contributions of this thesis to current research. We touch upon a methodological contribution before discussing how we inform current understanding of feature binding and visual perception.

### Combining Modelling and Electrophysiology

A common theme in most of this thesis has been the attempt to apply neural network modelling to make predictions about human electrophysiology. This novel technique, previously proposed in Craston (2009), embodies connectionist thinking in its approach to verifying high-level behaviour by simulating functional neural dynamics. It has enabled us to extend cognitive modelling beyond the explanation of behaviour. We have used neural models to interpret the preceding dynamics that produce the behaviour. In turn, we have also validated many of the mechanisms that simulate these dynamics. Owing to the nature of our methodology, the match between simulated and real dynamics has only been qualitative. Nevertheless, interpreting behavioural and EEG data within a common explanatory framework has provided us deeper insights into temporal attention and perception.

## **The Temporal Spotlight and Feature Binding**

The 2f-ST<sup>2</sup> model described in this thesis proposes a functional neural architecture for implementing feature binding in temporal perception. In particular, it hypothesises a crucial role for the temporal spotlight of attention therein, as the intermediary between two stages of information processing. Over the research described in this thesis, we have emphasised the distinction between this temporal spotlight and its spatial counterpart. Alongside, we have established that, though the processes of feature binding in space and time share fundamental properties, there are also important distinctions. With the 2f-ST<sup>2</sup> model, we have demonstrated how the temporal spotlight provides transient attentional enhancement to establish a binding between temporally overlapping featural representations of stimuli (presented in succession at a particular spatial location). This functional description of temporal feature binding at the level of neural network dynamics improves upon previous modelling efforts, and feeds into current research into the binding problem in general.

In this regard, it is important to note that the description of temporal feature binding provided by 2f-ST<sup>2</sup> does not necessarily conflict with proposals based on temporal synchrony (Gray, 1999). Indeed, it is possible that temporal correlations between oscillatory patterns in neuronal populations might be employed in conjunction with attentional enhancement (Singer, 1999). At its level of abstraction, the 2f-ST<sup>2</sup> model describes how such concurrent patterns of activity might be functionally influenced by the temporal spotlight. Further, it proposes a consequent architecture for maintaining multiple such bindings in a token-based working memory, once they have been established. In doing so, the model reaches up to the level of behaviour, explaining the formation of correct reports and illusory conjunctions in the temporal domain.

## **The Episodic Nature of Consciousness**

As pointed out in chapter 3, the ST<sup>2</sup> model embodies the notion of episodic distinctiveness in temporal perception. The 2f-ST<sup>2</sup> model remains faithful to this idea and extends it to temporal feature binding. Generally speaking, it proposes that the cognitive architecture involved in temporal perception aims to provide conscious awareness with a coherent picture of an ever-changing reality. To elaborate, at the level of raw visual input, the real world

presents a continuously changing environment, where events take place in uninterrupted succession. However, for us to make sense of it, this input needs to be transformed into distinct, episodic memories that occur in a particular temporal order. According to the 2f-ST<sup>2</sup> model, the temporal spotlight mediates this transformation, effectively by enabling the visual system to take ‘snapshots’ of specific segments of time, in response to the occurrence of salient events (Wyble, Bowman, & Nieuwenstein, 2009). These snapshots ‘capture’ groups of featural representations that are conjoined into working memory. Each such snapshot, represented by a token in the model, is intended to be a separate, discrete episode accessible to conscious awareness. The model suggests that many related behavioural phenomena manifest because of the temporal limitations in a system that is attempting to create such episodic representations of reality. In particular, the AB is caused by the suppression of the temporal spotlight during the ongoing creation of an episode. Similarly, illusory conjunctions occur when the temporal spotlight highlights an incorrect group of visual representations to be combined into an episode. Over the course of this thesis, we have studied this system as implemented in the ST<sup>2</sup> and 2f-ST<sup>2</sup> models, and characterised the role of temporal spotlight in shaping conscious experience.

## **10.3 Future Outlook**

In this final section, we look at potential directions in which the research described in this thesis could be taken further. In the course of this research, we have combined computational modelling with EEG experimentation to study temporal attention. Consequently, in the following sections, we speculate on future lines of enquiry that could be pursued along these two directions.

### **10.3.1 Experimental Directions**

At many points in this thesis, we have highlighted interesting predictions from the ST<sup>2</sup> and 2f-ST<sup>2</sup> models that could not be tested with the empirical data collected herein. This section returns to these predictions, and discusses potential experimental ideas that could serve to verify the models and inform their further development.

## **Connecting T1 Duration with T2 Latency**

In chapter 7, we measured the single-trial latencies of P3s (as estimated by their phases) evoked in the T1 Lag 3 and T2 Lag 3 conditions (see section 7.5.3). In the discussion section therein, we discussed potential reasons for why we did not observe a direct trial-by-trial correlation between these P3 latencies. As pointed out there, Experiment 2 was not designed to generate much variation in T1 strength, and consequently, a weak correlation between the P3 latencies could have been obscured by noise. With sufficient variation in T1 strength, the dynamics of the ST<sup>2</sup> model propose a stronger relationship between the duration of the T1 Lag 3 P3 and the latency of the T2 Lag 3 P3. Indeed, the model suggests that there should be a reciprocal influence of T1 strength on its encoding duration (Bowman et al., 2008), which would in turn have implications for T2 P3 latency.

One possible method to test this prediction from the ST<sup>2</sup> model is to devise an experiment that incorporates a stronger variation in T1 strength, and then investigate the correlation between T1 and T2 P3 latencies across this variation, in addition to across T2's presentation outside and inside the AB window. This is because the ST<sup>2</sup> model suggests that, within the appropriate range, T1 P3 duration is driven by its bottom-up strength. An experiment that builds on the sort of designs we have described in this thesis could incorporate a strong variation in T1 strength produced by explicitly manipulating its psychophysical characteristics. This could be done by varying the backward masking of the T1 item in RSVP, i.e., by replacing the distractor following the T1 with a blank screen. Going further, a more fine-grained modulation of T1 strength could be achieved by varying the relationship between its presentation duration and that of the blank following it, thereby introducing a variable inter-stimulus interval following the T1. Such an experimental configuration would allow us to gradually increase T1 strength along a linear scale, and measure the consequent effect on the duration of its P3 and the latency of T2's P3.

## **Two-Feature AB with EEG**

Chapter 7 highlighted results from previous research (Chun, 1997a; Popple & Levi, 2007; Vul et al., 2008) involving experiments where items with pairs of features were presented in RSVP. In these studies, participants were required to detect the occurrence of two targets

(T1 and T2) with unique key features within the RSVP stream, and identify the associated response features. They all reported finding an AB effect for T2 in this context. In addition, they also reported specific changes in the response distributions for the T2 when it was presented during the AB (see section 7.9). Therein, we connected their findings with our hypothesis of reduced temporal precision during the AB, and showed that the ST<sup>2</sup> model could explain the pattern of behavioural effects observed in these studies. In this regard, it would be informative to conduct a study that extends the experimental paradigm used in these previous ones, by recording EEG in conjunction with behavioural responses. The data generated therefrom would inform our understanding of the influence of the AB on the neural dynamics of temporal feature binding, and guide theoretical research in this regard. In particular, as discussed later in this chapter, EEG data from the proposed ‘two-feature AB’ study would directly inform the further development of the 2f-ST<sup>2</sup> model, to enable it to explicitly simulate influence of the AB on feature binding in time.

### **Response Feature Manipulation with EEG**

In chapter 8 we showed how the 2f-ST<sup>2</sup> model can simulate behavioural effects produced by experimental manipulations of key and response processing times. In particular, we described results from a pair of experiments conducted by Botella et al. (2001), one involving a key feature manipulation and another involving a response feature manipulation. As described in section 8.3, the 2f-ST<sup>2</sup> model was able to simulate the behavioural effects of both manipulations. Then, in chapter 9, we went further and generated ERP predictions from the 2f-ST<sup>2</sup> model about the effects of such systematic manipulations on the N2pc and P3 (see section 9.3). Using EEG data from Experiment 3, we compared the virtual ERPs generated by 2f-ST<sup>2</sup> to human ERP data across a pair of conditions involving a manipulation of key feature processing time. However, as pointed out in the discussion section in chapter 9, Experiment 3 did not incorporate a complementary response feature manipulation. Hence, an appropriate EEG study consisting of a pair of conditions differing only in response processing times would provide data that could be used as an additional test of the ERP predictions from 2f-ST<sup>2</sup>. As an example, the design of such a study could invert the task from Experiment 3, by presenting coloured easy/hard alphanumeric/symbol stimuli in RSVP, and requiring participants to identify the item presented in a particular unique

colour. This would produce a pair of conditions across which the average processing time for the key feature (colour) remained the same, while that for the response feature (identity) varied depending on whether the target item was an easy or hard alphanumeric/symbol stimulus. N2pc and P3 data from this study could be compared with virtual ERPs from figure 53. This comparative evaluation would help further validate 2f-ST<sup>2</sup>'s mechanisms, and add to our understanding of the interplay between temporal attention and binding.

### 10.3.2 Theoretical Directions

We now turn to directions in which the modelling work on the 2f-ST<sup>2</sup> model introduced in this thesis could be continued. These directions aim not only to broaden the explanatory scope of the model, but also to explore more neurocomputationally viable implementations.

#### Modelling Two-feature AB with 2f-ST<sup>2</sup>

As pointed out earlier in this chapter, a 'two-feature AB' EEG study extending from behavioural studies (Chun, 1997a; Popple & Levi, 2007; Vul et al., 2008) would generate new data to inform further development of the 2f-ST<sup>2</sup> model. In parallel, the extension of the 2f-ST<sup>2</sup> model to explicitly simulate the influence of the AB on temporal feature binding would generate testable ERP predictions that could be verified with this data. In this thesis, the 2f-ST<sup>2</sup> model has been used to simulate the binding of pairs of features in RSVP streams consisting of a single target. In this scenario, we have manipulated the feature processing time in the key and response pathways and shown that some of the main behavioural and ERP predictions from the 2f-ST<sup>2</sup> model about the effect of such manipulations are validated by empirical data. The model could be further extended to explicitly simulate the influence of the AB additional to these manipulations. To do so, it would need to simulate the feature binding of two targets, T1 and T2, presented in an RSVP stream consisting of items with pairs of features, in close succession so as to produce an AB effect for T2. This addition would naturally increase the computational complexity of the model, and further optimisations might be required in order to keep simulation time within feasible limits. Overall, this combination of theoretical and experimental enquiry would significantly add to the 2f-ST<sup>2</sup> model's capabilities as a broad-based description of temporal visual processing.

## Distributed Representations in the Binding Pool

The binding pool in the 2f-ST<sup>2</sup> model implements an activation based memory for type-token associations. In other words, the binding pool remembers which types were associated with which tokens during binding, thereby providing the model with a way to later recall the types of seen targets. For this purpose, the binding pool contains one binding node for each combination of type node and token, which gets turned on only if the type and token are associated during binding. Such a representation, also referred to as *localist* (O'Reilly & Munakata, 2000), allows for simple and sufficient implementation of the binding pool in the model, where only a few types are represented. However, the binding pool is likely to be implemented in a *distributed* fashion in the brain. This is because a localist representation does not scale well when considering all the possible types of items the brain can represent. Hence, mandating a unique cortical micro-circuit for each combination of type and token would require an unreasonable number of neurons dedicated to the task of maintaining bindings. For such problems, distributed representations (Rumelhart et al., 1986) have been proposed as a neurophysiologically feasible alternative. Indeed, in many cases, the brain appears to rely on distributed activation patterns over neuronal cell assemblies to store mappings<sup>1</sup> (Haxby et al., 2001; Ishai, Ungerleider, Martin, Schouten, & Haxby, 1999; also see Desimone & Ungerleider, 1989; Tanaka, 1996 for reviews). Another unrealistic aspect of a localist binding pool is that it would allow for perfectly accurate retrievals of previously stored associations, and have theoretically unbounded capacity. This follows from the fact that there is a unique binding pool node whose state of activation unambiguously determines whether an association was created between the corresponding type and token during binding. As there is no theoretical limit on the number of binding pool nodes, an unbounded number of associations can be stored and correctly retrieved. Again, this notion is unrealistic, and is refuted by previous cognitive and neurophysiological research into the limitations of human working memory (Luck & Vogel, 1997; Alvarez & Cavanagh, 2004; Callicott et al., 1999; also see Cowan, 2001 for a review). It has been found that there is a limit to the number of type-token associations that humans can store in working memory,

---

<sup>1</sup>In reality, it might be that a combination of localist and distributed representations is implemented in the brain (Page, 2001).

and that the decreasing probability of correct retrieval gradually is modulated by the number and complexity of previously stored associations. On the whole, these arguments make a convincing case for investigating a distributed binding pool implementation in the 2f-ST<sup>2</sup> model. However, in this context, it is important to note that we are not proposing that all neural constructs in the model might be implemented in a distributed fashion. For example, it is likely that token-like mechanisms are more suited to localist representations in the brain (Page, 2001).

As pointed out earlier in this chapter, from a neurophysiological perspective, binding is a complex phenomenon, thought to tap into temporal correlations in the firing patterns of many neuronal cell assemblies (Milner, 1974; Gray, 1999; Koch, 2004). However, within the context of the 2f-ST<sup>2</sup> model, it is interesting to investigate the implementation of a distributed binding pool that functionally approximates this complexity<sup>2</sup>. In a distributed binding pool, nodes are not specific to a combination of type and token. Rather, the process of binding involves creating a type-token association that activates a randomly chosen subset of binding pool nodes to different degrees. In other words, a binding is stored in a distributed fashion, as a ‘spread of activation’ over a group of binding pool nodes. Importantly, a given binding pool node can be involved in multiple type-token associations. Conversely, the sets of binding pool nodes used by different type-token associations can overlap, i.e., have nodes in common between them. In order to retrieve a stored association in such a distributed memory, activation is fed ‘backwards’ from the active token, via the binding pool nodes that were randomly chosen during binding, to ‘re-activate’ the associated type node. In contrast to a localist binding pool, this retrieval process in a distributed binding pool is not deterministic, i.e., there is a certain probability with which the correct type node associated with an active token can be re-activated. This probability is a function of many parameters, including the total number of nodes available in the distributed binding pool, the number of types and tokens, etc. In particular, as the number of stored associations increases, the average amount of overlap in a binding pool of a given size also increases. Consequently, the probability of correct retrieval degrades gracefully with increasing overlap, imposing a natural limit on the number of associations that can be stored while keeping this probability

---

<sup>2</sup>Preliminary modelling work with the ST<sup>2</sup> model suggests that a relatively small distributed binding pool could store mappings involving a large number of types (Wyble, Bowman, & Nieuwenstein, 2009).

above chance level.

A move to a distributed binding pool implementation would not produce significant changes in the overall behaviour and dynamics in the model, at least within the context of the simulations we have conducted in this thesis. This is because, in our simulation of RSVP streams, only a few types and tokens are involved in the binding process. Consequently, retrieval accuracy will be relatively high, even with a distributed implementation. Nevertheless, adding this implementation would make the model more neurocomputationally feasible, i.e., more in-line with what is known about how the brain processes and stores information across patterns of activation over groups of neuronal assemblies. The distributed binding pool in itself could then be employed in simulations to test the limits of its performance, and its dependence on the main parameters controlling its implementation. A better knowledge of these parameters could be used to inform our understanding of working memory performance in humans, and allow us to make predictions about the nature and functioning of binding pool-like mechanisms in the brain.

## Part IV

# Appendix

# Appendix A

## Computational Methods

### A.1 The ST<sup>2</sup> Model

The ST<sup>2</sup> model (Bowman & Wyble, 2007) is a neural-network model of temporal attention and working memory. Neurons in the ST<sup>2</sup> model are implemented using the O'Reilly and Munakata (2000) model of rate-coded neurons. The mechanisms operating in these neuro-physiologically plausible abstractions of real neurons are based on the Hodgkin and Huxley (1952) equations (Koch, 1998). The following sections outline some of the common neural constructs employed in the model.

#### A.1.1 On-Off Circuits

Individual nodes in the Item and TFL layers, and the Blaster Input and Blaster Output are implemented as on-off micro-circuits, each consisting of a pair of such neurons. As shown in figure 57, the circuit consists of a self-sustaining on neuron that excites an inhibitory off neuron. The on neuron is activated by incoming input, and due to its self-loop, temporally sustains its activation for a while, even after the input has been removed. During this time, the off neuron also builds up excitation, and once it crosses its output threshold, it strongly suppresses the on neuron. This interaction emulates the behaviour of excitatory and inhibitory interneuron cell assemblies in the brain (see Bowman & Wyble, 2007 for more details).

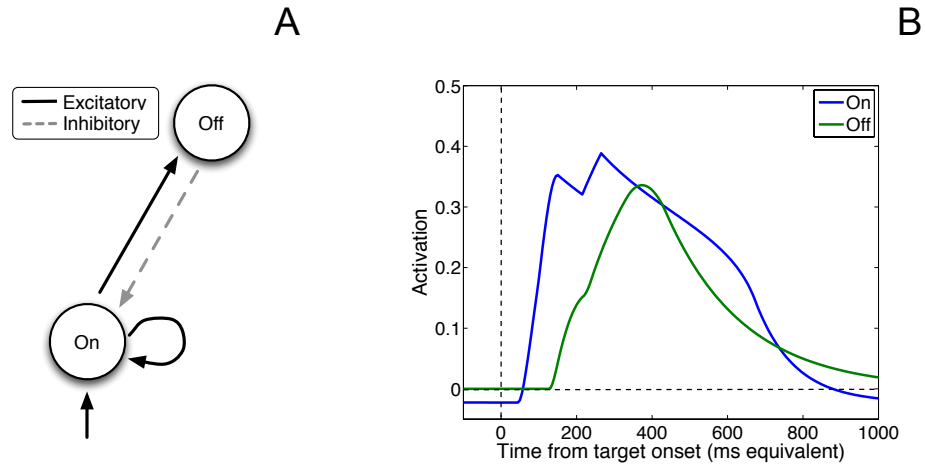


Figure 57 **An on-off circuit.** Nodes in the Item and TFL layers, and the Blaster Input and Blaster Output in the ST<sup>2</sup> model have this internal structure.

### A.1.2 Gate-Trace Pair

A gate-trace pair (Bowman et al., 2008; Bowman & Wyble, 2007) is an inhibitory interneuron circuit, involving an excitatory gate neuron and a self-sustaining inhibitory trace neuron. Each token in figure 11 has this internal structure, depicted in figure 58A. The gate neuron is so named because it acts as a gate to the trace neuron. That is, activation of the trace neuron (which is in a closed circuit with the gate) follows activation of and is driven by the gate. The trace neuron is so named because, once activated above threshold, it will self sustain; i.e., it maintains the trace of an item in WM. However, once over threshold, the trace neuron will also suppress the gate neuron. This interplay between the gate and trace neurons of a token can be seen in the membrane potentials plotted in figure 58B. A single target presented in an RSVP stream excites the gate neuron of the currently active token. This increased activation gradually feeds into the trace neuron, which eventually enters an attractor due to the excitatory self-loop. Once in the stable attractor, the trace neuron strongly suppresses the gate neuron and prevents it from being activated again.

Importantly, when gate neurons are placed in an inhibitory competition, as is the case with tokens in the ST<sup>2</sup> model, a receptive competitive active memory is obtained. Because trace neurons maintain representations and gates are removed from the competition once their traces have been allocated, the layer can engage in a series of (competitive) encoding episodes. Gate-trace circuits have the further benefit that encoding time is inversely related

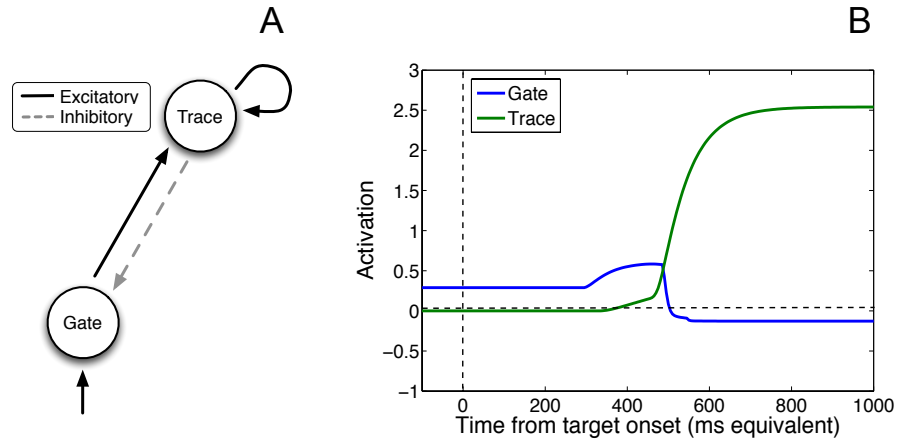


Figure 58 **A gate-trace pair.** Binding pool nodes and tokens in the  $ST^2$  model have this internal structure.

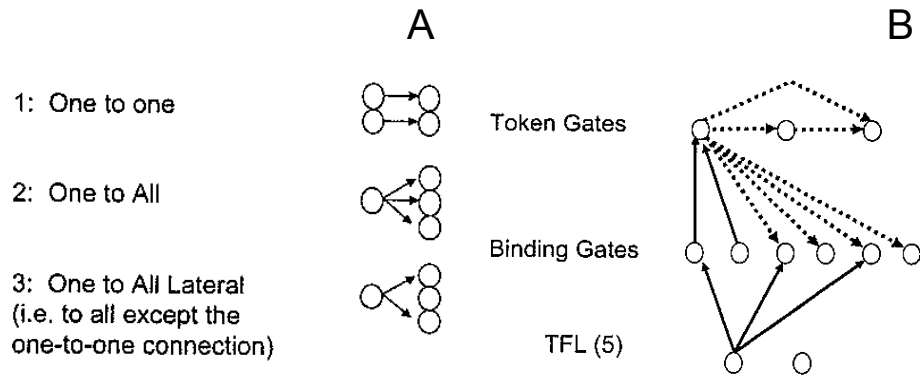


Figure 59 **Weight types and connectivity patterns in the  $ST^2$  model.** Panel A: Different connection types between layers. Panel B: Connectivity into and out of the binding pool. For visual clarity, connectivity is shown only for one neuron in each layer. Solid connections are excitatory, and dashed connections are inhibitory.

to activation strength. The time to encode a stimulus using a gate-trace pair is the interval from when the gate starts to be active to when its corresponding trace neuron crosses threshold. Importantly, this time will be shorter the stronger the extrinsic (bottom-up) activation of the gate. Because of this property of gate-trace pairs, they naturally yield a reciprocal relationship between bottom-up trace strength and encoding time, a property which underlies the depth of the AB in  $ST^2$  (Bowman et al., 2008).

From Layer	To Layer	SOA (ms)	New Weight	Old Weight
Input	Masking	100	.023	0.022
Input	Masking	50	.058	0.05
TFL	Blaster input on	100, 50	.02003	0.018
Blaster input off	Blaster input off	100, 50	.0112	0.01

*Table 1* Connection weights in the ST<sup>2</sup> model that were modified in this thesis.

### A.1.3 Weights and Connectivity

Connections between layers in the ST<sup>2</sup> model are one of three types, as shown in figure 59A. One-to-one connections link corresponding nodes in the source and destination layers (e.g., feedforward excitatory connections from Item to TFL). One-to-all connections link each individual node in the source layer to all nodes in the destination layer (e.g., feedback excitatory connections from Blaster output to TFL). One-to-all-lateral connections are identical to one-to-all connections, except for the one-to-one connection between corresponding nodes in the source and destination layers (e.g., feedforward inhibitory connections from Input to Masking). Figure 59B depicts the pattern of fan-out and fan-in connectivity in the binding pool, using an example scenario with 2 TFL type nodes and 3 tokens. This configuration requires 6 binding pool nodes to maintain associations between each combination of type and token. As can be seen, a TFL type is connected to only those binding pool nodes that associate it with each token. Further, a token inhibits other tokens, and the binding pool nodes associated with them.

### A.1.4 Model Configuration

For all the simulations of the ST<sup>2</sup> model in this thesis, the model was configured with as few parameter changes as possible compared to the version published in Bowman and Wyble (2007). Table 1 contains a list of the neural network weight values that were modified. Note that, despite these changes, the model still reproduced all behavioural data published in Bowman and Wyble (2007). In addition, the number of distractor nodes in Stage 1 were increased from 10 to 15 nodes. This had no effect on behavioural accuracy, but was required to generate virtual ERP traces at 50ms SOA.

## A.2 The Re-implemented LC-NE Model

The original LC-NE model described in Nieuwenhuis, Gilzenrat, et al. (2005) was re-implemented as a part of the research leading up to this thesis. In this re-implementation, the equations and parameters governing the LC-NE system and the behavioural network remained exactly the same as that in the original model. The only exception was the number of iterations comprising a simulation trial, which was increased from 2200 to 2400 to extend the trial over 48 units of model time and incorporate 8 lag positions for T2.

### A.2.1 Simulating Blanks in the LC-NE Model

Consideration of the T1+1 blank condition in the LC-NE model was confused by the fact that placing an actual blank after the T1, i.e. presenting ... D T1 \_ D ... to the model, obliterated the blink. However, this was not due to absence of backward masking, and indeed would have been inconsistent with the afterimage persistence of visual stimuli (Keysers & Perrett, 2002; Keysers et al., 2005). The blink was attenuated with ... D T1 \_ D ... because the T2 benefits from reduced inhibitory competition. The blank interval in the T1+1 position allowed the activation level of the distractor node to fall to nearly resting level. In the LC-NE model, a T in a sequence ... D \_ T D D ... (or, indeed, ... D \_ D T D ..., etc) always had an advantage over a T in a sequence not containing a blank (e.g... . D D T D D ...). Thus, blanks placed anywhere in the stream generated a forward going (in the sense of the stream) competitive advantage. However, there were a number of reasons why this could not have served as an explanation of AB attenuation with T1+1 blank. For example, if the LC-NE decision layer set-up had been taken as a model of target-blank effects in the AB, it would have predicted that T1-1 blank should massively improve T1 performance and attenuate the blink, which it does not (Breitmeyer, Ehrenstein, Pritchard, Hiscock, & Crisan, 1999).

## A.3 The Extended LC-NE Model

The re-implemented LC-NE model (see appendix A.2) was extended using constructs from the ST<sup>2</sup> model, as a part of the comparative evaluation of the two models. In this extension,

pairs of gate-trace neurons (see section 3.1) for each target stimulus, connected to their corresponding detection layer nodes, formed the “read out” system for WM encoding. In addition, interface nodes translate gate neuron activation into inhibition of the LC-NE system. The parameters and simulation procedure for the extensions to the LC-NE model are described in the following sections.

### A.3.1 Extension Parameters

In the extended LC-NE model, the state  $Z$  of a node is updated once every iteration, by numerically integrating the ordinary differential equation for that node using a simple Euler method and then computing the activity of the node, using its sigmoidal activation function  $f(Z)$ , which is defined as,

$$f(Z) = \frac{1}{1 + e^{-g(Z-b)}} \quad (4)$$

where  $g$  is the multiplicative gain and  $b$  is the tonic bias input.

The differential equation for computing the state of a gate neuron  $G$  is given by

$$\frac{dX_G}{dt} = -X_G + w_{GT}[f(X_T) - \theta]_+ + w_{GR}f(X_R) \quad (5)$$

where  $X_G$  is the state of  $G$ ,  $w_{GT}$  (4) is the weight of the connection from the detection layer node  $T$  to  $G$ ,  $w_{GR}$  (-10) is the weight of the connection from  $G$ 's trace neuron  $R$  to  $G$ ,  $\theta$  (0.532) is the baseline activity level of  $T$  and  $[x]_+ = \max(x, 0)$ . The equation above is used to compute the state of  $G$  only after  $f(X_T)$  crosses the threshold of 0.67 used in the original LC-NE model. The activation function for  $X_G$ , i.e.  $f(X_G)$ , uses a gain ( $g$ ) of 1 and a bias ( $b$ ) of 1.

The equation for computing the state of a trace neuron  $R$  is given by:

$$\frac{dX_R}{dt} = -X_R + w_{RG}f(X_G) + w_{RR}f(X_R) \quad (6)$$

where  $X_R$  is the state of  $R$ ,  $w_{GR}$  (0.2) is the weight of the connection from the gate neuron  $G$  to  $R$  and  $w_{RR}$  (3) is the weight of the self-loop on  $R$ . The activation function for  $X_R$ , i.e.  $f(X_R)$ , uses a gain ( $g$ ) of 20 and a bias ( $b$ ) of 0.3.

The equation for computing the state of an interface node  $I$  is given by:

$$\tau_I \frac{dX_I}{dt} = -X_I + w_{IG} \min(f(X_G), \mu) \quad (7)$$

where  $X_I$  is the state of  $I$ ,  $w_{IG}$  (20) is the weight of the connection from the gate neuron  $G$  to  $I$ ,  $\tau_I$  (10) is the time constant of  $X_I$  and  $\mu$  (0.8) is an upper threshold on the activity level of  $G$  that is received by  $I$ . The activation function for  $X_I$ , i.e.  $f(X_I)$ , uses a gain ( $g$ ) of 4 and a bias ( $b$ ) of 1.4.

In the extended model, the LC-NE system receives inhibitory input from the interface nodes. Consequently, the equation modelling the LC state variable  $v$  is modified to:

$$\begin{aligned} \tau_v \frac{dv}{dt} = & w_{vX} [f(X_{T1}) + f(X_{T2})] \\ & + w_{vI} ([f(X_{I1}) - \rho]_+ + [f(X_{I2}) - \rho]_+) \\ & + v(a - v)(v - 1) - u \end{aligned} \quad (8)$$

where  $w_{vI}$  (-0.4) represents the weights of the inhibitory connections from the interface nodes  $I1$  and  $I2$  with activities  $f(X_{I1})$  and  $f(X_{I2})$ , respectively, and  $\rho$  (0.8) represents a lower threshold on the activity of the interface nodes.  $w_{vX}$  (0.3) is the link weight from decision layer to LC, and  $X_{T1}$  and  $X_{T2}$  are the states of the decision units.

## A.4 The 2f-ST<sup>2</sup> Model

### A.4.1 Architecture

The 2f-ST<sup>2</sup> model is an extension of the ST<sup>2</sup> model as described in Bowman and Wyble (2007), and later modified as outlined in section A.1. However, in order to integrate the extension with the original ST<sup>2</sup> model into a coherent architecture that could replicate the

Layer	Leak
Input	.07
Masking	.01
Item on	.04
Item off	.02
Type on	.07
Type off	.02

*Table 2* **Leak current values in Stage 1 of the response pathway of the 2f-ST<sup>2</sup> model.**

behavioural data related to temporal feature binding, some of its parameters had to be modified. These are detailed in the following sections.

### **Stage 1**

The 4 layers in Stage 1 of the original ST<sup>2</sup> model became the key feature pathway in the 2f-ST<sup>2</sup> model. The parallel response feature pathway was added by replicating these layers, namely Input, Masking, Item and Type. For each replicated layer, the number of nodes in it was the same as that in its counterpart in the existing key pathway. However, there were differences in many parameters in the two pathways, as described below.

**Key Pathway** The following changes were made to the configuration of the Stage 1 layers in the original ST<sup>2</sup> model to convert them into the key feature pathway of the 2f-ST<sup>2</sup> model.

1. The weights of the connections from the Item layer to the Type layer were reduced from 0.015 to 0.013, to decrease activation strengths at the Type layer. In addition, the strength of the leak current at the Type layer was increased from 0.07 to 0.0715.

2. The weights of the connections from the off neurons to the on neurons of the Type layer micro-circuits were increased from -0.12 to -0.15, to ensure that the on neurons were suppressed at the correct times.

3. The weight of the connection from the Type layer to the blaster Input was increased from 0.02003 to 0.02803, so that the blaster received more of the activation generated by target type nodes.

**Response Pathway** Table 2 lists the leak current settings for the layers in Stage 1 of the response pathway, and table 3 lists the weights of the connections between the layers. An

From Layer	To Layer	Type	Weight
Input	Masking	1	.023
Input	Masking	3	-.105
Masking	Masking	3	-.06
Masking	Item on	1	.014
Item on	Type on	1	.015
Item on	Item off	1	.02
Item on	Item on	1	.0095
Item off	Item on	1	-.15
Item off	Item off	1	.0095
Type on	Type on	1	.022
Type on	Type on	3	-.05
Type on	Type off	1	.01
Type off	Type on	1	-.5
Type off	Type off	1	.01
Blaster out on	Item on	2	.3
Blaster out on	Type on	2	.8

*Table 3 Connection weights in Stage 1 of the response pathway of the 2f-ST<sup>2</sup> model.* Connection type (column 3) specifies the whether the connection was a one-to-one (1), one-to-all (2) or one-to-all lateral (3). See figure 59 for a pictorial description of these connection types.

From Layer	To Layer	Weight	Remarks
Type on	Binding pool gate	.1	(1)
Binding pool gate	Token gate	.01	(2)
Token gate	binding pool gate	-4.5	(3)

*Table 4 Connection weights in Stage 2 of the 2f-ST<sup>2</sup> model.* (1) Excitatory weight from Type layer nodes to associated binding pool gates. (2) Excitatory weight from binding pool gates to associated tokens (3) Inhibitory weight from token to binding pool gates not associated with it.

important addition was the weak lateral inhibition between Type layer nodes, indicated by the small negative weight between Type layer on neurons. In addition, activity in the Item and Type layers did not influence the blaster. However, the blaster provided enhancement to the Item and Type layers. Finally, task demand did not operate at the response pathway Type layer.

## Stage 2

The binding pool in Stage 2 of the ST<sup>2</sup> model was expanded to include nodes that represented associations between response pathway type nodes and tokens. To this end, a total of 100 binding pool nodes were added, one for each combination of 4 tokens and 25 response

types (including all targets and distractors). The extension of the ST<sup>2</sup> model resulted in the alteration of its activation dynamics, which needed to be compensated for to ensure that the model’s behaviour remained within bounds. Importantly, the tokens were now receiving double the input (from two binding pool nodes compared to one in the original model). Table 4 lists the Stage 2 weights that were adjusted to account for this alteration.

#### **A.4.2 Dynamics**

A typical simulation run of the 2f-ST<sup>2</sup> model consisted of multiple trials. Across these trials, the strength of key feature of the target was varied across a range, while the strengths of the key features of distractor items were kept constant. However, in the response pathway, in order to simulate the generation of correct reports and conjunction errors, the strengths of the response features of the target as well as distractors around the target had to be varied. In order to keep the simulation time within feasible limits, only the strengths of response features of proximal (-1, -2, +1 and +2) distractors were varied, in addition to that of the target’s response feature. The strengths of all other distractor response features were kept constant across all trials.

Additional reductions in simulation times were obtained by minimising the number of strength combinations simulated in the response pathway. Specifically, strengths of the target’s response feature and one of the proximal distractors were varied in a pair-wise fashion, while the strengths of the other proximal distractors were kept constant. By doing so, we produced a set of trials that simulated competitive interactions between the response features of the target and a particular proximal distractor, over all possible response feature strengths. In effect, this set comprised a representative (but not an exhaustive) subset of all the possible outcomes that could be generated by the 2f-ST<sup>2</sup> model.

#### **A.4.3 General Configuration**

During the simulation of each trial in the 2f-ST<sup>2</sup> model, a randomly selected +ve/-ve delay  $\tau_D$  was added to the processing of all features in both pathways.  $\tau_D$  was repeatedly sampled within each trial run, once per item in the stream, from a gaussian distribution with mean of 0 and standard deviation of 15ms. This effectively introduced temporal noise in the model’s

dynamics, and allowed for the simulation of a larger number of conjunction errors and broader response distributions. Further, isolated manipulations of the feature processing time in the key or the response pathway were simulated. To do so, for all trials within a simulation run, a fixed additional +ve/-ve delay was introduced in the processing of all features in the desired pathway. This delay parameter was referred to as  $\tau_K$  in the key pathway and  $\tau_R$  in the response pathway. In the default configuration of the 2f-ST<sup>2</sup> model, both  $\tau_K$  and  $\tau_R$  were set to 0. To simulate a particular key (response) feature manipulation,  $\tau_K$  ( $\tau_R$ ) was appropriately set at the beginning of a complete simulation run, and stayed the same for all trials within that run.

In all simulations of the 2f-ST<sup>2</sup> model described in this thesis, the input RSVP streams presented to it were comprised of 25 items presented for 20 time steps each, equivalent to 100ms in model. The target item was presented at position 10 in the stream. Each item presented to the model had a pair of strength values, one in the key pathway and another in the response pathway. Distractors had constant key feature strength of 0.526. The key feature and response feature strengths of targets were independently iterated from 0.442 to 0.61 in steps of 0.028. For each response feature strength value of the target, that of a proximal distractor (i.e., in the -1, -2, +1 or +2 positions) was in turn iterated from 0.442 to 0.61 in steps of 0.028. During each such iteration, the response feature strength of all other proximal distractors was kept constant at 0.526. This iterative sequence was repeated for each proximal distractor. On the whole, this process generated a total of 1372 trials comprising a complete simulation run of the 2f-ST<sup>2</sup> model.

#### **A.4.4 Configuration for Behavioural Simulations in Section 8.3**

The previous sections have described the general configuration of the 2f-ST<sup>2</sup> model used for all the conditions simulated below. Only the  $\tau_K$  and  $\tau_R$  parameters that controlled the processing delays in the key and response pathways were changed according to the condition being simulated.

##### **Key Feature Manipulation**

To simulate the behavioural key feature manipulation from Experiment 1A in Botella et al. (2001) described in chapter 8, the high-frequency word condition was simulated by running

the 2f-ST<sup>2</sup> model in its default configuration (i.e.,  $\tau_K = 0\text{ms}$  and  $\tau_R = 0\text{ms}$ ). Of the total of 1372 trials making up a complete simulation in this configuration, a token was bound to a pair of features in 1122 trials. In 113 of these trials, two response features were bound to the same key feature, in which case one of them was randomly selected for behavioural report.

The low-frequency word condition was simulated by introducing a delay of 40ms (i.e.,  $\tau_K = 40\text{ms}$  and  $\tau_R = 0\text{ms}$ ) in the processing of all features in the key pathway in each trial. Of the total of 1372 trials making up a complete simulation in this configuration, a token was bound to a pair of features in 1117 trials. In 120 of these trials, two response features were bound to the same key feature, in which case one of them was randomly selected for behavioural report.

### **Response Feature Manipulation**

To simulate the behavioural response feature manipulation from Experiment 2 in Botella et al. (2001) described in chapter 8, the high-frequency word condition was simulated by running the 2f-ST<sup>2</sup> model in its default configuration (see above for details).

The low-frequency word condition was simulated by introducing a delay of 10ms (i.e.,  $\tau_K = 0\text{ms}$  and  $\tau_R = 10\text{ms}$ ) in the processing of all features in the response pathway in each trial. Of the total of 1372 trials making up a complete simulation in this configuration, a token was bound to a pair of features in 1115 trials. In 125 of these trials, two response features were bound to the same key feature, in which case one of them was randomly selected for behavioural report.

## Appendix B

# Experimental Methods

### B.1 Experiment 1

#### B.1.1 Participants

Twenty-two university students were paid 10 GBP to participate in the experiment. Two were excluded due to an excessive number of EEG artefacts, and a further three were excluded because of insufficient number of trials in the Onset condition, leaving 17 participants for the behavioural and EEG analysis (mean age 22.2; SD 3.3). Participants were free from neurological disorders and had normal or corrected-to-normal vision. The study was approved by the local ethics committee.

#### B.1.2 Stimuli and Apparatus

We presented alphanumeric characters in black, against a white background, on a 21" CRT computer screen (1024x768 @ 85Hz) placed at a distance of at a distance of 100cm from the viewer. All stimuli were presented using the Psychophysics toolbox version 2 (Brainard, 1997) running on MATLAB version 6.5 under Microsoft Windows XP. Stimuli were in Arial font and had an average size of  $2.1^\circ \times 3.4^\circ$  visual angle.

#### B.1.3 Procedure

Participants viewed four blocks (3 RSVP/1 Onset, counterbalanced between subjects) of 100 trials each. Within each block, there were 96 trials containing a single target, and 4

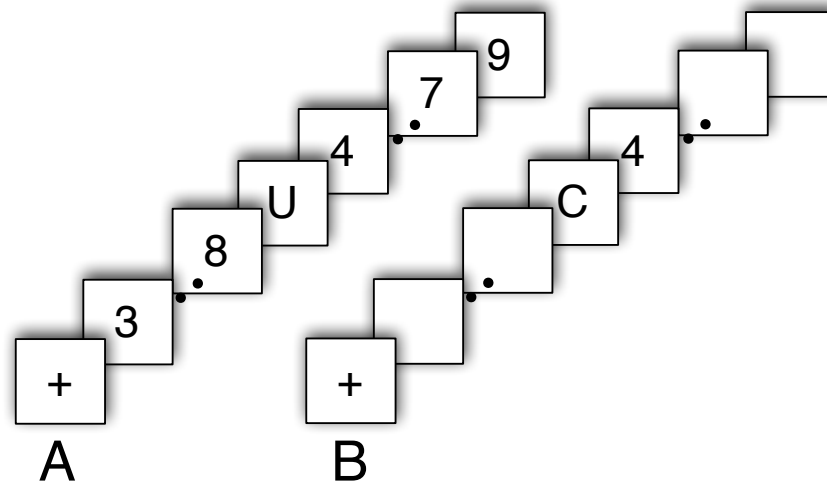


*Figure 60* **The RSVP and Onset presentation paradigms.** Panel A: A regular RSVP stream where a target letter is embedded in a stream of digit distractors. Panel B: The Onset presentation paradigm, which contains only the target letter and the following digit distractor as its mask.

trials consisting only of distractors. Five practice trials preceded the first block in both the RSVP and Onset conditions, and were not included in the final analysis. The underlying structure and timing of RSVP and Onset streams were the same. However, in the RSVP condition, the target was embedded in a continuous stream of distractors. In comparison, Onset streams contained only the target and a following distractor that served as a backward mask. The target for each trial was chosen at random from a list of 14 capital letters (B, C, D, E, F, G, J, K, L, P, R, T, U, V); distractors could be any digit except 1 or 0. The target item's position in the stream varied between positions 10 and 54. The 'distractor only' trials were randomly inserted to make the occurrence of the target less predictable. Trials were randomly ordered and 50% of targets were followed by a blank in both RSVP and Onset trials to equate patterns within blocks. However, the data from the Onset unmasked and RSVP unmasked conditions (streams where the target was not followed by a distractor) were not analysed. Figure 60 depicts the conditions (Panel A: regular RSVP, Panel B: Onset presentation) that were analysed from Experiment 1. Figure 60A depicts a single target embedded in a regular RSVP stream. Figure 60B shows a Onset stream consisting solely of the target and the following distractor. Although some studies (Ward et al., 1997) employ patterns instead of digits to mask the targets, the important difference with respect to RSVP is that all other distractor items are omitted.

A fixation cross presented for 500ms preceded the first item of each stream. Items were presented at the unconventionally fast rate of approx. 20 items per second (item duration 47.1ms; no inter-stimulus interval) to ensure participants' detection accuracy was not at ceiling in this relatively easy single target detection task.

An RSVP stream consisted of 70 items (total stream length 3.3 seconds) to allow a sufficient amount of time between target presentation and the end of the stream. The Onset condition contained a blank screen for 471ms to 2.5 seconds (depending on the target position), then the target (and its mask in the masked condition) for 47.1ms each, followed by another 706ms to 2.8 seconds of blank screen. The relatively long time period between the presentation of the target and the end of the stream ensured that the subject's behavioural response did not interfere with the EEG signal evoked by the target. Each stream ended with a dot or a comma presented for 47.1ms. Following stream presentation, participants were asked 'Was the final item a comma or a dot?' and in the following screen 'If you saw a letter, type it. If not, press Space.'. Participants entered their responses using a computer keyboard. The dot-comma task was included to ensure that participants maintained their attention on the stream after the target had passed.

#### **B.1.4 EEG Recording and Analysis**

EEG activity was recorded from Ag/Ag-Cl electrodes mounted on an electrode cap (FMS, Munich, Germany) using a high input impedance amplifier (1000M $\Omega$ , BrainProducts, Munich, Germany) with a 22-bit analogue-to-digital converter. Electrode impedance was reduced to less than 25 k $\Omega$  before data acquisition (Ferree, Luu, Russell, & Tucker, 2001). EEG amplifier and electrodes employed actiShield technology (BrainProducts, Munich, Germany) for noise and artefact reduction.

EEG data was recorded using Vision Recorder (BrainProducts, Munich, Germany), The sampling rate was 2000Hz (digitally reduced to 1000Hz at a later stage) and the data was digitally filtered at low-pass 85Hz and high-pass 0.5Hz during recording. 22 electrodes were placed at the following standard locations according to the international 10/20 system (Jasper, 1958): Fp1, Fp2, Fz, F3, F4, F7, F8, Cz, C3, C4, C7, C8, Pz, P3, P4, P7, P8, Oz, O1, O2, T7 and T8. In addition, a pair of electrodes recorded activity from both earlobes, which were used to re-reference the data offline. Electrooculographic (EOG) activity

was bipolarly recorded from below and to the right side of the right eye.

The EEG data was analysed using Vision Analyzer (BrainProducts, Munich, Germany), in conjunction with EEGLAB 6.01b (Delorme & Makeig, 2004) and custom MATLAB scripts. The data was referenced to a common average online and re-referenced to linked earlobes offline. Left mastoid acted as ground. Signal deviations in the EOG channel of more than  $50\mu\text{V}$  within an interval of 100ms were identified as eye blink and movement artefacts. These were removed by rejecting data in the window of 200ms before and after an eye artefact. To verify that these trials were accurately identified by the algorithm, we performed a manual inspection after the algorithm had been applied. ERPs were time-locked to the onset of the target and extracted from -200ms to 1200ms with respect to target onset. After segmentation, direct current drift artefacts were removed using a DC detrend procedure employing the average activity of the first and last 100ms of a segment as starting and end point, respectively. Following this, the baseline was corrected to the prestimulus interval (-200ms to timepoint 0) and segments were averaged to create ERPs.

ERP component amplitudes were derived from mean amplitude values within a certain window. ERP component latencies were calculated using 50% area latency analysis (Luck & Hillyard, 1990). Amplitude and latency values from subject averages were submitted to MATLAB scripts (Trujillo-Ortiz, Hernandez-Walls, & Trujillo-Perez, 2004) to perform repeated measures Analysis of Variance (ANOVA). After all statistical analyses, a 25Hz low pass filter was applied to enhance visualisation of ERP components.

We analysed EEG data from occipital-parietal scalp locations, more precisely, the P7 and P8 electrode sites. We averaged across these two sites as we were not interested in lateralised effects, but rather on ERP components that were not specific to one of the hemispheres. The analysis also focused on early visual processing, and the ERP trace averaged across the P7 and P8 electrodes contained both the P3 component and ERP components associated with early visual processing.

All ERPs contained only those trials in which the target was correctly identified. After artefact rejection, there were a total of 1517 trials left where the target was seen in the RSVP condition (with an average of 89 trials per subject, and the smallest trial count being 52), and 560 trials where the target was seen in the Onset condition (with an average of 33 trials per subject, and the smallest trial count being 19). We verified that this large difference,

due effectively to the experimental design, did not influence the statistical results. For each statistical comparison, this was done by redoing the statistical tests after randomly sampling trials from the RSVP condition for each subject, equal in number to Onset condition, and ensuring that the results did not change qualitatively.

### **B.1.5 Computational Modelling**

In order to simulate single target RSVP streams with 50ms presentation rate, the input stream presented to the ST<sup>2</sup> model contained 40 items, with the single target appearing at position 14 of the stream. Each item was presented for 10 timesteps, equivalent to 50ms in model time. Each item presented to the model had a certain strength value. Distractors had a constant value of 0.526. The strength of the single target was varied from 0.442 to 0.61 in steps of 0.014, resulting in a total of 13 trials making up a complete simulation run. All other model parameters and settings were as described in section A.1.

### **Virtual ERPs**

To simulate data from Experiment 1, we focused on the virtual ssVEP and P3 ERPs, which were compared with the human ssVEP and P3 for the Onset and RSVP conditions. The virtual ssVEP was generated by recording activation from the Input and Masking layers, and the virtual P3 was generated by summing activation across the Item, TFL, binding pool and token layers (see chapter 4).

## **B.2 Experiment 2**

### **B.2.1 Participants**

We recruited 20 new under- and postgraduate university students (mean age 23.1, SD 3.2; 10 female; 18 right-handed) who provided written consent and received 10 GBP for participation. Two participants were excluded from the analysis. The first one seemed to be a non-blinker (Martens, Munneke, et al., 2006), as his performance was at ceiling across all three lags. The second participant was excluded due to persistently high oscillations in the alpha band throughout the experiment. Hence, 18 participants remained for behavioural

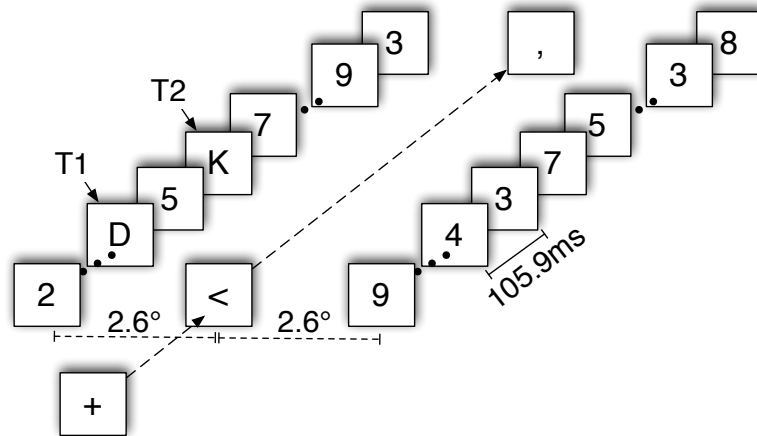


*Figure 61* **The two-target bilateral RSVP paradigm used in Experiment 2.** A typical trial began with a central fixation cross that turned into an arrow pointing toward the stream in which two letter targets would appear amongst digit distractors in RSVP sequence. At the end of the trial, the arrow turned into a dot or a comma. Reproduced from Craston et al. (2009).

and EEG analysis (mean age 22.5, SD 2.7; 9 female; 18 right-handed). Participants were free from neurological disorders and had normal or corrected-to-normal vision. The study was approved by the local ethics committee.

### B.2.2 Stimuli and Apparatus

Stimulus presentation settings were the same as that in Experiment 1, except for a reduction in average stimulus size ( $1.03^\circ \times 0.69^\circ$  visual angle) to ensure that the paradigm produced a reliable AB effect.

### B.2.3 Procedure

Participants viewed four blocks of 100 trials. Before starting the experiment, participants were asked to make 5 eye blinks and 5 horizontal eye movements to record the typical pattern of EOG activity. This was used to configure the algorithm for eye blink artefact rejection. Participants performed 8 practice trials, which were not included in the analysis. As shown in figure 61, RSVP streams were preceded by a fixation cross in the centre of the screen. After 400ms, the cross turned into an arrow indicating the side at which the targets would be presented. After 200ms, two streams of digits were simultaneously presented at an equal distance of  $2.6^\circ$  visual angle to the left and right of fixation. The RSVP stream

consisted of 35 items presented for 105.9ms each with no inter-stimulus interval. For 84% of trials in a block, the stream on the side indicated by the arrow contained 2 targets (T1 & T2), in 16% of trials both streams were made up of distractor digits only. The ‘distractor only’ trials were randomly inserted to make the occurrence of targets less predictable. In a trial, T1 and T2 were selected from a list of 18 possible targets (A, B, C, D, E, F, G, H, J, K, L, N, P, R, T, U, V, Y); distractors could be any digit except 1 or 0. T1 appeared between position 5 and 17; T2 followed T1 at position 1 (no intervening distractors - lag 1), position 3 (2 intervening distractors - lag 3) or position 8 (7 intervening distractors - lag 8). The arrow remained in the centre of the screen until the streams were over and then turned into either a dot or a comma.

Before the experiment started, participants were told to keep their eyes fixated on the centre of the screen from presentation of the cross until the dot/comma, as trials with eye movements would be identified in the EOG and excluded from the analysis. Participants were told to direct their covert attention towards the indicated stream, search for the two target letters and remember whether the last item was a dot or a comma. They were also informed that streams could contain either two or zero targets. Following stream presentation, participants were presented with the message ‘If you saw letters - type them in order, then dot or comma for the final item’ and entered their response without time pressure using a computer keyboard. The dot-comma task was included to ensure that participants kept their eyes fixated on the centre of the screen throughout the duration of the RSVP stream.

#### **B.2.4 EEG Recording and Analysis**

EEG recording hardware was identical to that employed for Experiment 1. EEG data was recorded using Vision Recorder (BrainProducts, Munich, Germany), at a sampling rate of 1000Hz. The left mastoid acted as ground. Online referencing to the average of all channels and filtering at 80Hz low-pass and 0.25Hz high-pass were applied. 20 electrodes were placed at the following standard locations according to the international 10/20 system (Jasper, 1958): Fp1, Fp2, Fz, F3, F4, F7, F8, Cz, C3, C4, Pz, P3, P4, P7, P8, Oz, O1, O2, T7 and T8. In addition, a pair of electrodes recorded activity from both earlobes, which were used to re-reference the data offline. Horizontal eye movements, recorded from a bipolar

Condition	Trials
Targets Presented Outside the AB	1873
Targets Presented Inside the AB	1561
Targets Seen Outside the AB (T1 Lag 8)	1581
Targets Seen Inside the AB (T2 Lag 3)	859
T2 Lag 8	1208
T1 Lag 3	851

*Table 5* **Conditions of interest analysed in Experiment 2.** The second column lists the number of trials in each condition after artefact rejection.

EOG channel placed below and to the left of the participant’s left eye, and indicated that participants had moved their eyes away from fixation and towards one of the RSVP streams.

EEG data was analysed using Vision Analyzer (BrainProducts, Munich, Germany), in conjunction with EEGLAB 6.01b (Delorme & Makeig, 2004) and custom MATLAB scripts. Signal deviations in the EOG channel of more than  $50\mu\text{V}$  within an interval of 100ms were identified as eye blinks and movement artefacts, and a window of 200ms before and after an artefact were marked for rejection. To verify that these artefacts were accurately identified by the algorithm, we performed a manual inspection after the algorithm had been applied.

ERP component amplitudes were derived from mean amplitude values within a certain window. ERP latencies were calculated using jackknife analysis (with an onset criterion of 50% of peak amplitude; see J. Miller et al., 1998) for the N2pc and 50% area latency analysis (Luck & Hillyard, 1990) for the P3. Amplitude and latency values from subject averages were submitted to MATLAB scripts (Trujillo-Ortiz, Hernandez-Walls, & Trujillo-Perez, 2004; Trujillo-Ortiz, Hernandez-Walls, & Trujillo-Perez., 2004; Trujillo-Ortiz, Hernandez-Walls, Castro-Perez, & Barba-Rojo, 2006) to perform repeated measures Analysis of Variance (ANOVA). Where appropriate, p-values were adjusted using Greenhouse-Geisser correction.

We analysed EEG data from parietal-occipital electrode sites. Specifically, to localise the N2pc ERP component, we used the P7, P8, O1 and O2 electrode sites. To localise the P3 ERP component, we used the Pz electrode. The continuous EEG data from each participant was loaded into MATLAB and low-pass filtered at 25Hz. The data was then segmented into trials, by extracting a time window of -500ms to 1000ms around the target onset times for the conditions of interest listed in table 5.

Trials marked as containing artefacts by the procedure defined above were excluded from further analysis. After artefact rejection, the total number of trials in the above conditions of interest are listed in table 5. A linear detrend function was applied to all retained trials. Each such trial was then baselined to the -200ms to 0ms window before presentation of the target to which it was time-locked. The only exceptions were the trials comprising the N2pc ERPs evoked by targets presented and seen inside the AB, which were baselined to the -500 to -300ms window before T2 presentation to ensure that there was no T1-related activity in the baseline window.

### **ITC-ERSP Analysis**

For the analysis of ITC and ERSP, continuous EEG data was segmented into trials by extracting time windows from -1000ms to 1000ms around target onset. After rejecting artefacts, this produced 1519 and 836 trials in the targets seen outside and inside the AB conditions, respectively. The ERSP and ITC evoked by the N2pc and the P3 in these two conditions were estimated with the EEGLAB v6.01b *newtimef* function. For both conditions and ERPs, the time-frequency analysis performed by *newtimef* used half-cycle Morlet-like wavelets of discrete frequencies between 1 and 5Hz, a spectral baseline window of -500ms to -300ms, and a padding ratio of 16. A bootstrap method (Delorme & Makeig, 2004) was used to construct a surrogate distribution for each time-frequency estimate by repeated temporal shuffling and accumulation that was repeated 200 times. The significance of each time-frequency estimate was then tested against its surrogate distribution at a significance level of 0.01. All other parameters were set to *newtimef* defaults. Please refer to EEGLAB documentation for more details on these parameters.

### **ERPimage Analysis**

To plot the ERPimages, trials were vertically sorted by phase angle, calculated using wavelet-based time-frequency analysis performed separately for each trial. For the time-frequency analysis, half-cycle Morlet-like wavelets (Delorme & Makeig, 2004) at 2.45Hz and 1.53Hz were used as templates for the N2pc and P3, respectively. These frequencies were selected by identifying the peaks of the ITC difference plots in figures 35E and 35F, within the time window of interest for the ERP in question. The time-frequency analysis returned a pair

of two-dimensional matrices, indexed by trial number and timepoint, and consisting of the power and phase values calculated at the specified frequency. The phases of the N2pc/P3 across all trials in a condition were selected at the peak of the corresponding grand average for that condition. For targets seen outside the AB, this peak occurred at 204ms and 428ms, respectively, for the N2pc and the P3. For targets seen inside the AB, the corresponding peaks occurred at 252ms and 496ms, respectively. For the T2 Lag 8 and T1 Lag 3 conditions, the peaks of the P3s occurred at 444ms and 424ms, respectively. ERPimages were plotted for each condition by sorting the trials based on their corresponding phase values. Trials were vertically smoothed using sliding window of 50 trials to improve visual clarity.

### **Phase Analysis**

Single N2pc/P3 trials for each condition were grouped by subject. For each trial in each group, phase values estimated at the frequencies mentioned above were selected at the peak latencies of the subject-wise average ERPs. For each subject and condition, this produced a circular distribution (Mardia & Jupp, 2000) of phase values within the range  $[-\pi, +\pi]$ . A concentration parameter  $\kappa$  was estimated for each of these subject-wise phase distributions, using maximum likelihood estimation in the R statistical package (R Development Core Team, 2008). The  $\kappa$  values were then statistically compared outside and inside the AB by feeding them into a standard one-way repeated measures ANOVA in MATLAB (Trujillo-Ortiz, Hernandez-Walls, & Trujillo-Perez, 2004).

### **B.2.5 Computational Modelling**

In order to simulate the two-target paradigm in the ST<sup>2</sup> model, the input RSVP streams presented to it were comprised of 25 items presented for 20 time steps each, equivalent to 100ms in model. T1 appeared at position 7 in the stream and T2 followed T1 after 0 to 7 (lags 1 - 8) intervening distractors. Each item presented to the model had a certain strength value. Distractors had a constant value of 0.526. Strength values for T1 and T2 were iterated from 0.442 to 0.61 in steps of 0.014. Hence, the model simulated a total of 169 target strength combinations at each lag position. All other model parameters and settings were as described in section A.1.

## Virtual ERPs

To generate virtual ERPs and ERPimages comparable to their human counterparts in Experiment 2, we combined simulated trials across multiple complete runs of the model. For each of the 18 subjects in the human data, a complete simulation run of the ST<sup>2</sup> model was executed once, over all combinations of T1 and T2 strengths. For all trials in each such run, a small delay (fixed per subject) was introduced in the processing of all stimuli presented to the model. This delay was a positive or a negative integer value, randomly sampled once per run, from a normal distribution with a mean of 0ms and a standard deviation of 50ms.

To simulate ERP data from Experiment 2, we focused on generating virtual N2pc and P3 ERPs for targets outside and inside the AB. The virtual N2pc was generated by recording activation from the blaster, and the virtual P3 was generated by summing activation across the item, TFL, binding pool and token layers (see chapter 4).

## Virtual ERPimages

To generate the virtual ERPimage for a particular condition, the corresponding trials from all the runs were collected together, sorted by 50% area latency (Luck & Hillyard, 1990) within the 200-1100ms window in each trial, and plotted as a colour-map with a vertical smoothing window of 10 trials to improve visual clarity.

## B.3 Experiment 3

### B.3.1 Participants

We recruited 14 new under- and postgraduate university students (mean age 22.3, SD 5.7; 9 female; 12 right-handed) who provided written consent and received 10 GBP for participation. Participants were free from neurological disorders and had normal or corrected-to-normal vision. The study was approved by the local ethics committee.

### B.3.2 Stimuli and Apparatus

We presented dark grey (RGB value of [64, 64, 64]) alphanumeric characters and symbols surrounded by coloured squares. The squares themselves were presented on a dark

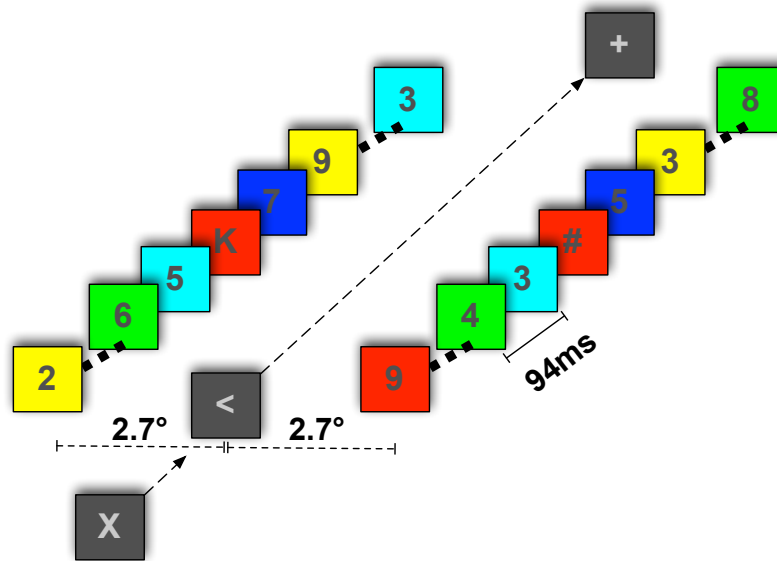


*Figure 62* **The single-target coloured bilateral RSVP paradigm used in Experiment 3.** A typical trial began with a central fixation cross that turned into an arrow pointing to the stream in which the target letter or symbol would appear amongst digit distractors. All items were presented against a coloured background square. At the end of the trial, the arrow turned into a '+' or an '=' sign.

grey (RGB value of [64, 64, 64]) background on a 21" CRT computer screen (1024x768 @ 85Hz) placed at a distance of 100cm from the viewer. All stimuli were presented using the Psychophysics toolbox version 3 (Brainard, 1997) running on MATLAB version 7.6 under Microsoft Windows XP. All stimuli were in Arial font. The characters and symbols subtended a maximal visual angle of  $1.2^\circ \times 1.2^\circ$ , while the coloured squares surrounding them subtended a maximal visual angle of  $1.36^\circ \times 1.36^\circ$ .

### B.3.3 Procedure

Participants viewed two blocks of 180 trials each. A block began with a task instruction indicating that the target item within all trials in the block would be either a letter or a symbol. The ordering of 'letter' blocks and 'symbol' blocks was counterbalanced across participants. Trials in both blocks had the structure depicted in figure 62. A trial began with a white fixation cross in the centre of the screen. After 500ms, the cross turned into a white arrow indicating the side at which a target would be presented. After 200ms, two streams of 16 items were simultaneously presented at an equal distance of  $2.7^\circ$  visual angle

to the left and right of fixation, at a rate of 94ms per item with no inter-stimulus interval. Colours for the squares surrounding items were sampled from a set of 5 values (Red: [255, 0, 0], Green: [0, 255, 0], Blue: [0, 0, 255], Yellow: [255, 255, 0], Cyan: [0, 255, 255]).

Both streams began with digits that were randomly sampled from a set of 8 possible values (2, 3, 4, 5, 6, 7, 8, 9) such that there were no repetitions of identity or colour within 3 consecutive positions. The target item was presented on one side of fixation chosen randomly with counterbalancing across trials within a block, at a random position between 6 and 12 in the stream. Targets were letters or symbols (depending on the block), randomly chosen from sets of 8 items: (D, E, G, K, L, T, U, V) for letters and (#, %, £, ¥, <<, ×, P, ÷) for symbols. Colours for the target and the proximal distractors (i.e., distractors in -1, -2, +1 and +2 positions relative to the target) in its stream were assigned using a random permutation of the above five colours listed above. This random permutation was counterbalanced across trials within a block. In a particular block, if letters were designated as targets, the item on the opposite side of the target in every trial within that block (i.e., in the same relative position but in the other stream) would be a symbol, and vice versa. The combinatorial pairing of a target item with a corresponding item in the opposite stream was counterbalanced across trials within a block. The colour of this item was always the same as that of the target. Further, the colours of the proximal distractors surrounding this item in its stream were the same as the colours of the corresponding proximal distractors surrounding the target. Effectively, this design ensured that the overall psychophysical structure of the blocks and the trials within them remained relatively invariant, and only the task relevance of letters and symbols as targets varied according to the task instruction for the block.

The arrow indicating the lateral position of the target remained in the centre of the screen until both streams were over, and then turned into either a '+' sign or an '=' sign (see figure 62). At the beginning of a block, participants were told to keep their eyes fixated on the centre of the screen from the time the cross was presented, until the +/- sign indicated the end of the streams. In addition, they were told to direct their covert attention towards the stream indicated by the arrow, and search for the target item, note its identity and the colour of the square surrounding it. In addition, they were asked to remember whether the last item was a + sign or an = sign. This final +/- task was included to

ensure that participants kept their eyes fixated on the centre of the screen throughout the duration of the trial.

At the end of a trial, participants were asked 3 questions. For each question, they were presented with a response menu with multiple options in a list. They were instructed to navigate the list using the up and down arrows, and select an option using the enter key of a standard UK keyboard. In the first menu, they were asked to select the last item that they saw, and were given 3 options: '+', '=', and 'None of the above'. Following that, they were presented with a second response menu where they were asked to select the identity of the target item, and were given 6 options. The first 5 consisted of the target item plus 4 other items, randomly chosen without repetition from the target set (i.e., letters or symbols) for the block. The order of these 5 items in the menu were randomised. The final option in the menu was the 'None of the above' option. This identity question effectively ensured that participants could not perform the task of identifying the target's colour by attending to the item opposite to the target in the other stream. The third response menu asked participants to select the colour of the square surrounding the target, and were again given 6 options. The first 5 options consisted of a random permutation of the 5 colours used in the experiment, and the last option was 'None of the above'. In all 3 menus, participants were instructed to use the last 'None of the above' option only if they were completely uncertain about all of the other five responses.

### **B.3.4 EEG Recording and Analysis**

EEG recording hardware was identical to that employed for Experiment 1. EEG data was recorded using Vision Recorder (BrainProducts, Munich, Germany), at a sampling rate of 1000Hz. Electrode channel locations used were identical to that used in Experiment 2. Online referencing to the average of all channels, de-trending and filtering at 80Hz low-pass and 0.25Hz high-pass were applied.

EEG data was analysed using EEGLAB 7 (Delorme & Makeig, 2004) and custom MATLAB scripts. The raw data was filtered at 25Hz. Following that, signal deviations in the EOG channel of more than  $50\mu V$  within an interval of 100ms were identified as eye blinks and movement artefacts, and a window of 200ms before and after an artefact were marked for rejection. Later, segmented trials containing such marked regions were excluded from

Condition	N2pc Trials	P3 Trials
Letter+Symbol	3417	3017
Letter	1629	1435
Symbol	1788	1582
Correct reports	1117	956
Pre-target errors	881	801
Post-target errors	1417	1258

*Table 6* **Conditions of interest analysed in Experiment 3.** Columns 2 and 3 list the total number of trials that were retained for N2pc and P3 plotting and analysis after artefact rejection.

further analysis. The data was then re-referenced to the earlobe channels and down-sampled to 250Hz.

Trials for conditions of interest were extracted from the raw EEG data, by segmenting the data into windows of -200 to 800ms around target onset for N2pc analysis and -200 to 1000ms for P3 analysis. For all conditions, the trials containing artefacts were rejected, and were further restricted to those in which the last item question and the target identity question had been correctly answered. The number of retained trials in each condition are listed in table 6. These trials were baselined to the -200 to 0ms window preceding target onset. ERP amplitudes for a condition were derived from mean voltage values within a window identified by examining the grand average for that condition. ERP latencies were calculated using jackknife analysis (with an onset criterion of 50% of peak amplitude; see J. Miller et al., 1998) for the N2pc and 50% area latency analysis (Luck & Hillyard, 1990) for the P3. Amplitude and latency values from subject-wise averages were submitted to MATLAB scripts (Trujillo-Ortiz, Hernandez-Walls, & Trujillo-Perez, 2004) to perform repeated measures Analysis of Variance (ANOVA).

### **B.3.5 Computational Modelling**

Section A.4 describes the general configuration of the 2f-ST<sup>2</sup> model used for all the conditions simulated below. Only the  $\tau_K$  and  $\tau_R$  parameters that controlled the processing delays in the key and response pathways were changed according to the condition being simulated.

## Key Feature Manipulation

The *early key feature* condition was simulated by introducing a delay of -40ms (i.e.,  $\tau_K = -40\text{ms}$  and  $\tau_R = 0\text{ms}$ ) in the processing of all features in the key pathway in each trial. Of the total of 1372 trials making up a complete simulation in this configuration, a token was bound to a pair of features in 1123 trials. In 164 of these trials, two response features were bound to the same key feature, in which case one of them was randomly selected for behavioural report.

The *late key feature* condition was simulated by running the 2f-ST<sup>2</sup> model in its default configuration (i.e.,  $\tau_K = 0\text{ms}$  and  $\tau_R = 0\text{ms}$ ). Of the total of 1372 trials making up a complete simulation in this configuration, a token was bound to a pair of features in 1122 trials. In 113 of these trials, two response features were bound to the same key feature, in which case one of them was randomly selected for behavioural report.

## Response Feature Manipulation

The *early response feature* condition was simulated by running the 2f-ST<sup>2</sup> model in its default configuration (see above for details).

The *late response feature* condition was simulated by introducing a delay of 40ms (i.e.,  $\tau_K = 0\text{ms}$  and  $\tau_R = 40\text{ms}$ ) in the processing of all features in the response pathway in each trial. Of the total of 1372 trials making up a complete simulation in this configuration, a token was bound to a pair of features in 1123 trials. In 164 of these trials, two response features were bound to the same key feature, in which case one of them was randomly selected for behavioural report.

## Virtual ERPs

To simulate ERP data from Experiment 3, we focused on the virtual N2pc and P3 ERPs. The virtual N2pc was generated by recording activation from the blaster, and the virtual P3 was generated by summing activation across the item, Type, binding pool and token layers in both key and response pathways (see figure 49).

# Bibliography

- Alvarez, G. A., & Cavanagh, P. (2004). The Capacity of Visual Short-Term Memory Is Set Both by Visual Information Load and by Number of Objects. *Psychological Science*, *15*(2), 106-111.
- Anderson, A. K. (2005). Affective Influences on the Attentional Dynamics Supporting Awareness. *Journal of Experimental Psychology: General*, *134*(2), 258-281.
- Arend, I., Machado, L., Ward, R., McGrath, M., Ro, T., & Rafal, R. D. (2008). The role of the human pulvinar in visual attention and action: evidence from temporal-order judgment, saccade decision, and antisaccade tasks. In C. Kennard & R. J. Leigh (Eds.), *Using Eye Movements as an Experimental Probe of Brain function - A Symposium in Honor of Jean Büttner-Ennever* (Vol. 171, p. 475-483). Elsevier.
- Ashby, F. G., Prinzmetal, W., Ivry, R., & Maddox, W. T. (1996). A formal theory of feature binding in object perception. *Psychological Review*, *103*(1), 165-192.
- Aston-Jones, G., & Cohen, J. D. (2005). An Integrative Theory of Locus Coeruleus-Norepinephrine Function: Adaptive Gain and Optimal Performance. *Annual Review of Neuroscience*, *28*(1), 403-450.
- Aston-Jones, G., Rajkowski, J., & Cohen, J. (2000). Locus coeruleus and regulation of behavioral flexibility and attention. *Progress in Brain Research*, *126*, 165-182.
- Averbach, E., & Coriell, A. S. (1961). Short-term memory in vision. *Bell System Technical Journal*, *40*, 309-328.
- Baillet, S., Mosher, J., & Leahy, R. (2001). Electromagnetic brain mapping. *IEEE Signal Processing Magazine*, *18*(6), 14-30.
- Battye, G. (2003). *Connectionist Modelling of Attention and Anxiety*. Unpublished doctoral dissertation, The Medical Research Council's Cognition and Brain Sciences unit,

Cambridge.

- Behrmann, M., Zemel, R. S., & Mozer, M. C. (1998). Object-based attention and occlusion: Evidence from normal participants and a computational model. *Journal of Experimental Psychology: Human Perception and Performance*, *24*(4), 1011-1036.
- Berger, H. (1929). Uber das Elektroencephalogramm des Menschen. *Arch. Psychiatr. Nervenkr.*, *87*, 527-570.
- Bichot, N. P., & Schall, J. D. (1999). Effects of similarity and history on neural mechanisms of visual selection. *Nat Neurosci*, *2*(6), 549-554.
- Botella, J. (1992). Target-specified and target-categorized conditions in RSVP tasks as reflected by detection time. *Bulletin of the Psychonomic Society*, *30*(3), 197-200.
- Botella, J., Barriopedro, M. I., & Suero, M. (2001). A Model of the Formation of Illusory Conjunctions in the Time Domain. *Journal of Experimental Psychology: Human Perception and Performance*, *27*(6), 1452-1467.
- Botella, J., & Eriksen, C. (1992). Filtering versus parallel processing in RSVP tasks. *Perception & Psychophysics*, *51*(4), 334-343.
- Botella, J., & Eriksen, C. W. (1991). Pattern changes in rapid serial visual presentation tasks without strategic shifts. *Bulletin of the Psychonomic Society*, *29*(2), 105-108.
- Botella, J., Garcia, M. L., & Barriopedro, M. (1992). Intrusion patterns in rapid serial visual presentation tasks with two response dimensions. *Perception & Psychophysics*, *52*(5), 547-552.
- Boucart, M., Moroni, C., Fuentes, L. J., & Belin, C. (1998). Variations of attentional blink as a function of task and semantic similarity. *Abstracts of the Psychonomic Society*, *3*, 685.
- Bouma, H. (1970). Interaction Effects in Parafoveal Letter Recognition. *Nature*, *226*(5241), 177-178.
- Bowman, H., Su, L., Wyble, B., & Barnard, P. (2009). Saliency Sensitive Control, Temporal Attention and Stimulus-Rich Reactive Interfaces. In C. Roda (Ed.), *Human Attention in Digital Environments*. Cambridge University Press.
- Bowman, H., & Wyble, B. (2007). The Simultaneous Type, Serial Token Model of Temporal Attention and Working Memory. *Psychological Review*, *114*(1), 38-70.
- Bowman, H., Wyble, B., Chennu, S., & Craston, P. (2008). A Reciprocal Relationship

- Between Bottom-up Trace Strength and the Attentional Blink Bottleneck: Relating the LC-NE and ST<sup>2</sup> Models. *Brain Research*, 1202, 25-42.
- Brainard, D. H. (1997). The Psychophysics Toolbox. *Spatial Vision*, 10, 433-436.
- Breitmeyer, B. G., Ehrenstein, A., Pritchard, K., Hiscock, M., & Crisan, J. (1999). The roles of location specificity and masking mechanisms in the attentional blink. *Perception & Psychophysics*, 61(5), 179-809.
- Broadbent, D. E. (1958). *Perception and Communication*. London: Pergamon Press.
- Broadbent, D. E. (1977a). Colour, localisation and perceptual selection. In *Psychologie Experimentale et Comparée* (p. 95-98). Paris: Presses Universitaires de France.
- Broadbent, D. E. (1977b). The hidden preattentive process. *American Psychologist*, 32, 109-118.
- Broadbent, D. E., & Broadbent, M. H. P. (1987). From Detection to Identification: Response to Multiple Targets in a Rapid Serial Visual Presentation. *Perception & Psychophysics*, 42, 105-113.
- Callicott, J. H., Mattay, V. S., Bertolino, A., Finn, K., Coppola, R., Frank, J. A., et al. (1999). Physiological Characteristics of Capacity Constraints in Working Memory as Revealed by Functional MRI. *Cerebral Cortex*, 9(1), 20-26.
- Castiello, U., & Umiltà, C. (1992). Splitting focal attention. *Journal of Experimental Psychology: Human Perception and Performance*, 18(3), 837-848.
- Cave, K. R., & Bichot, N. P. (1999). Visuospatial attention: beyond a spotlight model. *Psychonomic bulletin & review*, 6(2), 204-223.
- Chalmers, D. (1990). Syntactic Transformations on Distributed Representations. *Connection Science*, 2, 53-62.
- Chartier, S., Cousineau, D., & Charbonneau, D. (2004). A Connectionist Model of the Attentional Blink Effect During a Rapid Serial Visual Presentation Task. In L. Earlbaum (Ed.), *Sith International Conference on Cognitive Modeling* (p. 64-69).
- Chelazzi, L., Miller, E. K., Duncan, J., & Desimone, R. (2001). Responses of Neurons in Macaque Area V4 During Memory-guided Visual Search. *Cereb. Cortex*, 11(8), 761-772.
- Chennu, S., Craston, P., Wyble, B., & Bowman, H. (2008). Transient Attentional Enhancement during the Attentional Blink: ERP correlates of the ST<sup>2</sup> models. In R. M. French

- & E. Thomas (Eds.), *FROM ASSOCIATIONS TO RULES: Connectionist Models of Behavior and Cognition* (Vol. 17, p. 236). 5 Toh Tuck Link, SINGAPORE 596224: World Scientific.
- Chennu, S., Craston, P., Wyble, B., & Bowman, H. (2009a). Attention Increases the Temporal Precision of Conscious Perception: Verifying the Neural-ST<sup>2</sup> Model. *PLoS Computational Biology*, *5*(11), e1000576.
- Chennu, S., Craston, P., Wyble, B., & Bowman, H. (2009b). The influence of target discriminability on the time course of attentional selection. In N. A. Taatgen & H. van Rijn (Eds.), *Proceedings of the 31st Annual Conference of the Cognitive Science Society* (p. 1506-1511). Austin, TX: Cognitive Science Society.
- Chua, F. (2005). The effect of target contrast on the attentional blink. *Perception & Psychophysics*, *67*(5), 770-88.
- Chua, F., Goh, J., & Hon, N. (2001). Nature of Codes Extracted During the Attentional Blink. *Journal of Experimental Psychology: Human Perception and Performance*, *27*(5), 1229-1242.
- Chun, M. (1997a). Temporal binding errors are redistributed by the attentional blink. *Perception & Psychophysics*, *59*(8), 1191-1199.
- Chun, M. (1997b). Types and Tokens in Visual Processing: A Double Dissociation Between the Attentional Blink and Repetition Blindness. *Journal of Experimental Psychology: Human Perception and Performance*, *23*(3), 738-755.
- Chun, M., & Potter, M. (1995). A Two-Stage Model for Multiple Target Detection in Rapid Serial Visual Presentation. *Journal of Experimental Psychology: Human Perception and Performance*, *21*(1), 109-127.
- Chun, M., & Potter, M. (2000). The attentional blink and task switching within and across modalities. In K. Shapiro (Ed.), *Temporal constraints on human information processing* (p. 20-35). Oxford: Oxford University Press.
- Cohen, A., & Ivry, R. (1989). Illusory conjunctions inside and outside the focus of attention. *Journal of Experimental Psychology: Human Perception and Performance*, *15*(4), 650-663.
- Coltheart, M. (1983). Iconic memory. *Philosophical Transactions of the Royal Society B: Biological Sciences*, *302*(1110), 283-94.

- Corbetta, M., Miezin, F., Dobmeyer, S., Shulman, G., & Petersen, S. (1991). Selective and divided attention during visual discriminations of shape, color, and speed: functional anatomy by positron emission tomography. *J. Neurosci.*, *11*(8), 2383-2402.
- Corbetta, M., & Shulman, G. L. (2002). Control of goal-directed and stimulus-driven attention in the brain. *Nat Rev Neurosci*, *3*(3), 201-215.
- Cowan, N. (2001). The magical number 4 in short-term memory: A reconsideration of mental storage capacity. *Behavioral and Brain Sciences*, *24*(1), 87-114.
- Craston, P. (2009). *Applying cognitive electrophysiology to neural modelling of the attentional blink*. Unpublished doctoral dissertation, University of Kent.
- Craston, P., Wyble, B., Chennu, S., & Bowman, H. (2009). The attentional blink reveals serial working memory encoding: Evidence from virtual & human event-related potentials. *Journal of Cognitive Neuroscience*, *21*(3), 550-566.
- David, O., Harrison, L., & Friston, K. J. (2005). Modelling event-related responses in the brain. *NeuroImage*, *25*(3), 756-770.
- David, O., Kilner, J. M., & Friston, K. J. (2006). Mechanisms of evoked and induced responses in MEG/EEG. *NeuroImage*, *31*(4), 1580-1591.
- Dehaene, S., Sergent, C., & Changeux, J.-P. (2003). A Neuronal Network Model linking Subjective Reports and Objective Physiological Data during Conscious Perception. *Proceedings National Academie of Sciences*, *100*(14), 8520-8525.
- Delorme, A., & Makeig, S. (2004). EEGLAB: an open source toolbox for analysis of single-trial EEG dynamics including independent component analysis. *Journal of Neuroscience Methods*, *134*(1), 9-21.
- Desimone, R. (1996). Neural mechanisms for visual memory and their role in attention. *Proceedings of the National Academy of Sciences of the United States of America*, *93*(24), 13494-13499.
- Desimone, R., & Duncan, J. (1995). Neural Mechanisms of Selective Visual Attention. *Annual Review of Neuroscience*, *18*, 193-222.
- Desimone, R., & Ungerleider, L. G. (1989). Handbook of Neuropsychology. In F. Boller & J. Grafman (Eds.), (Vol. 2, p. 267-299). New York: Elsevier.
- Deutsch, J. A., & Deutsch, D. (1963). Attention: Some theoretical considerations. *Psychological Review*, *70*, 80-90.

- Di Lollo, J., V. and Kawahara, Ghorashi, S., & Enns, J. (2005). The Attentional Blink: Resource depletion or temporary loss of control? *Psychological Research*, *69*(3), 191-200.
- Di Russo, F., Teder-Sälejärvi, W., & Hillyard, S. (2003). Steady-state VEP and attentional visual processing. In A. Z. . A. Proverbio (Ed.), *The Cognitive Electrophysiology of Mind and Brain* (p. 259-274). San Diego: Academic Press.
- Donchin, E. (1981). Surprise! . . . Surprise? *Psychophysiology*, *18*, 493-513.
- Donchin, E., & Coles, M. (1988). Is the P300 component a manifestation of context updating? *Behavioral and Brain Sciences*, *11*, 357-374.
- Donk, M. (1999). Illusory Conjunctions Are an Illusion: The Effects of Target-Nontarget Similarity on Conjunction and Feature Errors. *Journal of Experimental Psychology: Human Perception and Performance*, *25*(5), 1207-1233.
- Donk, M. (2001). Illusory conjunctions die hard: A reply to Prinzmetal, Diedrichsen, and Irvy (2001). *Journal of Experimental Psychology: Human Perception and Performance*, *27*(3), 542-546.
- Downing, C. J., & Pinker, S. (1985). Attention and Performance XI. In M. I. Posner & O. S. M. Marin (Eds.), (chap. The spatial structure of visual attention). Hillsdale, NJ: Erlbaum.
- Driver, J. (2001). A selective review of selective attention research from the past century. *British Journal of Psychology*, *92*, 53-78(26).
- Driver, J., & Baylis, G. C. (1989). Movement and visual attention: The spotlight metaphor breaks down. *Journal of Experimental Psychology: Human Perception and Performance*, *15*(3), 448-456.
- Duncan, J. (1980). The locus of interference in the perception of simultaneous stimuli. *Psychological Review*, *87*, 272-300.
- Duncan, J. (1981). Directing attention in the visual field. *Perception and Psychophysics*, *30*(1), 90-93.
- Duncan, J. (1984). Selective attention and the organization of visual information. *Journal of Experimental Psychology: General*, *113*, 501-517.
- Duncan, J. (2001). An adaptive coding model of neural function in prefrontal cortex. *Nat Rev Neurosci*, *2*(11), 820-829.

- Duncan, J., & Humphreys, G. (1992). Beyond the search surface: Visual search and attentional engagement. *Journal of Experimental Psychology: Human Perception and Performance*, 18(2), 578-588.
- Duncan, J., & Humphreys, G. W. (1989). Visual search and stimulus similarity. *Psychological Review*, 96(3), 433-458.
- Eimer, M. (1996). The N2pc component as an indicator of attentional selectivity. *Electroencephalography and Clinical Neurophysiology*, 99(3), 225-234.
- Elman, J. L. (1991). Distributed representations, simple recurrent networks, and grammatical structure. *Machine Learning*, 7(2), 195-225.
- Eriksen, B. A., & Eriksen, C. W. (1974). Effects of noise letters upon the identification of a target letter in a nonsearch task. *Perception & Psychophysics*, 16, 143-149.
- Eriksen, C. W., & St James, J. D. (1986). Visual attention within and around the field of focal attention: a zoom lens model. *Perception and Psychophysics*, 40(4), 225-240.
- Eriksen, C. W., & Yeh, Y.-y. (1985). Allocation of attention in the visual field. *Journal of Experimental Psychology: Human Perception and Performance*, 11(5), 583-597.
- Falkenstein, M., Hohnsbein, J., & Hoormann, J. (1994). Time pressure effects on late components of the event-related potential (ERP). *Journal of Psychophysiology*, 8(1), 22-30.
- Falkenstein, M., Hohnsbein, J., Hoormann, J., & Blanke, L. (1991). Effects of crossmodal divided attention on late ERP components. II. Error processing in choice reaction tasks. *Electroencephalography and Clinical Neurophysiology*, 78(6), 447-455.
- Ferree, T. C., Luu, P., Russell, G. S., & Tucker, D. M. (2001). Scalp electrode impedance, infection risk, and EEG data quality. *Clinical Neurophysiology*, 112(3), 536-544.
- Fitzhugh, R. (1969). Biological Engineering. In H. P. Schwan (Ed.), (p. 1-85). McGraw-Hill Book Company.
- Fodor, J. A. (1975). *The Language of Thought*. Crowell Press.
- Fournier, L. R., & Eriksen, C. W. (1991). All-or-none versus a graded process conception of attention. In *Thirty-second Annual Meeting of the Psychonomic Society*. San Francisco, CA.
- Fournier, L. R., Eriksen, C. W., & Bowd, C. (1998). Multiple-feature discrimination

- faster than single-feature discrimination within the same object? *Perception & Psychophysics*, 60(8), 1384-1405.
- Fox, E., Russo, R., & Georgiou, G. A. (2005). Anxiety modulates the degree of attentive resources required to process emotional faces. *Cognitive, Affective, & Behavioral Neuroscience*, 5(4), 396-404.
- Fragopanagos, N., Kockelkoren, S., & Taylor, J. G. (2005). A neurodynamic model of the attentional blink. *Cognitive Brain Research*, 24(3), 568-586.
- Gathercole, S. E., & Broadbent, D. E. (1984). Combining attributes in specified and categorized target search: further evidence for strategic differences. *Memory & cognition*, 12(4), 329-337.
- Gazzaniga, M. S., Ivry, R., & Mangun, G. R. (2002). *Cognitive Neuroscience: The Biology of the Mind* (2nd ed.). New York, NY: W. W. Norton and Company.
- German, D., Walker, B., Manaye, K., Smith, W., Woodward, D., & North, A. (1988). The human locus coeruleus: computer reconstruction of cellular distribution. *J. Neurosci.*, 8(5), 1776-1788.
- Giesbrecht, B., & Di Lollo, V. (1998). Beyond the Attentional Blink: Visual Masking by Object Substitution. *Journal of Experimental Psychology: Human Perception and Performance*, 24(5), 1454-1466.
- Gilzenrat, M. S., Holmes, B. D., Rajkowski, J., Aston-Jones, G., & Cohen, J. D. (2002). Simplified dynamics in a model of noradrenergic modulation of cognitive performance. *Neural Networks*, 15(4-6), 647-663.
- Gray, C. M. (1999). The Temporal Correlation Hypothesis of Visual Feature Integration: Still Alive and Well. *Neuron*, 24(1), 31-47.
- Grieve, K. L., Acuña, C., & Cudeiro, J. (2000). The primate pulvinar nuclei: Vision and action. *Trends in Neurosciences*, 23(1), 35-39.
- Hampshire, A., Duncan, J., & Owen, A. M. (2007). Selective Tuning of the Blood Oxygenation Level-Dependent Response during Simple Target Detection Dissociates Human Frontoparietal Subregions. *J. Neurosci.*, 27(23), 6219-6223.
- Hampshire, A., Thompson, R., Duncan, J., & Owen, A. M. (2009). Selective tuning of the right inferior frontal gyrus during target detection. *Cognitive, Affective, & Behavioral Neuroscience*, 9(1), 103-112.

- Haxby, J. V., Gobbini, M. I., Furey, M. L., Ishai, A., Schouten, J. L., & Pietrini, P. (2001). Distributed and Overlapping Representations of Faces and Objects in Ventral Temporal Cortex. *Science*, *293*(5539), 2425-2430.
- He, S., Cavanagh, P., & Intriligator, J. (1996). Attentional resolution and the locus of visual awareness. *Nature*, *383*(6598), 334-337.
- Hebb, D. O. (1949). *The Organization of Behaviour*. New York: John Wiley and Sons.
- Hillyard, S. A., & Anllo-Vento, L. (1998). Event-related brain potentials in the study of visual selective attention. *Proceedings of the National Academy of Sciences of the United States of America*, *95*(3), 781-787.
- Hillyard, S. A., & Picton, T. W. (1987). Handbook of Physiology. In F. Plum (Ed.), (Vol. 5, p. 519-584). Bethesda, MD: American Physiological Society.
- Hochstein, S., & Ahissar, M. (2002). View from the Top: Hierarchies and Reverse Hierarchies in the Visual System. *Neuron*, *36*(5), 791-804.
- Hodgkin, A. L., & Huxley, A. F. (1952). A quantitative description of membrane current and its application to conduction and excitation in nerve. *The Journal of Physiology*, *117*(4), 500-544.
- Hopf, J.-M., Luck, S. J., Girelli, M., Hagner, T., Mangun, G. R., Scheich, H., et al. (2000). Neural Sources of Focused Attention in Visual Search. *Cereb. Cortex*, *10*(12), 1233-1241.
- Ishai, A., Ungerleider, L. G., Martin, A., Schouten, J. L., & Haxby, J. V. (1999). Distributed representation of objects in the human ventral visual pathway. *Proceedings of the National Academy of Sciences of the United States of America*, *96*(16), 9379-9384.
- Ivry, R. B., & Prinzmetal, W. (1991). Effect of feature similarity on illusory conjunctions. *Perception & Psychophysics*, *49*(2), 105-116.
- James, W. (1890). *The Principles of Psychology* (Vol. 1). New York: Holt.
- Jasper, H. H. (1958). The ten-twenty electrode system of the International Federation. *Electroencephalography & Clinical Neurophysiology*, *10*, 371-375.
- Jolicoeur, P., Sessa, P., Dell'Acqua, R., & Robitaille, N. (2006). Attentional control and capture in the attentional blink paradigm: Evidence from human electrophysiology. *European Journal of Cognitive Psychology*, *18*(4), 560-578.
- Kahneman, D. (1973). *Attention and Effort*. Englewood Cliffs, NJ: Prentice Hall.

- Kahneman, D., & Treisman, A. (1984). Varieties of Attention. In R. Parasuraman & R. Davies (Eds.), (p. 29-61). New York: Academic Press.
- Kahneman, D., Treisman, A., & Gibbs, B. J. (1992). The reviewing of object files: Object-specific integration of information. *Cognitive Psychology*, *24*, 175-219.
- Kanwisher, N. (1987). Repetition Blindness: Type recognition without token individuation. *Cognition*, *27*, 117-143.
- Kanwisher, N. (1991). Repetition Blindness and Illusory Conjunctions : Errors in Binding Visual Types With Visual Tokens. *Journal of Experimental Psychology: Human Perception and Performance*, *17*(2), 404-421.
- Kanwisher, N., & Driver, J. (1992). Objects, Attributes, and Visual Attention: Which, What, and Where. *Current Directions in Psychological Science*, *1*(1), 26-31.
- Keele, S. W., Cohen, A., Ivry, R., Liotti, M., & Yee, P. (1988). Tests of a temporal theory of attentional binding. *Journal of Experimental Psychology: Human Perception and Performance*, *14*(3), 444-452.
- Keele, S. W., & Neill, W. T. (1978). Handbook of Perception. In E. C. Carterette & M. P. Friedman (Eds.), (Vol. 9, p. 3-47). New York: Academic Press.
- Kessler, K., Schmitz, F., Gross, J., Hommel, B., Shapiro, K., & Schnitzler, A. (2005). Target consolidation under high temporal processing demands as revealed by MEG. *NeuroImage*, *26*(4), 1030-1041.
- Keysers, C., & Perrett, D. I. (2002). Visual masking and RSVP reveal neural competition. *Trends in Cognitive Sciences*, *6*(3), 120-125.
- Keysers, C., Xiao, D. K., Földiák, P., & Perrett, D. I. (2005). Out of sight but not out of mind: the neurophysiology of iconic memory in the superior temporal sulcus. *Cognitive Neuropsychology*, *22*(3), 316-332.
- Kikuchi, T. (1996). Detection of Kanji words in a rapid serial visual presentation task. *Journal of Experimental Psychology: Human Perception and Performance*, *22*(2), p332-341.
- Kiss, M., Jolicoeur, P., Dell'Acqua, R., & Eimer, M. (2008). Attentional capture by visual singletons is mediated by top-down task set: New evidence from the N2pc component. *Psychophysiology*, *45*, 1013-1024(12).
- Koch, C. (1998). *Biophysics of Computation: Information Processing in Single Neurons*

- (*Computational Neuroscience*) (1 ed.). Oxford University Press, USA.
- Koch, C. (2004). *The Quest for Consciousness: A Neurobiological Approach*. Englewood, CO: Roberts & Company Publishers.
- Kok, A. (2001). On the utility of P3 amplitude as a measure of processing capacity. *Psychophysiology*, *38*(3), 557-577.
- Kovács, G., Vogels, R., & Orban, G. A. (1995). Cortical correlate of pattern backward masking. *Proceedings of the National Academy of Sciences of the United States of America*, *92*(12), 5587-5591.
- Kranczioch, C., Debener, S., & Engel, A. K. (2003). Event-Related Potential Correlates of the Attentional Blink Phenomenon. *Cognitive Brain Research*, *17*(1), 177-187.
- Kranczioch, C., Debener, S., Schwarzbach, J., Goebel, R., & Engel, A. K. (2005). Neural Correlates of Conscious Perception in the Attentional Blink. *NeuroImage*, *24*(3), 704-714.
- Kristjansson, A., Mackeben, M., & Nakayama, K. (2001). Rapid, object-based learning in the deployment of transient attention. *Perception*, *30*(11), 1375-1387.
- Kristjansson, A., & Nakayama, K. (2003). A primitive memory system for the deployment of transient attention. *Perception & Psychophysics*, *65*, 711-724(14).
- Lawrence, D. (1971). Two studies of visual search for word targets with controlled rates of presentation. *Perception and Psychophysics*, *10*, 85-89.
- Luck, S. J. (1998). Attention. In H. Pashler (Ed.), (p. 257-295). London, UK: University College London Press.
- Luck, S. J. (2005). *An Introduction to the Event-Related Potential Technique*. MIT Press, Cambridge, MA.
- Luck, S. J., Chelazzi, L., Hillyard, S. A., & Desimone, R. (1997). Neural Mechanisms of Spatial Selective Attention in Areas V1, V2, and V4 of Macaque Visual Cortex. *J Neurophysiol*, *77*(1), 24-42.
- Luck, S. J., & Hillyard, S. A. (1990). Electrophysiological evidence for parallel and serial processing during visual search. *Perception & Psychophysics*, *48*, 603-617.
- Luck, S. J., & Hillyard, S. A. (1994). Spatial Filtering During Visual Search: Evidence From Human Electrophysiology. *Journal of Experimental Psychology: Human Perception and Performance*, *20*(5), 1000-1014.

- Luck, S. J., & Vogel, E. K. (1997). The capacity of visual working memory for features and conjunctions. *Nature*, *390*, 279-281.
- Luck, S. J., Vogel, E. K., & Shapiro, K. L. (1996). Word meanings can be accessed but not reported during the attentional blink. *Nature*, *383*(6601), 616-618.
- Makeig, S. (2009). Foundations of Augmented Cognition. Neuroergonomics and Operational Neuroscience. In (Vol. 5638, p. 749-758). Berlin, Germany: Springer.
- Makeig, S., Debener, S., Onton, J., & Delorme, A. (2004). Mining event-related brain dynamics. *Trends in Cognitive Sciences*, *8*(5), 204-210.
- Makeig, S., Delorme, A., Westerfield, M., Jung, T., Townsend, J., Courchesne, E., et al. (2004). Electroencephalographic Brain Dynamics Following Manually Responded Visual Targets. *PLoS Biology*, *2*(6), e176.
- Makeig, S., & Onton, J. (2009). Oxford Handbook of Event-Related Potential Components. In S. Luck & E. Kappenman (Eds.), (chap. ERP Features and EEG Dynamics: An ICA Perspective). Oxford University Press.
- Mardia, K. V., & Jupp, P. E. (2000). *Directional statistics*. Chichester; New York: J. Wiley.
- Marois, R., Chun, M., & Gore, J. (2000). Neural Correlates of the Attentional Blink. *Neuron*, *29*, 229-308.
- Marois, R., Yi, D., & Chun, M. (2004). The Neural Fate of Consciously Perceived and Missed Events in the Attentional Blink. *Neuron*, *41*, 465-472.
- Marr, D. C. (1982). *Vision: A Computational Investigation into the Human Representation and Processing of Visual Information*. New York, NY: W.H. Freeman and Company.
- Martens, S., Elmallah, K., London, R., & Johnson, A. (2006). Cuing and stimulus probability effects on the P3 and the AB. *Acta Psychologica*, *123*(3), 204-218.
- Martens, S., Munneke, J., Smid, H., & Johnson, A. (2006). Quick Minds Don't Blink: Electrophysiological Correlates of Individual Differences in Attentional Selection. *Journal of Cognitive Neuroscience*, *18*(9), 1423-1438.
- McCormick, P., Klein, R., & Johnston, S. (1998). Splitting versus sharing focal attention: comment on Castiello and Umiltà (1992). *Journal of Experimental Psychology: Human Perception and Performance*, *24*(1), 350-357.
- McLaughlin, E., Shore, D., & Klein, R. (2001). The attentional blink is immune to masking-induced data limits. *The Quarterly Journal of Experimental Psychology: Section A*,

- 54(1), 169-196.
- McLean, J. P., Broadbent, D. E., & Broadbent, M. H. (1983). Combining attributes in rapid serial visual presentation tasks. *Quarterly Journal of Experimental Psychology (A)*, 35(1), 171-186.
- Miller, E. K., & Cohen, J. D. (2001). An integrative theory of prefrontal cortex function. *Annual Review of Neuroscience*, 24(1), 167-202.
- Miller, E. K., Erickson, C. A., & Desimone, R. (1996). Neural Mechanisms of Visual Working Memory in Prefrontal Cortex of the Macaque. *J. Neurosci.*, 16(16), 5154-5167.
- Miller, J. (1991). The flanker compatibility effect as a function of visual angle, attentional focus, visual transients, and perceptual load: A search for boundary conditions. *Perception & Psychophysics*, 49(3), 270-288.
- Miller, J., Patterson, T., & Ulrich, R. (1998). Jackknife-based method for measuring LRP onset latency differences. *Psychophysiology*, 35(1), 99-115.
- Milner, P. M. (1974). A model for visual shape recognition. *Psychological review*, 81(6), 521-535.
- Mozer, M. (1989). Types and Tokens in Visual Letter Perception. *Journal of Experimental Psychology: Human Perception and Performance*, 15(2), 287-303.
- Mueller, M. M., & Hillyard, S. (2000). Concurrent recording of steady-state and transient event-related potentials as indices of visual-spatial selective attention. *Clinical Neurophysiology*, 111(9), 1544-1552.
- Mueller, M. M., & Hubner, R. (2002). Can the Spotlight of Attention be Shaped Like A Doughnut? *Psychological Science*, 13(2), 119-124.
- Mueller, M. M., Picton, T. W., Valdes-Sosa, P., Riera, J., Teder-Salejarvi, W. A., & Hillyard, S. A. (1998). Effects of spatial selective attention on the steady-state visual evoked potential in the 20-28 Hz range. *Cognitive Brain Research*, 6(4), 249-261.
- Müller, H. J., & Rabbitt, P. M. (1989). Reflexive and voluntary orienting of visual attention: Time course of activation and resistance to interruption. *Journal of Experimental Psychology: Human Perception and Performance*, 15(2), 315-330.
- Nagumo, J., Arimoto, S., & Yoshizawa, S. (1964). An active pulse transmission line simulating nerve axon. In *Proceedings of the Institute of Radio Engineers* (Vol. 50, p. 2061-2070).

- Nakayama, K., & Mackeben, M. (1989). Sustained and transient components of focal visual attention. *Vision Research*, *29*(11), 1631-1647.
- Neisser, U. (1967). *Cognitive Psychology*. Appleton-Century-Crofts.
- Newell, A., & Simon, H. A. (1976). Computer science as empirical inquiry: symbols and search. *Communications of the ACM*, *19*(3), 113-126.
- Nieuwenhuis, S., Aston-Jones, G., & Cohen, J. (2005). Decision Making, the P3, and the Locus Coeruleus-Norepinephrine System. *Psychological Bulletin*, *131*(4), 510-532.
- Nieuwenhuis, S., Gilzenrat, M., Holmes, B., & Cohen, J. (2005). The role of the locus coeruleus in mediating the attentional blink: A neurocomputational theory. *Journal of Experimental Psychology: General*, *134*(3), 291-307.
- Olivers, C. N. L., & Meeter, M. (2008). A boost and bounce theory of temporal attention. *Psychological review*, *115*(4), 836-863.
- Olivers, C. N. L., Stigchel, S. van der, & Hulleman, J. (2005). Spreading the sparing: against a limited-capacity account of the attentional blink. *Psychological Research*, *1*, 1-14.
- O'Reilly, R., & Munakata, Y. (2000). *Computational Explorations in Cognitive Neuroscience*. MIT Press.
- Page, M. (2001). Connectionist modelling in psychology: A localist manifesto. *Behavioral and Brain Sciences*, *23*(04), 443-467.
- Pashler, H. (1996). *The Psychology of Attention*. Cambridge, MA: MIT Press.
- Passingham, D., & Sakai, K. (2004). The prefrontal cortex and working memory: physiology and brain imaging. *Current Opinion in Neurobiology*, *14*(2), 163-168.
- Polich, J., & Donchin, E. (1988). P300 and the word frequency effect. *Electroencephalography and Clinical Neurophysiology*, *70*(1), 33-45.
- Popple, A. V., & Levi, D. M. (2007). Attentional blinks as errors in temporal binding. *Vision Research*, *47*(23), 2973-2981.
- Posner, M. I., & Peterson, S. E. (1990). The attention system of the human brain. *Annual Review of Neuroscience*, *13*, 25-42.
- Posner, M. I., Snyder, C. R., & Davidson, B. J. (1980). Attention and the detection of signals. *Journal of Experimental Psychology: General*, *109*(2), 160-174.
- Potter, M. C. (1975). Meaning in visual search. *Science*, *187*, 965-966.

- Potter, M. C. (1993). Very short-term conceptual memory. *Memory & Cognition*, *21*(2), 156-161.
- Potter, M. C., Chun, M., Banks, B., & Muckenhoupt, M. (1998). Two Attentional Deficits in Serial Target Search: The Visual Attentional Blink and an Amodal Task-Switch Deficit. *Journal of Experimental Psychology: Human Perception and Performance*, *24*(4), 979-992.
- Potter, M. C., Staub, A., & O'Connor, D. (2002). The Time Course of Competition for Attention: Attention Is Initially Labile. *Journal of Experimental Psychology: Human Perception and Performance*, *28*(5), 1149-1162.
- Prinzmetal, W. (1981). Principles of feature integration in visual perception. *Perception & Psychophysics*, *30*(4), 330-340.
- Prinzmetal, W. (1995). Visual feature integration in a world of objects. *Current Directions in Psychological Science*, *4*, 90-94.
- Prinzmetal, W., Diedrichsen, J., & Ivry, R. B. (2001). Illusory Conjunctions Are Alive and Well: A Reply to Donk (1999). *Journal of Experimental Psychology: Human Perception and Performance*, *27*(3), 538-541.
- Prinzmetal, W., Henderson, D., & Ivry, R. (1995). Loosening the constraints on illusory conjunctions: Assessing the roles of exposure duration and attention. *Journal of Experimental Psychology: Human Perception and Performance*, *21*(6), 1362-1375.
- Pylyshyn, Z. W. (1984). *Computation and Cognition*. Cambridge, MA: MIT Press.
- Pylyshyn, Z. W. (1989). The role of location indexes in spatial perception: a sketch of the FINST spatial-index model. *Cognition*, *32*(1), 65-97.
- Pylyshyn, Z. W., & Storm, R. W. (1988). Tracking multiple independent targets: Evidence for a parallel tracking mechanism. *Spatial Vision*, *3*, 179-197.
- R Development Core Team. (2008). *R: A Language and Environment for Statistical Computing*. Vienna, Austria.
- Raymond, J., Shapiro, K., & Arnell, K. (1992). Temporary Suppression of Visual Processing in an RSVP Task: An Attentional Blink? *Journal of Experimental Psychology: Human Perception and Performance*, *18*(3), 849-860.
- Reeves, A., & Sperling, G. (1986). Attention Gating in Short-term Visual Memory. *Psychological Review*, *93*(2), 180-206.

- Reynolds, J. H., Chelazzi, L., & Desimone, R. (1999). Competitive Mechanisms Subserve Attention in Macaque Areas V2 and V4. *J. Neurosci.*, *19*(5), 1736-1753.
- Rolke, B., Bausenhart, K. M., & Ulrich, R. (2007). Impaired temporal discrimination within the attentional blink. *Perception and Psychophysics*, *69*, 1295-1304(10).
- Rolke, B., Heil, M., Streb, J., & Hennighausen, E. (2001). Missed Prime Words within the Attentional Blink evoke an N400 Semantic Priming Effect. *Psychophysiology*, *38*, 165-174.
- Rolls, E. T., Tovée, M. J., & Panzeri, S. (1999). The Neurophysiology of Backward Visual Masking: Information Analysis. *Journal of Cognitive Neuroscience*, *11*(3), 300-311.
- Rosenblatt, F. (1958). The Perceptron: A Probabilistic Model for Information Storage and Organization in the Brain. *Psychological Review*, *65*, 386-408.
- Rösler, F., Borgstedt, J., & Sojka, B. (1985). When perceptual or motor sets are changed: Effects of updating demands on structure and energy of P300. *Acta Psychologica*, *60*(2-3), 293-321.
- Rousselet, G. A., Thorpe, S. J., & Fabre-Thorpe, M. (2004). How parallel is visual processing in the ventral pathway? *Trends in Cognitive Sciences*, *8*(8), 363-370.
- Rumelhart, D. E., McClelland, J. L., & the PDP Research Group. (1986). *Parallel Distributed Processing* (Vol. 1:Foundations). Cambridge, MA: MIT Press.
- Schmolesky, M. T., Wang, Y., Hanes, D. P., Thompson, K. G., Leutgeb, S., Schall, J. D., et al. (1998). Signal Timing Across the Macaque Visual System. *J Neurophysiol*, *79*(6), 3272-3278.
- Seiffert, A., & Di Lollo, V. (1997). Low-Level Masking in the Attentional Blink. *Journal of Experimental Psychology: Human Perception and Performance*, *23*(4), 1061-1073.
- Serences, J. T., Shomstein, S., Leber, A. B., Golay, X., Egeth, H. E., & Yantis, S. (2005). Coordination of Voluntary and Stimulus-Driven Attentional Control in Human Cortex. *Psychological Science*, *16*(2), 114-122.
- Sergent, C., Baillet, S., & Dehaene, S. (2005). Timing of the brain events underlying access to consciousness during the attentional blink. *Nature Neuroscience*, *10*(10), 1391-1400.
- Sessa, P., Luria, R., Verleger, R., & Dell'Acqua, R. (2006). P3 latency shifts in the attentional blink: Further evidence for second target processing postponement. *Brain Research*, *1137*, 131-139.

- Shapiro, K. L., & Raymond, J. E. (1994). Temporal allocation of visual attention: Inhibition or interference? In D. Dagenbach & T. H. Carr (Eds.), *Inhibitory processes in attention, memory, and language*. (p. 151-188). Academic Press: San Diego.
- Singer, W. (1999). Neuronal Synchrony: A Versatile Code for the Definition of Relations? *Neuron*, *24*(1), 49-65.
- Sperling, G. (1960). The information available in brief visual presentations. *Psychological monographs: General and Applied*, *74*(11), 1-29.
- Sperling, G., Budiansky, J., Spivak, J. G., & Johnson, M. C. (1971). Extremely rapid visual search: The maximum rate of scanning letters for the presence of a numeral. *Science*, *174*, 307-311.
- Su, L., Bowman, H., Barnard, P., & Wyble, B. (2008). Process Algebraic Modelling of Attentional Capture and Human Electrophysiology in Interactive Systems. *Formal Aspects of Computing*, *21*, 513-539.
- Swartz, B. (1988). Timeline of the history of EEG and associated fields. *Electroencephalography & Clinical Neurophysiology*, *106*, 173-176.
- Tallon-Baudry, C., Bertrand, O., Delpuech, C., & Pernier, J. (1996). Stimulus Specificity of Phase-Locked and Non-Phase-Locked 40Hz Visual Responses in Human. *J. Neurosci.*, *16*(13), 4240-4249.
- Tanaka, K. (1996). Inferotemporal Cortex and Object Vision. *Annual Review of Neuroscience*, *19*(1), 109-139.
- Tanji, K., Suzuki, K., Delorme, A., Shamoto, H., & Nakasato, N. (2005). High-Frequency gamma-Band Activity in the Basal Temporal Cortex during Picture-Naming and Lexical-Decision Tasks. *J. Neurosci.*, *25*(13), 3287-3293.
- Taylor, J. G., & Rogers, M. (2002). A control model of the movement of attention. *Neural Networks*, *15*(3), 309-326.
- Treisman, A. (1991). Search, similarity, and integration of features between and within dimensions. *Journal of Experimental Psychology: Human Perception and Performance*, *17*(3), 652-676.
- Treisman, A. (1996). The binding problem. *Current Opinion in Neurobiology*, *6*(2), 171-178.
- Treisman, A. (1998). Feature Binding, Attention and Object Perception. *Philosophical Transactions: Biological Sciences*, *353*(1373), 1295-1306.

- Treisman, A., & Gelade, G. (1980). A feature-integration theory of attention. *Cognitive Psychology*, *12*(1), 97-136.
- Treisman, A., & Gormican, S. (1988). Feature analysis in early vision: Evidence from search asymmetries. *Psychological Review*, *95*(1), 15-48.
- Treisman, A., & Schmidt, H. (1982). Illusory conjunctions in the perception of objects. *Cognitive Psychology*, *14*(1), 107-141.
- Trippe, R. H., Hewig, J., Heydel, C., Hecht, H., & Miltner, W. H. (2007). Attentional Blink to emotional and threatening pictures in spider phobics: Electrophysiology and behavior. *Brain Research*, *1148*, 149-160.
- Trujillo-Ortiz, A., Hernandez-Walls, R., Castro-Perez, A., & Barba-Rojo, K. (2006). *epsGG: Greenhouse-Geisser epsilon. A MATLAB file.* (Available at <http://www.mathworks.com/matlabcentral/fileexchange/loadFile.do?objectId=12839>. Retrieved on 27/11/2009.)
- Trujillo-Ortiz, A., Hernandez-Walls, R., & Trujillo-Perez, R. (2004). *RMAOV1: One-way repeated measures ANOVA. A MATLAB file.* (Available at <http://www.mathworks.com/matlabcentral/fileexchange/5576>. Retrieved on 27/11/2009.)
- Trujillo-Ortiz, A., Hernandez-Walls, R., & Trujillo-Perez, R. (2004). *RMAOV2: Two-way repeated measures ANOVA. A MATLAB file.* (Available at <http://www.mathworks.com/matlabcentral/fileexchange/5578>. Retrieved on 27/11/2009.)
- Turing, A. M. (1937). On Computable Numbers, with an Application to the Entscheidungsproblem. *Proc. London Math. Soc.*, *s2-42*(1), 230-265.
- Turing, A. M. (1948). Turing, A. M., Intelligent machinery. In D. C. Ince (Ed.), *Collected Works of A.M. Turing: Mechanical Intelligence*. Amsterdam: Elsevier Science Publishers, 1992.
- Usher, M., Cohen, J. D., Servan-Schreiber, D., Rajkowski, J., & Aston-Jones, G. (1999). The Role of Locus Coeruleus in the Regulation of Cognitive Performance. *Science*, *283*(5401), 549-554.
- Verleger, R. (1988). Event-related potentials and cognition: A critique of the context updating hypothesis and an alternative interpretation of P3. *Behavioral Brain Science*, *11*, 343-427.
- Verleger, R., Jaskowski, P., & Wascher, E. (2005). Evidence for an Integrative Role of P3b

- in Linking Reaction to Perception. *Journal of Psychophysiology*, 19, 165-181.
- Visser, T., Bischof, W., & Di Lollo, V. (2004). Rapid serial visual distraction: Task-irrelevant items can produce an attentional blink. *Perception & Psychophysics*, 66, 1418-32.
- Visser, T., Bischof, W. F., & Di Lollo, V. (1999). Attentional switching in spatial and non-spatial domains: Evidence from the attentional blink. *Psychological Bulletin*, 125(4), 458-469.
- Vogel, E., & Luck, S. (2002). Delayed Working Memory Consolidation during the Attentional Blink. *Psychonomic Bulletin & Review*, 9(4), 739-743.
- Vogel, E., Luck, S., & Shapiro, K. (1998). Electrophysiological Evidence for a Postperceptual Locus of Suppression During the Attentional Blink. *Journal of Experimental Psychology: Human Perception and Performance*, 24(6), 1656-1674.
- Vul, E., Nieuwenstein, M., & Kanwisher, N. (2008). Temporal Selection Is Suppressed, Delayed, and Diffused During the Attentional Blink. *Psychological Science*, 19(1), 55-61.
- Ward, R., Duncan, J., & Shapiro, K. (1997). Effects of similarity, difficulty, and nontarget presentation on the time course of visual attention. *Perception & Psychophysics*, 59(4), 593-600.
- Weichselgartner, E., & Sperling, G. (1987). Dynamics of automatic and controlled visual attention. *Science*, 238(4828), 778-780.
- Winer, G. A., & Cottrell, J. E. (1996). Does anything leave the eye when we see? Extramission beliefs of children and adults. *Current Directions in Psychological Science*, 5(5), 137-142.
- Wolfe, J. M. (1994). Guided Search 2.0: A revised model of visual search. *Psychonomic Bulletin and Review*, 1(2), 202-238.
- Wolfe, J. M. (1998). Attention. In H. Pashler (Ed.), (p. 13-73). London, UK: University College London Press.
- Wolfe, J. M., & Bennett, S. C. (1997). Preattentive Object Files: Shapeless Bundles of Basic Features. *Vision Research*, 37(1), 25-43.
- Wolfe, J. M., & Cave, K. R. (1999). The Psychophysical Evidence for a Binding Problem in Human Vision. *Neuron*, 24(1), 11-17.

- Wolford, G. (1975). Perturbation model for letter identification. *Psychological Review*, *82*, 184-199.
- Woodman, G. F., & Luck, S. J. (2003). Serial deployment of attention during visual search. *Journal of Experimental Psychology: Human Perception and Performance*, *29*(1), 121-138.
- Wurtz, R., Goldberg, M., & Robinson, D. (1980). Behavioral modulation of visual responses in the monkey: Stimulus selection for attention and movement. *Progress in Psychobiology and Physiological Psychology*, *9*, 43-83.
- Wyble, B., & Bowman, H. (2005). Computational and Experimental Evaluation of the Attentional Blink: Testing The Simultaneous Type Serial Token Model. In B. Bara, L. Barsalou, & M. Bucciarelli (Eds.), *CogSci 2005, XXVII Annual Conference of the Cognitive Science Society* (p. 2371-2376). Cognitive Science Society.
- Wyble, B., Bowman, H., & Nieuwenstein, M. (2009). The attentional blink provides episodic distinctiveness: Sparing at a cost. *Journal of Experimental Psychology: Human Perception and Performance*, *35*(3), 787-807.
- Wyble, B., Bowman, H., & Potter, M. C. (2009). Categorically defined targets trigger spatiotemporal visual attention. *Journal of Experimental Psychology: Human Perception and Performance*, *35*(2), 324-337.
- Yantis, S. (1992). Multielement visual tracking: attention and perceptual organization. *Cognit Psychol*, *24*(3), 295-340.
- Yantis, S. (1998). Attention. In H. Pashler (Ed.), (p. 223-256). London, UK: University College London Press.